Potential of ozone to enable the low load operation of a Gasoline Compression Ignition engine

Pietro Matteo Pinazzi

UNIVERSITÉ D'ORLÉANS

***ÉCOLE DOCTORALE** ENERGIE, MATERIAUX, SCIENCES DE LA TERRE ET DE L'UNIVERS*

LABORATOIRE PRISME

THÈSE présentée par :

Pietro Matteo PINAZZI

soutenue le : 18 Décembre 2018

Pour obtenir le grade de : **Docteur de l'université d'Orléans**

Discipline/ Spécialité : Energétique

Potential of ozone to enable the low load operation of a Gasoline Compression Ignition engine.

THÈSE dirigée par :

Mr Fabrice FOUCHER Professeur, Université d'Orléans

RAPPORTEURS :

Mr Francesco CONTINO Professeur, Vrije Universiteit Brussel

Mr Robert DIBBLE Professeur, KAUST

JURY :

Mr Philippe DAGAUT Directeur de Recherche, ICARE-CNRS

Mr Olivier GUÉZET Ingénieur de Recherche, PSA Groupe

Mr Toni TAHTOUH Docteur, Ingénieur de Recherche, IFPEN

Mr Guillaume PILLA Docteur, Ingénieur de Recherche, IFPEN

UNIVERSITÉ D'ORLÉANS

ÉCOLE DOCTORALE ENERGIE, MATERIAUX, SCIENCES DE LA TERRE ET DE L'UNIVERS

LABORATOIRE PRISME

THÈSE présentée par :

Pietro Matteo PINAZZI

soutenue le : 18 Décembre 2018

Pour obtenir le grade de : **Docteur de l'université d'Orléans**

Discipline/ Spécialité : Energétique

Potentiel de l'ozone pour atteindre le fonctionnement en faible charge d'un moteur essence a allumage par compression.

THÈSE dirigée par :

Mr Fabrice FOUCHER Professeur, Université d'Orléans

RAPPORTEURS :

Mr Francesco CONTINO Professeur, Vrije Universiteit Brussel

Mr Robert DIBBLE Professeur, KAUST

JURY :

Mr Philippe DAGAUT Directeur de Recherche, ICARE-CNRS

Mr Olivier GUÉZET Ingénieur de Recherche, PSA Groupe

Mr Toni TAHTOUH Docteur, Ingénieur de Recherche, IFPEN

Mr Guillaume PILLA Docteur, Ingénieur de Recherche, IFPEN

1. Index

2. Abbreviations

CAI	Controlled Auto Ignition
CAD	Crank Angle Degree
CFD	Computational Fluid Dynamics
CI	Compression Ignition
CH_2O	Formaldehyde
CO	Carbon Monoxide
CO_2	Carbon Dioxide
CR	Compression Ratio
COV	Coefficient of Variation
DI	Direct Injection
DOC	Diesel Oxidation Catalyst
EGR	Exhaust Gas Recirculation
FSN	Filter Smoke Number
GCI	Gasoline Compression Ignition
GPPC	Gasoline Partially Premixed Combustion
HC	Unburned Hydrocarbon
HCCI	Homogeneous Charge Compression Ignition
IGR	Internal Gas Recirculation
IMEP	Indicated mean effective pressure
LTC	Low Temperature Combustion
NO	Nitrogen monoxide
NO_2	Nitrogen dioxide
ON	Octane Number
O	Oxygen atom
O_2	Diatomic oxygen molecule
O_3	Ozone
PRF	Primary Reference Fuel
RON	Research Octane Number
SACI	Spark Assisted Compression Ignition
SI	Spark Ignition
SOI	Start of Injection
SOI1	Start of first Injection
SOI2	Start of second Injection
TDC	Top Dead Center
VVT	Variable Valve Train

1. Background and Motivation

1.1. ENERGY OUTLOOK

1.1.1. Gasoline: the fuel for future transportation

In recent decades, the global energy demand has continued to grow and forecasts indicate that this trend will remain unchanged in the near future. As can be seen in Figure 1, world energy consumption is forecast to increase from 579 quadrillion KJ in 2012 to 664 quadrillion KJ in 2020 and then to 860 quadrillion KJ in 2040, a 48% increase (1.4%/year) [1]. The regions of Asia outside the Organization for Economic Cooperation and Development (Non-OECD Asia), including China and India, account for more than half of the increase. The industrial sector continues to account for the largest share of delivered energy consumption, and will consume over half of global delivered energy in 2040. Data from [1,2] show that although renewable energy will be the world's fastest-growing energy source, fossil fuels will continue to supply more than three-fourths of world energy use in 2040.

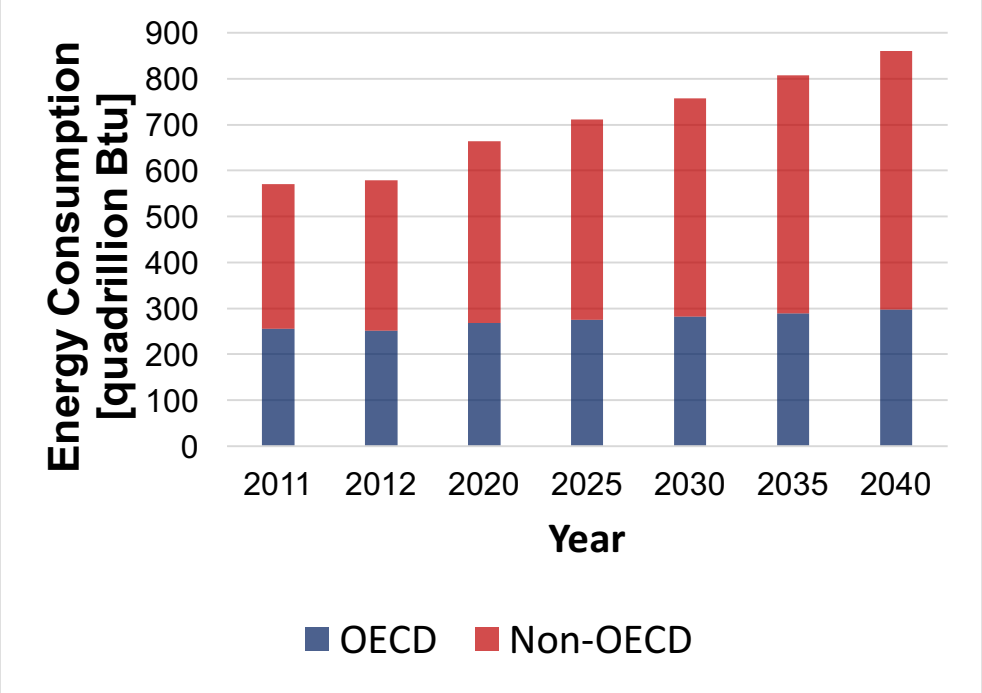

Figure 1. World total energy consumption by region. Data from [3].

The ever-increasing economic activity and population growth (forecasts [4] indicate a rise in population from 7.3 billion people in 2012 to 9.7 billion in 2050) drive the increases in energy use. A more detailed analysis, shown in Figure 2, indicates that Non-OECD nations drive the increase in total energy use, with non-OECD Asia accounting for 55% of the world increase in energy consumption. It is also important to understand which sectors consume the most energy. The three main categories are industry, transportation,

and buildings. Although total energy consumption will grow in the years to come, the share of total consumption by end-use sector will remain relatively unchanged. The industrial sector is predicted to account for approximately half (~53%) of the energy consumption, with the remainder consumed by buildings (~21%) and a slightly higher ratio (~26%) by transportation, as indicated in Figure 3.

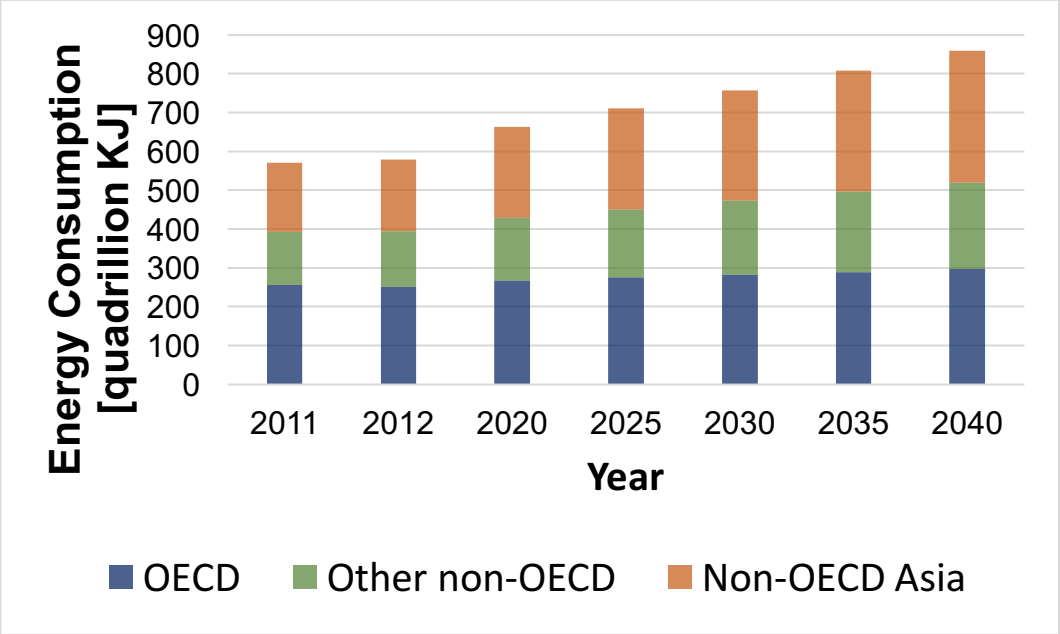

Figure 2. World total energy consumption by region (detailed). Data from [3].

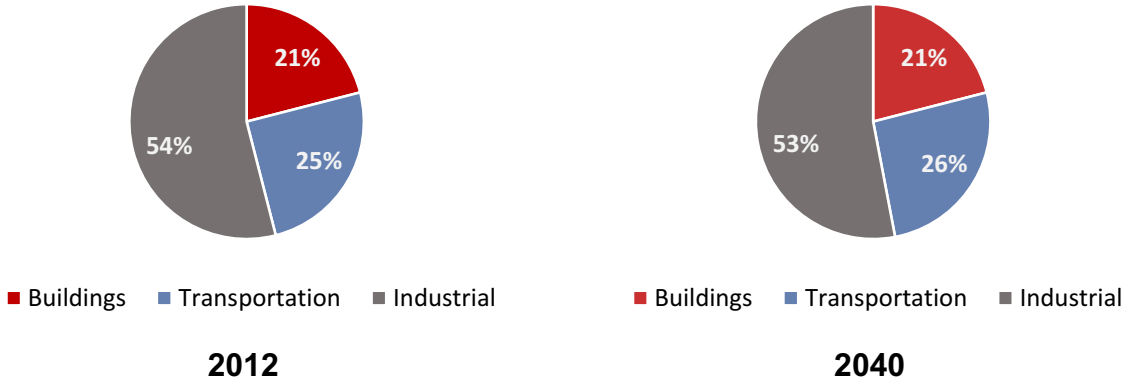

Figure 3. Energy consumption by end-use sector. Data from [3]

The delivered energy consumption of transportation is approximately one fourth of the global demand, and will increase at an annual average rate of 1.4%, from 110 quadrillion KJ in 2012 to 164 quadrillion KJ in 2040. Transportation energy demand growth occurs almost entirely in regions outside the Organization for Economic Cooperation and Development (non-OECD), with transportation demand remaining roughly flat in OECD regions, reflecting different expectations for economic growth in developing regions compared with developed regions [2]. Worldwide, petroleum and other liquid fuels are the dominant source of transportation energy: despite electrification and the search for alternative energy sources, their share of total transportation energy is expected to decline only slightly over the projection period [5], from 96% in 2012 to 88% in 2040, as shown in Figure 4.

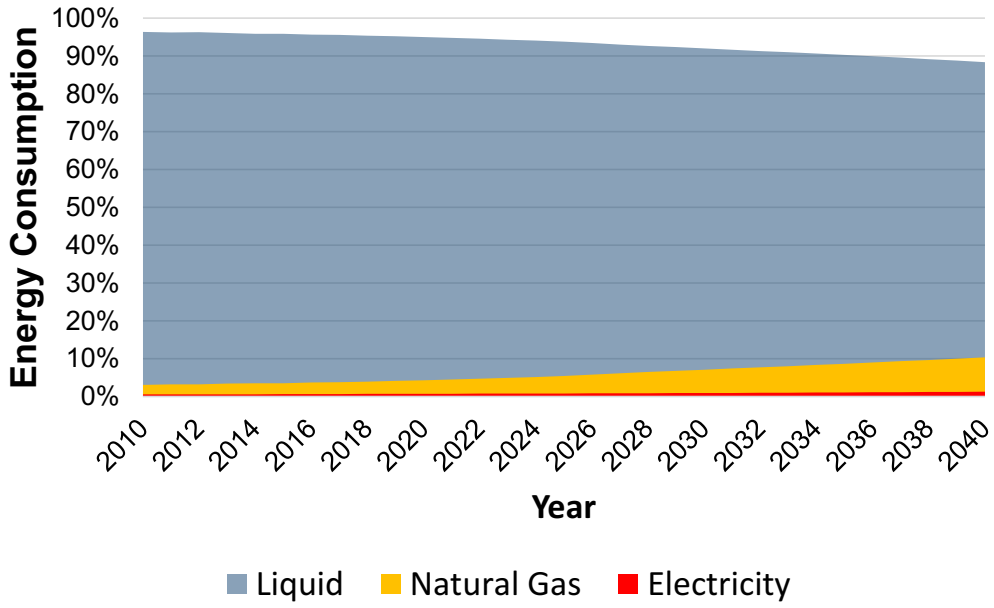

Figure 4. World transportation sector energy consumption by energy source. Data from[5,6]

Among liquid fuels, motor gasoline will remain the most widely used fuel in transportation, even though its share of total transportation energy consumption will probably decline from 2012 to 2040. From 2012 to 2040 the total transportation market share of diesel fuel (including biodiesel), which is the second-largest transportation fuel, will decline and the share of jet fuel will increase (Figure 5). Electricity will remain a minor fuel for the world's transportation energy use, although its importance in passenger rail transportation will remain high: in 2040, electricity will account for 40% of total passenger rail energy consumption. The electricity share of total light-duty vehicle energy consumption is forecast to increase to 3% in 2040 in the reference case, as increasing sales of new plug-in electric vehicles penetrate the total light-duty stock.

Gasoline fuel will remain the reference fuel for transportation, however, particularly for light duty passenger vehicles. This is an important factor to be considered when investigating future powertrain systems.

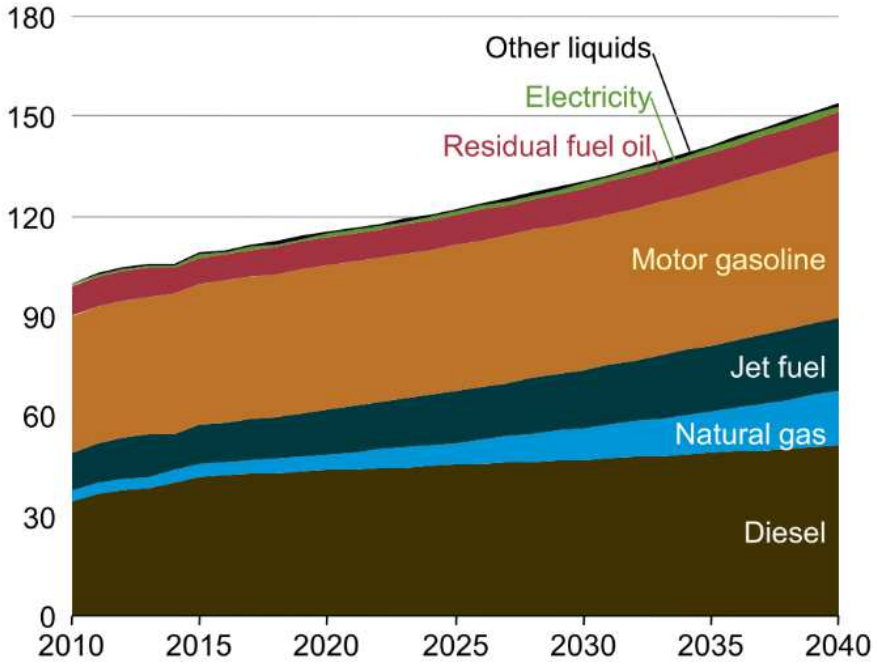

Figure 5. World transportation sector liquid fuel consumption by type. [5]

1.1.2. Reducing the impact of transportation on the environment

Over the past century the carbon dioxide concentration in the atmosphere has increased significantly. Compared to the pre-industrial era, this increase corresponds to approximately 280 ppm [7]. Because of the continually increasing energy consumption, the average concentration of CO_2 has increased by 2 ppm/year in the last ten years. Significant increases have also occurred in the levels of methane and nitrous oxide [7].

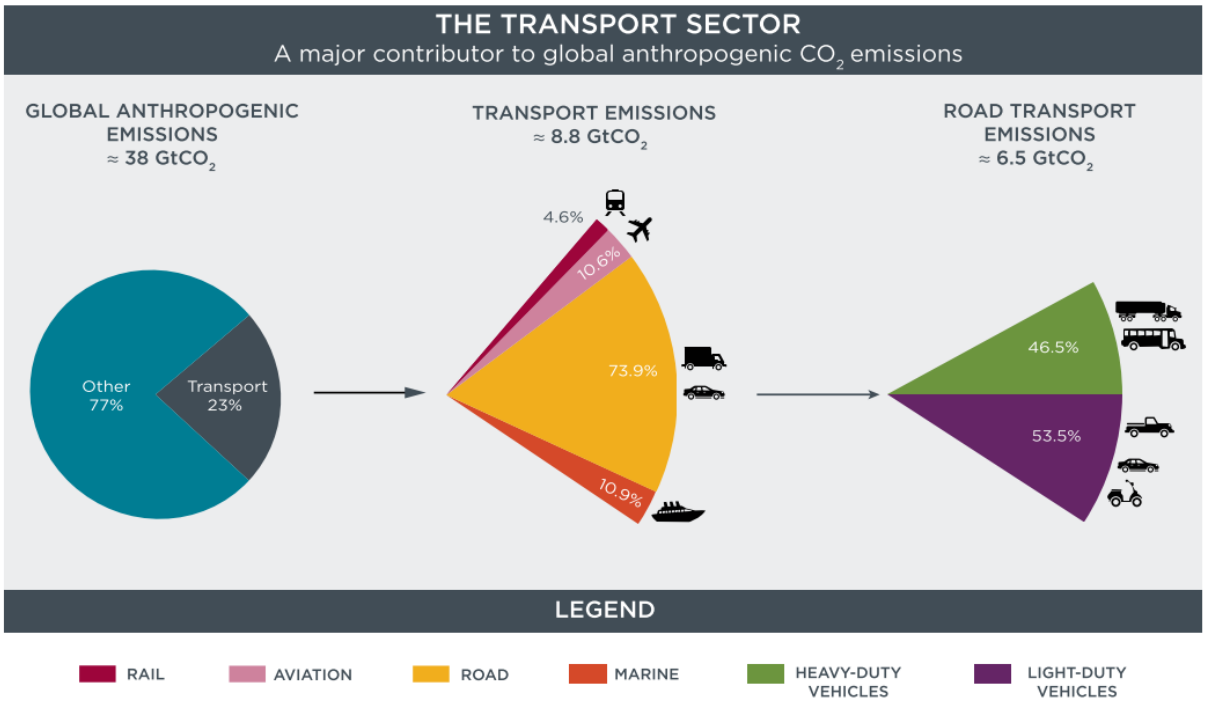

Figure 6. Distribution of CO_2 emissions in the transportation sector. [8]

The anthropic influence on the climate system is clear [9]. Among the many human activities that produce greenhouse gases, the use of energy represents by far the largest source of emissions. Within the energy sector, CO_2 resulting from the oxidation of carbon in fuels during combustion dominates total greenhouse gas (GHG) emissions, and the transport sector is, in order of importance, the third source of CO_2, two-thirds of which is produced by electricity and heat generation. In order to mitigate CO_2 emissions from the transportation sector, the European community introduced a series of norms, the European Emission Standards, which define the acceptable limits for exhaust emissions of new vehicles sold in the European Union (EU) and European Economic Area (EEA) member states. The emission standards are defined in a series of European Union directives staging the progressive introduction of increasingly stringent standards. For CO_2, a target of 95 grams per kilometer will apply from 2021, but this value will be dramatically reduced in the near future. The Euro norms also limit pollutant emissions of carbon monoxide (CO), unburned

hydrocarbon (HC), and particulate matter (PM). Consequently, despite the huge efforts already made in the last decade to provide the technology currently available on the market, the study of

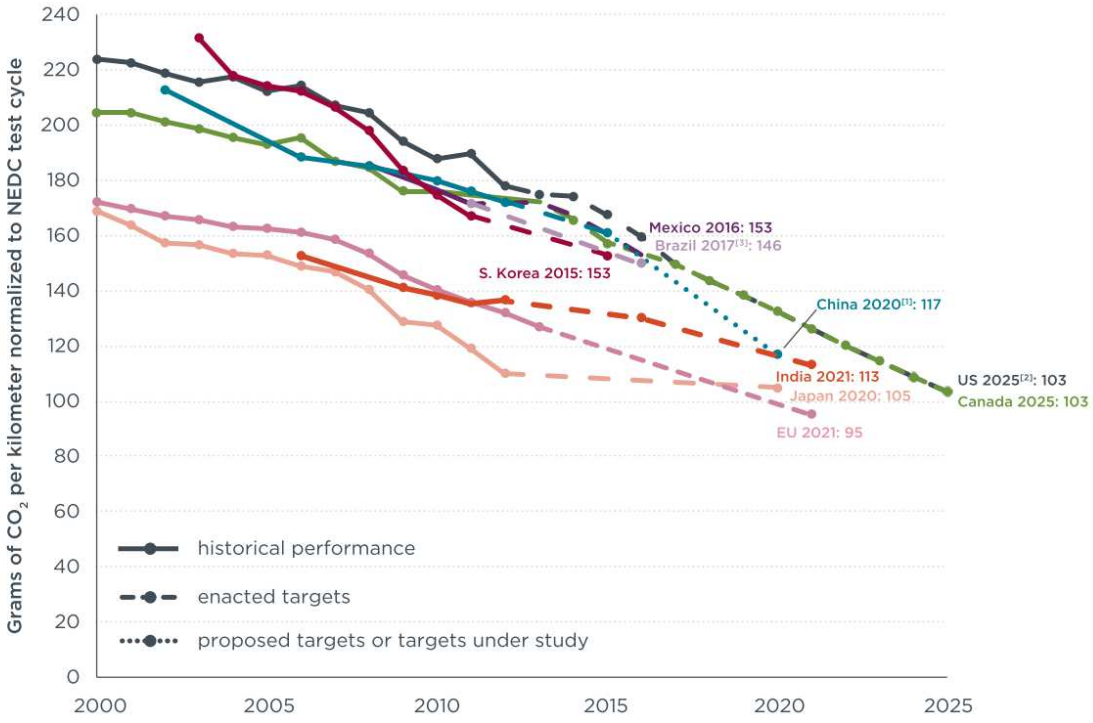

Figure 7. Global comparison of passenger car efficiency standards. [8]

more advanced, clean and efficient combustion strategies for internal combustion engines (ICE) still represents a major concern of the scientific community.

1.2. RESEARCH OBJECTIVE

In view of the environmental context, the transportation sector has to participate in the creation of sustainable development. A reduction of CO_2 and pollutant emissions is necessary to provide a clean living environment, so research must strive to provide efficient and clean vehicles.

Since its invention over a century ago, the internal combustion engine has been the main propulsion system for human and goods transportation. While the introduction of electrical and hybrid engines is undoubtedly an efficient means to reduce the environmental impact of transportation, a full conversion to an electric powertrain is more difficult. Several issues are related to the increase in electricity demand and battery system production, which can result in a negative environmental impact. Future transportation will be based on a mix of thermal and electrical powertrains. Internal combustion engines will still largely exist, as will the need to reduce the CO_2 and pollutant emissions caused by their use as a propulsion system. For these reasons, the development of clean and efficient vehicle propulsion has become a major objective.

Two types of internal combustion engines are currently employed: Gasoline Spark Ignition (SI) engines, and Diesel Compression Ignition (CI) engines. The key features of the SI engine are the lower cost of production and the relatively clean operation, at the expense of a relatively low efficiency. The diesel engine is the reference in terms of efficiency, but requires a more expensive aftertreatment system to avoid dispersion of the high level of pollutants formed during the combustion process. For these reasons advanced combustion engines combining high efficiency, low pollutants and reduced cost have been developed.

Gasoline Compression Ignition (GCI) engines are a promising engine concept aiming for efficient and clean operation. In GCI engines, high octane number gasoline is employed to fuel a high compression ratio CI engine. The combination of the CI mode and the gasoline fuel properties enables Low Temperature Combustion (LTC) characterized by ultra-low emissions of Nitrogen Oxides (NOx) and Soot. GCI provides very good performances but some challenges have to be overcome before it can be employed for practical applications. Specifically, the high octane number which yields several advantages at high load, in fact limits the ignitability of gasoline in low load operating conditions, making it difficult to achieve low load operations.

The aim of this research was to demonstrate the potential of using an ozone generator to extend the operating range of a GCI engine. Ozone is a strong oxidizing agent which has been shown to improve the oxidation chemistry of hydrocarbon fuels. Ozone can be produced from natural air by means of ozone generators, which could become a compact and low cost solution that is easily integrable and controllable in a passenger car. By placing an ozone generator in the intake manifold of the engine, ozone can be produced and

employed to seed the intake air and therefore promote gasoline autoignition under critical GCI low load operation. The aim of the present work was therefore to investigate the possibility of using ozone to extend the ignitability range of gasoline and to ascertain whether an ozone generator could be an efficient solution for achieving low load operation and extending the operating range of a GCI engine.

2. Introduction

2.1. INTERNAL COMBUSTION ENGINES

The internal combustion engine has been employed for passenger and goods transportation for more than a hundred years. It is a robust and affordable power generator with a high power to weight ratio, making it optimal for transportation applications. Nowadays, conventional gasoline spark ignition (SI) engines and diesel compression ignition (CI) engines dominate the transportation market.

2.1.1. SI Gasoline Engine

SI engines work under the principle of the Otto thermodynamic cycle with the heat introduction taking place at constant volume. In most SI engines a homogeneous fuel-air mixture is obtained by means of different fuel injections during the intake stroke or beginning of the compression stroke. The ignition of the intake charge is controlled by the timing of the electrical discharge across the spark plug gap. Efficient and clean combustion requires the mixture to have a stoichiometric fuel-air equivalence ratio. Load is then controlled by throttling the mass of air admitted, leading to pumping losses which affect the net indicated efficiency at part load. Increasing the thermal efficiency by means of a higher compression ratio is possible but knock related issues demand increasingly high fuel quality in terms of octane index. This is why SI engines generally cannot reach the efficiency of high compression ratio diesel engines. However, there is a range of low cost technologies that can reduce the losses traditionally encountered at both low and high engine loads: cylinder deactivation systems, cooled exhaust gas recirculation (EGR), hybridization and water injection systems. In SI engines, after the ignition induced by the electric discharge, a flame front propagates in the cylinder, increasing the local temperature and gas pressure. Nitrogen oxides (NO) are thus formed by the Zeldovich mechanism in the high temperature post flame gases. Carbon monoxide (CO) is formed due to the presence of rich regions caused by the inhomogeneity in the fuel-air mixture, while large amounts of unburned hydrocarbons (HC) are formed due to flame quenching on the combustion chamber wall and the crevices. The three-way catalytic converter allows for the simultaneous reduction of the above-mentioned pollutants, making SI engines a relatively clean powertrain with respect to CI diesel engines. Soot production is relatively low for conventional SI engines and particulate filters are not required. In the most recent SI engines working with stratified fuel-air mixtures, higher amounts of soot are produced, so a Gasoline Particulate Filter (GPF) is included in the exhaust gases aftertreatment system.

2.1.2. Compression Ignition Engine

In a diesel CI engine the intake air flow is compressed and highly reactive diesel fuel is injected into the cylinder only near the end of the compression stroke. After the injection, the fuel spray atomizes in small droplets, evaporates and mixes with air. Meanwhile, the piston continues to compress the mixture, and when the mixture temperature reaches the fuel's ignition temperature, ignition of a premixed quantity of fuel and

air occurs. If the injection event has not yet been completed, the remaining fuel that did not participate in premixed combustion is consumed in the rate-controlled combustion phase, creating a diffusion flame. Due to the absence of an actuator triggering the ignition event, the fuel has to have a high autoignition propensity in terms of Cetane number. Diesel CI engines are currently the most efficient powertrain for automotive transportation. Their lower fuel consumption is mainly due to the higher compression ratio employed and to the fact that the power output is controlled by merely adjusting the amount of fuel injected, avoiding the introduction of throttling losses at part load. CI diesel engines generally run on lean fuel, meaning that lower in cylinder temperatures are reached and a lower amount of heat is rejected to the coolant and toward the exhaust. As an additional benefit, the gamma, or specific heat ratio, is higher for lean burn engines than for engines that operate at stoichiometry. Less of the thermal energy generated by the combustion reactions is lost in the excitation states of larger triatomic species (CO_2 and H_2O vapor), resulting in more thermal energy available for raising the pressure and temperature of the working fluid, increasing the work that can be extracted. Because of the higher peak pressure and temperature, diesel CI engines demand a more expensive engine layout. The high rotational inertia limits the maximum speed and increases the cost of all the hardware that has to be very durable. A further drawback of CI engines is the pollutant emissions. Diffusion-controlled combustion is a significant source of soot and NOx due to the ignition of non-homogeneous mixtures. Because the engine is run in non-stoichiometric conditions, it cannot rely on the economic three-way catalytic converter, and a more complex, and hence expensive, aftertreatment system has to be included at the exhaust. A Diesel Oxidation Catalyst (DOC) for HC oxidation, a Diesel Particulate Filter (DPF) for soot, and a Selective Catalytic Reduction (SCR) system for NOx reduction by NH_3 have to be installed to clean up the exhaust gases.

2.2. ADVANCED INTERNAL COMBUSTION ENGINES WORKING ON LOW TEMPERATURE COMBUSTION

In recent years considerable research has been conducted to provide advanced combustion strategies with the aim of improving internal combustion engines. The characteristics of the two major engine families, CI and SI, can be summarized as follows. On the one hand, compression engines are the benchmark for high efficiency and low fuel consumption, albeit at the expense of a significant production of NOx and soot and a higher cost of production. On the other hand, gasoline SI engines are relatively low-polluting and cheaper, but with a limited efficacy due to throttled part load operation.

Advanced combustion strategies have emerged from the study and the development of existing engine technologies. The goal is to achieve the best tradeoff between efficiency, pollutant emissions and costs, maintaining the strengths of existing engines and overcoming their weaknesses. The ideal engine should be efficient like a CI engine, cos-effective like an SI engine, and the production of pollutants should be

eliminated at the source, allowing for a less complex aftertreatment system. This is possible only by developing advanced ICE relying on advanced combustion processes.

Two major approaches can be adopted to improve current combustion engines: increasing the thermal efficiency of SI engines, or reducing the pollutant emissions of already efficient CI engines.

Starting from an SI layout, the idea is to improve efficiency by increasing the CR while overcoming knock issues, for example by using water injection [10,11]. Another possible way is employ advanced spark ignition devices, i.e. microwave assisted [12], which make it possible to increase the thermal efficiency by running the SI engine with a leaner fuel-air mixture and reducing pump losses.

Starting from a CI engine layout, the main objective is to maintain the already good efficiency while reducing the production of NOx and soot that mainly affect diesel combustion. To achieve clean combustion in IC engines, a wide range of advanced combustion modes have been introduced. For the sake of clarity, in this work, all these strategies will be grouped together under the term Low Temperature Combustion (LTC) strategy.

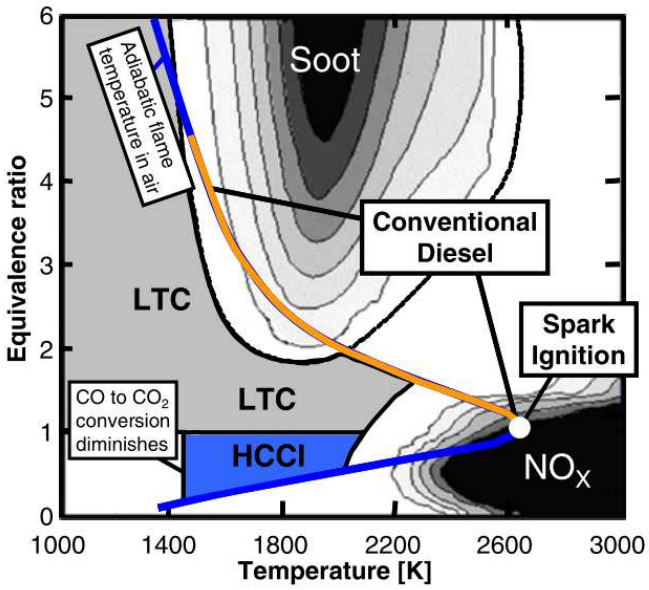

Figure 8. Diagram showing the equivalence ratio-temperature ranges for soot and NOx formation and the regions for conventional diesel, SI, HCCI, and LTC. From [13]

As shown in Figure 8, NOx and Soot are produced when combustion is characterized by certain in-cylinder conditions of temperature and equivalence ratio. The basic principle of LTC consists in preventing the formation of NOx and Soot by circumnavigating the regions on a T-ϕ plane which are responsible for the

production of these pollutants. Specifically, soot can be suppressed by burning lean mixtures ($\phi<2$) and NOx production is overcome by attaining low combustion temperatures (T<2200K) [13].

Homogeneous Charge Compression Ignition (HCCI) is an advanced combustion mode in which a well premixed, lean fuel/air mixture is compression-ignited. In this way, combustion originates from a lean mixture and low combustion temperatures are generated, as shown in Figure 8. HCCI can be ideally employed for the combustion of any kind of fuel. HCCI is an important concept here because it is the basic principle of all the LTC which will be described hereafter. Despite the different methodologies employed, all LTC strategies are fundamentally related to the HCCI combustion strategy. Several ways have been studied to achieve LTC combustion and simultaneously avoid soot and NOx formation, but this kind of clean combustion has then to be implemented on engines for widespread commercial application. A feasibility study of the implementation of LTC combustion for practical engine applications must take into account the constraints to which manufacturers, oil companies, and the final customers are subject. For these reasons, a realistic solution that can be applied in the short-medium term should be based on a currently available engine layout and should run on fuels available on the market, i.e. Diesel or Gasoline.

	Engine Layout	
Fuel	*Spark Ignition*	*Compression Ignition*
Gasoline	SACI, CAI	Gasoline HCCI, GCI, GPPC
Diesel	-	Diesel HCCI/LTC

Table 1. Advanced combustion modes for SI and CI engines.

Based on this consideration, it is possible to schematize the different strategies developed to implement LTC in real engines depending on the base engine architecture layout and the fuel employed. LTC mainly refers to CI combustion. However, by deactivating the spark ignition system, the CI mode can be achieved in SI engines. This is the case of Controlled Auto-Ignition (CAI) and Spark Assisted Compression Ignition (SACI) strategies, which aim to run SI engines in CI mode at least for a certain part of the load speed map (low and part load). In CI engines, LTC can be achieved by running the engine with conventional Diesel fuel, leading to the Diesel LTC strategy. Gasoline Compression Ignition (GCI) is an engine concept which relies on the use of gasoline fuel in CI diesel engines to achieve Low Temperature Combustion.

As already mentioned, there are several different ways in which the LTC strategy can be realized, and the characteristics and challenges of applying this combustion mode depend on the fuel and the engine layout employed. In the following sections, a short presentation of the main ways in which LTC are realized is reported. Because GCI engines are the main topic of the present research, they will be given particular attention.

2.2.1. HCCI

A homogeneous charge compression ignition (HCCI) engine uses a well-mixed fuel-air charge like spark-ignition engines and relies on compression ignition like diesel engines [14]. Similar to diesel engines, the use of high compression ratios and the removal of the throttling valve in HCCI allow for high efficiency operation, thereby resulting in lower CO_2 emissions per unit of work delivered by the engine. In HCCI engines, a homogeneous fuel-air mixture can be obtained by port fuel injection or early direct injections. Under the compression work of the piston, the highly diluted (air or EGR) fuel-air mixture ignites when the in-cylinder temperature and pressure reach the ignitability point of the fuel. It is clear that without the use of an actuator that directly triggers combustion, autoignition is driven by the chemical kinetics. The charge autoignites in several locations simultaneously. Depending on the chemistry of the fuel employed, autoignition spots are located in the regions in which the equivalence ratio and temperature conditions are the most favorable for the oxidation reactions to occur. There is no flame propagation and the combustion rate is fast. HCCI has several strengths. The most important one is that this combustion mode combines both high efficiency and ultra-low emissions of NOx and soot. Thermal efficiency is generally high because of unthrottled operation, the high compression ratio, and the high effective expansion ratio. Moreover, the formation of soot and NOx can be simultaneously suppressed by burning lean mixtures ($0.3<\phi<0.6$) and maintaining low peak combustion temperatures. Another additional feature of the HCCI strategy is that in this combustion mode the fuel ignition is governed by chemical kinetics. As a result, any kind of fuel can be burned in HCCI mode provided that the thermodynamic conditions necessary for autoignition are achieved. This can be done by modulating the intake conditions (pressure and temperature) in order to supply the necessary pressure-temperature path. However, there are some drawbacks related to HCCI combustion.

Firstly, HCCI can only be implemented over a narrow region of the load speed operating range at which a CI engine is required to operate for automotive applications. At high load, HCCI is difficult to achieve because premixed combustion leads to intense heat release responsible for a high pressure gradient which can cause excessive mechanical stress and noise. Low load operations are also difficult to achieve. This is mainly due to the fact that low power output corresponds to extremely lean mixtures, in which combustion is problematic because of the high energy required to initialize and because the in-cylinder temperatures are too weak to sustain the oxidation reactions. It should be mentioned that the low load limit is fuel dependent. Autoignition of high CN diesel fuel is less difficult to achieve, while low load with a high ON gasoline fuel or alcohol fuel is particularly challenging.

As the combustion process is driven by chemical kinetics, controlling the combustion phasing is challenging due to the lack of an actuator, such as a spark plug, that would provide direct control over the ignition event.

Combustion phasing therefore depends on the physical and chemical properties of the fuel-air mixture, as well as the history of the in-cylinder thermodynamic conditions. The combustion process can thus be indirectly controlled by various parameters such as intake temperature and pressure, equivalence ratio, EGR, composition of the IGR, and on-demand use of chemical additives.

Generally, high CO and HC emission results from incomplete oxidation of the fuel. High HC comes from fuel deposited on the cylinder liner and in crevices. CO emissions are also high because of the low temperature achieved during combustion and the subsequent lack of energy necessary to complete the CO to CO_2 conversion. Cold start is another challenging aspect to be addressed when considering HCCI combustion, since the lowering of the intake temperature can prevent the in-cylinder conditions necessary for autoignition from being reached, leading to misfire.

Due to its limitations, it is difficult to apply HCCI across the entire operating range of engines for practical automotive use. Therefore, the other advanced combustion modes based on LTC strategies can be seen as a way to apply the HCCI strategy over those portions of the load speed range of a conventional IC engine where the challenges are less difficult to overcome, using the actuators provided according to the specific engine layout. For example, the CAI strategy uses HCCI at low load in gasoline fueled SI engines by deactivating the spark plug. Although applying the HCCI strategy at low load may seem somewhat counterintuitive because of the above-mentioned low load limitations with high ON fuels, the CAI mode can rely on the Variable Valve Train (VVT) available in an SI engine to trap hot residual burnt gases in order to increase the intake charge temperature. Alternatively, other advanced combustion strategies have tried to introduce some variation in the ideal HCCI mode in order to extend its operating range. This is the case of GCI engines relying on the partially premixed combustion of gasoline. In this case, the mixture is not totally premixed but a certain degree of stratification is induced by a more complex multiple direct injection strategy which is commonly employed in diesel engines. This makes it easier to achieve heat release control and clean and efficient high load operations, but lower loads are more challenging because of the CI engine layout which does not always provide VVT and ignition can be difficult depending on the autoignition propensity of the fuel employed.

2.2.2. CAI-SACI: HCCI in SI engines

The application of the HCCI strategy to SI engines is generally denoted Controlled Auto Ignition CAI. In this kind of combustion, gasoline fuel is premixed with the intake charge by port fuel injection or early direct injections in the admission stroke. CAI is a potential solution to increase the thermal efficiency at engine part and low load [15]. Pumping losses are suppressed by operating the engine at wide throttle

openings, and the spark is deactivated to let the fuel autoignite by means of the compression work of the piston. To regulate the load, the mass of fuel is adjusted. Consequently, for a low power output demand, i.e. low load and idle, the fuel air mixture becomes extremely lean ($\phi<0.4$), and because of the relatively low compression ratio of SI engines, the in-cylinder thermodynamic conditions necessary for gasoline autoignition are not achieved. To overcome this issue, CAI makes use of VVT [16] systems that generally equip the SI engine to regulate the IGR trapped mass. In this way, the in-cylinder charge temperature can be increased by trapping hot burnt gases [17,18], favoring the spontaneous ignition of the high ON gasoline fuel. The amount of IGR can be controlled by regulating the intake and exhaust valve opening. Two main strategies are employed:

- Negative valve overlap NVO. Burnt gases are trapped in the cylinder by separating and shortening both the exhaust valve opening period at the exhaust stroke and the intake valve opening period during the intake stroke. This strategy introduces some gas-exchange efficiency losses related to the recompression of trapped gases.

- Rebreathing of exhaust gases is performed by a second opening of the exhaust valve during the compression stroke. In this way, the cylinder charge is filled with both the fresh air coming from the inlet duct and the burnt gases which have not yet evacuated the exhaust duct. The advantage over the NVO strategy is that it involves no recompression losses.

In CAI mode, the amount of trapped burnt residuals determines the reactivity of the intake charge, and the higher IGR rate increases the reactivity of the fuel-air mixture. Consequently, the IGR rate can be employed to achieve autoignition and control the combustion phasing. This is particularly necessary near TDC as the load decreases, due to the lower reactivity of leaner mixtures. At low load, when the mixture is highly diluted, the ignition can be further improved by re-activation of the spark plug. This strategy goes under the name of SACI, Spark assisted compression ignition. There are several variations of CAI and SACI. The CAI strategy can lead to high part load efficiency with low emissions of NOx compared to SI engine operation. There are, however, several challenges that have to be addressed to employ CAI combustion in practical applications. Operating in CAI mode over the entire load-speed range of an engine is extremely difficult. Low loads are difficult to achieve because of the high IGR rate required to achieve autoignition. High loads are difficult to achieve because of a high pressure rise rate. Nonetheless, CAI operation can be employed in a reduced portion of the load speed map of an SI engine. In this case, it is necessary to provide a switching strategy from CAI to SI mode and vice versa. Independently of the operating range width, controlling the combustion phasing always requires particular attention. A complex control strategy

simultaneously involving VVT, hot and cooled EGR, and direct fuel injection should be employed, especially when considering transient operations.

2.2.3. HCCI for CI Diesel Engines

Engine-out emission regulations concerning Diesel engines specify that CI diesel engines must be equipped with aftertreatment systems for NOx and diesel particulate matter. In order to reduce the complexity and the cost of exhaust gas posttreatment systems, diesel combustion has been extensively investigated. HCCI is considered as the major candidate capable of providing an in-cylinder approach to overcome the formation of pollutants at the source. In conventional Diesel combustion fuel readily ignites after being injected at the end of the compression stroke near TDC. The strategy to attain HCCI operation in CI engines is to advance the injection event and use a high EGR rate in order to give the fuel more time to mix with air, to form a mixture with a lower equivalence ratio and to generate a lower flame temperature. This could potentially enable the simultaneous attenuation of the mechanisms governing the production of NOx and soot. Initial approaches [19–21] employed diesel port fuel injection to create a homogeneous fuel/air mixture as in SI engines. However, several problems were encountered due to poor evaporation and mixing because of the low volatility of diesel fuel. Moreover, because of the high reactivity, diesel fuel tends to easily ignite when compressed and the compression ratio needed to be reduced in order to avoid knocking and combustion before TDC. To overcome the limitations of port fuel injection, HCCI can be implemented by using direct injection. However, the conventional diesel injection strategy has to be modified accordingly to meet HCCI requirements. In order to achieve a well-mixed charge the injection should be advanced earlier during the compression stroke [22–25] and to improve mixing, special nozzles designed to disperse and soften the spray [25–27] can be employed. A drawback of early fuel injections is fuel impingement on the cylinder wall, leading to very high HC emissions and to the deterioration of lubrication oil, especially with conventional wide umbrella angle diesel injectors. Special injectors with reduced umbrella angles [28] were then specially designed to direct the fuel toward the piston head bowl even at very early injection timing. Because of the high CN of diesel, early injection leads to early ignition. A high EGR rate has therefore to be employed regardless of the injection strategy to slow down the oxidation reactions, avoid knocking and prevent autoignition from taking place too early in the compression stroke [22,26,28,29]. Other techniques made use of a low compression ratio [30] or late intake valve closing to reduce the effective compression ratio while preserving a high expansion ratio [31,32]. Diesel HCCI research showed that the high reactivity and low volatility of diesel fuels make it difficult to achieve the desired mixing quality and the necessary ignition delay to achieve low temperature combustion. A branch of the research on HCCI strategies introduced the possibility of running diesel CI engines with less reactive and more volatile gasoline fuels.

2.2.4. Gasoline Compression Ignition engine

The need to meet the increasingly stringent regulations concerning diesel engines led researchers to find a way to reduce the pollutant emissions of diesel CI engines without affecting the high thermodynamic efficiency of this powertrain family. Because of the difficulties in applying the HCCI concept with diesel fuel, various research groups have demonstrated the interest of using of gasoline fuel in CI engines in order to achieve LTC combustion. As this doctoral research will focus on GCI engines, an entire section is dedicated to this topic and is presented below.

2.3. GASOLINE COMPRESSION IGNITION ENGINE

Gasoline compression ignition engines have the potential to realize LTC by combining a CI engine and gasoline fuel. As for conventional diesel engines, high thermal efficiency is achieved by using a high compression ratio and unthrottled operation over the entire operating range. The autoignition resistance and the high volatility of gasoline improves the fuel-air mixing process, enabling LTC and avoiding the local equivalence ratios (ϕ) and combustion temperatures responsible for NOx and soot production. Direct injection strategies make it possible to control the combustion process by controlling the degree of fuel stratification. Several studies have focused on Gasoline combustion in CI engines and different approaches have been employed, that converged on the development of GCI engines. In this section, the most important concepts underlying the GCI engine concept are reviewed and presented.

2.3.1. Partial fuel stratification

Partial fuel stratification is an important notion in understanding the combustion process in GCI engines. A major contribution to the comprehension of the impact of fuel stratification on gasoline compression ignition combustion can be found in the work of Dec [13,33–37] and it is well reviewed by Dempsey et al. [38]. Fuel stratification measures the degree of inhomogeneity present in the combustion chamber following the introduction of the fuel in the cylinder. The stratification level ranges in scale and its boundaries are defined by the conditions that can be found in traditional combustion systems. The minimum level of stratification is the premixed conditions that can be found in gasoline engines. Under these conditions, the charge is homogeneous and the local equivalence ratio values correspond to the global value that characterizes the mixture. The maximum level of stratification corresponds to the diffusion flame typical of conventional diesel combustion. In this case, combustion occurs when the injection event is not yet completed and the degree of heterogeneity is maximum. Regions where the equivalence ratio is extremely low (the periphery of the jet) coexist with regions where the equivalence ratios exceed the stoichiometric value by multiple times. The level of stratification is directly controlled by the injection strategy. Port fuel or early injection during the compression stroke gives low stratification while injection near TDC at the end of the

compression stroke gives higher fuel stratification. Partial fuel stratification can be obtained by intermediate injection timings during the final part of the compression stroke or by using more complex multiple injection strategies which split the total fuel mass, combining a first early premixed fuel portion with a further stratified injection close to the end of the combustion stroke. The importance of partial fuel stratification is that it is strongly linked to the combustion behavior. The main advantages of low fuel stratification are the low NOx and soot, but the downside is a limited combustion efficiency, controllability and noise. At the other extreme, high stratification is characterized by high combustion efficiency and controllability, at the expense of higher NOx and soot formation due to the higher temperature and equivalence ratio. An intermediate level of stratification presents behavior which lies in between the two extremes. So a potentially efficient and clean combustion can be achieved by precisely modulating the level of stratification. Another important aspect of fuel stratification is that it also contributes to determining the mixture reactivity. Dec et al. [33,34,37] showed that depending on the fuel chemistry, richer fuel pockets are more reactive than leaner regions. This is generally valid for double stage ignition fuels (such as n-heptane or naphtha) and it can be extended to single stage fuels under certain conditions, i.e. gasoline or gasoline-ethanol blends under boosted intake pressure conditions [36,39,40]. A direct consequence is that the different levels of fuel stratification can be employed differently depending on the operating range of the engine. At high load, stratification should be high enough to slow down the heat release rate but not too high in order to avoid NOx and soot, whereas low load operation requires higher stratification to improve fuel reactivity and combustion stability.

The importance of partial fuel stratification is that it can be governed through the injection strategy, which consequently becomes the actuator on which GCI engines rely to control the LTC process. Therefore, the injection strategy plays a fundamental role in GCI engines because it makes it possible to extend the application range of LTC over wider load speed ranges. This determines the potential of the GCI strategy to represent a strong candidate for practical, clean, and efficient engine applications.

2.3.2. Advantages of using gasoline in CI engines

Gasoline fuels are designed with a high antiknock quality and are characterized by a high octane number (ON). This makes gasoline extremely resistant to compression ignition. As demonstrated by studies on the CAI mode, without a spark plug, gasoline is difficult to ignite in engines with a CR in the range of 9-11 and the intake charge temperature has to be increased by using large amounts of IGR. However, if gasoline fuel is injected in a conventional diesel CI engine with a CR in the order of 14-20, the in-cylinder temperature and pressure near TDC can reach values which meet the conditions required for gasoline autoignition. The interesting feature of gasoline is that, compared to Diesel, it has a much larger ignition delay for any given

set of operating conditions [41]. The characteristic diesel diffusion flames are avoided and instead, auto-ignition occurs after completion of the injection event [42–47]. In addition, because of the high volatility and low boiling point [48], gasoline readily evaporates in the range of in-cylinder temperatures which characterize the compression stroke of a conventional CI engine. This dramatically improves the propensity of gasoline to mix with the in-cylinder air, making it possible to reduce the local strength of the fuel air mixture, which is characterized by a lower local ER value. The ease with which gasoline evaporates and mixes, together with the tendency to generate longer ignition delays, ensure that at the moment of ignition, the local equivalence ratio values are well below the limits for soot formation. Moreover, because the mixture is diluted, the peak temperatures achieved during combustion are low, avoiding NOx formation. This makes gasoline fuel an intrinsically good candidate to implement LTC strategies in CI engines and achieve efficient and clean combustion [45].

2.3.3. Gasoline Partially Premixed Combustion

Gasoline PPC is a combustion strategy employed in a large region of the operating map of a GCI engine. This concept is directly linked to PFS and to the chemical and physical properties of gasoline fuel. Injecting gasoline in a CI engine can lead to premixed combustion as in an HCCI engine. In order to overcome the issues related to the excessive heat release rate generated by premixed combustion, GCI engines are based on a Partially Premixed Combustion PPC strategy. To achieve PPC, fuel direct injection is employed to create a fuel-air mixture which is homogeneous enough to avoid soot and NOx, but at the same time sufficiently stratified to prevent autoignition occurring simultaneously in the whole volume as in typical HCCI combustion [33]. Because of the fuel and temperature stratification [33,34] induced by a specific direct injection strategy, different degrees of reactivity characterize the mixture inside the combustion chamber. Combustion therefore originates from the most reactive regions, and then sequentially extends to the rest of the volume, leading to a progressive consumption of the fuel and staged heat generation. Thanks to this staged combustion process, the heat release is significantly smoothed, as are the noise and mechanical stress [37]. The high load limitations typical of the HCCI mode can be overcome: excessive pressure gradients are avoided. If the injection strategy is employed properly, the presence of richer and highly reactive fuel pockets will be enough to trigger autoignition but not excessively so, so that the production of NOx and soot will be lower if compared to conventional diesel engines. PPC also enables a second relevant issue, which particularly affects HCCI operations, to be overcome, namely control of the combustion phasing. In PPC, the combustion process is not exclusively controlled by chemical kinetics as in HCCI. Instead, the equivalence ratio and temperature stratification caused by direct injection induced

inhomogeneities mainly drive the fuel ignition. The timing of combustion can be therefore controlled by managing the injection strategy as is commonly done in diesel engines.

2.3.4. Efficient and clean part and high load operation

The effectiveness of gasoline partially premixed combustion has been demonstrated in several studies focusing on achieving high load operation while maintaining low levels of NOx, soot and noise. Efficient and clean combustion at part and high load can be achieved in GCI by combining different injection strategies, EGR levels, and intake boosting. Kalghatgi was the first to focus on applying the concept of gasoline partially premixed combustion at high load [41,49]. In [49], the authors used a gasoline with 94.7 RON and 85.9 MON to fuel a 2.0 L single cylinder diesel engine with a compression ratio of 14 at an engine speed of 1200 rpm. Because the ignition delay was longer for gasoline compared to diesel, much higher IMEP were attained with gasoline for a given intake pressure and EGR level while maintaining lower NOx and smoke emissions. The highest IMEP reached with gasoline was 14.86 bar with a soot level of 0.36 FSN and an ISNOx level of 1.21 g/kWh. In [41], a double injection strategy consisting in a pilot injection at the beginning of the compression stroke and the main injection close to TDC further increased the IMEP and simultaneously reduced the pollutant emissions. A maximum IMEP of 15.95 bar was achieved, with an FSN < 0.07, ISNOx of 0.58 g/kWh, ISFC of 179 g/kWh, ISHC of 2.9 g/kWh and ISCO of 6.8 g/kWh. In the same operating conditions, to get such a low level of smoke with Swedish MK1 diesel fuel, the IMEP had to be below 6.5 bar. At Lund, Manente et al. [50–52] also carried out a detailed investigation of the PPC of gasoline, and results clearly highlighted the potential of the gasoline compression ignition engine to achieve high efficiency with low NOx and soot emissions. In a heavy duty engine, a high boost level combined with ~50% of EGR yielded a gross indicated efficiency of 53% with a maximum IMEP of 25 bar. It should be noted that an estimated brake efficiency close to 50% was maintained constant in the 16 to 25 bar IMEP range, while the level of pollutants was most of the time below the limits laid down by the US 10 and EU VI legislations. In [53], Dec et al. from Sandia investigated the use of fuel stratification to extend the high load of a gasoline fueled CI engine. In a single cylinder 0.98L engine, using a combination of premixed and direct injected fuel supply, the engine was run at 14 bar IMEP with an indicated thermal efficiency of ~44.7%. Sellnau and coworkers from Delphi developed a light duty Gasoline Direct Injection Compression Ignition (GDCI) engine [54–62]. In [55], the Delphi GDCI engine was tested under different load speed conditions, and results indicated that very low NOx and particulate matter productions were achieved at all operating conditions including 3500rpm - 16 bar IMEP and 2500rpm -18 bar IMEP. These results indicate the potential of the gasoline compression ignition engine to reduce the complexity of the aftertreatment systems that equip conventional diesel CI engines.

2.3.5. GCI Low Load Limitations

Although GCI has shown a potential for efficient and clean operation at high load, achieving low load can be challenging due to the high octane number of commercial gasoline. A high resistance to autoignition offers several advantages at high load, but when the power output demand decreases, the injected fuel mass is reduced, and the intake charge mixture becomes increasingly leaner and less reactive. In [63], the authors assessed the difficulty of achieving stable low load conditions when 87 AKI gasoline autoignites in a light duty CI engine. The influence of several parameters, such as uncooled Exhaust Gas Recirculation (EGR), injection timing, injection pressure and nozzle geometry was analyzed, emphasizing the need to concentrate a sufficiently stratified fuel-air mixture in the piston bowl. Without enhancing the intake temperature or pressure conditions, autoignition of commercial gasoline is challenging and characterized by excessive emission of HC and CO, and low combustion efficiency [42,45,46]. The in-cylinder pressure and temperature reached during the compression stroke are not enough to meet the autoignition requirement of the high ON fuel and misfire occurs. In order to achieve the autoignition of lean gasoline mixtures, the intake temperature or pressure needs to be increased. However, at low load the enthalpy content of the exhaust gases would not be enough to supply the energy necessary to the turbocharging system to boost the intake pressure. Increasing the intake temperature by intake air heaters is not a suitable solution because the system will be too slow to enable accurate control of the intake conditions. Research focusing on the low load operation of GCI engines has proposed two main solutions. The first effective solution consists in equipping the CI engine architecture with a VVT system allowing for flexible control of the valve timing to trap hot residual gases and increase the in-cylinder temperature. The second approach concerns the type of fuel used. Replacing high ON gasoline with more reactive naphtha fuel characterized by an intermediate ON and high volatility can reduce the fuel thermodynamic demand necessary for autoignition, making it possible to achieve GCI operation over the entire load speed range.

2.3.5.1. VVT for rebreathing of Hot Burnt gases

As shown by the work of Sellnau at Delphi [55,59,60,62] and by Borgqvist et al. in Lund [64–66], increasing the intake charge temperature is possible by trapping hot burnt gases, thus improving the reactivity of the mixture and therefore achieving gasoline ignition. Using VVT in [55] demonstrated to be a key enabler of RON 91 gasoline autoignition. The study reported that at low load conditions of 1500 rpm-2 bar IMEP, a secondary-exhaust-valve-lift event was employed to rebreathe hot exhaust gas and promote autoignition. A specially designed cam was used to maximize the effective compression ratio. An ISFC of about 230 g/kWh was obtained. The exhaust port temperatures were about 250°C. In [60], the performance of a gen II Delphi GDCI was presented. Concerning low load operations, an improved VVT, continuously-variable mechanical valve train system, and injection system design enabled 2.4 bar at 2000 rpm with an ISFC of

206g/KWh and an indicated efficiency of 44.2% to be achieved. At idle conditions (800 rpm – 2bar IMEP) the engine showed an indicated efficiency of 36.6 % and ISFC of 249.8 g/KWh. Although the use of an advanced engine architecture enriched with VVT demonstrated the potential for efficient operation also at low load, the increased cost of the engine and the additional complexity of the control strategy may discourage the implementation of such a solution for practical automotive applications.

2.3.5.2. Use of Low Octane Gasoline (Naphtha)

The second research approach suggested the use of low octane gasoline fuel, in the range of naphtha fuel in CI engines. The key limitation for GCI low load operations is related to the ON of gasoline available on the market. Ideally, the optimal fuel for CI engines should be resistant enough to autoignition to achieve LTC at high load, but reactive enough to be ignited at low load when the mixture is leaner and less reactive. In this context, in [45], the authors suggested that the octane number of the ideal fuel for PPC should be in the range of 70-85 RON, while the boiling range should be similar to that of commercial gasoline. According to several studies [42,45,46,48,67] naphtha fuel, which has a volatility in the range of gasoline but a lower resistance to autoignition, matches the reactivity demand of CI engines, enabling clean and efficient high load operations and stable operations down to idle and low load. In [68] the author compared Diesel and naphtha fuel in the same CI engine. Naphtha was shown to improve the particulate/NOx trade-off in the drive cycle relevant conditions with a significant reduction in CO_2 emission. Moreover, reductions in CO and HC could also be possible. Other positive properties leading to a tendency to promote the use of naphtha as a key fuel for the future are the higher energy density compared to gasoline, and the lower refining costs. The use of an intermediate octane number fuel such as naphtha has therefore several advantages in the context of GCI engines. However, for short-term application, the use of such a fuel is not possible because it will take time to adapt the fuel distribution system.

2.4. CHEMICAL AGENTS FOR COMBUSTION IMPROVEMENT

As concluded in the previous section, the main limitation which affects GCI low load operation could be overcome by achieving the compression ignition of a lean fuel air mixture. Chemically promoting the autoignition propensity of lean gasoline-air mixtures can be a possible way to achieve low load operations in GCI engines without using complex VVT to increase the intake temperature or without relying on fuel which is still not available in the market. Because of its strong oxidizing properties, ozone can strongly promote combustion. Moreover, the on-board production of ozone is possible by means of a compact and cheap ozone generator. The chemistry of ozone-interaction along with more details about the ozone generator are therefore presented in this section. Nitrogen oxides (NOx) are another chemical compound that can promote combustion. Because of the use of EGR or IGR, nitrogen oxides, such as NO and NO_2, can be present inside the combustion chamber of a GCI engine and consequently react with gasoline fuel. An additional interest in studying the chemistry of nitrogen oxides is related to the fact that such chemical compounds, as will be showed later in this chapter, can react with ozone. Therefore, a review of the formation mechanisms along with the chemistry of the interaction with hydrocarbon is included in this section.

2.5. OZONE AS A COMBUSTION IMPROVER

2.5.1. Ozone – hydrocarbon interaction

Ozone is an inorganic molecule with the chemical formula O_3. Ozone is an allotrope of oxygen that is much less stable than the diatomic allotrope O_2.

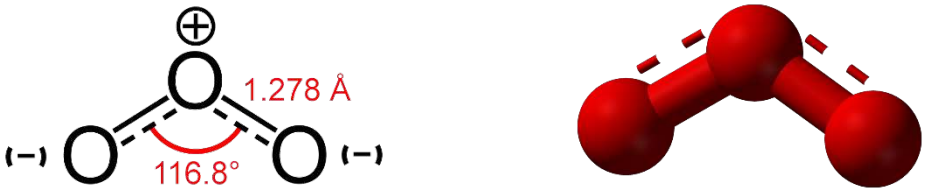

(a) (b)

Figure 9. Skeletal formula of ozone (a). Ball and stick model of the Ozone molecule (b).

Ozone is a powerful oxidant (far more so than dioxygen) and has many industrial and consumer applications related to oxidation, such as water treatment, manufacture of pharmaceuticals, the ozonation of oleic acid and others. In recent years, because of its strong oxidizing features, ozone has been investigated for combustion-related applications.

2.5.1.1. Ozone impact on the oxidation chemistry of small chain hydrocarbons

Because of its strong oxidizing properties, ozone has been shown to improve the combustion of hydrocarbons. The impact of ozone on the chemistry of hydrocarbon oxidation was fundamentally investigated in flame-related studies [69–84] for small hydrocarbons with C1 – C4 carbon chains. Small hydrocarbon chains and relatively simple systems such as a laminar flame burner offer the optimal environment for studying the impact of ozone on oxidation chemistry. In [81], results from experiments showed that the addition of high ozone concentration can enhance the flame propagation speed of CH_4 and C_3H_8 air mixtures. By way of example, Figure 10 shows the flame speed enhancement induced by different ozone concentrations for CH_4 flames, for different equivalence ratios. The reasons behind the effect of ozone should be sought in the chemical kinetics. The effect of this agent is due to its ability to alter the hydrocarbon oxidation path, opening the way for reactions that would not occur in conventional oxygen-driven combustion.

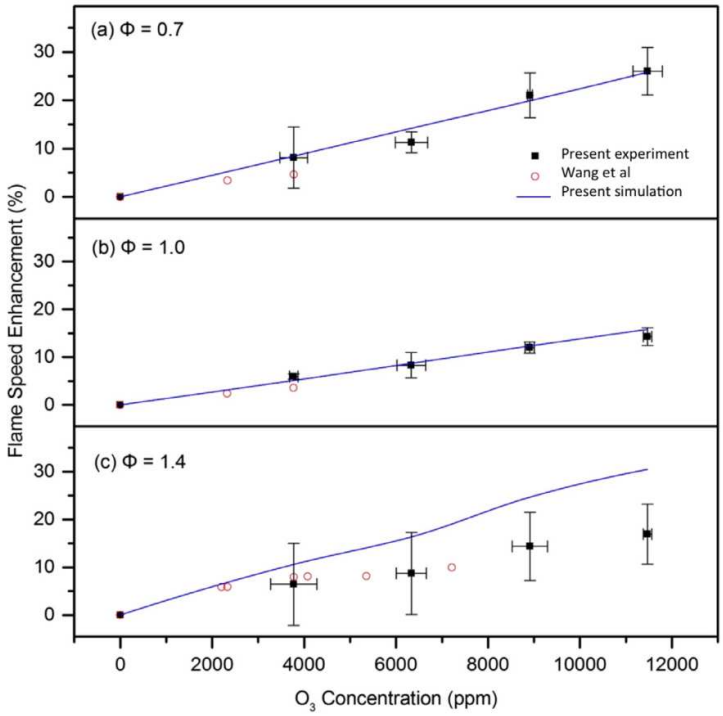

Figure 10. Promoting effect of ozone on the laminar flame speed of CH_4.
P = 1 bar and T= 300 K. Adapted from [81]

There are two combined effects related to the presence of ozone that lead to an improvement in the oxidation process. The first is due to a direct interaction between the O_3 molecules and other species present in the

reactive mixture. More specifically, in [73], the authors suggested that the reason for the burning velocity enhancement with ozone addition is the acceleration of chain-branching reactions due to the presence of O_3 molecules in the gas mixture. The presence of the O_3 molecules in the pre-flame zone results in a much faster growth of intermediate species such as HO_2, H_2O_2, and CH_2O due to the reactions:

$$O_3 + H \leftrightarrow O + HO_2 \quad (1)$$

$$O_3 + OH \leftrightarrow O_2 + HO_2 \quad (2)$$

$$O_3 + H_2O \leftrightarrow O_2 + H_2O \quad (3)$$

$$O + CH_3 \leftrightarrow H + CH_2O \quad (4)$$

Then, subsequent chain-branching reactions through CH_3, CH_2O, HCO, etc. can accelerate the whole flame propagation process. Results also showed that ozone induced an increase in the concentrations of H, O and OH radicals in the flame front and in the post-flame region. It should be noted that the presence of O_3 also leads to a temperature increase in the pre-heat region. However, the burning velocity enhancement was shown to be dominated by the radical related chain-branching reactions rather than by the thermal effect [70,71].

The direct interaction of O_3 molecules is not the only mechanism that governs the impact of this chemical agent on the oxidation process. As highlighted by Foucher et al. in [85] and by Halter et al. in [72], ozone increases the reactivity of the system mostly because it is a carrier of highly reactive O atoms coming from the decomposition of unstable O_3 molecules. For CH_4 flames, this effect was described in detail in [72], in

which results from chemical simulations showed that without ozone the main source of O atoms were the reactions:

$$O_2 + H \leftrightarrow O + HO \quad (5)$$

$$O_2 + HO_2 \leftrightarrow O + H_2O \quad (6)$$

while when ozone was added, the combustion was enhanced because of the extra O atoms generated by the reactions

$$O_3 + N_2 \leftrightarrow O_2 + O + N_2 \quad (7)$$

$$O_3 + O_2 \leftrightarrow 2O_2 + O \quad (8)$$

$$H + HO_2 \leftrightarrow O + H_2O \quad (9)$$

The production of O radicals through O_3 molecules is responsible for the whole chain-branching mechanism. Then, the diffusion of O atoms acts as an initiator of the promoting effect on the oxidation process. In fact, when ozone is added, the extra O atoms are consumed by CH_3 and CH_4 and the whole chain-branching combustion process is accelerated because of the proliferation of O, H and OH radicals. In [72], results from chemical simulations showed that when ozone was added to the CH_4 air mixture, the production of OH and H radicals increased by a factor of 5, while the production of CH_3O increased by a factor of 4. The increase in the production of radicals is the main reason for the improvement in the ignition process. The impact of ozone addition on the ignition of hydrocarbon-air mixture is higher for lean fuel-air equivalence ratio, while it reduces as the equivalence ratio gets closer to stoichiometric values. It should be noted that high ozone concentration are needed to accelerate the laminar flame speed, demonstrating that the stronger impact of the O_3 molecules addition concerns the ignition process more than the flame propagation.

2.5.1.2.Effect of ozone on the combustion characteristics

Adding ozone was shown to introduce a new pathway in the oxidation mechanism. This alteration in the combustion chemistry leads to consequences in the combustion behavior such as the formation of extra OH and formaldehyde which can be experimentally observed. In [76], the effect of ozone was investigated on premixed methane air flames. Planar Laser Induced Fluorescence of CH_2O was performed in order to understand the mechanism behind the impact of ozone on the oxidation of methane. As can be seen in Figure

11, a considerable increase in formaldehyde production was observed when ozone was added to a CH_4-air mixture. This effect was observed for different temperatures and equivalence ratios.

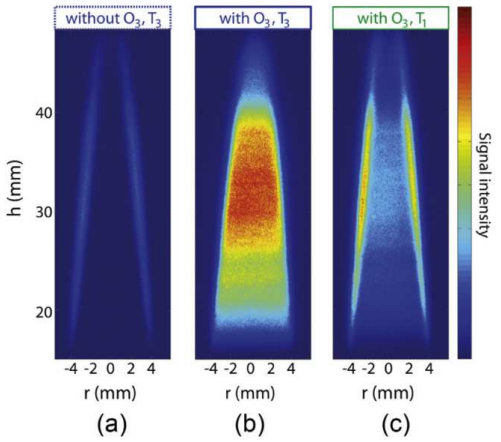

Figure 11. CH_2O production enhancement induced by ozone. From [76]

Oxidation chemistry easily reveals the mechanism behind the enhancement of formaldehyde production. Once ozone seeds the fuel-air mixture, the oxygen atoms coming from the decomposition of O_3 molecules react with the CH_4 molecules, producing OH radicals which rapidly react with methane. Methane is then transformed to formaldehyde via the reaction sequence $CH_4 \rightarrow CH_3 - CH_3O \rightarrow CH_2O$. Throughout this reaction path several OH radicals are produced, further increasing the overall reactivity of the system.

2.5.2. Ozone impact on IC engine combustion

The first ozone application for IC engines was proposed by Tachibana et al. in 1991 [86]. In their study, the authors investigated the effect of ozone on the combustion in a Diesel CI engine. An experiment performed in a Diesel Cooperative Fuel Research CFR engine showed that the effect of adding ozone was the same as that of increasing the CN of the fuel. The results showed that depending on the initial conditions chosen,

500 ppm of ozone corresponded to an increase in CN from 2 to 4, clearly demonstrating the promoting effect of ozone on the fuel reactivity.

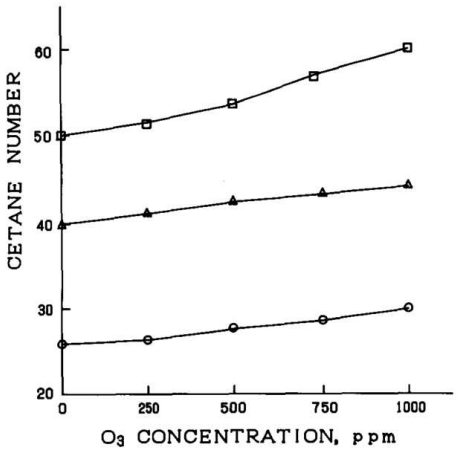

Figure 12. Correlation between ozone and CN of the fuel for different initial conditions. From [86]

Most of the following studies regarding ozone applications for IC engines concerned innovative advanced combustion modes. In particular, ozone applications were investigated as a possible solution to overcome the practical limitations that impeded this potentially clean and efficient advanced combustion strategy from being employed in IC engines for large scale commercial applications.

The use of ozone was investigated as a potential means to overcome the lack of control in combustion phasing which particularly affects HCCI and PCCI engines. Ozone has the ability to promote ignition and advance the combustion phasing, thus making it possible to control the combustion phasing. Aceves et al. [87] and Foucher et al. [85] showed that ozone is an effective chemical agent able to advance the premixed combustion of hydrocarbon fuels in HCCI engines because of its capacity to release O atoms once the intake air flow has been seeded. Other studies investigated the possibility of using ozone to control combustion phasing with different fuels and engine configurations. Ozone applications for a stationary natural gas fueled engine were investigated in [88,89]. In [88], ozone was employed to improve the reactivity of methane in a heavy duty single cylinder stationary CI engine. Results showed that some ppm of ozone strongly promoted methane autoignition, typically under low equivalence ratios. In, [89] the promoting effect of ozone was applied to the generation of OH radicals coming from H_2O_2 decomposition. Moreover, the authors compared ozone with other chemical agents, demonstrating that seeding O_3 molecules had a similar effect of directly injecting O radicals and an impact of an order of magnitude greater than directly adding OH radicals to the intake flow. With the final purpose of controlling the combustion phasing in light duty HCCI engines, the effect of ozone was extensively investigated at the University of Orleans [85,90–95] for a variety of

conditions and for different fuels. The use of an on-board ozone generator positioned at the intake of the engine was proposed by Foucher et al. in [85] as a potential cost-saving solution to improve the combustion of n-heptane and to overcome the control issues affecting HCCI engines. The potential of an ozone generator for the cycle-to-cycle control of combustion was investigated, and results showed that by switching the power supply of the ozone generator, the consequent change from 0 to 49 ppm ozone concentration in the intake air flow induced a variation of the combustion phasing of 7 CAD in one engine cycle, as can be observed in Figure 13.

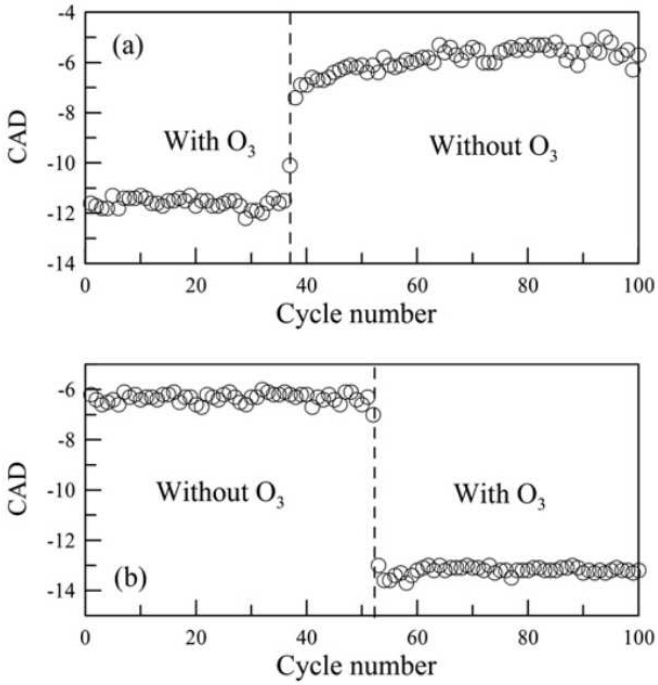

Figure 13. Variation of the phasing of the main flame induced by switching on and off the ozone generator. (a) Direct case off – on. (b) Reverse case off-on. From [85]

The study concerning the potential of ozone to control the combustion timing in HCCI conditions was then extended to other fuels such as Alcohol [93], Natural Gas [92] and PRF blends [91]. Moreover, a large range of engine operating conditions including nitrogen dilution [94] and Exhaust Gas Recirculation (EGR) dilution [96] were investigated. In [91], the impact of ozone on the combustion of different PRF blends was studied. Results showed that single stage fuels are the most sensitive to the impact of ozone, with iso-octane combustion phasing showing the highest sensitivity to ozone. For PRF blends exhibiting a two-stage heat

release, the ozone impact is split between the cool and the main flame. In such fuels, the advance in the cool flame was less pronounced than the advance of the main flame phasing.

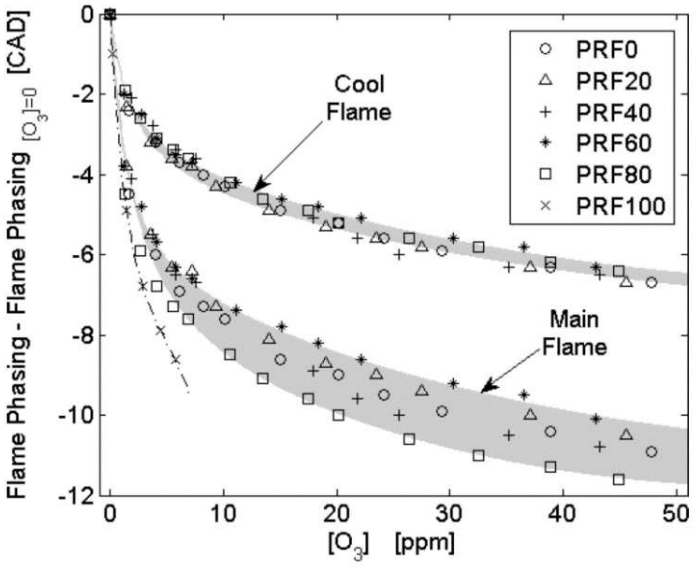

Figure 14. Variation of the main and cool flame phasing as a function of the intake ozone concentrations and for different PRF blends. From [91].

In [96], the promoting effect of ozone was investigated while nitrogen and other chemical species contained in the EGR were employed to dilute the intake fuel-air mixture. The products of Complete Combustion (N_2, H_2O, CO_2) were shown to reduce the impact of ozone mainly because of a thermal effect that slowed down ozone decomposition into O atoms. In [94] ozone interaction with nitrogen oxides (NO, NO_2) was investigated showing that when NO and O_3 simultaneously seeded the intake of the engine, the impact of ozone diminished because of an interaction between the two molecules, depending on the reaction:

$$NO \quad + O_3 \leftrightarrow NO_2 + O_2 \qquad (10)$$

2.5.3. Ozone generator

Ozone can be generated by means of an ozone generator. Different commercial ozone generators were employed in this study but the working principle is common to all the devices employed. Ozone is produced by an ozonizer working on the principle of a dielectric barrier discharge, which produces ozone between two electrodes separated by a dielectric material and powered by a high voltage signal. A scheme of the generator is presented in Figure 15.

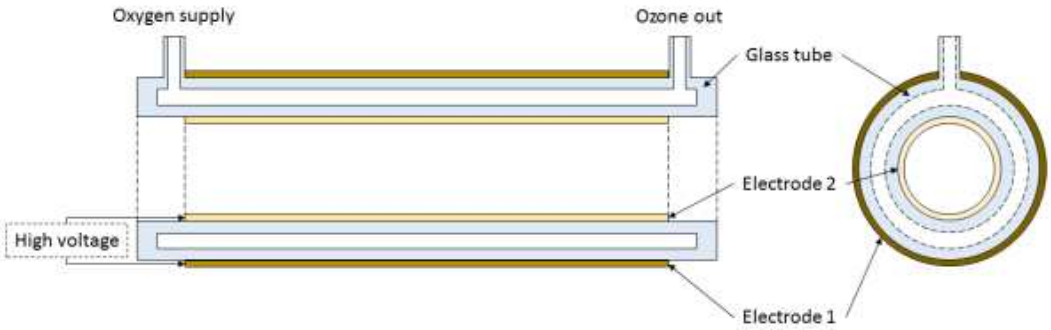

Figure 15. Schematic representation of an ozone generator working on the principle of a dielectric barrier discharge

As shown in the scheme, two electrodes surround the glass: one inside the cylinder and the other one outside. The electrodes are powered by high voltages (~ 10 kV) which produce pulsed discharges inside the cylindrical volume supplied with the working air. Ozone is produced from the oxygen molecules which break down inside the cylinder under the effect of the high voltage discharge and then recombine, forming O_3 molecules. The amount of ozone can therefore be controlled by varying the pulse frequency of the ozonizer. The other way to control the ozone produced is to manage the flow crossing the cylindrical volume. The ozone generator previously described produces ozone based on a capacity given as a percentage but the device does not indicate the quantity of ozone that is produced. An ozone analyzer is therefore used to measure the concentrations which seed the intake of the engine. The device used to monitor the ozone concentration was an Ozomat MP (Anseros GmbH). The determination of the ozone concentration is based on the absorption of UV radiation by ozone. Commercial ozone generators, whose size is not compatible with the integration in light-duty engines, were employed in the present study. However, in a recent patent [97], an engine prototype includes in its layout an ozone generator, demonstrating that small ozonizers integrable on real passenger cars are feasible.

2.6. NITROGEN OXIDES

Small concentrations of highly reactive chemical species such as nitric oxide (NO) have a very important impact on the onset of combustion. In engine conditions, a fraction of the nitric compounds produced during combustion can be retained in the combustion chamber as residual burnt gases or as a component of EGR. NO_x are consequently present in the cylinder before injection of the fuel takes place and can actively interact in the oxidation chemistry impacting the autoignition process, generally leading to an increase in the global reactivity and advancing the combustion phasing. In this section a brief review of the mechanism governing the formation of nitric compounds is firstly given. Then, a description of the chemical mechanism governing the sensitization of hydrocarbon oxidation is presented.

2.6.1. Nitrogen Oxide formation in IC engines

2.6.1.1. Kinetics of NO formation

Nitrogen monoxide (NO) and nitrogen dioxide (NO_2), usually grouped together as NO_x, are produced inside the cylinder during the combustion process. Of the two species, NO is the predominant nitric compound produced inside the combustion chamber of the engine. Because of the high temperatures generated by the combustion event, oxidation of atmospheric nitrogen occurs in the hot burnt gases [98], and NO forms according to the Zeldovich mechanism which can be summarized by the following reactions:

$$O + N_2 \leftrightarrow NO + N \quad (11)$$

$$N + O_2 \leftrightarrow NO + O \quad (12)$$

$$N + OH \leftrightarrow NO + H \quad (13)$$

In SI engines, NO generally forms in the region behind the expanding flame front generated by the spark ignited homogeneous fuel-air mixture [99]. In a direct injection CI engine, a locally non-uniform distribution of temperature and equivalence ratio is induced by the spray injection. In these conditions, NO is mainly formed in the high-temperature burnt gases in the periphery of the spray during both the premixed and mixing-controlled diffusion flame, with the NO formation rates being highest in the close-to-stoichiometric regions. Analysis of the reaction kinetics shows that the rate of NO production is dependent on the temperature and the oxygen concentration in the post flame gases. High temperature and high O concentrations result in high NO formation rates. NO can also form from the nitric compounds contained in the fuels (amines and ring compounds such as pyridine, quinolone and carbazoles). These compounds are thermally unstable and decompose under the effect of increasing temperature before entering the

combustion zone. Nitrogen-containing compounds such as NH_3, HCN, and CN are thus formed [100], and act as precursors of NO formation. Several reactions involving the above-mentioned compounds and other molecules such as O_2, OH, H, and H_2O take place in the cylinder, leading to NO_x. The NO_x formation reactions involving the previously mentioned compounds are available in the literature [101,102] and are included in the NOx submechanisms which can merge with the chemical set describing the oxidation of the fuel.

2.6.1.2.Kinetics of NO_2 formation

Although chemical equilibrium considerations indicate that at typical burnt gas temperatures, NO_2 should be negligible, experiments have shown that nitric dioxide may represent up to 30% of the NOx emissions in Diesel CI engines [103]. A possible explanation for this is that NO_2 is generated from the conversion of the NO previously produced by the Zeldovich mechanism. NO_2 forms according to reactions such as

$$NO + HO_2 \leftrightarrow NO_2 + OH \quad (14)$$

Then, it subsequently reconverts to NO via

$$NO_2 + O \quad \leftrightarrow NO + O_2 \quad (15)$$

or by quenching of NO_2 with cooler fluid.

2.6.2. Nitrogen Oxide interaction with hydrocarbon oxidation.

2.6.2.1. Residual Nitrogen Oxides

Nitric compounds are not only a passive product of the combustion, but also actively participate in the fuel oxidation process. In fact, after combustion, the exhaust flow drives the NOx-containing burnt gases toward the exhaust pipe, but depending on the aerodynamics of the combustion chamber, the burnt gases remain trapped the cylinder as residuals. Nitric compounds consequently seed the intake charge before injection of the fuel and can actively contribute to the oxidation of the fuel. Moreover, Diesel CI engines make an extensive use of EGR, with exhaust gases employed to reduce the oxygen content or to increase the intake charge temperature. IGR can also carry NOx into the combustion chamber of Gasoline fueled spark ignition SI engines. Advanced IC engine concepts such as gasoline compression ignition GCI engines also make great use of EGR or VVT to trap hot burnt gases in the cylinder, causing NOx species to coexist with gasoline fuel in CI conditions. Consequently, nitric compounds interact with fuel oxidation in several kinds of IC under a variety of thermo-chemical conditions. Understanding the impact of NO and NO_2 on the oxidation of hydrocarbon fuels is therefore of primary importance for understanding the in-cylinder process in advanced combustion engines.

2.6.2.2. Chemistry of Nitrogen oxides–hydrocarbon interaction

Several studies [102,104–108] have focused on understanding the impact of NO and NO_2 on the oxidation of hydrocarbon. In most cases, the effect of NO_x on fuel oxidation kinetics has been experimentally studied in jet stirred reactors (JSR) with the aim of developing chemical sets to be employed for chemical kinetic computations. NO-hydrocarbon fuel interaction is here discussed since NO is the largest fraction of the NO_x produced during combustion and the one most likely to be present in the combustion chamber of IC engines. Among the hydrocarbons, iso-octane and n-heptane are considered as major compounds of gasoline fuel.

Adding NO in a fuel-air mixture generally improves the global reactivity of the system. Previous studies demonstrated that NO could strongly affect the oxidation kinetics of hydrocarbons through the NO-promoted production of OH radicals. The main reaction affecting the autoignition of the fuel is also called NO to NO_2 conversion:

$$NO + HO_2 \leftrightarrow OH + NO_2 \quad (16)$$

$$NO_2 + H \leftrightarrow NO + OH \quad (17)$$

which globally corresponds to a catalyzed production of OH involving the consumption of H and HO_2:

$$H \quad + HO_2 \leftrightarrow 2O \qquad (18)$$

However, the NO impact on hydrocarbon oxidation is more complex and depends on several factors including the temperature and the fuel considered. Figure 16 shows the fuel concentration measured in a JSR as a function of the temperature and for different NO concentrations, for iso-octane and n-heptane as fuel. In the case of iso-octane, adding NO increases fuel consumption during the oxidation process regardless of the initial mixture temperature. A similar impact of NO was observed with n-heptane as a fuel, except at low temperatures, when adding NO resulted in a reduction of the rate of fuel consumption, indicating a reduction in the reactivity of the system. Reactions (15)(16)(17) are not enough to describe the effect of NO on a multicomponent fuel such as gasoline, especially in complex conditions such as those of IC engines where the temperature and equivalence ratio vary greatly, changing the relative importance of the chemical reactions that compete in the oxidation process. In [106], a more complex model of n-heptane oxidation sensitized by NO was proposed and is summarized here.

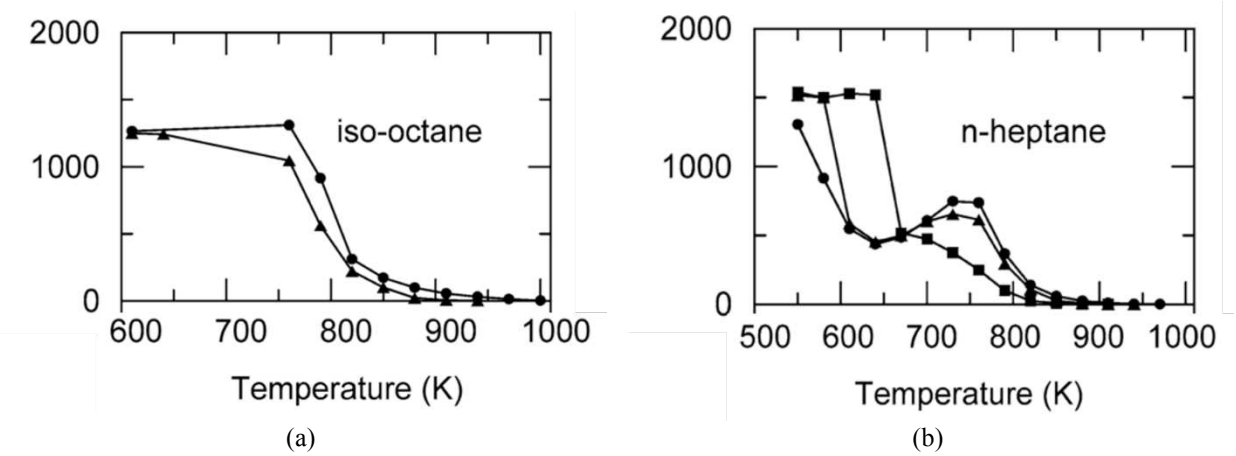

Figure 16. Impact of NO addition on iso-octane (a) and n-heptane (b) oxidation, adapted from [105]. Figures show the Species concentration profiles during the stoichiometric oxidation of n-heptane in a jet-stirred reactor at 10 atm with a residence time of 1 s in the presence of various amounts of NO: 0 ppmv (circles), 50 ppmv (triangles), 500 ppmv (squares).

Figure 17 (a) shows the commonly accepted scheme for the oxidation of an alkane at low temperatures (665 K) in the absence of NOx. The main reaction channel is the formation of alkyl (R•) radicals from the initial reactant followed by an addition of oxygen molecules and an isomerization of the obtained peroxy radicals (ROO•) to give hydroperoxyalkyl (•QOOH) radicals. These radicals can decompose into stable species, such as cyclic ethers or ketones, involving the expulsion of •OH radicals. They can also react by the addition with another oxygen molecule producing hydroperoxyalkylperoxy (•OOQOOH) radicals. The isomerization and decomposition of •OOQOOH radicals lead to the formation of hydroperoxide molecules. The

decomposition of these hydroperoxide molecules involves a multiplication of the radical production, which in a chain reaction induces an exponential acceleration of the reaction rate. At temperatures around 750 to 800 K, the reversibility of the addition of alkyl (R•) radicals to oxygen molecules becomes more pronounced. The oxidation of these radicals leading to the formation of alkenes and the very unreactive •OOH radicals is then favored. This reduces the overall reactivity and is the main reason for the appearance of the NTC regime.

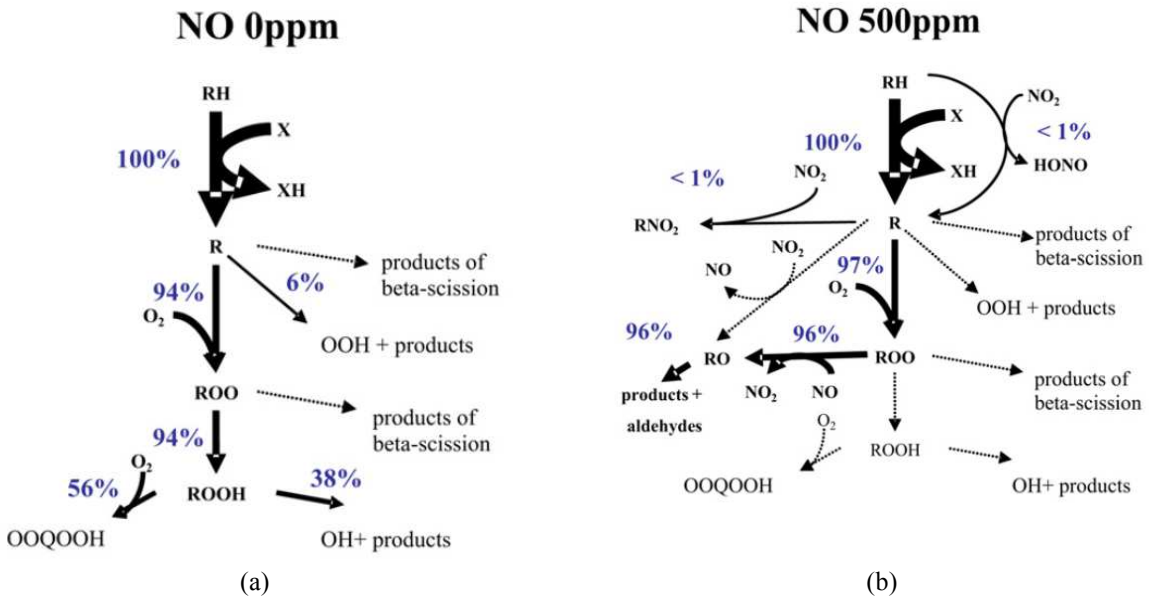

Figure 17. Flow analysis for the stoichiometric oxidation of 1500 ppm of n-heptane in a PSR at a pressure of 10 atm and a temperature of 665 K with addition of (a) 0 ppm of NO and (b) 500 ppm of NO. Adapted from [106].

Figure 17 (b) shows the oxidation schemes in presence of NO. The reaction of peroxy radicals with NO gives alkoxy (RO•) radicals and NO_2:

$$\mathrm{ROO}\bullet + NO \leftrightarrow \mathrm{RO}\bullet + NO_2 \quad (19)$$

The resulting RO• radicals decompose, yielding aldehydes and smaller alkyl radicals

$$\mathrm{RO}\bullet \rightarrow \text{aldehyde} + R' \quad (20)$$

This reaction channel competes with the second addition of oxygen molecules that occurs in the neat oxidation process. Reactions (19) and (20) can reduce the rate of formation of hydroperoxide species, causing a disadvantage to the branching steps which are normally induced by the decomposition of •OOQOOH. This reaction channel actually slows down fuel oxidation, particularly at lower temperatures

(T < 750K). Consequently, at low temperature, it can be said that adding NO actually reduces the reactivity of the system. Under engine conditions, however, the boundary conditions offer higher temperatures at which NO has a promoting effect on combustion. The promoting effect is mainly due to the reactions of NO with smaller hydrocarbon molecules, such as:

$$\bullet CH_3 + NO_2 \leftrightarrow CH_3O \bullet + NO \quad (21)$$

$$\bullet NO + \bullet OOH \leftrightarrow \bullet OH + NO_3 \quad (22)$$

$$CH_3OO \bullet + NO \leftrightarrow CH_3O \bullet + NO_2 \quad (23)$$

$$NO_2 + \bullet OOH \leftrightarrow HONO + O_2 \quad (24)$$

Sensitivity analyses further show that the reactions of NOx with small C1—C2 species are of great importance whatever the temperature range. Reactions (21)(22)(23)(24) have a promoting or inhibiting impact on reactivity depending on the temperature range, and their combined effects determine the overall reactivity. Reaction (21) produces reactive CH3O• radicals from •CH3 radicals, while reaction (22) transforms the unreactive •OOH into the very reactive •OH radicals, thus increasing the overall reactivity. Reaction (23) has promoting impact at temperatures over 900 K, while it inhibits the reactivity at lower temperatures. Reaction (24) is a termination step competing with reaction (22). Reactions (25) and (26) also concur in the determination of the overall reactivity.

$$\bullet NO + \bullet OH \leftrightarrow HONO \quad (25)$$

$$C_2H_5 \bullet + NO_2 \leftrightarrow C_2H_5O \bullet + NO \quad (26)$$

Reaction (25) is responsible for a high consumption of the OH radical and the following inhibition of the oxidation process for temperatures below 650K. However, higher temperatures induce the decomposition of HONO and the dissociation of the products exceeds the consumption of the reactant, reversing the direction of reaction (25) and promoting overall reactivity. By contrast, reaction (26) has a promoting impact at lower temperatures while it inhibits fuel oxidation when the temperature exceeds 800 K.

2.7. CONCLUSIONS, GOALS, STRATEGIES AND CRITICAL ASPECTS

This first chapter has provided an overview of the fundamental principles that form the scientific background of this thesis. A short introduction to compression ignition and spark ignition engines was first presented, followed by a summary of the operating principles, the advantages and the technical aspects which could be improved for a more sustainable environmental impact. It was then shown how advanced combustion strategies represent a fundamental concept on which the internal combustion engines of the future will be based. It was highlighted that future engines should be characterized by the combined strengths of both conventional SI and CI engines. LTC combustion strategies have been identified as the key factor for enabling the development of efficient and clean internal combustion engines. The HCCI strategy, with its own advantages and drawbacks was presented as the main LTC mode which inspired the development of the other LTC strategies which are currently being studied and developed by the scientific community. The focus of this thesis is the study of the GCI engine. GCI has the potential for achieving clean and efficient combustion by combining the high CR of CI engines and the chemical and physical properties of gasoline fuel. The main notions underlying the operating principle of GCI engines were provided. Special attention was paid to the advantages of using gasoline in CI engines, the notion of fuel stratification and that of partially premixed combustion, which when combined make it possible to explain why high loads are easier to achieve in a GCI engine than in an HCCI engine while maintaining low rates of pollutant formation. Finally, the difficulties which still make the use of GCI engines challenging for widespread commercial applications were analyzed, highlighting that the main need is to improve the fuel-air mixture reactivity at low load. A literature review was introduced showing that ozone has strong oxidizing properties. The effect of ozone on the laminar flame speed of small hydrocarbon chains and the recent application to control the combustion phasing in HCCI engines were reviewed. The impact of ozone is complex and still not well understood. The engine conditions such as local temperature and fuel-air mixture composition have been shown to play an important role in the impact of ozone on fuel oxidation. Moreover, it has been shown that commercial ozone generators constitute an actuator with a low level of control complexity, and that cheap, compact ozone generators for real passenger car applications can be produced. Lastly, a review of the chemical mechanism driving NOx formation and its interaction with hydrocarbon fuel was given because of its relevance in GCI combustion.

2.7.1. Aim of the work

The aim of this work is to evaluate the potential of ozone to enable low load GCI operation. Considering the use of commercial gasoline, and given the layout of a standard diesel CI engine, the purpose of this work is to investigate how the oxidizing features of ozone can be employed to provide the reactivity improvement necessary to achieve compression ignition of lean gasoline/air mixtures. Ozone has been chosen because of

its strong oxidizing features and for the potential of ozone generators to be easily included in a CI engine architecture with a low economic impact and a low increase in the complexity of the engine control strategy. Because the behavior of ozone and its impact on combustion are still not completely understood, and because the GCI in-cylinder process is a complex combination of varying thermodynamic and chemical conditions, a precise strategy was followed to carry out the study presented here.

2.7.2. Critical issues, strategy, and structure of the work.

The challenges facing a practical application of GCI engines can be overcome if the reactivity of lean gasoline-air compression ignited mixtures is improved.

Ozone impacts the fuel oxidation chemistry. The local conditions characterizing the environment in which ozone operates, such as temperature, equivalence ratio, and the presence of other chemical species may strongly alter the effect that ozone has on combustion. Because the GCI engine relies on a complex injection strategy which can cause the local in-cylinder conditions to vary frequently during typical engine operations, for example with the aim of controlling the combustion phasing, it has to be understood how the main engine parameters and the in-cylinder conditions can impact the effect of ozone on combustion.

The first step consisted in characterizing low load GCI combustion in the absence of ozone. The GCI low load study involved experiments, CFD, and chemical simulations. Commercial gasoline was employed as a fuel and experiments were performed in a commercial CI converted for single cylinder operation. In order to achieve low load combustion, intake air heating had to be employed to enable gasoline autoignition and investigation of the impact of the injection strategy on gasoline combustion. The results of this first part of the work are detailed in Chapter 4.

The impact of ozone on gasoline combustion was also investigated. Several factors concur in determining whether ozone can be used in GCI engines at low load. Therefore, the main idea was to proceed by increasing level of complexity.

Because the effect of ozone on gasoline has never been investigated, the first step consisted in characterizing the impact of ozone on gasoline combustion under engine relevant conditions. A study of the impact of ozone on premixed, kinetically-driven HCCI combustion was performed. This was intended to limit as far as possible the number of parameters which could interfere with the ozone effect, such as the number and the timing of fuel injections or the in-cylinder fuel and temperature stratification induced by fuel spray injection. The results of this first part of the work are given in Chapter 5 and Chapter 6. Chapter 5 includes

results from experiments performed in a metallic engine, while Chapter 6 analyzes the results from experiments performed in an optically accessible HCCI engine.

The GCI engine uses direct fuel injection to control the combustion process. In a second stage, the impact of ozone was therefore investigated under direct injection operation. The purpose was to understand whether the method employed to supply the fuel would interfere with the impact of ozone on gasoline combustion. The results of this first part of the work are presented in Chapter 7.

In Chapter 8, the conclusions of this research are drawn.

3. Methodology

3.1. METALLIC ENGINE

The metallic engine test bench consisted of a commercial Peugeot DW10-series CI Diesel engine converted for single cylinder operation. The schematic of the engine setup and all the devices employed to control the engine and the intake boundary conditions are represented in Figure 18.

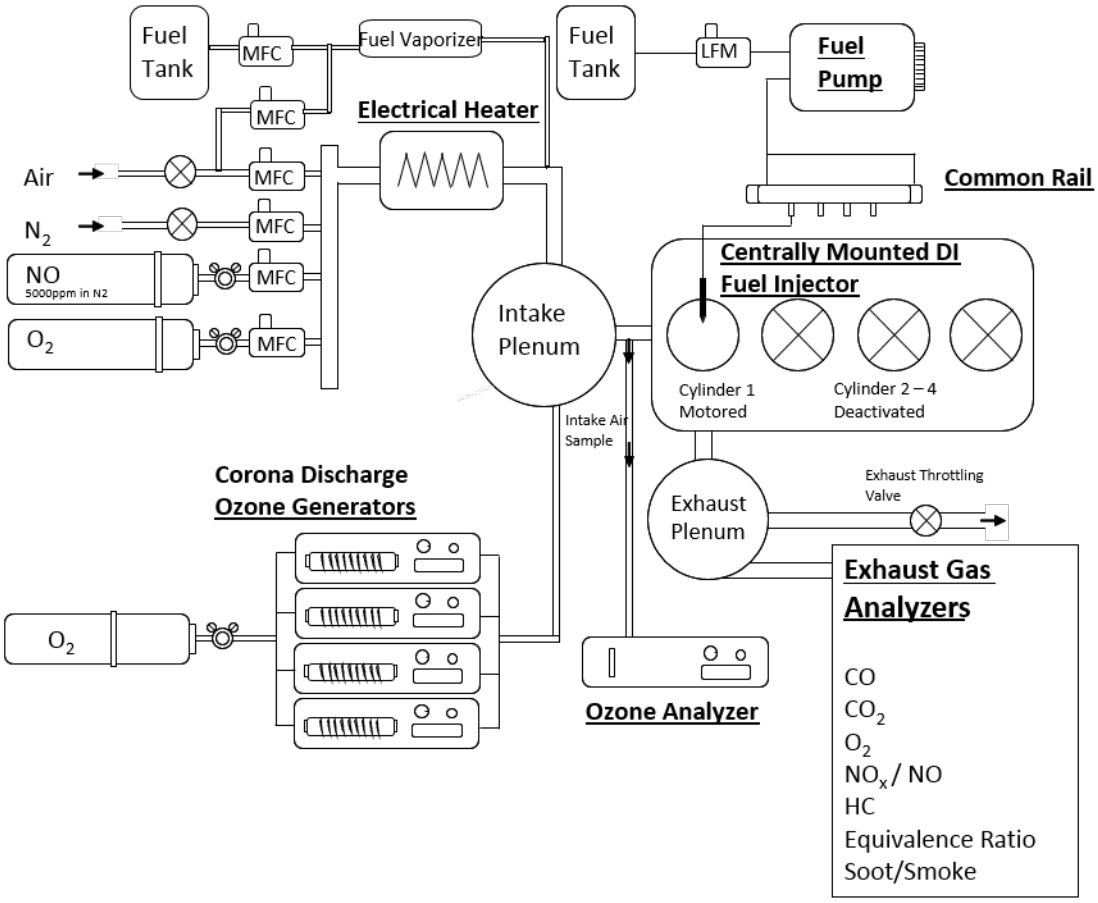

Figure 18. Schematic representation of the GCI metallic engine test bench.

The engine displacement and the other geometrical characteristics of the engine can be found in Table 1. The displaced volume of the engine is 0.5 L/cylinder and the piston geometry gives a compression ratio (CR) of 16. The swirl ratio of the engine was 1.1.

PSA DW-10	
Displaced Volume	499 mm^3
Bore	85 mm
Stroke	88 mm
Rod length	145 mm
Compression Ratio	16:1

Table 2. PSA DW-10 engine geometry

The test bench was developed to offer a flexible environment allowing for operating the engine under different combustion strategies. The engine can be operated in fully premixed HCCI mode thanks to the presence of an intake plenum positioned upstream the intake manifold. In HCCI mode, the fuel is evaporated by means of an electrical heater whose temperature can be controlled and adapted to the fuel employed. After being evaporated, the fuel is driven into the intake plenum where it mixes with a mixture of gases which compose the fresh intake charge. In normal operation the fresh intake charge is composed of dry air, but the intake system can be easily controlled to supply various other gases (N2, CO_2, CO, O2, CH4, NH3, NO, NO_2) or liquids (H20, H2). The flexibility of the intake gas control system makes it possible for example to easily simulate EGR by means of the products of complete combustion, or by simple nitrogen. Moreover, as in several experiments conducted in this research, the intake system is used to supply the desired concentration of chemical agents such as NO, or to supply the ozone generator with the desired working fluid (air or O2). The intake thermodynamic conditions can be controlled by independently setting the temperature and the pressure. Temperature control is performed thanks to a series of electrical heaters positioned upstream the intake plenum and the feedback of two thermocouples positioned in the intake manifold, 9 cm before the intake valve. Moreover, the intake plenum is covered by electrical heaters in order to reduce the power supply of the heating system and to increase the precision of the intake temperature control. The intake pressure can be quickly regulated by changing the output pressure of the compressor used to supply the intake air.

3.1.1. Direct Injection Fuel Supply for GCI operation

The engine is also supplied with a direct injection system, which makes it possible to use the engine bench for GCI direct injection operations. The injection system is composed of a Bosch diesel common rail system and a Delphi high pressure pump, a combination that enables the desired injection pressure to be set. The fuel supply circuit includes a liquid mass flow meter for direct measurement of the injected mass during the experiments. The fuel is directly injected into the cylinder by direct injection injectors. Different injectors were used in the experiments. All the injectors are solenoid actuated and have 8 holes and a nozzle diameter of 150µm but they have different umbrella angles, respectively 156°, 120° and 90°.

3.1.2. Combustion chamber

No modifications were made to the original piston head. The combustion chamber geometry is an axisymmetric, reentrant bowl with a central pip: the outer diameter of the bowl is 55 mm and the maximum bowl depth is 13 mm.

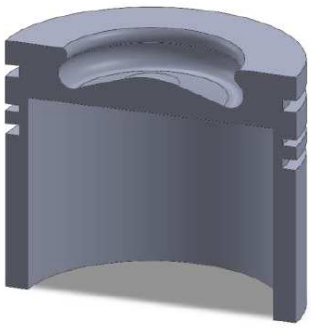

Figure 19. Vertical section of the piston in the DW-10 engine

3.1.3. Exhaust emission measurements

Exhaust concentrations of NO, NO_2, HC, CO, CH_4, CO_2 were measured with a Horiba 7100 gas analyzer. An AVL 415S Smoke meter was employed to measure the Filter Smoke Number FSN.

3.1.4. Accuracy of the acquisition system

Pollutant emissions at the exhaust were measured with a Horiba 7100 gas analyzer. The engine intake pressure was measured with a Kistler 4075A piezo-resistive absolute pressure sensor which presents an accuracy of ± 0.3% of the full scale. Intake temperature was measured with two K thermocouples, one in each pipe, with an accuracy of ± 2K. Lastly, the in-cylinder pressure was recorded with a Kistler 6043A piezo-electric pressure sensor with an accuracy of ± 2% and positioned by using an optical encoder allowing a measure every 0.1 CAD. For all the experiments performed in this study, data were recorded for 100 cycles and combustion characteristics were determined following a thermodynamic analysis.

3.2. OPTICALLY ACCESSIBLE ENGINE

In this work optical diagnostic techniques were employed to determine the impact of ozone on gasoline combustion. An optically accessible engine was used for this purpose. The single-cylinder optically accessible engine has the same PSA DW-10 base as the metallic engine described in the previous chapter. To enable direct visualization of the in-cylinder process, the engine base was modified by equipping the original piston with an extension which provides substantial optical access to the combustion chamber.

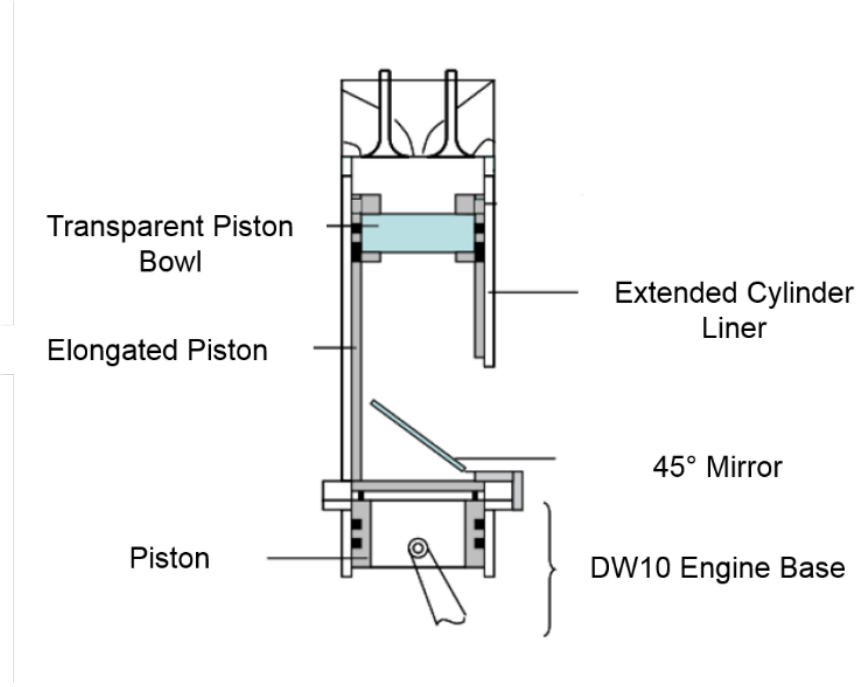

Figure 20. Schematic representation of the optically accessible engine.

A transparent piston made of fused silica is mounted on top of the elongated original piston in order to enable optical access from below and from the side. A 45° aluminum coated mirror is fixed to the engine block, below the piston, in order to redirect the light from the combustion chamber toward the optical access. Then the luminous signal can be collected by a camera or by photomultipliers positioned in front of the engine. To enable frontal visualization of the combustion chamber or to make the latter accessible to the laser sheet, a transparent quartz ring was added at the top of the cylinder liner. Operating conditions were controlled in the same way as in the metallic engine. Moreover, the same combination of several gaseous

and liquid mass flow controllers makes it possible to precisely control the in-cylinder charge composition and to use the engine under fully premixed operation.

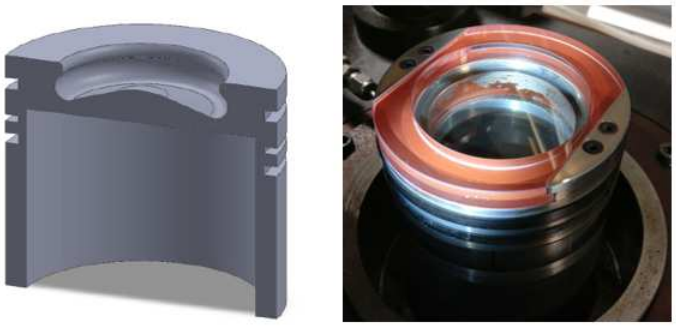

Figure 21. Section of the metallic piston (a) and image of the optical piston with transparent bowl and side (b).

3.2.1. OH* chemiluminescence

Direct visualization of OH* chemiluminescence, the emission spectra of which are shown in Figure 23, was performed to gain insight into the effect of ozone on combustion. The acquisition system comprised an intensified CCD camera and a set of filters.

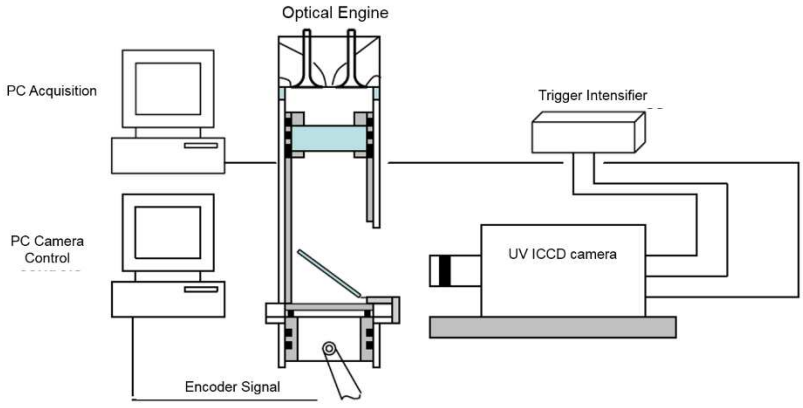

Figure 22. Schematic of the OH* chemiluminescence acquisition system.

The camera used for the experiments was a Princeton Instruments PI-MAX 4 ICCD UV camera, on which was mounted a B. Halle UV optic with a focal length of 100 mm. The camera was positioned in front of the 45° mirror of the optical engine to collect the light coming from the bottom of the transparent piston. The natural OH* chemiluminescence was recorded by filtering the light coming from the combustion chamber by means of an Asahi ZBPA310 Bandpass Filter. This filter wavelength is centered on 309 nm and has a bandwidth characterized by a FWHM of 10 nm. To maximize the image intensity while avoiding image blurring, a 90 μs exposure time was used. The image acquisition was synchronized with the engine shaft

encoder so that images could be acquired at any desired crank angle within the resolution of the shaft encoder. The image acquisition rate was limited so that only one frame could be acquired every four engine cycles. For each crank angle, at each operating condition, images were acquired in sets of fifty.

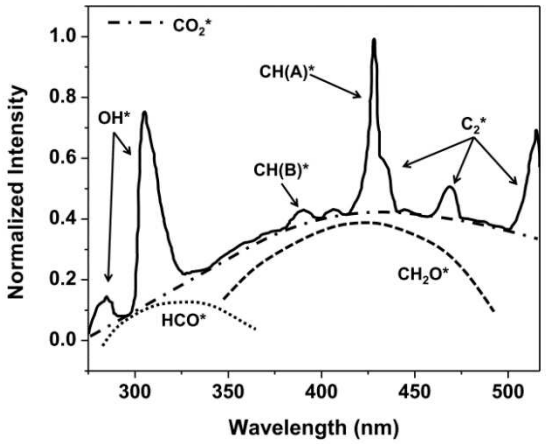

Figure 23. Chemiluminescence emission of OH*, CO_2*, HCO*, CH2O*. From [109]

3.2.2. CH_2O PLIF

For the formaldehyde-LIF the third harmonic (355 nm) of an Nd:YAG laser was used. The pulse energy at the source was approximately 50 mJ. A Pellin-Broca prism was positioned in front of the laser source to avoid contamination of the 355 nm light by the residual wavelength of the laser. During the test, the laser pulse-by-pulse intensity variation was measured by sampling 1% of the emitted fluency with a beam splitter and directing it to a Newport 1936 –R Power meter. The remaining 99% of the laser beam was then collected by a system of lenses and shaped into a horizontal laser sheet that was led through the combustion chamber via the transparent portion of the cylinder liner. The fluorescence signal was detected through the piston window and directed to the Princeton Instruments PI-MAX 4 ICCD UV camera positioned in front of the 45° mirror. The radiation from formaldehyde fluorescence emission spectra, which is reported in Figure 25, was selected by using an Andover Corporation 431 BP filter. This filter is characterized by a central wavelength of 431 nm and a bandwidth of 20 nm, enabling the CH_2O emitted fluorescence corresponding to the peak to be captured. To select the fluorescence signal while avoiding interference from other light emissions from combustion, the exposure time was set to 300 ns. The laser and the image acquisition were synchronized with the engine shaft encoder so that images could be acquired at any desired crank angle within the resolution of the shaft encoder. As in the case of OH chemiluminescence, the image acquisition

rate was limited so that only one frame could be acquired every four engine cycles. Fifty images were acquired for each experimental condition.

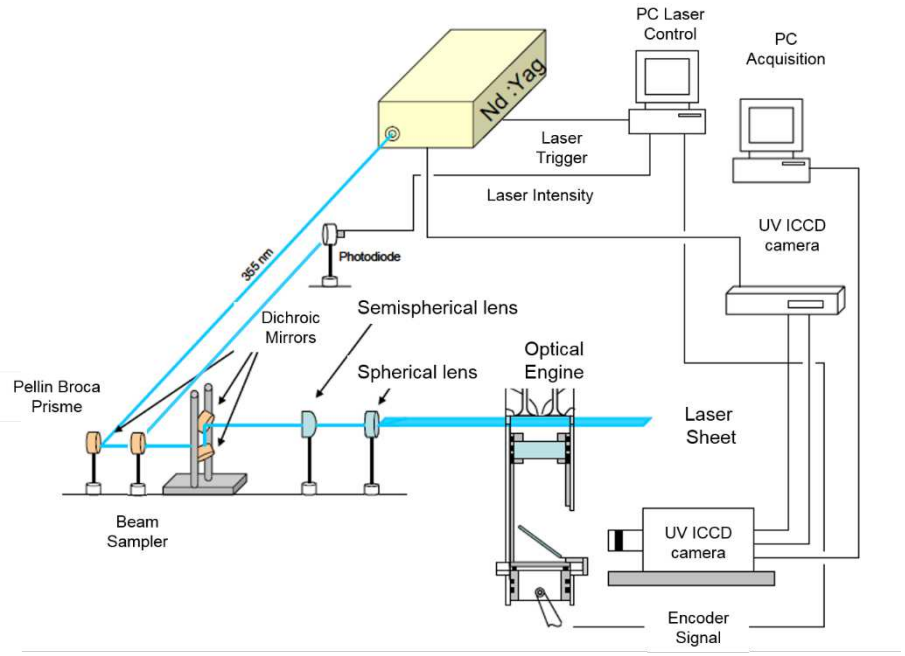

Figure 24. Schematic of the CH_2O PLIF acquisition system.

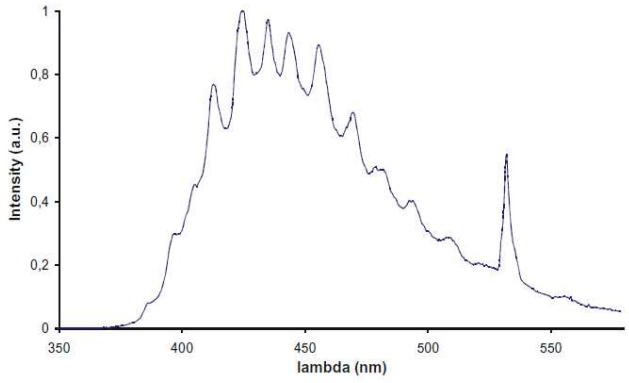

Figure 25. Emission spectrum of formaldehyde. From [110]

3.2.3. Simultaneous spatially integrated OH* and CH* chemiluminescence measurement

An Oriel Photomultiplier with two detectors was positioned in front of the optically accessible engine to enable the simultaneous measurement of OH* and CH* chemiluminescence. For OH* chemiluminescence, an Ealing 307 ± 10 bandpass filter was used. CH* natural chemiluminescence, whose emission wavelength is reported in Figure 23, was measured by filtering the light from the combustion chamber by means of a 430 ±10 nm filter.

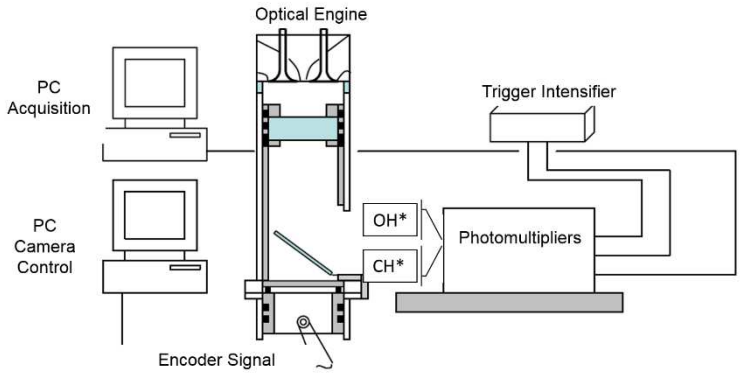

Figure 26. Schematic of the simultaneous OH* and CH* chemiluminescence acquisition system by means of a double detector photomultiplier.

3.3. 3D CFD SIMULATION

The main contribution of this thesis consists in the experimental part. CFD simulations were conducted to provide qualitative support for the analysis. In order to obtain reliable results from CFD, reference is made to other work in the literature. Considerable support was also provided by the technical assistance of the software producers. The results from this numerical study are simply intended to provide some insight into the trends and competing processes that affect GCI combustion.

3D CFD simulations were performed with the commercial software Converge. The RANS-based Re-normalization group (RNG) k–e model was used. A Lagrangian spray model based on the "blob" injection model of Reitz and Diwakar [111] was used wherein computational "parcels" of liquid with a characteristic size equal to the effective nozzle diameter are introduced into the computational domain. The subsequent breakup and atomization of the liquid blobs and resulting droplets was modeled using the Kelvin–Helmholtz and Rayleigh–Taylor instability mechanism without the use of a breakup length [112]. The no-time-counter (NTC) model of Schmidt and Rutland [113] was used in the current simulations to model droplet collision. Models were also included for dynamic drop drag [114], and droplet turbulent dispersion. The SAGE detailed chemistry solver was used for the simulations in this study along with a multizone approach to solve chemistry.

Concerning the mesh, closed-cycle computational fluid dynamics (CFD) simulations were performed using a 1/8th sector mesh which reproduces the DW-10 engine geometry. Grid generation was done during runtime in Converge with the ability to include fixed embedding of cells (increasing grid resolution over the base mesh size a priori in regions of interest such as along the walls and near the nozzle) as well as adaptive mesh refinement (AMR) based on gradients in key parameters. In the current work, AMR is based on velocity and temperature gradients. For example, a mesh with a base cell size of 1mm and with three levels of either fixed embedding or AMR will have a minimum cell size of 0.125 mm.

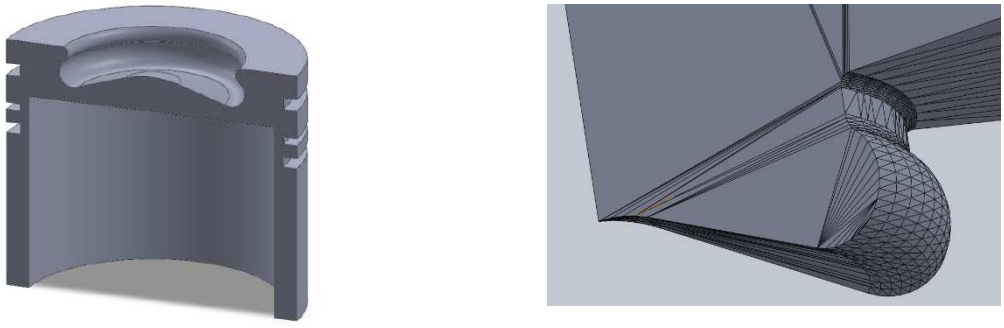

Figure 27. The CFD computational domain was built from the geometry of the customized DW-10 engine piston

The IVC pressure and temperature used in the CFD simulation were set by considering the intake conditions measured during the experiments. PIVC was 1 bar and the temperature at the IVC was assumed to be 470 K. The component temperatures (walls, head, and piston) were set to 550K. In this way, satisfactory agreement between experimental and CFD computed results was obtained, as shown later in Figure 30.

3.3.1. Surrogate fuel for 3D simulations

A five-component surrogate of gasoline from [115] was employed for the CFD simulations. The gasoline surrogate is composed of five hydrocarbons: iso-octane, n-heptane, n-pentane, iso-pentane and toluene. The precise composition is reported in Table 3. The five-component surrogate was developed in [116] using the methodology proposed by Mehl et al. [117] for targeting the combustion behaviour of a Haltermann research grade HF437 gasoline under GCI conditions.

	% vol
C8H18	24.8
C6H5CH3	30.9
iC5H12	35.1
nC5H12	4.6
nC7H61	4.6

Table 3. Formulation of the five-component gasoline surrogate [117].

During the experiments performed in this research, a commercial Total SPB-EH059 gasoline was used. However, as can be seen in Table 4, the properties of the Haltermann and the Total gasoline differ slightly. While this means that a certain degree of approximation may be introduced when comparing results from experiments performed with the SPB95 gasoline and the CFD simulations carried out with the five-component surrogate of the Haltermann gasoline, the differences in fuel properties are negligible; hence, the mixing and the combustion behaviour trends of the two fuels can be considered similar.

	HF437	Total SPB-EH059	Surrogate
AKI	92.7	90.65	91.6
RON	96.6	95.7	95.4
MON	88.7	85.6	87.8
Sensitivity	7.9	-	7.6
H/C ratio	1.81	1.9	1.86
Aromatics	30.7	29.6	30.9
Olefins	0.5	7.2	0
Saturates	68.8	58.3	69.1

Table 4. Some properties of the SPB95 gasoline employed for the experiments and of the five-component gasoline surrogate used for the CFD simulations, and of the HF437 gasoline used as a target for the surrogate development.

The chemical scheme used has 207 species and 992 reactions. The scheme was developed in [117] by implementing the Computer Assisted Reduction Mechanism (CARM) code [118] to correctly reproduce the

behaviour of the five-component gasoline surrogate. The reduced mechanism was obtained by reducing a previous mechanism from [116], which was used for analysing the combustion behaviour of several components relevant to gasoline surrogate formulation.

3.3.2. Grid Convergence Study

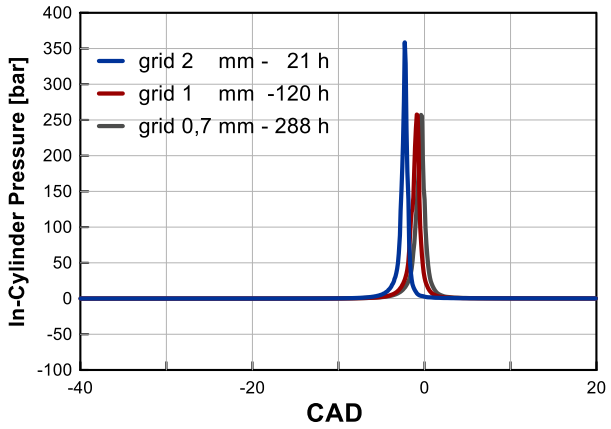

Figure 28. Heat release rate as a function of the base grid size.

Various cell sizes for the computational domain were evaluated to determine the minimum cell size needed for the convergence of results. For a fixed AMR level of 3, a swipe in base grid size was performed. The results, reported in Figure 28, showed that the heat release rate convergence was achieved for a base grid size of 1 mm, corresponding to a minimum cell size of 0.125 mm. It should be noted here that the recommendation for a standard diesel engine simulation is 0.25 mm minimum grid size, based on the literature [119]. In this work, a combination of 1 mm base grid and AMR level of 3 was employed for all the tests. With this setting, the maximum number of cells varied during the simulations depending on the temperature and velocity gradient, and the maximum cell count reached 700,000 elements during the combustion process, as indicated in Figure 29. With this setting, reactive computations needed 120 h to be carried out with an 8-core computer processor.

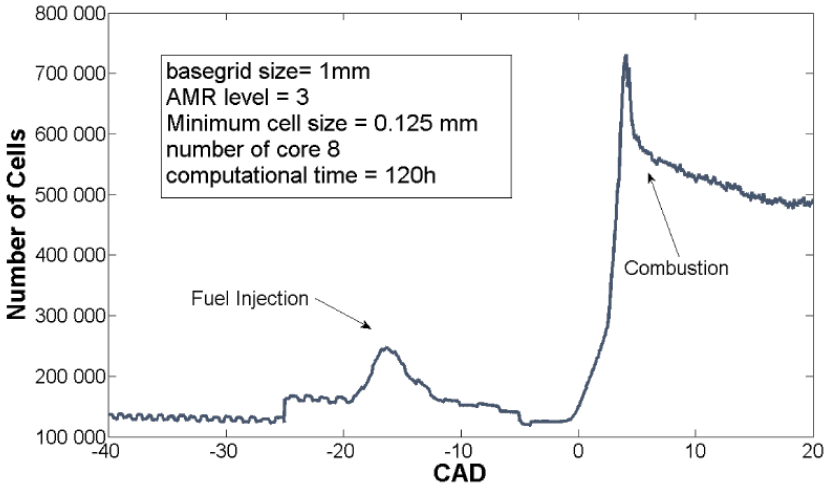

Figure 29. Cell count during the simulation of the engine cycle.

3.3.3. Evaluation of CFD Model Performance against Experiments

The CFD Converge computations were employed in this work as a support for the analyses of experimental data. Therefore, using the computational setup previously described, simulations of some relevant experimental conditions were performed to assess the capacity of the model to reproduce GCI combustion. Simulations were run by using the experimental boundary conditions determined from the experimental test as input. Figure 30 reports the experimental and simulated in-cylinder pressure, the in-cylinder temperature and the normalized cumulated heat release rate resulting from a swipe in injection timing. It can be seen that a good agreement between CFD computations and experimental results was obtained by using the setup previously described.

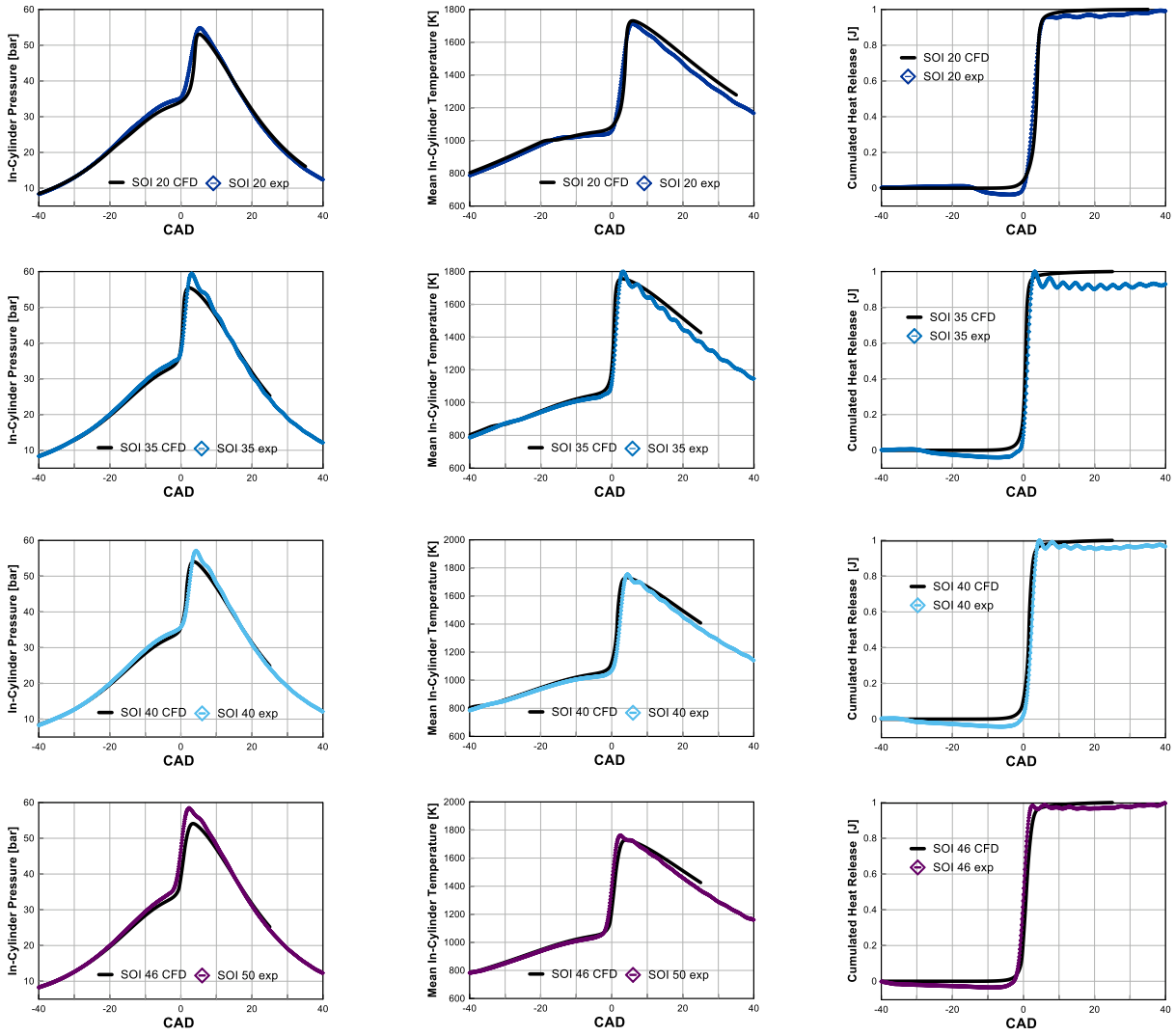

Figure 30. Experimental and calculated in-cylinder pressure, temperature and normalized cumulated heat release rate as a function of the injection timing.

4. Low load GCI combustion

4.1. INTRODUCTION

Gasoline Compression Ignition combustion is a complex process in which several factors act together to determine the behavior of combustion and the engine performances. Reactivity is one of the most important factors impacting GCI. From a global point of view, the lack of reactivity of lean gasoline/air mixtures is the limiting factor impeding the possibility of achieving GCI combustion at low load. Moreover, after injection, the fuel distributes inside the cylinder. The spray-induced local distribution of temperature and equivalence ratio can alter the local mixture reactivity. This determines the modality of autoignition and the combustion behavior, i.e. pollutant formation, once autoignition has been achieved. GCI combustion can also be impacted by the presence inside the combustion chamber of chemical species which can induce a change in reactivity, affecting the combustion behavior. In this section, GCI low load will be investigated, with a focus on the mechanism which can affect the reactivity and therefore the combustion behavior in such an engine.

4.2. INTAKE CONDITIONS

Fuel compression autoignition can be globally considered as the result of a matching between the in-cylinder thermodynamic conditions given by the piston compression and the thermodynamic conditions required by the fuel to autoignite. On the one hand, the thermodynamic conditions at the end of the compression process represent the thermodynamic state that the engine makes available to the fuel to start the oxidation process. For a given compression ratio, the in-cylinder pressure and temperature evolutions during the compression stroke are linked and can be controlled by varying the thermodynamic conditions corresponding to the intake valve closing. On the other hand, fuel autoignition chemistry determines the thermodynamic requirements for combustion to occur. Depending on the temperature and pressure, autoignition can be achieved or not. Moreover, the initial thermodynamic conditions experienced by the fuel, along with the fuel/air mixture equivalence ratio, determine the respective ignition delay. Compression ignition combustion takes place exclusively if the thermodynamic conditions at the end of the compression stroke are high enough to trigger the oxidation reactions with an ignition delay short enough to avoid the oxidation reactions being quenched during the expansion stroke. It should be borne in mind that both the fuel chemistry requirement and engine intake conditions are not totally independent and depend on the engine operating point. A simplified schematization of the autoignition process in GCI low load conditions is represented in Figure 31 by means of a pressure-temperature diagram. In GCI low load operations, small amounts of fuel are injected during the cycle because of the reduced power output demand. Intake pressure boosting is challenging because of the reduced enthalpy available in the exhaust gases and without heaters or VVT, it is difficult to increase the intake temperature. The engine consequently operates at atmospheric pressure but needs to burn a highly diluted fuel-air mixture characterized by a lean equivalence ratio (ϕ=0.3). A motoring curve of the PSA

DW10 diesel engine operating at 1 bar and 20°C intake conditions is plotted in Figure 31. On the same graph, the results of ignition delay calculations of a gasoline surrogate fuel are reported, indicating a simplified case in which the combustion originates from a homogeneous fuel-air mixture. A global ϕ=0.3 was considered as representative of the low load fueling rate. As shown in Figure 31, in these conditions, the in-cylinder compression pathway is extremely far from the autoignition region of a lean gasoline/air mixture. Figure 31 shows the motoring curve when the engine intake conditions were varied by increasing the intake air temperature to 175 °C. It can be seen that heating up the intake air charge can shift the motoring P-T trajectory in order to satisfy the high thermodynamic demand of such a lean and difficult to ignite gasoline/air mixture. In this chapter, high intake air temperatures were used to achieve autoignition of a RON 95 in a conventional DW10 Diesel engine and to make it possible to study the impact of other engine parameters on GCI low load combustion.

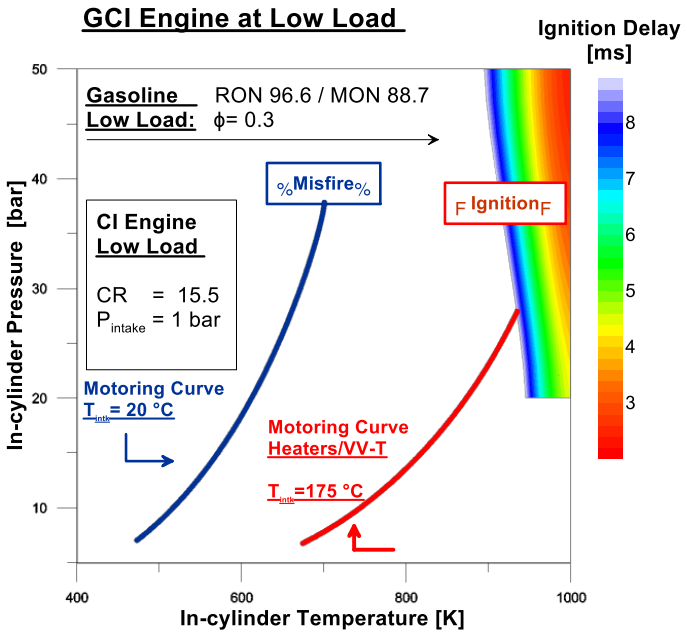

Figure 31. Schematic representation of the autoignition process inside a GCI engine at low load.

4.3. LOCAL FUEL DISTRIBUITION

In the previous section, a simplified case of the autoignition of a homogeneous mixture was considered. In this section, the effect of spray direct injection on autoignition is discussed.

In Figure 32, a representation of the fuel direct injection process is shown. On the left side, CFD fuel molar fraction distributions resulting from a single gasoline direct injection are represented. After injection, as a result of the spray-induced momentum and the in-cylinder air turbulent motion, the fuel mass distributes heterogeneously in the cylinder, evaporates and mixes with air. Depending on the injection strategy, a certain degree of fuel stratification is obtained and the in-cylinder fuel distribution is characterized by different local values of temperature and equivalence ratio.

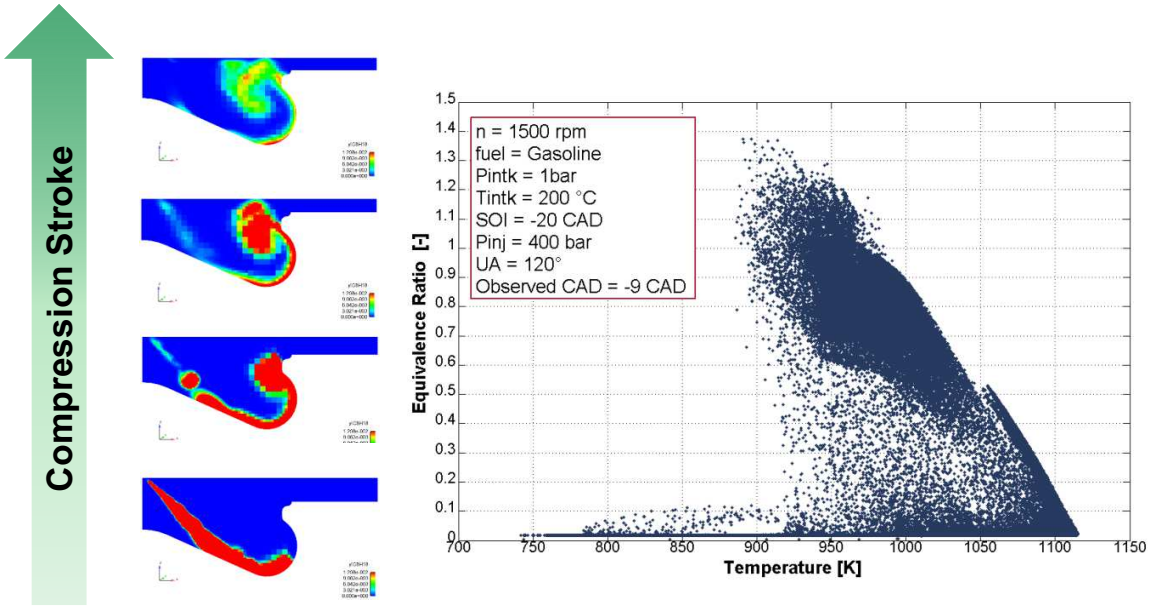

Figure 32. Representation of the direct injection process and example of an in-cylinder equivalence-ratio temperature distribution from reactive CFD computations. Initial conditions are reported in the graph.

In this case of partial fuel stratification, the charge reactivity can be analyzed by considering the reactivity of a multitude of locally homogeneous fuel/air cells experiencing different local conditions of equivalence ratio and temperature.

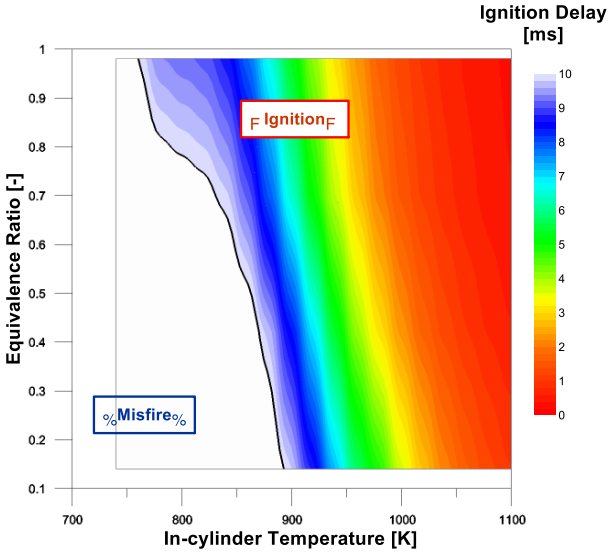

Figure 33. Constant volume ignition delay calculation for a gasoline surrogate fuel [117] as a function of equivalence ratio and temperature for a constant initial pressure of 32 bar.

As an example, Figure 33 reports the results for ignition delay calculations as a function of the local equivalence ratio and temperature, for a 5-component gasoline surrogate fuel. Results show that the ignition delay of the mixture is a function of both temperature and equivalence ratio. Higher reactivity and faster ignition delay result from an increased equivalence ratio or an increased local temperature. However, the ignition delay presents a non–linear dependence with temperature and equivalence ratio. As a result, iso-contours of the ignition delay can be observed in Figure 33. Different combinations of local temperature and equivalence ratio can give the same reactivity. It cannot therefore be ruled out that lean fuel/air mixtures may be more reactive than richer ones, depending on the temperature gradient. On the other hand, it can be assumed that despite the favorable intake thermodynamic conditions, the use of a non-optimal injection strategy can result in an extremely locally lean or extremely rich and cold mixture which will be unable to autoignite. Looking at both Figure 32 and Figure 33, it can be therefore deduced that the local distribution of temperature and equivalence ratio will affect the local reactivity and the subsequent development of the combustion process. The occurrence of autoignition, the combustion behavior and the pollutant formation will therefore be impacted by the injection strategy.

4.3.1. Autoignition and Combustion Development

The impact on combustion of the in-cylinder temperature and equivalence ratio distribution induced by the injection strategy is discussed in this section. Two different experimental conditions will be considered, differing only with respect to the injection timing. The experimental conditions are listed in Table 5.

Fuel	Engine Speed	Intake Temperature	Intake Pressure	Injection Pressure	Mass	SOI (variable)
SP95 Gasoline	1500 rpm	205 °C	1 bar	400 ppm	7.8 mg/cycle	-40CAD/ -20CAD

Table 5. Engine operating conditions employed during the experiments and as initial conditions for the CFD calculations (results reported in this chapter).

The engine speed was set at 1500 rpm. In both cases, 7.8 mg of SP95 gasoline were injected, corresponding to a low load operation of ~ 2 bar IMEP. In both cases, as discussed in the previous section, a high intake temperature was needed to achieve gasoline autoignition. A fixed injection pressure of 400 bar supplied the common rail system. Combustion behavior was compared when a single gasoline injection was performed using two different injection timings of respectively SOI = -40 CAD and SOI =-20 CAD. The same conditions were employed for the 3D-CFD computations. The five-component gasoline fuel described in Chapter 3 was used as a gasoline surrogate. Experimental and computed in-cylinder pressure and temperature traces for the two experimental cases are reported in Figure 34. Table 6 compares the combustion behavior as a function of the injection timing. Satisfactory agreement was found between experiments and simulations, indicating that the CFD model reproduced the combustion process well in the present conditions.

Table 6 reports the characteristics of the combustion process for the two different cases investigated, and shows that despite the different injection timing, combustion results were characterized by a similar combustion phasing. Heat release analysis indicated that 10% of the heat release occurred closer to 1 CAD aTDC in both cases. The CA50 was also similar, with 0.5 CAD of difference between the two experimental setups. At CA90, injecting the fuel later, at SOI = -20 CAD, increased the duration slightly. Table 6 shows that CFD simulations reproduced the experimental results well in terms of CA10, CA50 and CA90. Table 6 also shows the experimental measurement of the exhaust concentration of pollutants. It is interesting to note that despite the similar phasing of the combustion event, changing the injection timing had a significant impact on pollutant formation. The most strongly impacted case is that of NOx emissions, which were nine times higher for the SOI = -20 CAD than for the SOI = -40 case.

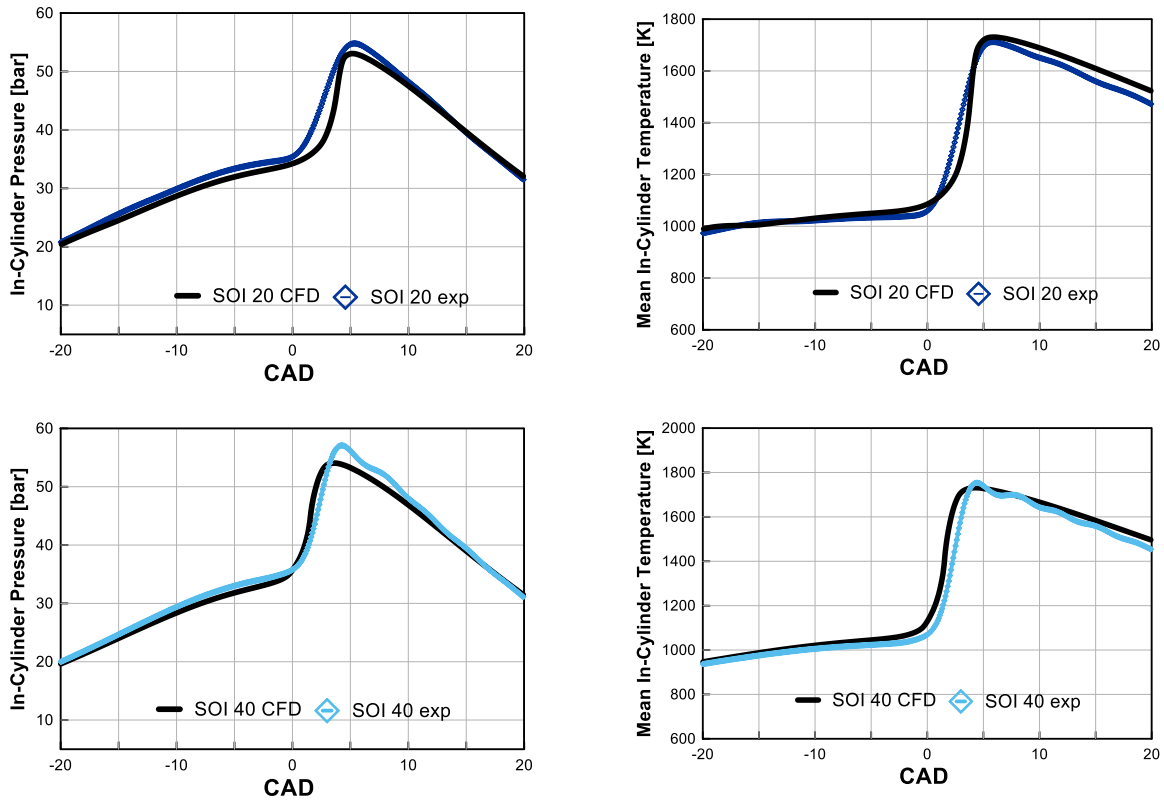

Figure 34. Experimental and CFD computed in-cylinder pressure and temperature traces for two different injection timings. Initial conditions are reported in **Table 5**.

	SOI = -40 CAD		SOI = -20 CAD	
	Exp.	CFD	Exp.	CFD
CA10	0.6	0.2	0.9	0.8
CA50	2.3	1.6	2.9	3
CA90	3.5	2.9	4.8	3.9
NOx	130 ppm	$2.97\text{-}10^{-7}$kg	1179 ppm	$3.652*10^{-7}$kg
HC	712	$4.42*10^{-7}$kg	649	$4.57x10^{-7}$ kg
CO	870 ppm	$2.159*10^{-7}$kg	580 ppm	$7.843x10^{-8}$ kg

Table 6. Results from Experiments.

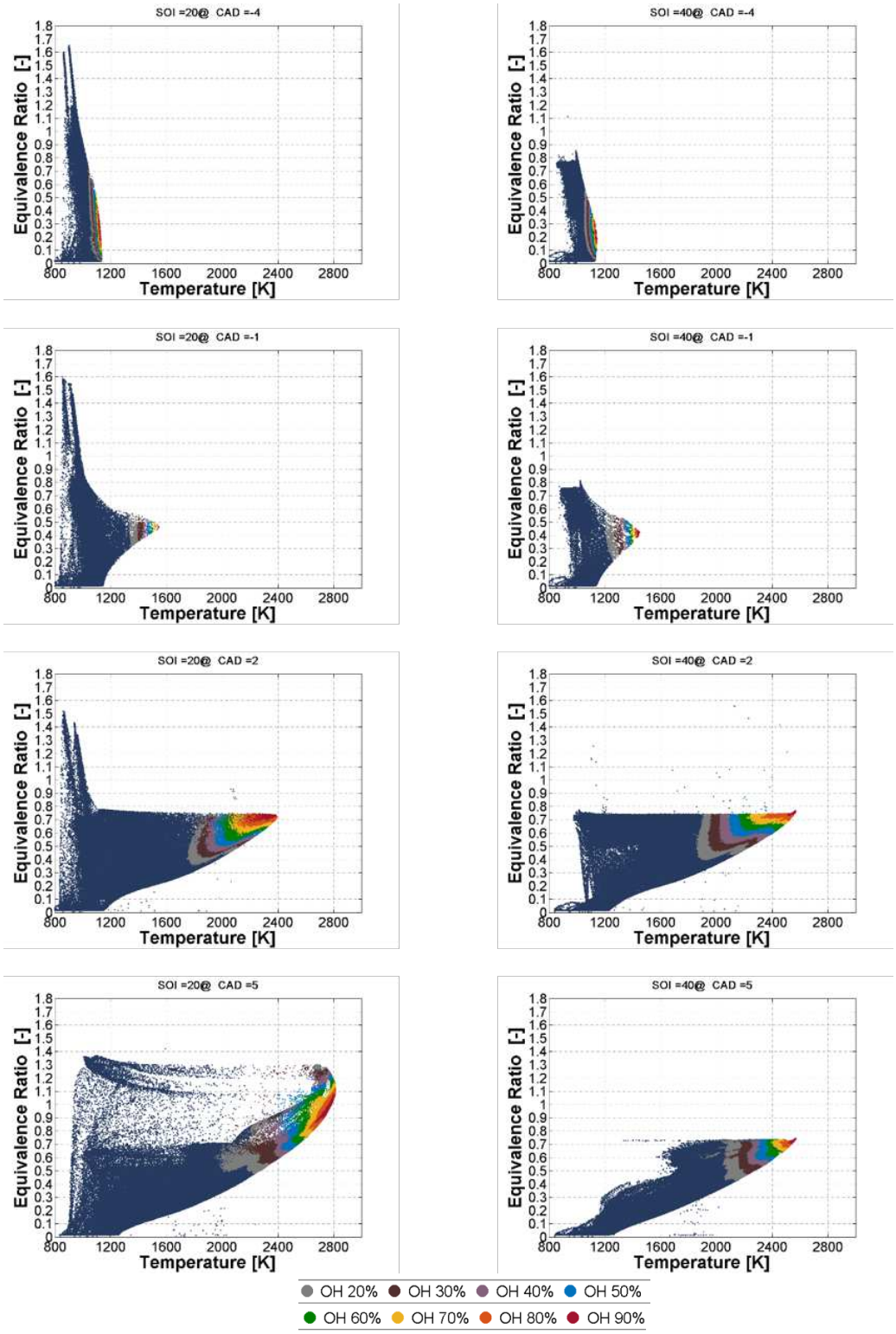

Figure 35. In-cylinder equivalence ratio and temperature distributions from CFD calculations corresponding to different CAD for SOI = -20 CAD (a) and SOI = -40 CAD (b). Relative Iso-contours of OH normalized concentrations are also reported. Initial conditions are reported in **Table 5**.

Figure 35 reports the local in-cylinder equivalence ratio and temperature distribution corresponding to different CAD for the two different injection timings investigated. After the injection event, as a result of the spray-induced momentum and in-cylinder turbulent flow, fuel air mixing occurs. Because of the different injection timing, the two cases are characterized by different T-ϕ fields.

Figure 35 reports the T-ϕ diagram corresponding to -4 CAD aTDC, just before initiation of the combustion process, for the SOI = -20 CAD case. It can be seen that although the injected mass was low, the fuel distributed over a wide range of equivalence ratios spanning from lean to values far from the global equivalence ratio value of ϕ =0.3. Because of the low amount of fuel injected, extremely lean regions with ϕ lower than 0.1 can be found in the cylinder. However, such fuel lean regions coexisted with fuel pockets characterized by an above-stoichiometric equivalence ratio of ϕ = 1.8. Richer fuel regions are generally characterized by a range of lower temperature. The maximum temperature for richer fuel regions was 1000K. As result of the lower cooling effect, leaner regions experienced higher local temperature, and lean ϕ = 0.1 with temperatures well over 1100K were found in the cylinder.

For the more advanced injection timing represented by the SOI =-40CAD case, the scatter plot of T- ϕ is markedly different. The in-cylinder fuel distribution is characterized by a narrower equivalence ratio range. The mixture is characterized by ϕ well below stoichiometry, and a maximum ϕ =0.8 was observed. The T-ϕ distribution indicates a low level of in-cylinder fuel stratification. Local inhomogeneities were smoothed as a result of the more vigorous mixing process induced by a longer ignition delay, resulting in a more homogeneous mixture.

Figure 35 also reports the iso-contour of OH concentration normalized relative to its maximum. It can be seen that regardless of the injection timing and the level of equivalence ratio stratification, the higher OH concentrations are located in the hotter region characterized by a lower equivalence ratio. This indicates the presence of an increased chemical activity in this region which anticipates the moment of autoignition that occurred later in the cycle.

Figure 35 shows the T-ϕ distribution corresponding to -2 CAD at TDC. The clear presence of a protrusion in the T-ϕ map following a significant temperature rise indicates the occurrence of mixture autoignition.

Despite the considerable difference in the in-cylinder T-ϕ distribution, in both the investigated cases, the most reactive combination of T and ϕ driving autoignition process did not involve the richer pockets. Inversely, irrespective of the injection timing, the autoignition event initiated in those regions was characterized by an intermediate equivalence ratio of approximately ϕ = 0.45 and a high temperature close to T = 1100K. These results indicated that in low load conditions, characterized by ambient intake pressures,

the gasoline has a reduced ϕ-sensitivity, contrarily to what observed in experimental conditions characterized by a boosted intake pressure [33,53,117].

After ignition had occurred in the region characterized by intermediate equivalence ratio values, the oxidation process evolved. The heat released during the first ignition of the leaner and more reactive fuel regions triggered the oxidation of the remaining fuel. The combustion was therefore progressively extended, involving a larger proportion of the injected fuel mass. As a result of the increased local temperature, the richer fuel pockets can also ignite. This results in the sequential, progressive ignition of increasingly richer fuel pockets. Due to the oxidation of these richer fuel pockets, a progressive increase in the maximum combustion temperature is observed. Figure 35 shows that because of the presence of richer fuel pockets in the moments immediately preceding combustion, the SOI=-20 CAD case is characterized by an in-cylinder peak temperature of 2800K generated by the late ignition of fuel-rich regions with equivalence ratios between $\phi = 0.9$ and $\phi = 1.2$. By contrast, for the SOI = -40 CAD case, the in-cylinder peak temperature was limited at 2400K because the maximum equivalence ratio was lower, at $\phi = 0.8$.

4.3.2. NOx emissions

The difference in the maximum in-cylinder temperature can therefore explain the substantial difference in the NOx emissions measured during the experiments in the two experimental cases. High NOx emission in the SOI = -20 CAD case could be explained by thermal stimulation of the nitrogen oxidation process. The difference in cylinder temperature can also explain the lower CO exhaust concentration measured in the SOI =-40 CAD case. Because of the lower in-cylinder temperature, earlier injection timings made it more difficult for the oxidation of CO to CO_2 to occur. Following the previous discussion, it can be deduced that the evolution of the in-cylinder temperature could have been qualitatively predicted by looking at the local distribution of the equivalence ratio prior to combustion. Results from this analysis showed that regardless of the injection timing, because of the low ϕ-sensitivity of gasoline under low load conditions, autoignition occurred in the regions characterized by a leaner fuel-air equivalence ratio. Therefore, combustion extends to the remaining fuel, and higher in-cylinder temperatures are generated as long as the injection strategy yields the in-cylinder presence of fuel-rich pockets. The presence in the moment just prior to combustion of fuel pockets characterized by a close to stoichiometric equivalence ratio can promote NO by the Zeldovich mechanism because of the higher in-cylinder temperature but also because of the presence of increased fuel concentrated over the equivalence ratio range between $0.9 < \phi < 1.1$.

4.3.3. Abnormal NOX emissions

For the same experimental conditions as in the previous experiments, an entire swipe in injection timing was employed and the impact of the injection timing on combustion was analyzed.

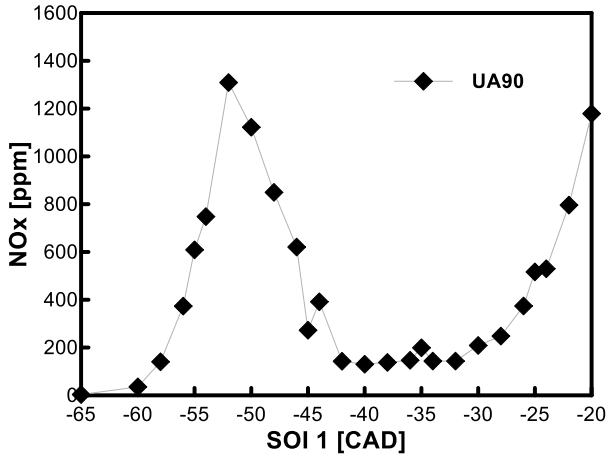

Figure 36. Experimental exhaust NOx measurement as a function of the start of injection SOI. Engine operating conditions are reported in **Table 5**.

Figure 36 shows measurements of the exhaust concentrations of NOx for the swipe in injection timing performed under the experimental conditions reported in Table 5.

As already shown in the previous sub-section, later SOI closer to TDC, i.e. SOI = -20CAD, are characterized by a significant level of fuel stratification which is correlated to the NOx production from the ignition of rich fuel pockets with ϕ>>1. Systematically advancing the injection timing could improve the mixing process and therefore reduce the NOx emissions occurring when SOI moves away from TDC. A constant minimum emission of NOx of ~130 ppm was observed between SOI = -30 CAD and SOI = -40 CAD, due to a less pronounced fuel stratification. However, advancing the injection timing further led to the presence of an abnormal increase in the emission of nitrogen oxides, and a bump in NOx emission can be observed for SOI between SOI = -45 CAD and SOI = -55 CAD. A maximum value of NOx=1400 ppm at SOI = -52 CAD was observed, even higher than the NOx production corresponding to a more stratified case such as SOI = -20 CAD. A detailed analysis of the exhaust gases showed that more than the 80% of the NOx were composed of NO. A possible explanation for the abnormal NOx emission for early injection timings can be the in-cylinder distribution of the fuel.

Figure 37 reports, for different injection timings, the in-cylinder fuel distribution as a function of the equivalence ratio. The fuel distributions are plotted as a function of -4 CAD aTDC, just before the initiation of combustion. In Figure 37 it can be seen that in the case of late injection timings represented by the SOI = -20 CAD case, the in-cylinder fuel distribution is characterized by a high local equivalence ratio which

can reach values well above stoichiometry, as indicated by the presence of fuel pockets with ϕ=1.6. As a consequence of the more vigorous mixing process, Figure 37 shows that for SOI earlier than -20 CAD aTDC, the mixture was less stratified and the equivalence ratio spanned a narrower range of values. Moreover, for the SOI = -40 CAD and SOI = -65 CAD cases, characterized by low NOx emission, the local equivalence ratio was below stoichiometry, close to ϕ = 0.8. However, it can be noticed that at SOI = -50 CAD, despite the typical ϕ-distribution shape of a well-mixed charge, there was a large mass of fuel distributed over the region between 0.8 and 1.1.

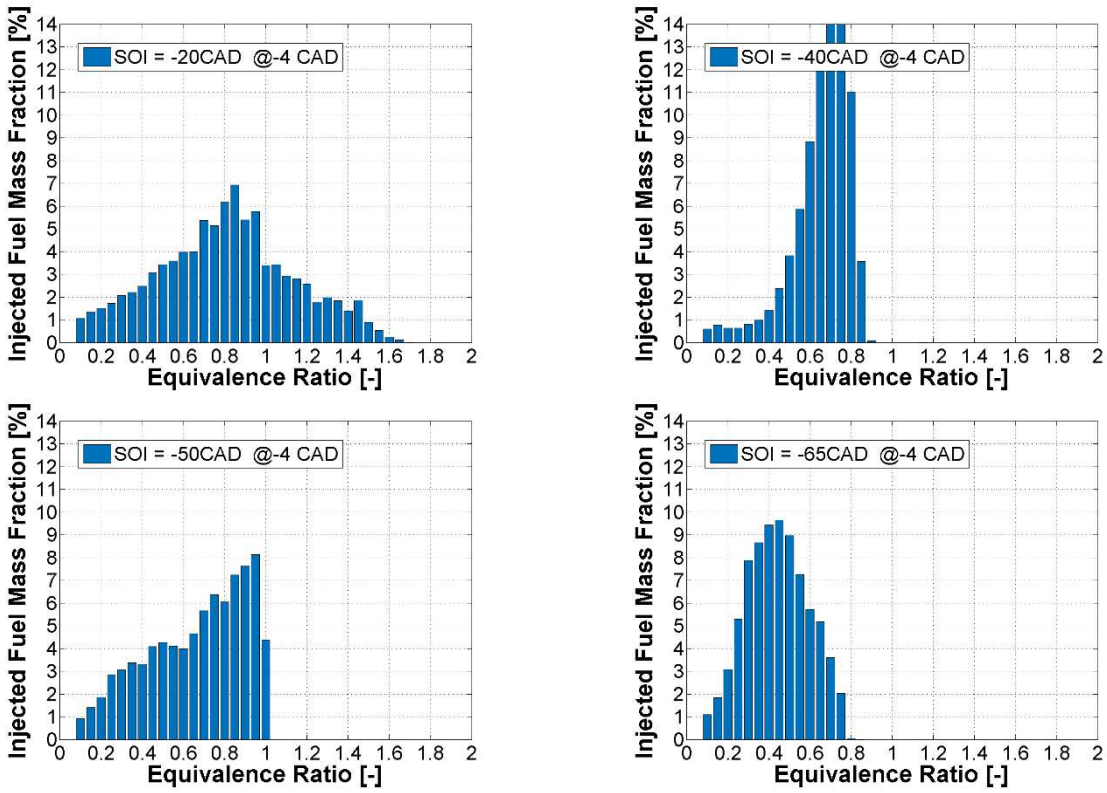

Figure 37. CFD computed fuel mass distribution as a function of the equivalence ratio at – 4 CAD aTDC and for different injection timings. Initial conditions are reported in **Table 5**.

The increase in this close-to-stoichiometric fuel region was not observed in the other early injection timing cases, and is well correlated with the peak in NOx emission reported in Figure 36. Simulations performed by Kim et al. [120] in a Diesel engine with a similar engine geometry showed that at particular injection timings, spray orientation and bowl conformation may cause the fuel to remain accumulated and constrained at the bottom of the bowl. This suggests that this condition occurred when the start of injection took place

between SOI = -45 CAD and SOI = -55 CAD, leading to local values of ϕ close to 0.9, incentivizing NO formation according to the Zeldovich mechanism.

Figure 38 reports the fuel mass fraction distributed over the 0.85<ϕ<1.1 interval as a function of the injection timing. At SOI = -20 CAD, more than 25% of the fuel had an equivalence ratio between 0.85<ϕ<1.1. It can be clearly seen that advancing the injection timing promoted the homogenization of the mixture, reducing the stratification and therefore the presence of fuel pockets with a high local equivalence ratio. For example, between SOI = -45 and SOI = -30 CAD the improved fuel/air mixing meant that less than 10% of the fuel was located in the close-to-stoichiometric regions. However, for further advanced SOI in the region between SOI = -45 CAD and SOI = -65 CAD, the local distribution of the equivalence ratio became extremely sensitive to the injection timing. At SOI = -50 CAD, despite the high level of homogeneity and because of a probable interaction between the spray trajectory and the piston head bowl conformation, a higher portion of the fuel accumulated over stoichiometric regions, with more than 25% of the fuel distributed over the 0.85<ϕ<1.1 interval. This can incentivize NO formation by the extended Zeldovich mechanism [99].

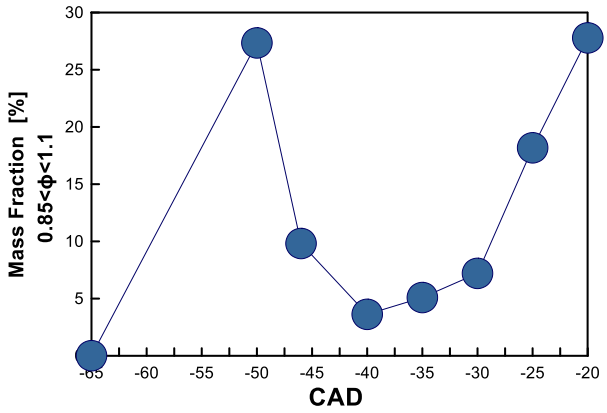

Figure 38. CFD computed fuel mass fraction distributed over the equivalence ratio interval 0.85<ϕ<1.1, as a function of the injection timing SOI. Initial conditions are reported in **Table 5**.

Figure 39 reports the in-cylinder maximum temperature reached during combustion as a function of the injection timings. Simulations showed that the presence of high in-cylinder peak temperatures correlate well with the presence of richer fuel regions. This suggests that although early SOI leads to a more homogeneous mixture, the occurrence of spray-bowl geometry interaction leads to the presence of close-to-stoichiometric

fuel pockets which stimulate the formation of abnormal amounts of NOx by promoting a high in-cylinder temperature, as indicated in Figure 39.

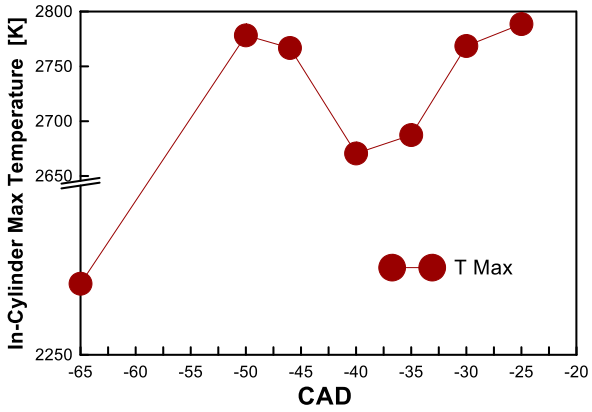

Figure 39. CFD computed maximum in-cylinder temperature as a function of the start of injection SOI. Initial conditions are reported in **Table 5**.

4.3.4. Evaluation of the impact of Residual NO on combustion

Figure 40 reports, for the same experiments, the CA50 trends as a function of the injection timing. It can be clearly observed that the peak in NOx emission correlated well with a strong advance of the combustion phasing in the SOI region between -55 CAD and SOI = -45 CAD. A widely accepted paradigm for NOx formation is that advanced combustion phasing promotes an increase in local temperature causing increased NOx emissions.

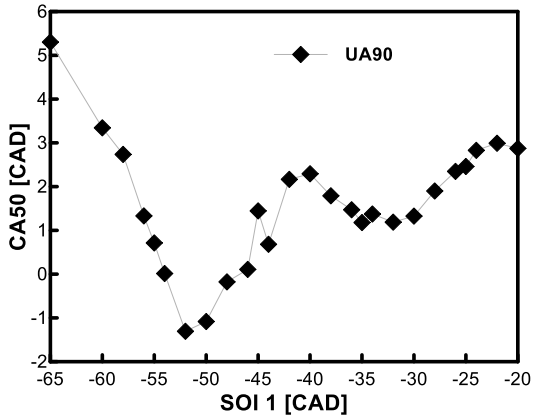

Figure 40. Experimental combustion phasing CA50 as a function of the injection timing SOI. Experimental conditions are reported in **Table 5**

In the introduction chapter the promoting impact of nitrogen oxides on hydrocarbon oxidation was already discussed. Moreover, in previous work by Contino et al. [108], and other previous work [94], NO and NO_2 were shown to possess a strong promoting effect on the premixed combustion of gasoline-like fuel. The

question that arises here, therefore, is whether in the SOI range between -45 CAD and -55 CAD, following the abnormal NO formation induced by the spray-piston bowl geometry, combustion phasing could have been accelerated even more by the NO concentration contained in the residual burnt gases trapped after each combustion cycle.

4.3.4.1.Experimental Evaluation of the residual NO

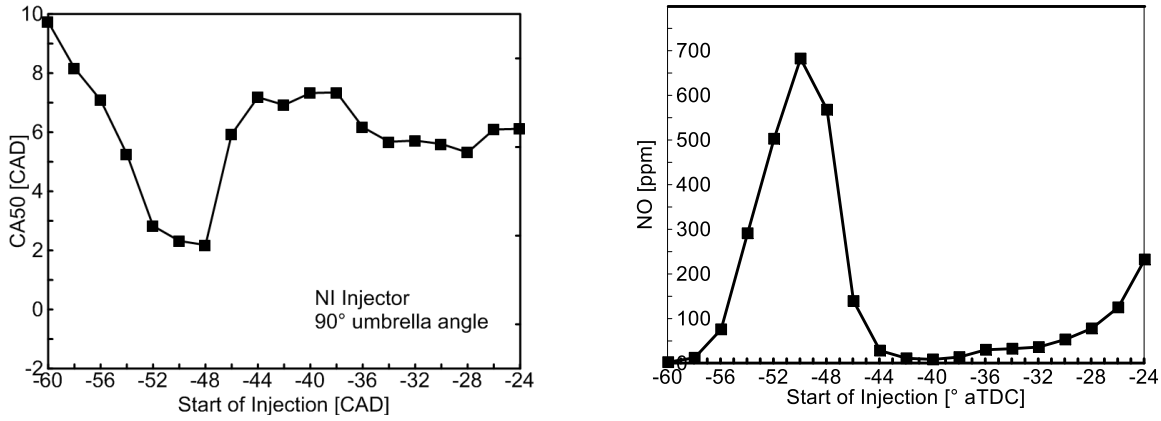

Figure 41. Experimental combustion phasing CA50 and exhaust NO measurements as a function of the start of injection SOI. Experimental conditions are reported in **Table 5**. Note that the intake temperature was reduced to T = 175°C.

Figure 41 reports the results of the same swipe in injection timing performed under the same experimental conditions as those reported in Table 5 but with the intake temperature reduced to 175°C. CA50 and NOx traces showed the same shape but both the CA50 trace and NO traces presented different specific values. CA50 exhibited a shift of approximately 4 CAD over the entire SOI range investigated. NO emission also contracted but maintained the same shape. The same NO bump was observed corresponding to a CA50 acceleration. This indicated that the mechanism underlying the abnormal NO production is unchanged and not sensitive to the intake thermodynamic conditions. This is further proof of the importance of spray-bowl interaction which can lead to the excitation of NOx emission by the Zeldovich mechanism. In these

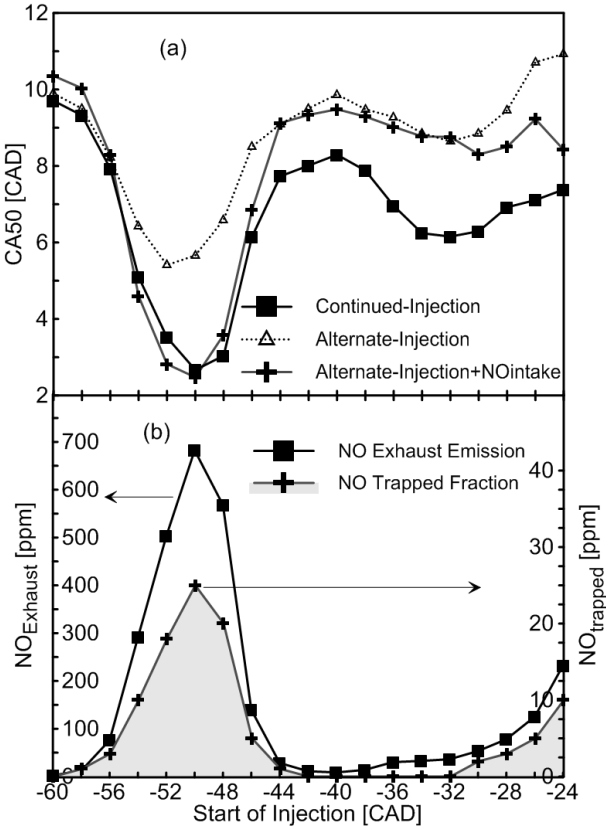

Figure 42. Experimental CA50 as a function of SOI for the continued-injection mode, alternate-injection mode and alternate-injection mode with NO addition at the intake (a). Experimental exhaust NO concentration measured in the continued-injection mode and the estimated NO trapped fraction (b). Experimental conditions are reported in **Table 5**. Note that the intake temperature was reduced to T = 175°C.

conditions, a special experiment was performed to assess the impact of the residual NO on gasoline combustion for the early injection timings. Results are reported in Figure 42.

An alternate-injection operating mode, in contraposition to the typical continued-injection mode was used to remove the effect of residual NO on gasoline autoignition. Under the alternate-injection mode, fuel was injected only every two cycles. In this way, each combustion cycle was followed by a cycle in which only fresh air flowed into the cylinder, enabling the dilution of the residual trapped gas and cleaning the combustion chamber of residual NO. Figure 42 compares the CA50 for the alternate and the continued injection mode for the same SOI sweep. In order to compensate for the reduced wall temperature induced by alternate combustion cycles, the intake temperature had to be increased up to 200°C. This 13°C increase was evaluated at SOI=-60 CAD, where NOx production was negligible and combustion phasing was independent of the effect of trapped NO, by matching the CA50 measured during continued-injections. According to [17], limiting the NO concentration coming from the preceding combustion cycle, retarded the CA50 over the whole range of SOI. Figure 42(b) shows the NO concentration measured at the exhaust in the continued-injection mode. Comparing Figure 42(a) and Figure 42(b), it can be seen that a maximum

offset between the two CA50 traces of ~3 CAD occurred for SOI=-50 CAD, matching with the 682 ppm peak in NO concentration at the exhaust.

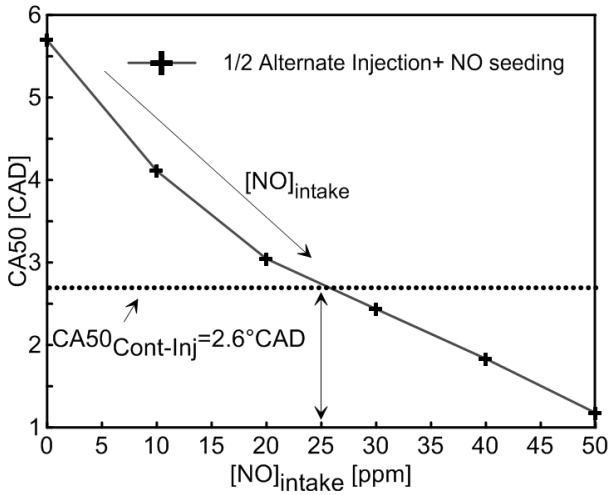

Figure 43. Experimental evaluation of the NO trapped fraction. CA50 as a function of NO concentration, during alternate-fired mode. Experimental conditions are reported in **Table 5**, but intake temperature was reduced to T = 175°C.

To estimate the trapped fraction of NO, the engine was run in alternate-injection mode, and the injection timing set as a function of the peak of NO production, at SOI =-50 CAD. Then, pure NO was systematically injected up to when the promoting effect of the nitric oxide was such as to restore the CA50 previously obtained in the continued-injection mode. As shown in Figure 43, 25 ppm of NO were needed to match this CA50. The NO trapped fraction was then estimated at SOI = -50 CAD as the ratio between the 25 ppm NO concentration at the intake and the 682 ppm measured at the exhaust under continued-injection operation. A value of 3.66% was obtained. Because in first approximation, this ratio depends only on the engine internal fluid dynamics, it could be applied to estimate the NO trapped over the entire SOI range. Therefore, the NO trapped fraction was calculated and used to seed the intake of the engine during alternate-injection operation over the entire SOI range investigated: results are reported in Figure 42(a). There is a good fit between the CA50 trends obtained and the continued-injection CA50 over the SOI range involved in high NOx production, i.e., up to an SOI of -46 CAD. It can be deduced that at early injection timings, if the piston geometry and injection strategy yield high NOx formation, a fraction depending on the speed and the engine geometry could remain trapped within residual gases, promoting autoignition. At later SOI, i.e. SOI > -44 CAD, the NO trapped fraction becomes negligible, and the onset of combustion is mainly regulated by local stratification of temperature and equivalence ratio.

4.3.4.2. CFD study of the impact of NO on combustion

The experiments reported in the previous section indicated that in certain conditions, NO trapped in the residual burnt gases can impact the premixed combustion of gasoline, leading to an abnormal advance in combustion phasing. In this work the impact of NO was assessed by using CFD simulations.

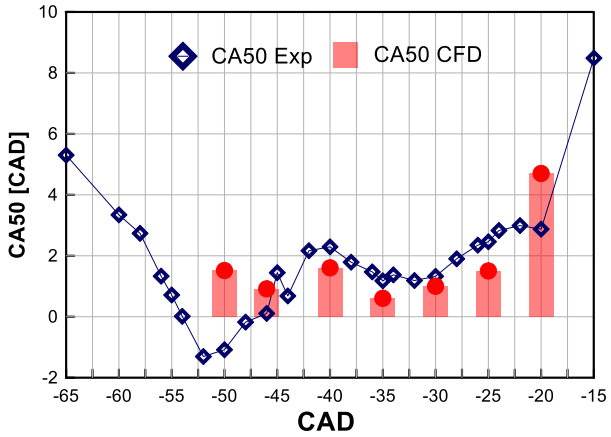

Figure 44. Experimental and CFD computed CA50 as a function of SOI. Experimental conditions are reported in Table 5. It should be noted that in the CFD simulations the intake charge is composed of pure air and that the presence of residual burnt gases trapped in the cylinder was not considered.

Figure 44 reports, for the same experimental conditions, the CA50 and NOx trends resulting from experiments and CFD simulations. The initial conditions used for the CFD calculations corresponded to those used for the experiments. However, the presence of a residual NO fraction coming from previous combustion cycles was not considered in the chemical composition of the intake charge. This methodology was adopted to reproduce the skip-fire method described in the previous cycle. For intermediate injection timing, characterized by low NOx production, computations reproduced the experimental combustion phasing trend well. However, a considerable discrepancy between experimental and simulation results was observed at SOI = -50 CAD and SOI = -20 CAD, where simulations considerably overestimated the CA50. Figure 45 shows the experimental NOx emissions and the residual NO trapped fraction estimated according to the method described in the previous section. Results clearly show that overestimation of the CA50 occurred in the experimental conditions characterized by the higher residual NO mass fraction.

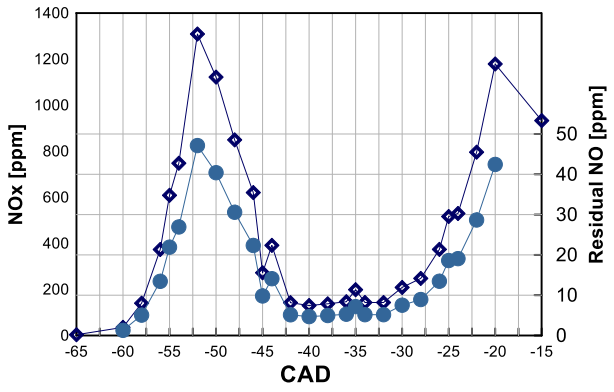

Figure 45. Experimental NOx and estimated residual NO as a function of SOI. Experimental conditions are reported in **Table 5**

Therefore, further simulations were performed with the aim of understanding whether the underestimation of the mixture reactivity in the high NOx production cases could have been caused by neglecting to take residual NO into consideration in the initial fresh charge composition. The CFD simulations were repeated in the case of SOI = -50 CAD and SOI = -20CAD by adding different concentrations of NO to the intake charge composition.

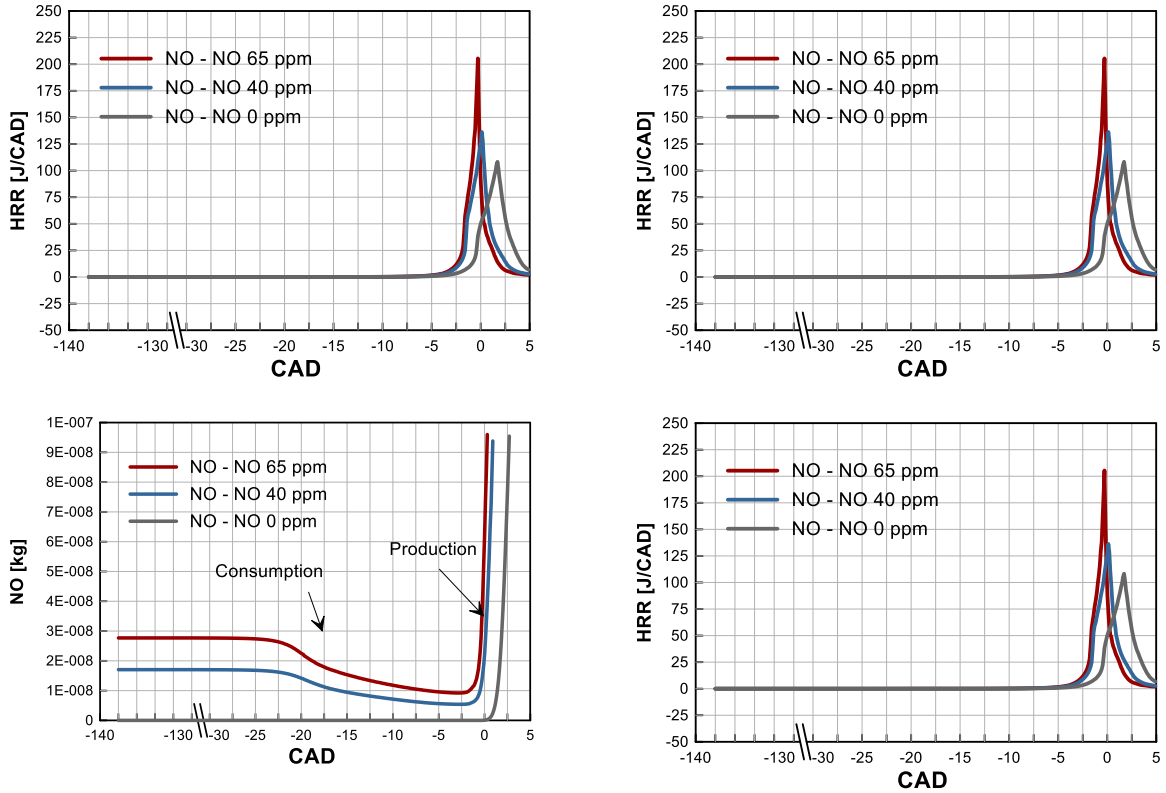

Figure 46. CFD computed heat release traces and NO in-cylinder mass traces as a function of the initial NO concentration and for two different operating conditions: SOI = -50 CAD and SOI = -20 CAD. Initial conditions are reported in **Table 5**.

Figure 46 shows the heat release traces and the NO in-cylinder mass for different initial NO concentrations for the SOI = -50 CAD and SOI = -20 CAD case. Results show that an advance and increase in the heat release rate traces occurred when the initial NO concentration varied from 0 ppm to 65 ppm. In the figure the in-cylinder mass of NO is also reported. When the initial NO concentration was neglected, the nitrogen oxide mass evolution showed a production phase close to TDC resulting from the onset of combustion. For initial NO concentrations of 45 ppm and 65 ppm, the NO mass profiles assumed an initial constant value corresponding to the initial concentrations. Then, at ~20 CAD before TDC, a reduction of NO indicated the progressive consumption of the nitric oxide which started to react and to participate in the fuel oxidation. Figure 46 also shows the NO mass in the case of SOI = -20 CAD. It can be noticed that the beginning of the NO consumption phase is sensitive to the injection timing. Indeed, in the SOI= -20 CAD case, NO consumption started later, approximately ~10 CAD before TDC. These trends demonstrate that the promoting impact of NO on gasoline combustion was associated to the NO consumption occurring some CAD after injection and before the onset of combustion.

Figure 47 reports the CA50 trends from experiments and simulations in which increasing NO concentrations were added at the engine intake. It can be seen that the CA50 considerably decreased under the effect of an increased initial NO concentration. Adding NO to the initial charge composition of the CFD simulation resulted in a better prediction of the experimental results. Figure 47 shows that in the CFD simulations, irrespective of the SOI, adding 40ppm of NO induced a shift of ~2 CAD in CA50. In the SOI = -20 CAD case, this led to a match between the CA50 from simulation and from experiments. In the case of SOI = -50 CAD, the larger gap with the experimental CA50 required even more nitrogen oxide to be added to further advance the combustion phasing. However, even with an initial nitrogen oxide concentration of 65 ppm, the discrepancy between experiments and simulations continued to exist.

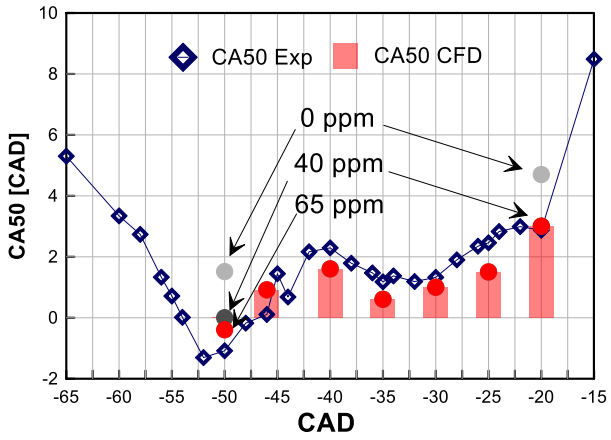

Figure 47. Experimental and CFD computed CA50 as a function of SOI. For SOI = -50 CAD and SOI = -20 CAD, the CA50 from CFD computations is reported for initial NO concentrations in the initial intake charge composition of 0, 40 and 65 ppm. Operating conditions are reported in **Table 5**

The CFD simulations reproduced the impact of NO experimentally observed. However, computations show a different sensitivity of the combustion phasing to NO addition compared to the experiments. This may depend on the sensitivity of the chemical set employed in reproducing the NO-hydrocarbon interaction. Further investigations have to be carried out in order to improve this aspect.

4.4. IMPACT OF THE INJECTION SYSTEM

In the present section the impact of the injector umbrella angle, the number and the timing of fuel injection on gasoline compression ignition combustion will be investigated.

All the experimental results reported in this section were performed in the conditions given in Table 7.

Fuel	Engine Speed	Intake Temperature	Intake Pressure	Injection Pressure	Mass
SP95 Gasoline	1500 rpm	205 °C	1 bar	400 ppm	7.8 mg/cycle

Table 7. Engine operating conditions during the experiments and as initial conditions for the CFD calculations for the results reported in this chapter.

In order to investigate the impact of the umbrella angle, three different Delphi Diesel injectors, with a wide (156°) intermediate (120°) and a narrow (90°) umbrella angle, (hereinafter UA156, UA120 and UA190, respectively), were used. All the injectors have 8 holes measuring 131μm in diameter.

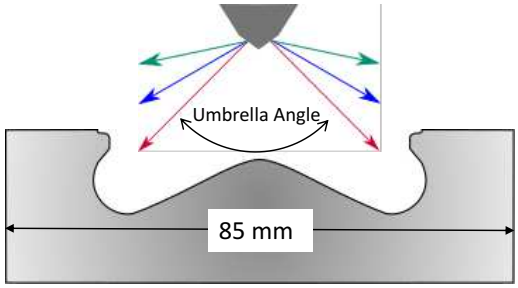

Figure 48. Schematic representation of the different injector umbrella angles.

4.4.1. Impact of the injector umbrella angle

The first experiments consisted in supplying in a single injection event a constant amount of fuel by using injectors with different umbrella angles. For every injector tested, starting from TDC, the injection timing was progressively advanced and a swipe in SOI was performed. Figure 49 reports the combustion efficiency as a function of the SOI for the three injectors tested. Results showed that the injector umbrella angle significantly impacted the combustion efficiency. More specifically, the injector umbrella angle defined the

range of SOI within which the ignition of the fuel was characterized by a high combustion efficiency, indicating a good onset and development of the oxidation reactions.

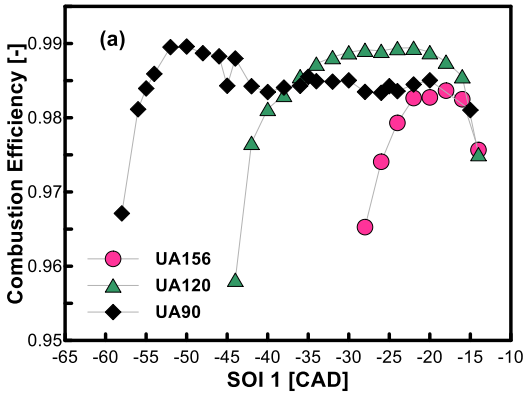

Figure 49. Combustion efficiency as a function of the start of injection timing SOI and for different umbrella angles. Experimental conditions are reported in Table 7.

From Figure 49 it can be seen that the high-efficiency SOI range is delimited by two drops in combustion efficiency. A late drop occurring close to TDC, whatever the injector employed, is noticeable for SOI =-15 CAD. This drop is mainly related to the minimum ignition delay necessary to avoid misfire. If SOI was moved closer to TDC, the long ignition delay characterizing lean gasoline/air mixtures caused autoignition to occur too late, and combustion reactions to be quenched by the lowering of the temperature occurring during the beginning of the expansion stroke. Therefore, a tendency to misfire characterized late SOI, which is noticeable by looking at the increased sensitivity of CA50 values reported in Figure 50 for SOI later than SOI = -20CAD.

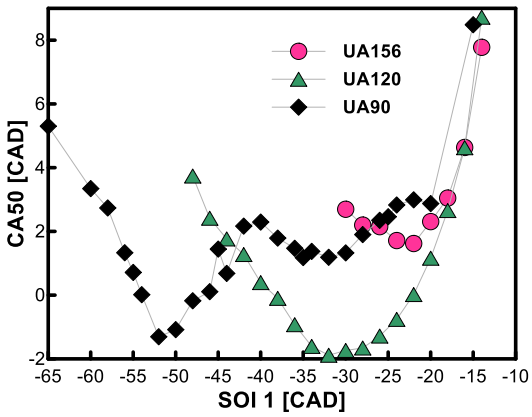

Figure 50. CA50 as a function of the start of injection timing SOI and for different umbrella angles. Experimental conditions are reported in Table 7.

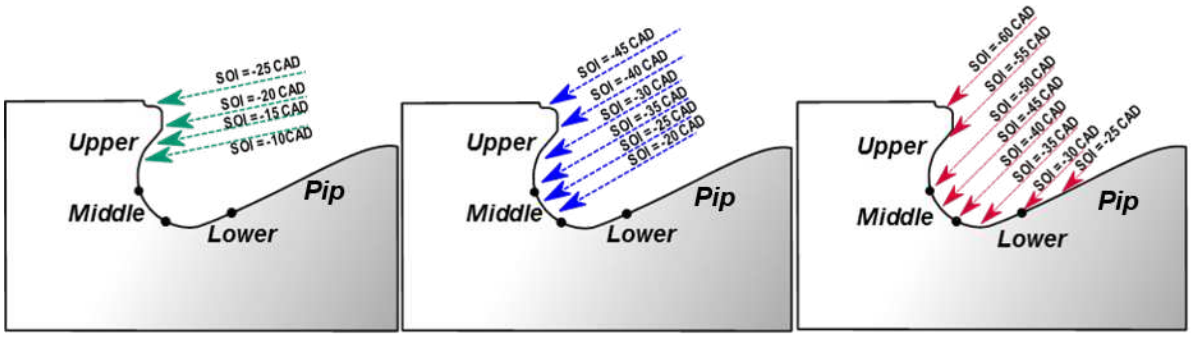

Figure 51. Spray target position as a function of the SOI different umbrella angles.

A second drop in combustion efficiency delimited the earlier admitted SOI, whose position was instead strongly dependent on the injector umbrella angle. Figure 49 shows that the extension of the high

efficiency SOI range could be considerably expanded by tightening the umbrella angle. The different extension of the high efficiency trends can be explained by observing Figure 51, which shows for each injector employed, the spray trajectory and the qualitative spray target position as a function of SOI for the three different injectors tested.

It can be seen that the high combustion efficiency range corresponded to the umbrella angle-SOI combination which allowed the spray to be directed inside the piston head bowl. Targeting the piston head bowl with a combination of spray trajectory and injection timing helped to concentrate the fuel charge, avoiding dispersion of the fuel and hence overleaning of the mixture. As a result, a strengthening of the combustion process occurred, as indicated by the high combustion efficiency in this SOI range. Contrarily, if the SOI was increasingly advanced, for each injector there was an early value of SOI for which the spray trajectory was too wide to allow the fuel to target the bowl. In these conditions, moving SOI increasingly farther from TDC directed an increasing part of the fuel toward the squish region. These SOI-UA combinations corresponded to a non-optimal configuration, as indicated by the HC and CO trends reported in Figure 52. It can be seen that when the SOI became too advanced for a given injector, excessive HC originated because of the increased amount of fuel dispersed in the coldest outmost boundary layers of the combustion chamber, such as crevices, where it can also be diluted in film wall oil. This fuel did not participate in the mixing process, reducing the mass of fuel effectively contributing to the combustion process. Moreover, at increasingly advanced SOI, spray misses the bowl. The spray trajectory is longer and the spray is dispersed in a larger volume, leading to overleaning and hence an increase in CO emission. The degradation of the combustion process caused by the non-optimal spray target position at early SOI is the

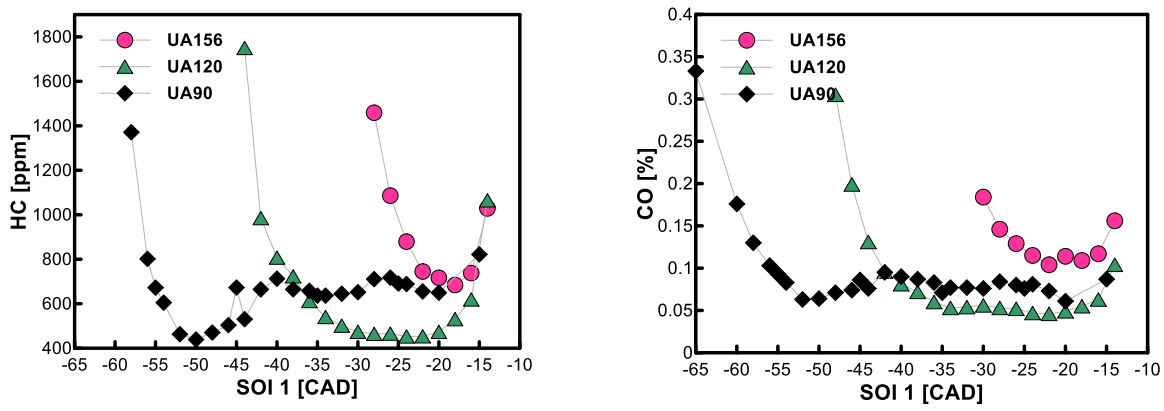

Figure 52. HC and CO exhaust concentration as a function of SOI and for the different umbrella angles. Experimental conditions are reported in Table 7

mechanism which determined the ability of the narrower umbrella angle to extend the high combustion efficiency SOI range.

The umbrella angle not only determined the expansion of the admitted SOI range, but also the combustion behavior within it.

Figure 49 shows that within the high efficiency SOI range, a narrower umbrella angle allowed a higher level of combustion efficiency to be achieved. The combustion efficiency values of the UA90 and UA120 injectors reached 99%. By contrast, with the customized diesel injector UA156, it was not possible to exceed a combustion efficiency of 98%. Figure 52 shows that the lower combustion efficiency achieved with the UA156 injector is due to the higher emission of HC and CO obtained by using this injector. The results in Figure 52 show that while the minimum HC and CO emission of respectively 400 ppm and 0.06% were achieved by both UA90 and UA120, the level of these pollutants was almost double in the case of the wider UA156 injector over an injection timing range between SOI = -25CAD and SOI = -15 CAD. Figure 53 shows the in-cylinder bulk temperature calculated from the in-cylinder pressure measurements. It can be seen that the UA156 injector presented a similar combustion temperature in the injection timing range going from SOI = -25 CAD to SOI = -15CAD, indicating that other factors could have contributed to the higher CO exhaust concentration observed for the UA156 injector. The excessive emission of CO and HC observed in the case of the wider umbrella angle can be explained by looking at the way in which fuel is distributed inside the combustion chamber. Figure 54 shows, for the three injectors tested, the fuel mass distribution as a function of the equivalence ratio at TDC. The fuel distribution indicates that in experiments performed using the UA165 injector, the in-cylinder process was characterized by a higher amount of fuel distributed over lean ($\phi<0.2$) or rich equivalence ratios ($\phi>1$), a fact that can affect the conversion of the C atoms contained in the fuel to CO_2. A low equivalence ratio affects CO to CO_2 conversion because of the low local temperature reached after oxidation. In fuel pockets with an above-stoichiometric equivalence rate, CO to

CO_2 conversion is affected by the low amount of available molecular oxygen. By contrast, the UA120 injector, which showed the lowest CO emission, was characterized by most of the fuel being distributed over intermediate equivalence ratio values which corresponded to an intermediate oxygen concentration and better conditions for the oxidation of CO into CO_2 to take place.

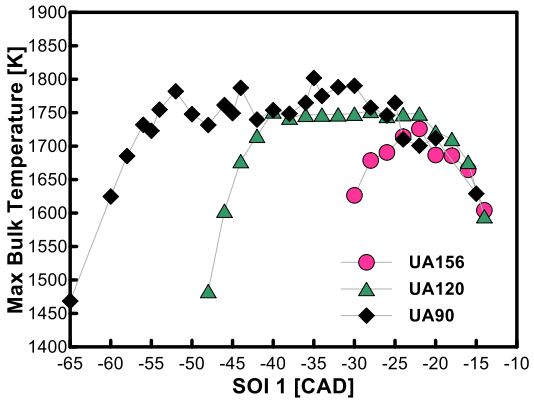

Figure 53. In-cylinder bulk temperature estimated from the in-cylinder pressure measurement. Experimental conditions are reported in Table 7

The higher combustion efficiency observed in the case of the narrower injector umbrella angle is reflected in the values of IMEP and indicated efficiency recorded during the experiments. Figure 55 clearly shows that narrower umbrella angles, because of their ability to better concentrate the fuel charge in the piston bowl, had a higher indicated efficiency and IMEP. The higher indicated efficiency can be explained by the higher combustion efficiency, indicating a better exploitation of the chemical energy made available by the fuel. Moreover, it can be assumed that because narrower umbrella angles are able to better concentrate the charge in the bowl, combustion is confined within the bowl, reducing heat exchange with the cylinder wall. This reduces thermal losses and increases the indicated efficiency.

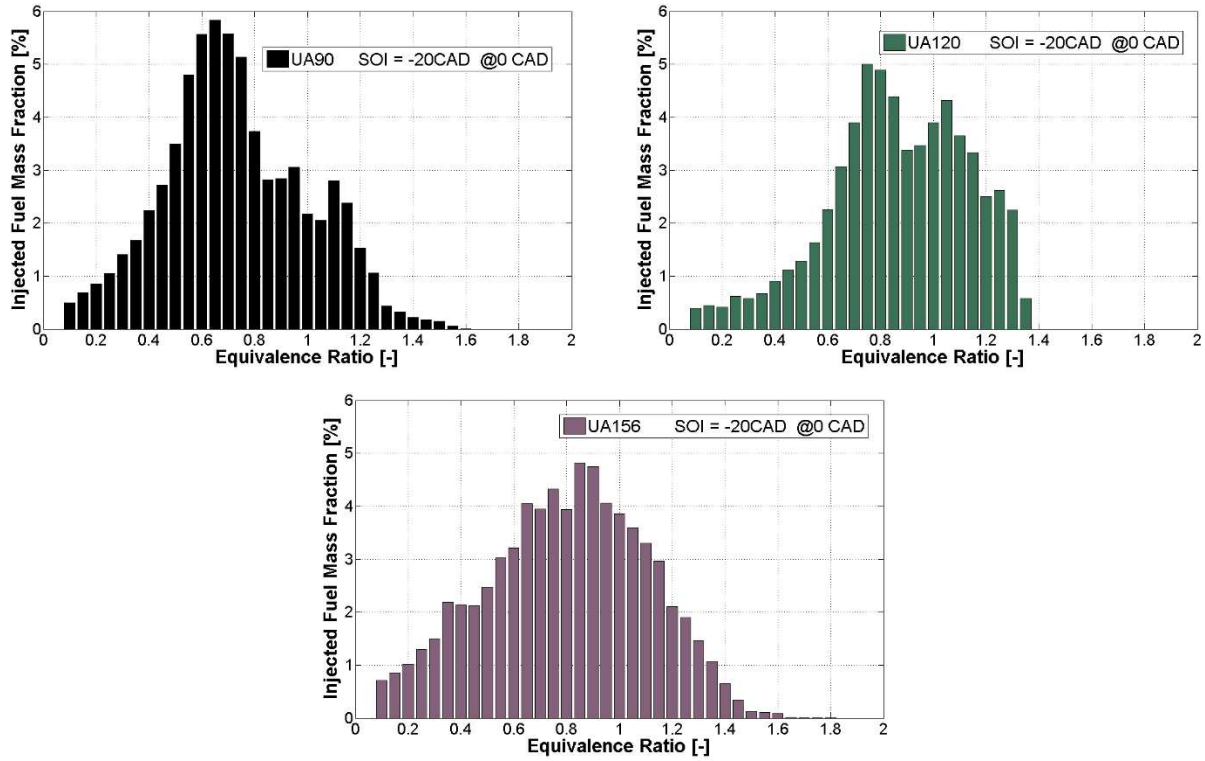

Figure 54. CFD computed in-cylinder fuel distribution as a function of the equivalence ratio at TDC, for different injector umbrella angles. Initial conditions are reported in Table 7

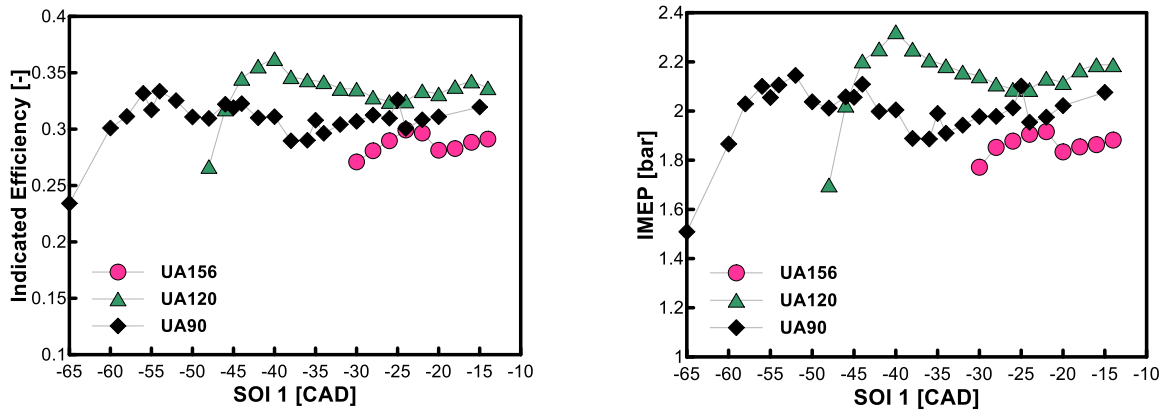

Figure 55. Experimental indicated efficiency and IMEP as a function of SOI and for the different umbrella angles. Experimental conditions are reported in Table 7

4.4.2.Spray target position

Figure 56 reports the NOx emission and the combustion phasing CA50 as a function of the SOI, for the three injectors tested.

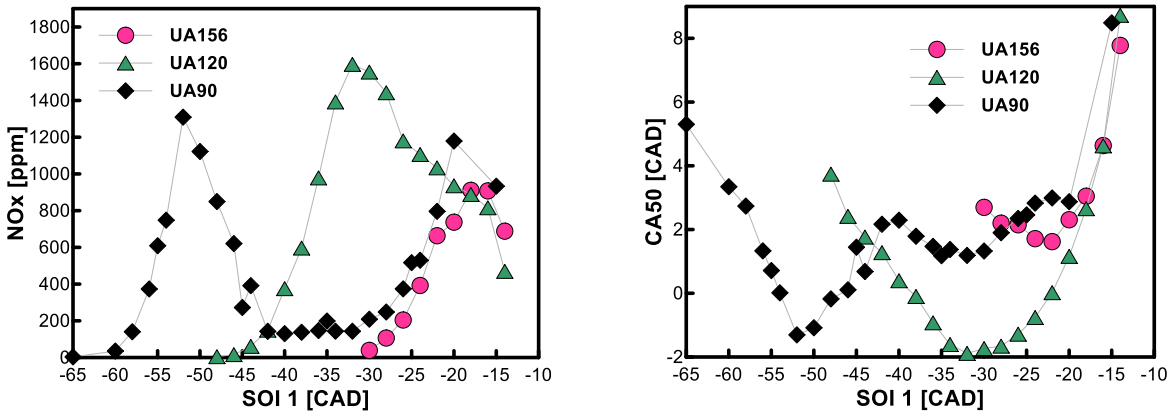

Figure 56. NOx emission and CA50 as a function of SOI and for the different umbrella angles. Experimental conditions are reported in **Table 7**

Unlike the CO and HC emissions and the combustion and the indicated efficiency, which had fairly stable values over the SOI range investigated, the NOx and CA50 trends were considerably impacted by SOI over the entire set of conditions investigated. Moreover, it can be seen how over the same SOI range, the three different injectors resulted in different trends in combustion phasing and NOx emissions. This is the case, for example, of the SOI range between SOI=-25 and SOI =-15 CAD, where the measured NOx for the injectors UA156 and UA90 increased under the effect of delayed injection, while in the same SOI range, using the UA120 injector caused NOx to decrease when SOI moved toward TDC. The CA50 values also showed different trends over the same SOI range depending on the umbrella angle of the injector. For example, for the injector timing range delimited by SOI = -50 CAD and SOI = -40 CAD, the UA90 and UA120 injectors showed opposed CA50 trends.

Figure 57 reports, for every injector, the spray target position as a function of the injection timing. The piston bowl was qualitatively divided into three different regions, named respectively upper, middle and lower part for the bowl. It should be noted that depending on the umbrella angle of the injector, a different SOI was needed to direct the spray and hit the piston in the same region. Table 8 reports the spray target position as a function of SOI and the umbrella angle of the injector. For example, with the UA120, an SOI between -20 CAD and -25 CAD directed the spray to the middle of the bowl, while for the UA90, fuel had

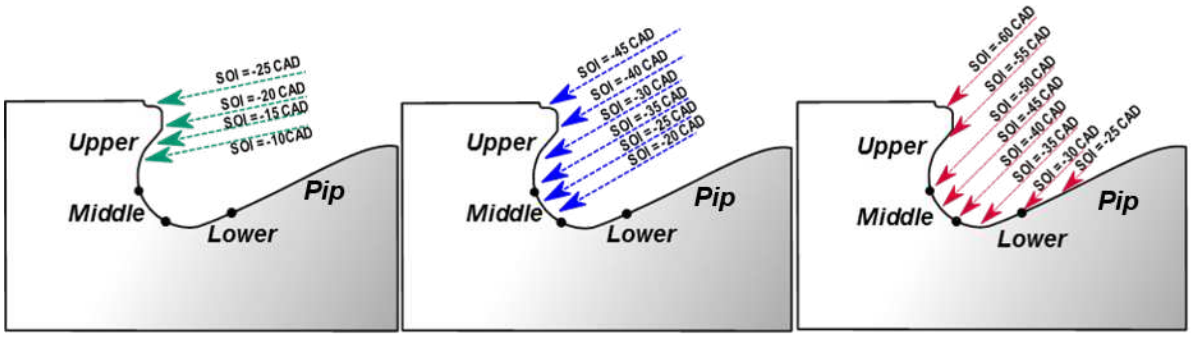

Figure 57. Spray target position as a function of the SOI different umbrella angles.

to be injected earlier during the compression stroke, between SOI = -35 CAD and SOI = -45CAD, to hit the piston in the same position.

Different combustion behaviors were associated to each spray target region.

	Spray Target Position			
	UPPER	**MIDDLE**	**LOWER**	**PIP**
UA 90°	-65/-50 CAD	-50/-40 CAD	-40/-30 CAD	-25/-15 CAD
UA 120°	-45/-35 CAD	-35/-15 CAD		
UA 156°	-25/-10 CAD			

Table 8. Start of Injection SOI as a function of the injector umbrella angle and the desired spray target position

Upper Bowl Region

The upper bowl region defines the more advanced SOI allowing a high combustion efficiency. For each injector, directing the spray towards the region defined as the upper bowl region caused the combustion to be extremely sensitive to the injection timing. Figure 49 shows that in this region, advancing the SOI could lead part of the fuel to be in the squish region, thereby increasing HC and CO followed by the combustion efficiency drop previously described and reported in Figure 49. By contrast, a delay of SOI toward TDC improved spray-bowl interaction, allowing an increased portion of the fuel to target the bowl and mix with air. Higher local equivalence ratio values characterized the fuel/air mixture when SOI moved toward TDC, as reported in the fuel distribution in Figure 58. This shows that by properly adjusting the injection timing, fuel dispersion can be avoided, maximizing the amount of fuel participating in the combustion process, leading to a reduction in HC and CO emission and thus a higher combustion efficiency, as indicated in Figure 49 and Figure 52. As the advanced SOI directs the fuel into the upper bowl region, this gives the fuel

longer to mix with air. Moreover, taking into account the high volatility of gasoline, it is highly likely that this spray target region promoted the formation of a well-mixed charge, which would be subject to HCCI-like combustion, governed by the chemical kinetics. It can be seen that as a result of the higher amount of fuel inside the piston head bowl, the equivalence ratio increased, enhancing the overall reactivity of the system. Consequently, the combustion phasing advanced when SOI was progressively delayed, as indicated in Figure 50. Figure 56 shows that NOx emissions increased in this range when SOI moved toward TDC, due to the increase in the local temperature reached during combustion. In this region, characterized by early injection timings and a well-mixed fuel/air mixture, the combustion phasing can also be driven by the in-cylinder presence of residual NO, as shown in the previous section.

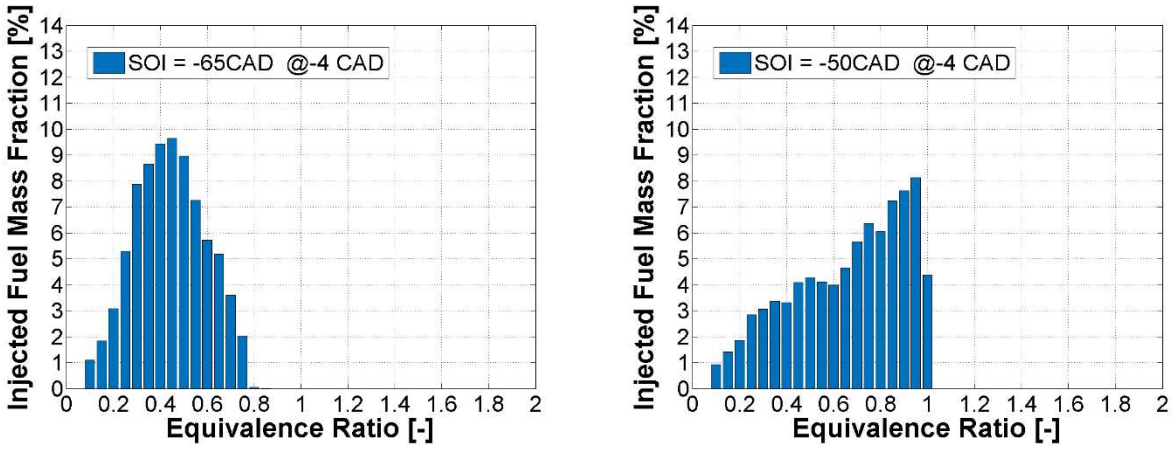

Figure 58. CFD computed fuel distribution as a function of the equivalence ratio for two injection timings corresponding to a spray target position in the upper bowl region. Initial conditions are reported in Table 7

Middle Bowl

The second region was named the middle bowl. More retarded SOI are needed to send the spray in this region, which is why it was not accessible to the wide UA156 injector. By targeting the middle of the bowl, the narrower injectors coupled with a retarded SOI were able to confine the fuel-air mixture preparation inside the bowl. Unlike what occurs when the spray targets the upper bowl region, the spray-bowl geometry interaction always avoided fuel being dispersed in the squish volume. All the injected fuel was concentrated inside the bowl, whatever the injection timing. Consequently, for SOI making it possible to enter this region, CO and HC are insensitive to the SOI, as well as the combustion efficiency, as indicated in Figure 49 and Figure 52. Moreover, with respect to the upper bowl region, the CA50 correlation with SOI is inverted, resulting in retarded combustion phasing when injection is delayed, as reported in Figure 50. As reported in Figure 56, the NOx trend is also inverted with respect to what was observed when spray targeted the upper bowl region, with NOx emission being reduced for delayed values of SOI. This is due to the fact that,

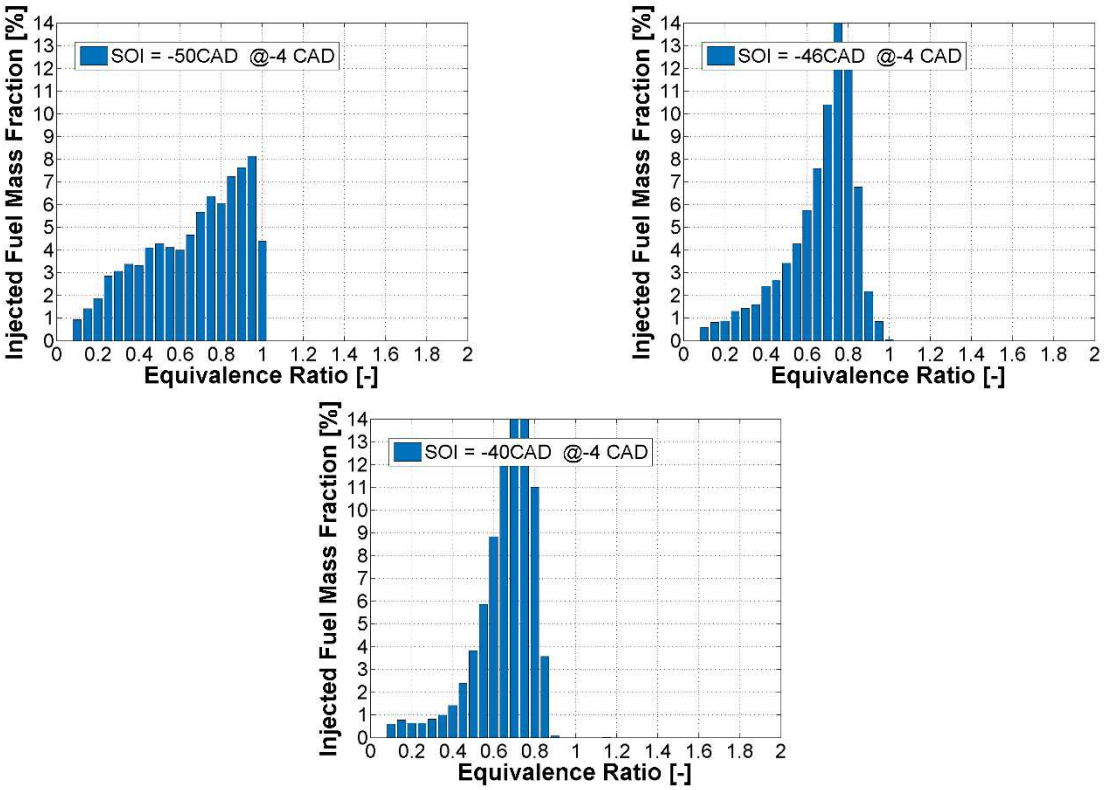

Figure 59. CFD computed Fuel distribution as a function of the equivalence ratio for different injection timings corresponding to a spray target position in the middle bowl region. Initial conditions are reported in Table 7

although the combustion was still characterized by a strong HCCI-like behavior, the equivalence ratio distribution was characterized by lower values of ϕ while the SOI was delayed, as reported in Figure 59.

Lower Bowl

Shifting the SOI closer to TDC moved the spray target position toward the third region, named lower bowl. In the case of the UA120, the SOI needed to enter this region was too late and the ignition delay of gasoline was too long to avoid the quenching of the oxidation reactions during the beginning of the expansion stroke. The lower bowl position was accessible only to the narrower UA90 for SOI occurring later than SOI = -40 CAD. As shown in Figure 56, Figure 52 and Figure 49, in this region, the NOx, the HC and CO emissions were less influenced by the SOI and the CA50 showed a reduced sensitivity to the injection timing. Figure 60 reports the fuel mass distribution as a function of the equivalence ratio prior to the onset of combustion. Differently from what happened in the previous regions, the shape of the fuel mass distribution was only slightly affected by the injection timing. The fuel distribution was similar for the different SOI, with the highest amount of fuel being distributed over the equivalence ratio range between 0.6 and 0.8. Exhaust measurements were characterized by low NOx emissions. This can be explained by the absence of fuel distributed over the close-to-stoichiometric regions responsible for NOx production. The low fuel stratification observed for this range of spray target positions can be due to the particular spray-bowl

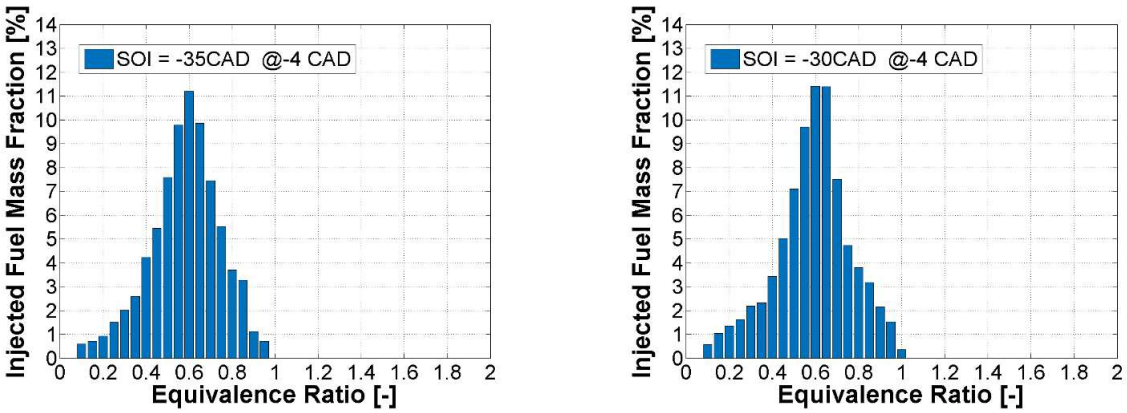

Figure 60. CFD computed fuel distribution as a function of the equivalence ratio for two injection timings corresponding to a spray target position in the lower bowl region. Initial conditions are reported in Table 7

geometry interference. In this regime, the direction of the spray-induced momentum is consistent with the slope of the bowl. Moreover, in view of the relatively early injection timing, there was a long time interval between injection and autoignition. Both factors favor the fuel-air mixing process, leading to a well-mixed fuel charge, with a stratification level almost independent of the injection timing. Combustion can therefore be considered to be characterized by a premixed-like regime, with autoignition and pollutant formations governed by chemical kinetics.

Bowl Pip

If fuel is injected late during the compression stroke with a 90° umbrella angle injector, the spray impacts the bowl pip. The increased stratification occurring with later injection timing frequently generated richer and colder fuel pockets. Reduced amounts of fuel were distributed over the leaner and hotter fuel regions characterized by higher reactivity. In this combustion regime, the CA50 and NOx were again sensitive to the injection timing, cf. Figure 56.

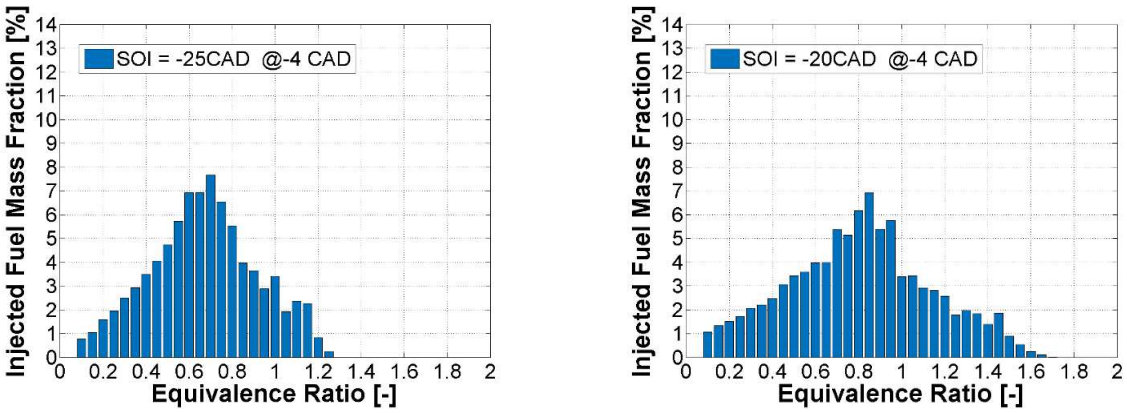

Figure 61. CFD computed fuel distribution as a function of the equivalence ratio for two injection timings corresponding to a spray target position in the lower bowl region. Initial conditions are reported in Table 7

In this region, an increase in NOx emission was observed when CA50 was retarded by the SOI. This trend was due to the impact on combustion of the increased fuel stratification occurring at later SOI. As can be seen in Figure 61, retarded SOI shifted the local equivalence ratio distribution making the presence of richer and colder fuel pockets more probable. Accordingly, combustion phasing was delayed as a consequence of the reduced amount of fuel distributed over the more reactive intermediate equivalence ratio. Delayed SOI therefore tended to induce slower combustion development, which can explain the CA50 trend. Moreover, higher local temperatures originated from the oxidation of over-rich fuel regions, promoting NOx emission.

4.5. DOUBLE INJECTION STRATEGY

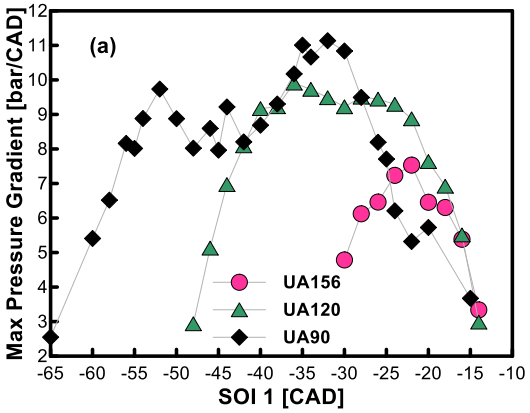

Figure 62. In-cylinder maximum pressure gradient as a function of SOI and for different injector umbrella angles under single injection GCI operation. Experimental conditions are reported in Table 7

Figure 62 reports the maximum in-cylinder pressure gradient as a function of SOI for the three injectors tested. Generally, in order to avoid excessive mechanical stress and noise, a maximum acceptable level of 5 bar/CAD should be considered. It can be seen that the pressure rise rate in most cases dramatically exceeded the accepted level, which is indicative of the motor's tendency to knock. Figure 62 shows that the maximum pressure rise rate tended to diminish for SOI closer to TDC. However, these more silent conditions corresponded to the experimental point characterized by low combustion efficiency and late combustion phasing. The results from the maximum pressure rise rate indicated that despite the low amount of fuel injected, single injection was not suitable for GCI operation in these operating conditions. In order to slow down the heat release and the pressure increase, double injection can be employed.

The influence of the umbrella angle was investigated while a double injection strategy was adopted. The injection duration was adjusted in order to obtain an equal distribution of the fuel mass over the two injection events. Both the injection timings of the first and second injection were varied over a wide range of SOI. In accordance with the results of the previous section, the maximum advance in injection timing of the first injection, SOI1, was chosen so as to contain the fuel charge in the bowl and to maximize the combustion

efficiency. Therefore, the most advanced injection timing of the first injection was -60 / -50 – 35 for UA90/UA120/UA156 respectively.

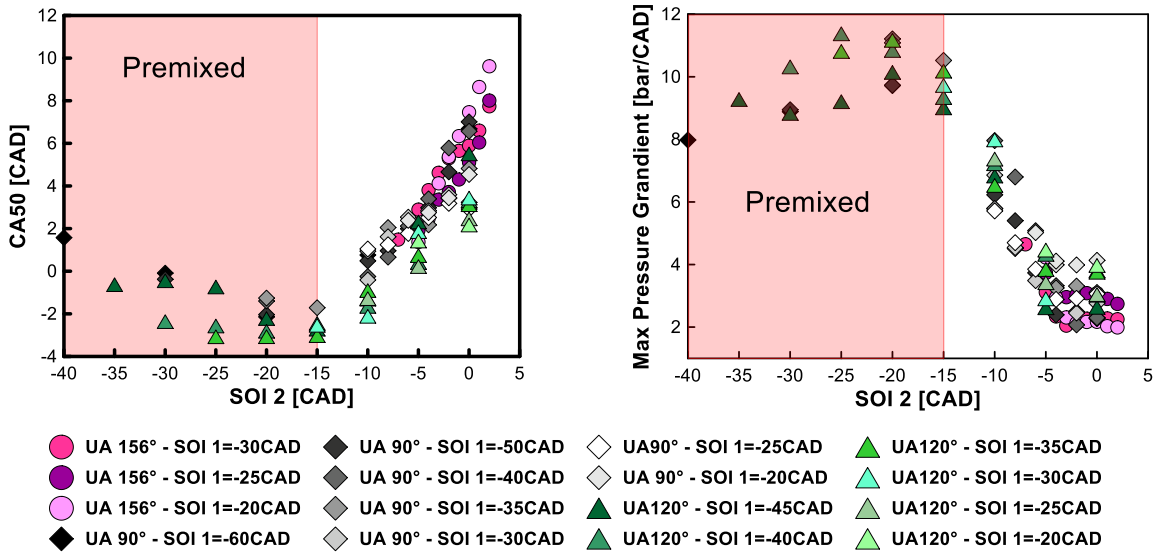

Figure 63. CA50 and in-cylinder maximum pressure gradient as a function of SOI1 and SOI2. Experimental conditions are reported in Table 7

Figure 63 shows the combustion phasing and the maximum pressure gradient as a function of the timing of the first and second injection for the three injectors tested. Irrespective of the timing of the first injection, a clear differentiation in combustion behavior was observed when the second injection went through SOI2 = -15 CAD.

For early second injection timings SOI2, the double injection strategy was ineffective. Both the CA50 and the maximum pressure gradient were mainly insensitive and not controllable by the injection timing. This result is related to the inability of early injections to induce a sufficient degree of stratification. With too advanced SOI2, combustion was generated from a well-mixed charge, and engine operation approached the HCCI-like regime characterized by a kinetically controlled premixed combustion leading to high heat release and pressure rise rate, similar to those observed in single injection operation, as can be seen in Figure 63. In order to become effective, the double injection strategy had to be performed by delaying the second injection timing. Supplying the second fuel mass later than SOI2 = -15 CAD led to a drastic variation in the combustion behavior, and the double injection strategy became an effective means of controlling the heat release. For SOI occurring later than SOI2 = -15 CAD, the CA50 became a monotonic function of the SOI2, allowing combustion phasing to be controlled. Moreover, the maximum pressure rise rate was dramatically reduced and the measured values of the in-cylinder pressure gradient decreased from 10 bar/CAD to 3

bar/CAD when SOI2 moved from SOI2=-15 CAD to SOI2 = -5 CAD. The double injection strategy was also an effective means to reduce NOx emissions, which are reported in Figure 64. It can be clearly seen that in the premixed regime, NOx emissions were high and not controllable by the timing of the second injection. As in the case of CA50 and the MPRR, NOx emissions became extremely sensitive when the second injection timing occurred later than SOI2 = -15CAD. A reduction from NOx= 2000 ppm to below NO = 250 ppm was observed by moving the SOI2 from SOI2 = -15CAD to SOI2 = 0 CAD. The reduced NOx emissions were in accordance with the above-mentioned delay in the CA50.

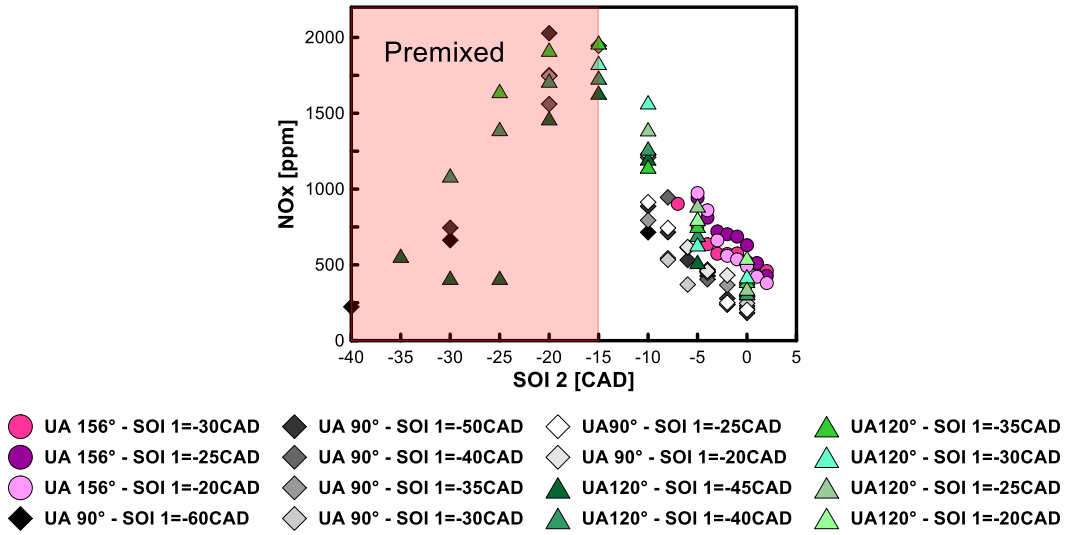

Figure 64. NOx as a function of SOI1 and SOI2. Experimental conditions are reported in Table 7

4.5.1. Impact of the timing of the second injection on combustion behavior

Figure 1 reports the heat release rate, the in-cylinder pressure gradient, and the in-cylinder temperature and pressure traces as a function of the SOI2 while the timing of the first injection was maintained constant at SOI1 = 35 CAD. The UA120 was chosen as an example but the observations are valid for all the other injectors tested. Heat release rate traces showed the typical premixed shape for SOI = -20 CAD, confirming that for SOI earlier than SOI2 = -15 CAD, combustion was characterized by a typical HCCI-like regime. When SOI2 was sufficiently delayed, combustion phasing became sensitive to the injection timing, and for SOI = -10 CAD, the heat release rate (HRR) shape presented a lower peak and a larger extension with respect to the case of SOI 2 = -20CAD. This indicates that the delaying impact of SOI2 on the CA50 was mainly due to an increased level of stratification of the fuel, which retarded combustion by introducing richer and colder fuel pockets responsible for the tailoring of the heat release. For further retarded SOI2, the mechanism underlying the shift in combustion phasing was different, as indicated by the double-peak shape of the heat release rate traces corresponding to SOI2=-5 CAD and SOI2= 0 CAD. The double peak

shape indicates that for the latter conditions, the first fuel mass ignited before its combustion was temporarily slowed down by the cooling effect induced by the second cold direct injected fuel portion. Combustion of the second injected mass occurred later, as indicated by the second peak in the HRR trace. In this SOI2 range, the ability of the second injection to control the combustion phasing has therefore to be attributed to the increase in combustion duration induced by the thermal cooling effect of the second mass rather than to the impact of local fuel stratification.

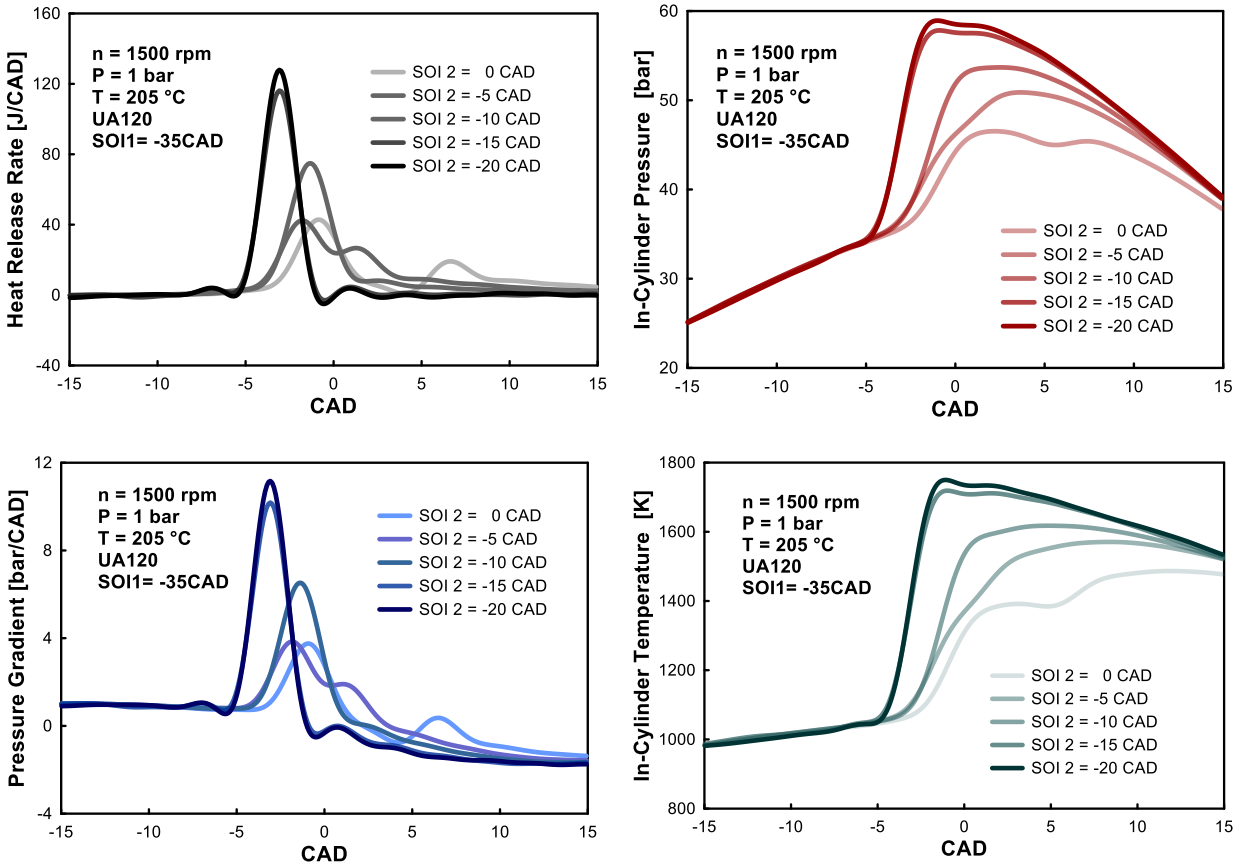

Figure 65. Heat release, in-cylinder pressure, in-cylinder pressure gradient, in-cylinder temperature traces for different timings of the second injection SOI 2 and for a fixed timing of the first injection at SOI 1 = -35 CAD. Experimental conditions are reported in Table 7.

This different combustion behavior at SOI2 = -5 CAD is also reflected in the trends of the in-cylinder maximum pressure gradient. Figure 65 shows that the in-cylinder pressure gradient can be significantly reduced by moving the second injection timing. On closer inspection, it can be seen that the maximum pressure gradient becomes insensitive to the timing of the second injection if the latter takes place later than SOI2 = -5 CAD. This is due to the change in combustion behavior previously discussed. As shown in Figure 65, the pressure gradient traces also exhibit a transition from a single to a double peak shape when SOI 2=-5 CAD. However, the maximum pressure gradient is always associated to the first peak, corresponding to the combustion of the first mass, as can be seen by looking at the in-cylinder pressure trace reported in

Figure 65. This second injection timing is consequently ineffective to reduce the maximum pressure gradient when the second injection occurs after the ignition of the second mass. Figure 65 gives the in-cylinder temperature traces for the same experimental conditions. It is evident that for an injection timing earlier than SOI2 = -5CAD, the reduction in bulk temperature is associated to a delay in the combustion phasing. For a further delay in SOI2, the reduction of the maximum in-cylinder bulk temperature was additionally favored by the cooling effect associated to the second fuel portion, which freezes the temperature rise associated to the combustion of the first fuel mass. The lowering of the mean in-cylinder temperature is the main cause of the NOx reduction with SOI2 observed in Figure 64.

4.5.2. Impact of the timing of the first injection on combustion behavior

Figure 66 shows the emission of unburned hydrocarbon HC and carbon monoxide CO as a function of SOI2 and SOI1 for the three injectors tested. It can be noticed that the biggest impact on HC was due to the first injection timing. As shown in Figure 66, unburned hydrocarbon may originate from the squish region when the first injection is too advanced (i.e. for SOI1=-60 and SOI1=-45CAD for the UA90 and UA120 cases respectively).

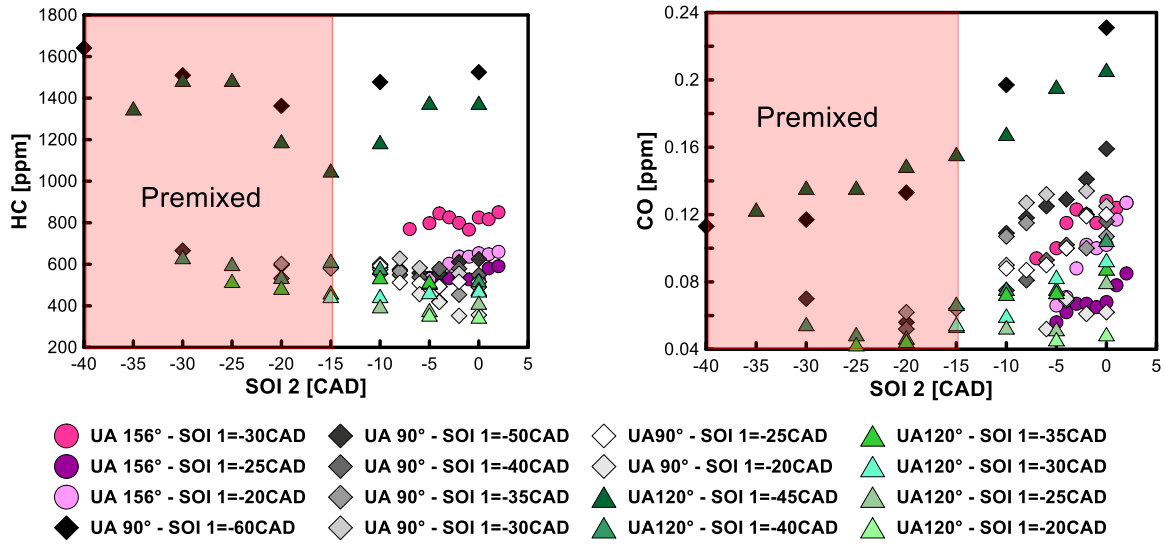

Figure 66. HC and CO as a function of SOI1 and SOI2. Experimental conditions are reported in Table 7

For the SOI1 range over which the charge is concentrated inside the bowl, HC emissions decreased when the SOI 1 was moved toward TDC, due to the reduced overleaning induced by the shorter mixing period. Similar remarks can be made for CO emissions, which are reported in Figure 66 for the same experimental conditions. Overleaning induced by the shorter mixing period and an advanced first injection timing led to an increase in CO formation. Moreover SOI2 also had a significant impact, with CO emission increasing for delayed SOI2; this is due to the decrease of the in-cylinder bulk temperature, which can be observed in

Figure 67. The reduction of the in-cylinder temperature, which is a consequence of the increased CA50, reduced the efficiency of the CO to CO_2 conversion.

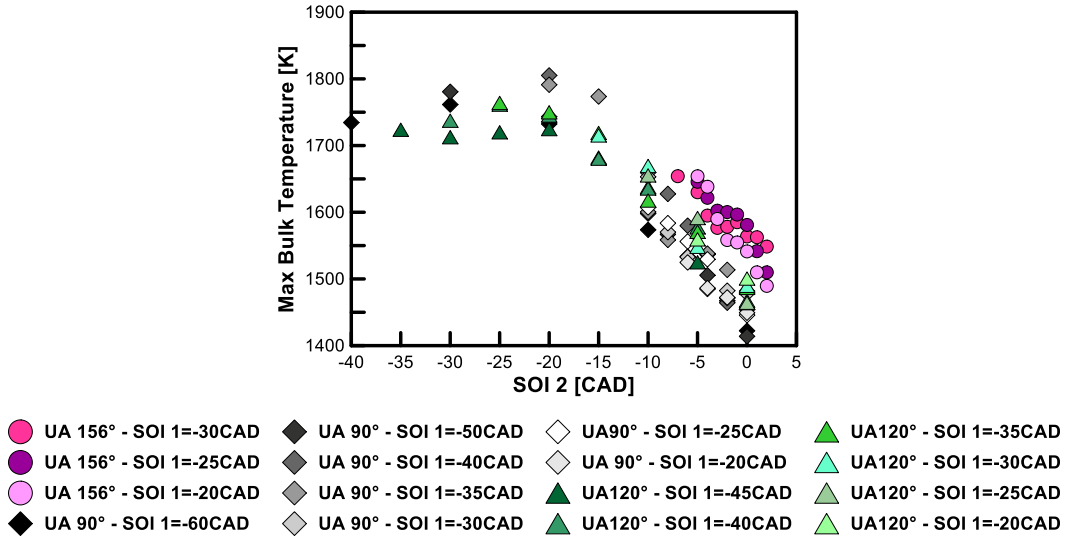

Figure 67. In-cylinder maximum bulk temperature as a function of the SOI1 and SOI2 and for different injector umbrella angles. Experimental conditions are reported in Table 7

4.5.3. Impact of the umbrella angle on the double injection strategy

The impact of the timing of both the injection events was similar for every injector tested. However, for the same intake thermodynamic conditions, different combustion phasings resulted from the use of different umbrella angles, cf. Figure 63. In order to compare the performances of the three injectors, it is useful to compare the results as a function of the CA50.

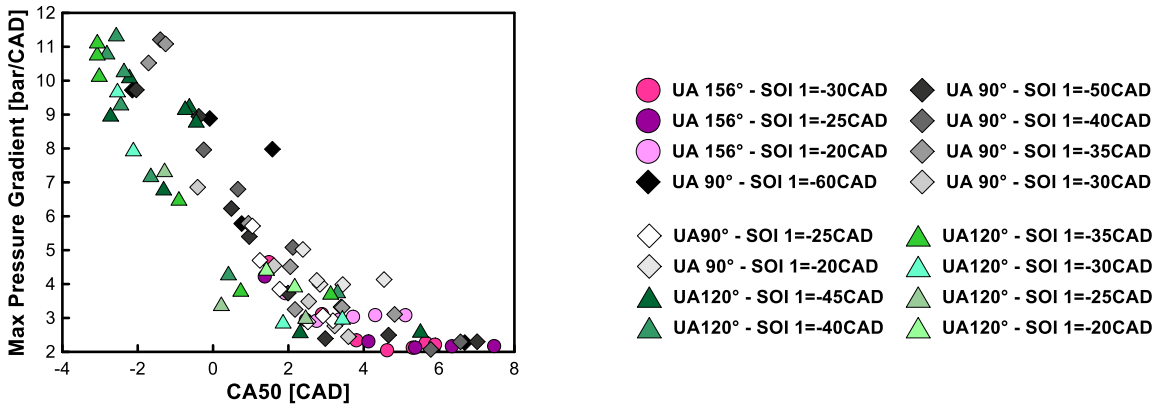

Figure 68. In-cylinder maximum pressure gradient as a function of CA50 for different injector umbrella angles. Experimental conditions are reported in Table 7

Figure 68 reports the trends for the maximum in-cylinder pressure gradient as a function of CA50 for all the injectors tested. Whatever the injection timing, the in-cylinder maximum rise rate proved to be much more sensitive to the combustion phasing than to the injector umbrella angle.

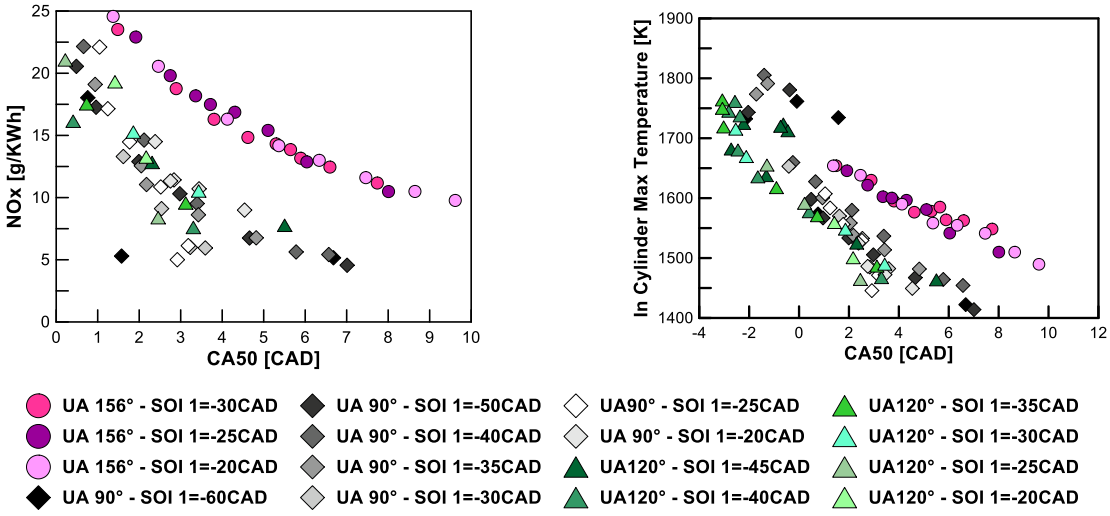

Figure 69. NOx emission and maximum bulk temperature as a function of CA50 and for different injector umbrella angles. Experimental conditions are reported in Table 7

Figure 69 reports the NOx emission and the in-cylinder maximum bulk temperature as a function of the combustion phasing. The scatterplot indicates that the production of nitrogen oxides was generally lower for the UA90 and UA120 injectors. UA156 showed a higher NOx production. Figure 69 indicates that the increased NOx exhaust concentration in the case of the UA156 injector can be attributed to an increase in the combustion temperature associated with the use of the larger umbrella angle injector. A possible explanation for the higher in-cylinder bulk temperature can be found by analyzing the combustion duration, which is reported in Figure 70. Results from experiments showed that the UA156 injector led to a shorter combustion process.

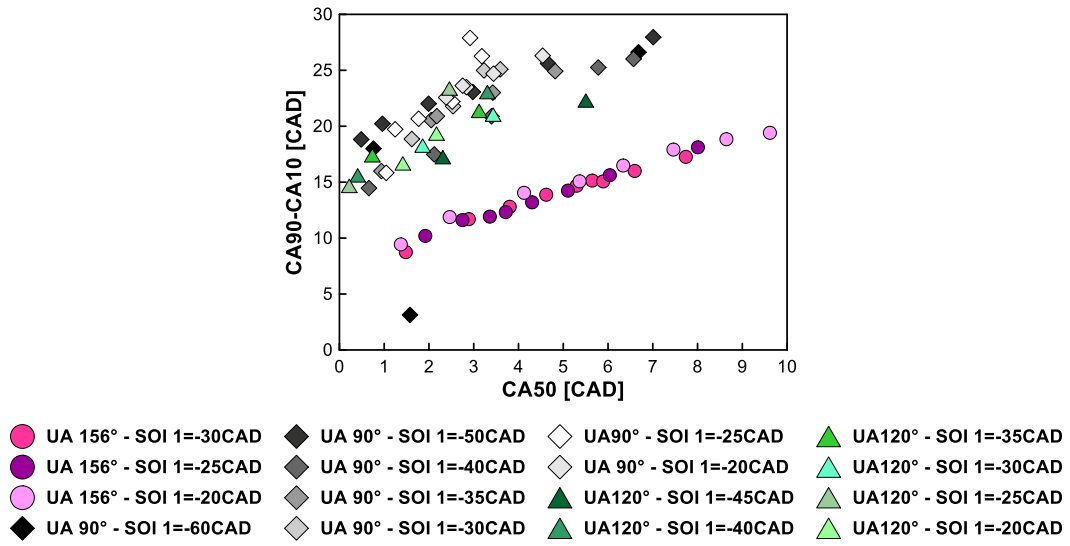

Figure 70. Combustion duration as a function of CA50 for different injector umbrella angles. Experimental conditions are reported in Table 7

The faster heat release observed in the UA156 case could be the reason for the greater in-cylinder temperature rise, and therefore for the increased production of nitrogen oxides.

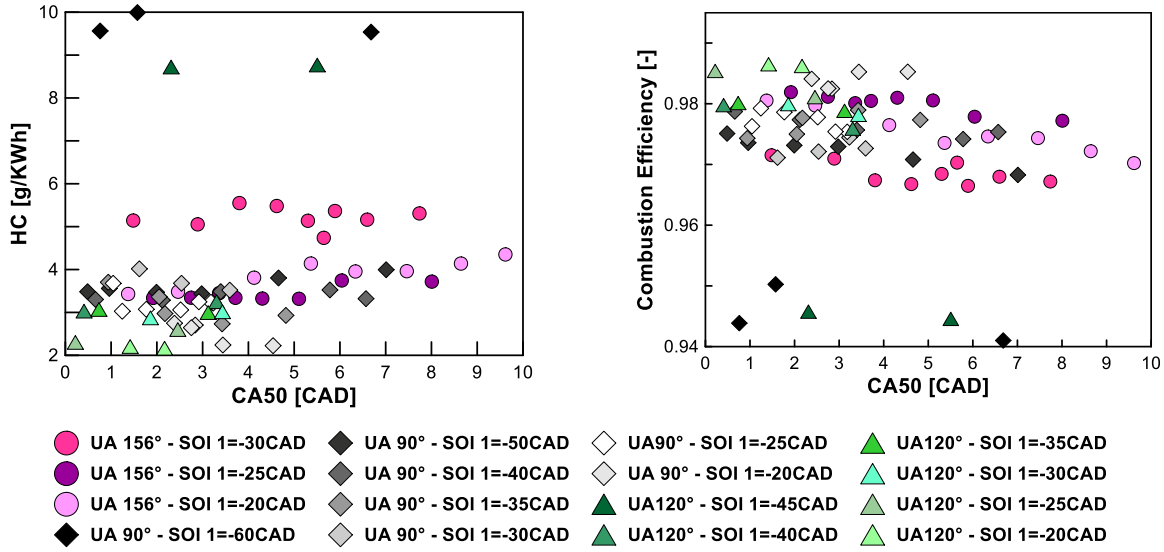

Figure 71. HC emission and combustion efficiency as a function of CA50 and for different injector umbrella angles. Experimental conditions are reported in Table 7

Despite the slower heat release rate and lower in-cylinder bulk temperature, Figure 71 shows that the UA120 and UA90 showed better performances in terms of HC and combustion efficiency for a given combustion

phasing. This result can be explained by the ability of a narrower umbrella angle to better concentrate the fuel charge inside the piston head bowl.

Figure 72 compares the pollutant emissions of NOx and HC and the indicated efficiency resulting from the use of different umbrella angles. It can be seen that the UA156 and UA120 injectors offered the best tradeoff between HC emission and indicated efficiency. In the case of the UA120 injector, the higher indicated efficiency can be explained by the higher combustion efficiency previously discussed. While the lower combustion efficiency observed in the case of the UA156 could penalize the indicated efficiency, this low combustion efficiency can compensate for the faster combustion, leading to a higher effective expansion ratio and therefore a reduction in the heat losses at the exhaust. The UA156 and UA120 also performed better in terms of indicated efficiency and NOx emission. Concerning the pollutant emission of HC and NOx, reduced umbrella angles offered better performances because of their ability to concentrate the fuel charge in the bowl, thus avoiding overleaning, and because of the reduced in-cylinder bulk temperature due to the slower heat release rate.

Although the three injectors tested did not substantially differ, the use of an intermediate UA120 could represent a good trade-off between pollutant emissions of NOx and HC and indicated efficiency. The use of the narrowest umbrella angle, UA90, can be motivated by the decision to adopt HCCI-like combustion with a first injection characterized by early injection timing. However, it is suggested here that the choice of the injector system should be evaluated by taking into account the engine operating over the entire load range. Moreover the injector characteristics have to be optimized by considering also the possibility of adapting the piston head shape according to the combustion mode. It has been demonstrated in the literature that the use of a wider umbrella angle is optimal for higher load operations. The results of the investigation performed at low load indicated that the choice of an intermediate umbrella angle such as the UA120 could be a suitable choice in order to achieve efficient combustion and relatively low pollutant formation over a wider operating range.

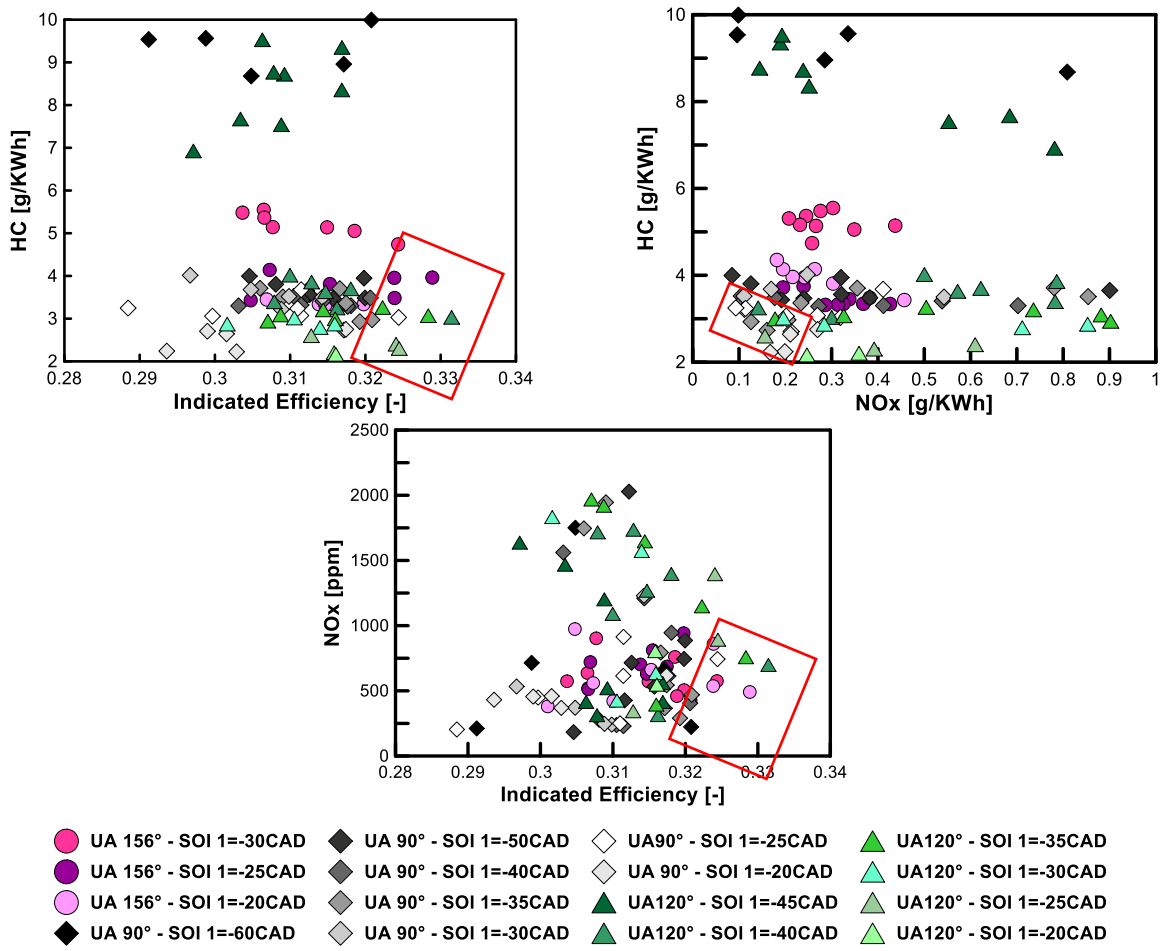

Figure 72. HC versus Indicated efficiency, HC versus NOx and NOx versus Indicated efficiency for the different injectors tested. Conditions are reported in Table 7

4.6. CONCLUSIONS

Under low load GCI operation, heating up the intake air charge is necessary to shift the motoring P-T trajectory in order to satisfy the high thermodynamic demand of lean and hard-to-ignite gasoline/air mixtures. In this chapter, high intake air temperatures were employed to achieve autoignition of a RON 95 commercial gasoline in a conventional DW10 Diesel engine.

The investigations first focused on understanding the combustion behavior when fuel was supplied through a single injection event.

The occurrence of autoignition, the combustion behavior and pollutant formation are impacted by the injection strategy due to its effect on the in-cylinder fuel distribution, which can be characterized by the induced in-cylinder temperature-equivalence ratio fields. Results from 3D CFD simulations using a five-component surrogate of a commercial gasoline indicated that at the low intake pressure conditions of low load operations, gasoline exhibits a low ϕ-sensitivity. The most reactive regions in which autoignition occurred are characterized by a lean equivalence ratio in the order of ϕ~0.45 and a high local temperature of T~1100K. The heat released during the initial ignition of the leaner fuel region sequentially triggers the combustion of progressively richer fuel pockets, which are responsible for increasing the in-cylinder temperature and therefore promoting the production of nitrogen oxides.

Results from experiments and CFD showed that under specific conditions, early injection can generate a well-mixed fuel/air mixture but that a substantial part of the fuel has close-to-stoichiometric values of equivalence ratio, i.e. $0.85<\phi<1.1$. Under this injection timing range, NO production can be promoted, leading to an abnormal increase in the exhaust concentration of nitric oxide. In the same conditions, an abnormal acceleration of the combustion phasing was observed. Results from experiments showed that this dramatic acceleration in combustion was partially driven by the promoting effect on gasoline oxidation due to the nitrogen oxide trapped in the residual burnt gases.

The impact of the injector umbrella angle on combustion was investigated under single injection operation. The umbrella angle defines the earliest injection timing allowed for each injector. Results showed that with a narrower umbrella angle it was possible to advance the injection timing without leading to excessive HC and CO emissions responsible for the deterioration of the combustion efficiency and indicated efficiency. This is due to the ability of narrower umbrella angles to direct the fuel spray more steeply downward, concentrating the fuel/air mixing inside the piston head bowl. In this way, fuel dispersion in the crevices and the overleaning occurring when fuel spray targeted the squish volume were avoided. Within the high efficiency injection timing range, combustion behavior depended on the spray target position, which is a

combination of the injection timing and the umbrella angle. Combustion behavior was shown to be mainly impacted by the spray target positon. For an SOI-UA combination leading the spray to target the same piston head position, the trends in combustion phasing and pollutant emission were similar whatever the injector employed.

Despite the low amount of fuel injected to attain low load operation, single injection operation proved to be characterized by an excessive in-cylinder pressure gradient. A double injection strategy was therefore adopted. Results showed that a double injection strategy was an effective means of combustion control. By appropriately timing the second injection, it was possible to simultaneously reduce the in-cylinder pressure rise rate and NOx emission by progressively delaying the combustion phasing. Depending on the timing of the second injection two mechanisms drive the combustion phasing delay. If the second mass is injected early enough, the second injection timing induces partial fuel stratification which delays autoignition by introducing richer and colder fuel pockets. If the timing of the second injection is delayed, autoignition of the first injected mass can occur, and then the cooling effect induced by the second fuel mass extends the combustion duration, increasing the combustion phasing. Moreover, in-cylinder temperatures are reduced and NOx emission drastically reduced.

The impact of the injector umbrella angle was also investigated under double injection low load operation. Results showed that under the experimental conditions considered in the study, a narrower umbrella angle generally reduced the emission of unburned hydrocarbon and that wider umbrella angles were characterized by a higher indicated efficiency. However, the absolute difference in the different injector performances was relatively small. The results suggested that the choice of the injection system has therefore to be made by considering the whole operating map of the engine.

5. Ozone Impact on HCCI Gasoline Combustion

5.1. INTRODUCTION

The aim of this section is to study the impact of ozone on the combustion of commercial gasoline fuel. Ozone has been shown to have a promoter effect based on the alteration of the complex chemical kinetics that governs the oxidation of hydrocarbons. Direct-injection compression ignition engines form an environment where complex physical phenomena such as multiple fuel injections in the form of sprays and the aerodynamics induced by the swirl overlap with the complex oxidation chemistry. To obtain an in-depth and fundamental understanding of the ozone-hydrocarbon interaction, it is necessary to simplify the study conditions to the greatest extent to isolate the effect of ozone on the combustion chemistry from other complex phenomena. To meet these requirements, this chapter will present the results of the experiments carried out in a light-duty CI engine converted to work under fully premixed conditions in which the thermodynamic and chemical composition of the intake charge, including the ozone concentration, can be accurately controlled. The impact of ozone on gasoline combustion can thus be studied before being investigated in a more complex environment such as that offered by direct injection conditions.

5.2. GASOLINE PREMIXED COMBUSTION UNDER NON SEEDED CONDITIONS

In this chapter the experiments performed under HCCI conditions will be discussed. In this engine mode, before entering the engine cylinder the liquid fuel is premixed with air according to the desired equivalence ratio and then heated up by an intake evaporator. The vapor phase fuel-air mixture thus obtained is then injected into an intake plenum whose thermodynamic conditions are maintained under control. Then, at every intake valve opening, the fuel-air mixture enters the cylinder. Although the fuel-air mixture is similar to that used in port fuel SI engines, autoignition of the mixture is not initiated by a spark but through compression by the piston. Once in the cylinder, the mixture is compressed and autoignition is governed by the chemical kinetics. At given initial thermodynamic conditions, the compression ratio and the wall losses, together with the equivalence ratio, define the temperature and pressure path that trigger the oxidation reactions responsible for autoignition of the fuel. In such a chemically-driven combustion mode, variations in the intake temperature and pressure have an important impact on autoignition and consequently on the characteristics of the combustion process such as heat release trace, noise and pollutants. If the use of EGR is excluded, for a given equivalence ratio the combustion phasing, which determines noise and pollutant emissions, is only a function of the intake thermodynamic conditions. By running the intake thermodynamic conditions it is possible to define on a T – P plane the region in which fuel autoignition takes place. Figure 73 shows the autoignition region obtained by fueling the engine with SP95 gasoline. The fuel-air equivalence ratio was set at 0.3 and the engine speed was fixed at 1500 rpm. No EGR was employed. The limits of self-ignition regions were arbitrarily defined as those pairs of P and T that corresponded to CA50

values between 0 and 7 CAD. The CA50 is here represented as a function of different variable sets. In Figure 73(a), the CA50 is shown as a function of the intake temperature and pressure.

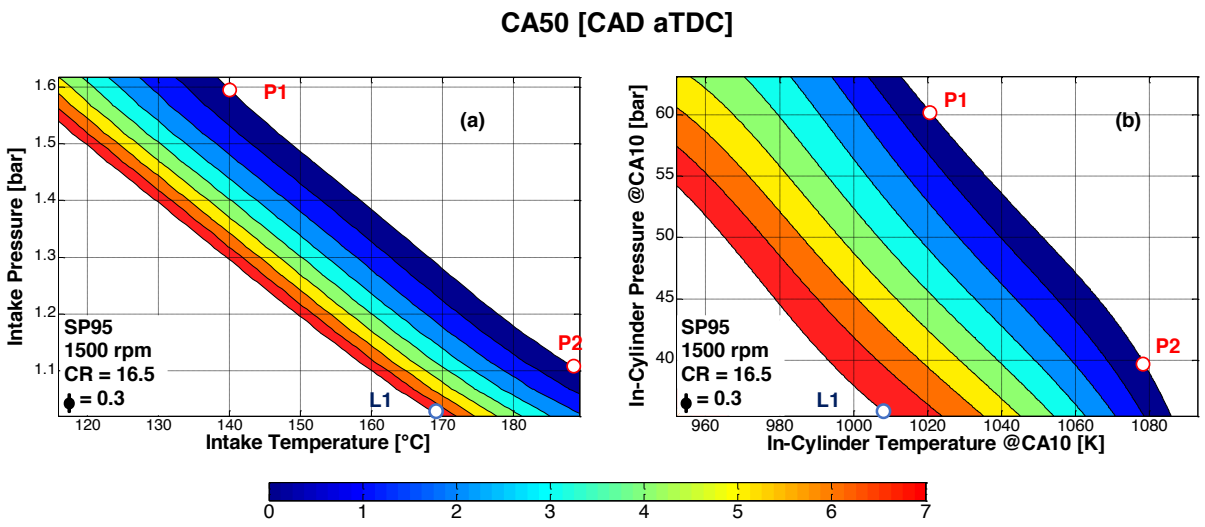

Figure 73. Combustion phasing CA50 as a function of intake temperature and pressure (a). CA50 as a function of the in-cylinder temperature and pressure at CA10 (b).

Figure 73(b) shows the CA50 as a function of the in-cylinder temperature and pressure estimated at autoignition, here considered as the CA10. This representation provides the results with a more universal value, making the data more easily comparable with experiments carried out in other experimental apparatus (combustion vessel, rapid compression machines). Figure 73 clearly shows how both temperature and pressure independently contribute to providing the minimum energy input required to activate the oxidation reactions. By independently tuning the pressure and temperature in the intake manifold, it is possible to obtain the in-cylinder thermodynamic conditions required for autoignition of the mixture in the final part of the compression stroke. Different combinations of T-P values enable combustion with the same combustion phasing. For example, consider the experimental conditions labeled P1 and P2 in the two graphs on Figure 73. At constant combustion phasing, increasing the intake pressure reduces the intake temperature and vice versa. As shown in Figure 73 (a), the CA50 can be set at TDC by means of 1.3 bar and 140 °C at the intake in P1. The same CA50 can be obtained in P2 by reducing the intake pressure to 1.1 bar and increasing the intake temperature up to 190°C. For the same experimental conditions, the in-cylinder values of pressure and temperature are shown in Figure 73 (b). P1 corresponded to the high pressure-low temperature combination, with the minimum estimated autoignition temperature of 1020 K for an in-cylinder pressure of 60 bar. In the transition from the high pressure-low temperature combination P1 to the low pressure-high temperature combination P2, the in-cylinder pressure decreased to 40 bar while the minimum temperature required for autoignition rose to 1080 K. This indicates that the lower the intake pressure is, the higher the intake temperature required for autoignition. These considerations are particularly important when

considering low-load operational conditions, when engine combustion originates from lean fuel-air mixtures, the exhaust gas enthalpy content is limited and the turbocharger does not provide extra pressure at the intake. The L1 experimental conditions reported in Figure 73 are representative of such low load atmospheric operations. As can be noted in Figure 73 (a), under atmospheric conditions the high octane number gasoline tested required an intake temperature above 170°C to autoignite. Such intake temperatures are not available on conventional CI engines. Intake air heaters or a Variable Valve Actuator necessary to trap hot residuals should be employed to improve the reactivity of the intake charge.. The following sections assess the potential of using an ozone generator to seed the intake air with ozone in order to improve the oxidizing power of the intake charge. Ozone seeding can provide a further degree of freedom in the control of the combustion event and a means of extending the autoignition region of gasoline fuel under compression ignition conditions.

5.3. OZONE ASSISTED GASOLINE PREMIXED COMBUSTION

This section describes the impact of ozone on gasoline combustion under HCCI operation. The analysis of the results from the experiments is divided in two main sections. The first section describes the effect of seeding the intake of the engine with ozone after combustion has already been established by means of intake thermodynamic conditions favorable to autoignition. The second section reports the results of the experiments concerning the use of ozone to extend the limits of the autoignition region of the fuel.

5.3.1. Effect on thermodynamically established combustion

The term "thermodynamically established combustion" here refers to experimental conditions in which fuel autoignition is obtained by sufficiently increasing the pressure and temperature at the intake at a fixed engine speed and for a given fuel-air equivalence ratio. Table 9 reports the experimental settings considered as a baseline condition for studying the impact of ozone on gasoline thermodynamically established combustion.

Thermodynamically Established Combustion Baseline Conditions				
Fuel	Engine Speed	Intake Temperature	Intake Pressure	Ozone
Gasoline	1500 rpm	134 °C	1.3 bar	0 ppm

Table 9. Experimental conditions leading to thermodynamically established combustion. These experimental conditions represent the baseline conditions for studying the effect of ozone.

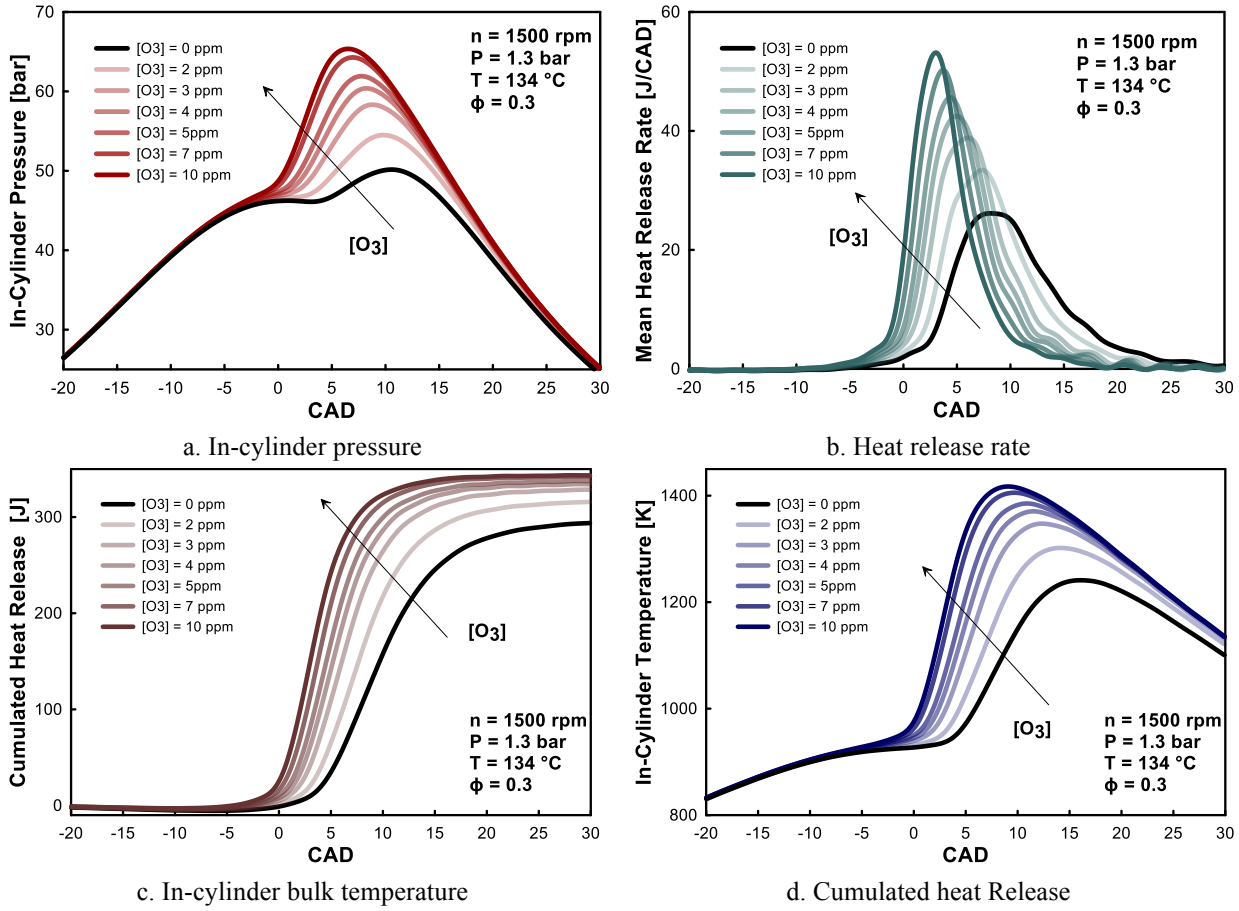

Figure 74. Impact of different intake ozone concentrations on HCCI combustion of gasoline.

Figure 74 shows the effect of seeding the intake of the engine with different concentrations of ozone on the in-cylinder pressure, temperature, heat release rate and cumulated heat release. It should be noted that ozone was added after autoignition had been ensured by means of high intake temperature and pressure. As can be seen, combustion is highly sensitive to ozone addition. Small intake concentrations of ozone, in the order of tens of ppm, can drastically modify the combustion of gasoline. Results clearly show an overall improvement in combustion when ozone was added at the intake of the engine. As can be seen in Figure 74 the in-cylinder pressure traces show an increase in the peak pressure and an advance in its location when ozone seeded the intake of the engine. Figure 74 (b) shows that the in-cylinder pressure trends are related to an advance of the heat release rate, which indicates that combustion took place earlier during the cycle. Moreover, the higher heat release rate indicates that the combustion reaction is speeded up and that combustion released a higher fraction of heat when ozone was added. As can be deduced by the higher value of the cumulated heat release reported in Figure 74 (c), ozone addition advanced and improved the quality of fuel oxidation. These results demonstrate that ozone allows for an improved exploitation of a certain mass of fuel, which is probably due to an improvement in the combustion efficiency. Because ozone advanced

the onset of the reaction leading to fuel autoignition, combustion took place earlier during the cycle and heat was released in a smaller volume. Accordingly, higher in-cylinder temperatures were registered for higher concentrations of ozone, as can be observed in Figure 74 (d). It should be noted that even if ozone is thought to alter the reaction path by acting mainly on the initiation of the oxidation process, no cool flame heat release was observed during the experiment. Gasoline is composed of several chemical components: iso-octane, n-heptane, toluene and several other compounds. Some of these fuels, if burned alone, can show a double stage heat release governed by a low temperature chemical kinetics. Previous studies showed that the cool flame was highly sensitive to ozone addition for fuels exhibiting double stage heat release. While the commercial gasoline tested undoubtedly contains compounds having such properties (n-heptane for example), no low temperature heat release associated to ozone additions was observed during the experiments, as evidenced in Figure 74 (b) and Figure 74 (c).

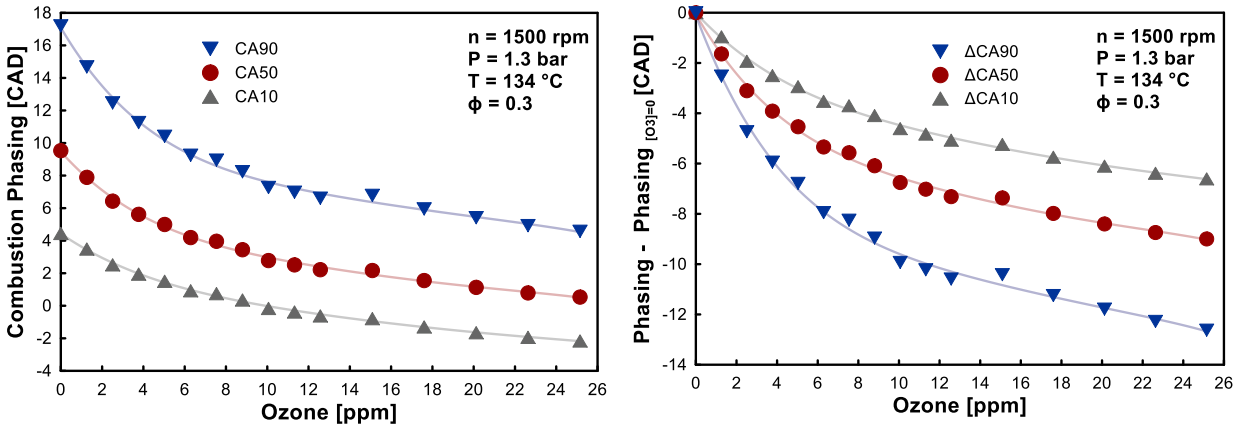

a. CA10, CA50 and CA90 as a function of ozone concentration

b. Shift in CA10, CA50 and CA90 as a function of ozone concentration

Figure 75. Impact of different ozone concentrations on the phasing of HCCI combustion of gasoline

5.3.1.1.Impact on the combustion phasing

From the results shown in Figure 74 it is possible to deduce that two combined effects occur when the fresh charge is seeded with ozone. A general strengthening of the combustion process is exhibited through the advance of combustion itself and through a greater energy release. To isolate the effect on the combustion phasing, Figure 75 shows, as a function of the initial ozone concentration, the evolutions of CA10, CA50 and CA90, respectively representative of the initial phase, the main phase and the end of the heat release. As can be seen from Figure 75 (a), all three combustion phases undergo an advance due to the addition of ozone. The effect is progressive and the phasing advance increases with the increase in the initial ozone concentration. It is interesting to note that the combustion advance is more pronounced for small concentrations of ozone, with CA10, CA50 and CA90 exhibiting an almost exponential behavior for ozone concentrations below 10 ppm. For higher concentrations, the sensitivity of the three parameters to ozone is slightly reduced, and the experimental points seem to align with an almost linear fit. In order to better assess

and quantify the impact of ozone on the combustion phasing, Figure 75 (b) shows the shift, with respect to the non-seeded case, that ozone induced in the CA10, CA50, and CA90. The most pronounced phase advance was recorded on CA90, while relatively lower impacts were observed respectively on CA50 and CA10. For example, for an intake concentration of 10 ppm of ozone, the start of combustion CA10 had an advance of 4 CAD, the main flame CA50 shifted 6 CAD towards TDC, while the combustion ended with 10 CAD of advance with respect to the non-seeded case. Chemical Kinetics Analysis showed that ozone alters the chemical reactions that initiate the fuel oxidation process. It could be therefore expected that the biggest effect would be recorded on the initial stages of heat release i.e. CA10. However, it should be kept in mind that combustion takes place in a dynamic environment such as the combustion chamber of an internal combustion engine. By favoring the initiation of autoignition by replacing oxygen molecules with oxygen atoms, ozone advances the appearance of exothermic reactions, which occur in a smaller volume compared to the non-seeded case, favoring a faster elevation of the in-cylinder temperature compared to the non-seeded case. Consequently, the more the exothermic chemical reactions succeed one another in the course of combustion, the more they benefit from the greater energy made available by the reactions that precede them. Each chemical reaction therefore originates from more favorable initial conditions compared to the case without ozone, leading to an overall acceleration of the heat release process. Consequently, the ozone-induced benefits accumulate as the combustion process progresses. As a result, the more the combustion process progresses, the more it will be in advance with respect to the non-seeded case. This mechanism could explain the trends observed in Figure 75. To further support this hypothesis, Figure 76 shows the evolution of the combustion duration for the same experimental conditions. As can be seen, combustion was faster as the ozone concentration increased, indicating a faster rate of heat release. Moreover, the reduction in combustion duration also increased with increased ozone concentration, as shown in Figure 76(b). This behavior constitutes a valid demonstration and a support for the hypotheses expressed above.

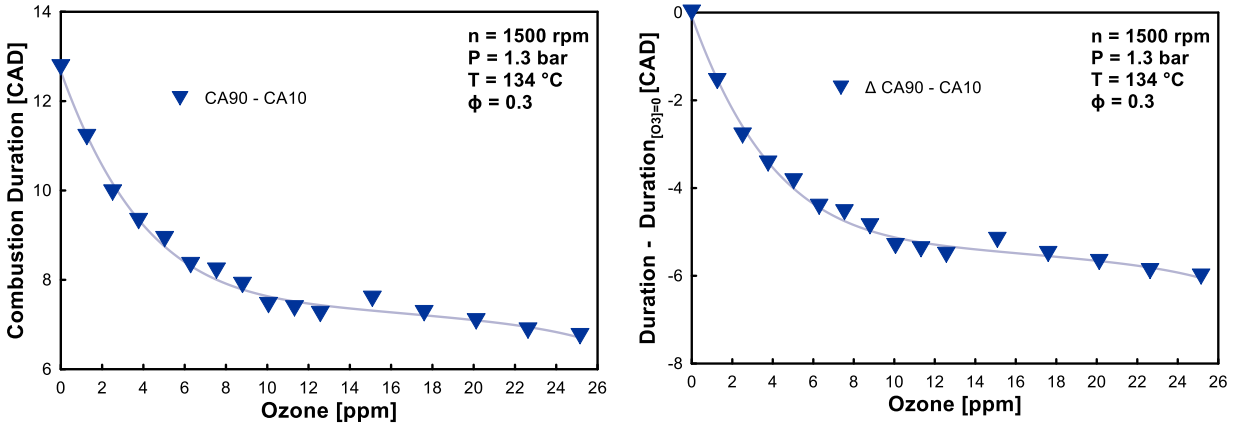

a. b.

Figure 76. Impact of ozone on combustion duration (a) and on the reduction of combustion duration with respect to the non-seeded case.

5.3.1.2.Impact on combustion efficiency and combustion stability

As stated above, the increase in the oxidation rate is accompanied by a general strengthening of the combustion process and a greater amount of heat released during combustion. In support of this, Figure 77 (a) shows the IMEP values as a function of the ozone concentration introduced in the fresh intake charge. As can clearly be seen from the graph in Figure 77 (a), systematically increasing the intake ozone concentration led to higher IMEP values, which rose from 2.3 bar in the non-seeded case to 2.8 bar when 12 ppm of ozone seeded the engine intake.

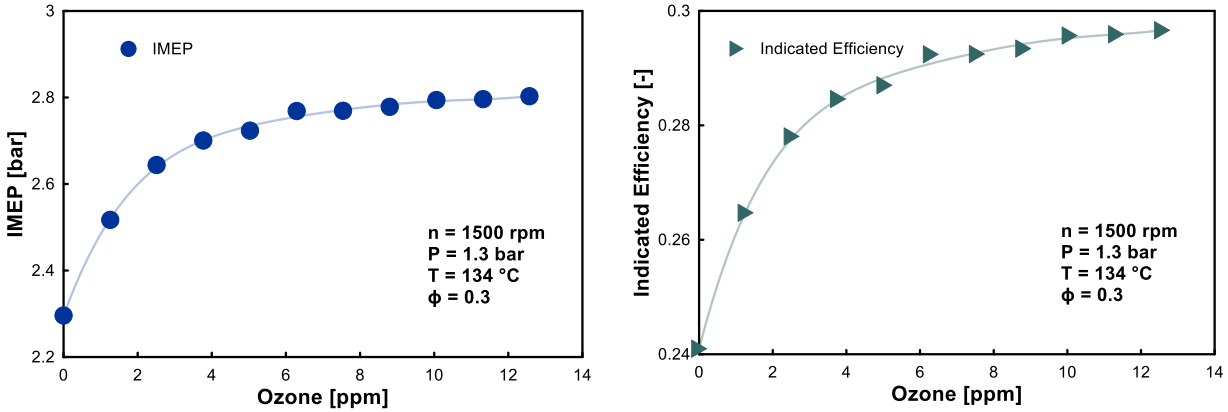

a. IMEP b. Indicated Efficiency

Figure 77. IMEP (a) and Indicated Efficiency (b) as a function of the intake ozone concentration.

Since the injected fuel mass did not change during the experiments, the increase in the IMEP corresponded to an improvement in the indicated efficiency. Figure 77 (b) shows the effect of the intake ozone concentration on this parameter. As can be seen, under non-seeded conditions, the indicated efficiency was close to 24%. Progressively increasing the intake ozone concentration up to 12 ppm induced an improvement in the indicated efficiency which increased up to ~30%. These trends show that the addition of increasing ozone concentrations causes a continuous, progressive improvement in the combustion process. However, as observed in the combustion phasing trends (Figure 75), the combustion process is much more sensitive to small ozone concentrations and a certain saturation effect is visible for higher intake ozone concentrations. Figure 78 reports the value for the coefficient of variation (COV) of IMEP as a function of the intake ozone concentration. Results show a significant reduction in the COV when ozone seeded the engine intake. This trend indicates that adding ozone corresponded to a considerable reduction of the cycle-to-cycle variations and thus to an improvement in the combustion stability. As discussed above, adding ozone simultaneously induces an advance in the combustion phasing and an improvement in the indicated efficiency and combustion stability. To highlight this phenomenon, Figure 79 shows the IMEP, the indicated efficiency and COV of IMEP values as a function of the CA50 for different intake ozone

concentrations. It is clear that higher IMEP and efficiency were registered along with a lower COV of IMEP when CA50 moved toward TDC. As widely demonstrated in other

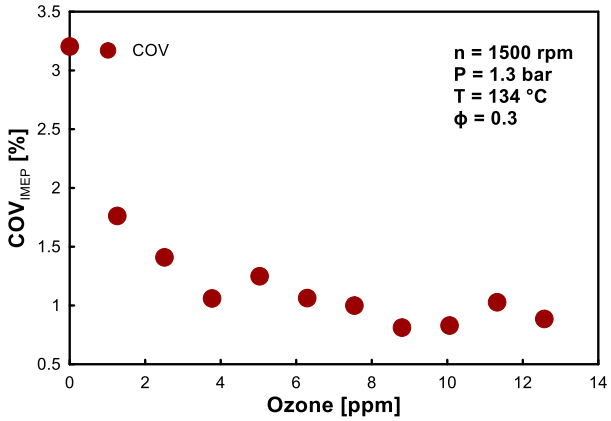

Figure 78. Coefficient of variation of IMEP as a function of the intake ozone concentration.

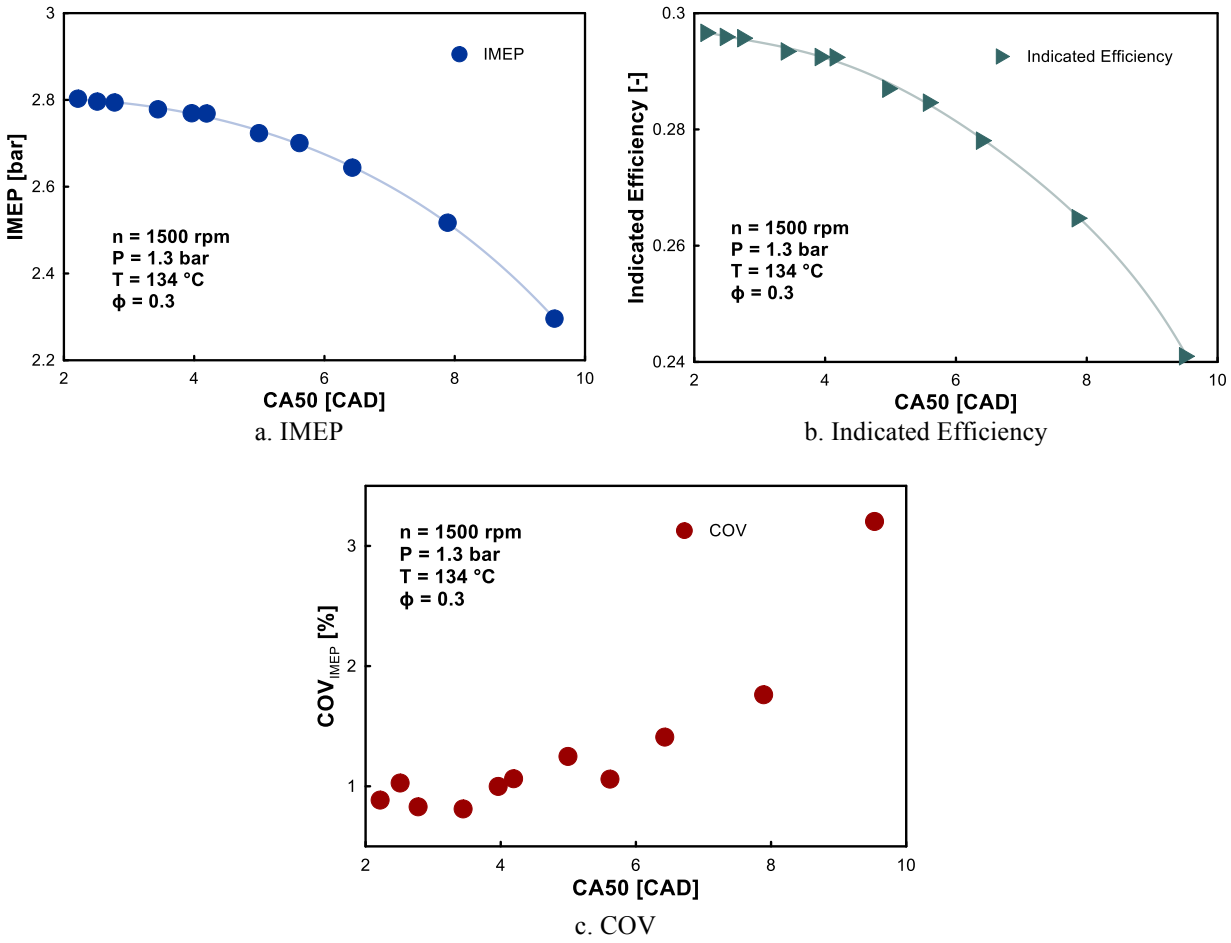

Figure 79. IMEP (a), Indicated Efficiency (b) and COV of IMEP (c) as a function of the change in CA50 induced by different intake ozone concentrations.

studies, the indicated efficiency in this type of premixed combustion is strongly related to its phasing and maintaining the CA50 closer to TDC generally corresponds to higher indicated efficiency. It is evident that the effect of ozone on the indicated efficiency cannot be separated from its effect on the combustion timing. Consequently, it is difficult to determine whether the increase in the IMEP is due to a chemical effect, with ozone leading to an improvement in the fuel to heat conversion, i.e. combustion efficiency, or whether it is simply due to better positioning of the heat release within the cycle. To try to isolate the effect of combustion phasing from that of ozone, a particular type of experiment was designed. Figure 80 illustrates the strategy followed during this experiment.

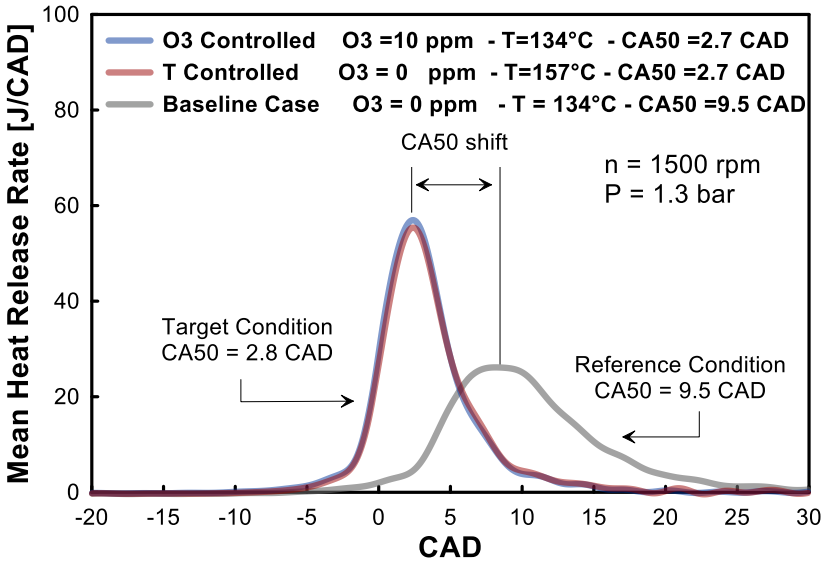

Figure 80. Experimental strategy employed to isolate the impact of ozone from that of the combustion phasing.

In the reference conditions, combustion was achieved by means of a combination of temperature and pressure; the values are listed in Table 10. Under these reference conditions, the heat release was characterized by a CA50 of 9.5 CAD.

	Experimental Conditions						
	Engine Speed *[rpm]*	E.R *[-]*	Fuel Mass *[mg/cycle]*	Intake Pressure *[Bar]*	Intake Temperature *[°C]*	Ozone *[ppm]*	CA50 *[CAD]*
Reference Case	1500	0.3	10.68	1.3	134	0	9.5
O_3 Controlled Case	1500	0.3	10.68	1.3	134	10 ppm	2.7
T Controlled Case	1500	0.3	10.36	1.3	157	0	2.7

Table 10. Values of the main engine parameters for the experiments described in Figure 80

Starting from the reference conditions, the heat release was then advanced, reaching an arbitrary target CA50 of 2.7 CAD, by means of two different methods. In the first case, the advance of the heat release was induced through the use of ozone, while the thermodynamic conditions at the intake were maintained unchanged. In the second case, the same shift in the CA50 was achieved by raising the intake air temperature. It should be noted that because of the change in the intake charge density caused by the higher intake temperature, in this second experimental configuration the injected fuel mass was reduced to maintain the same equivalence ratio as that of the reference conditions.

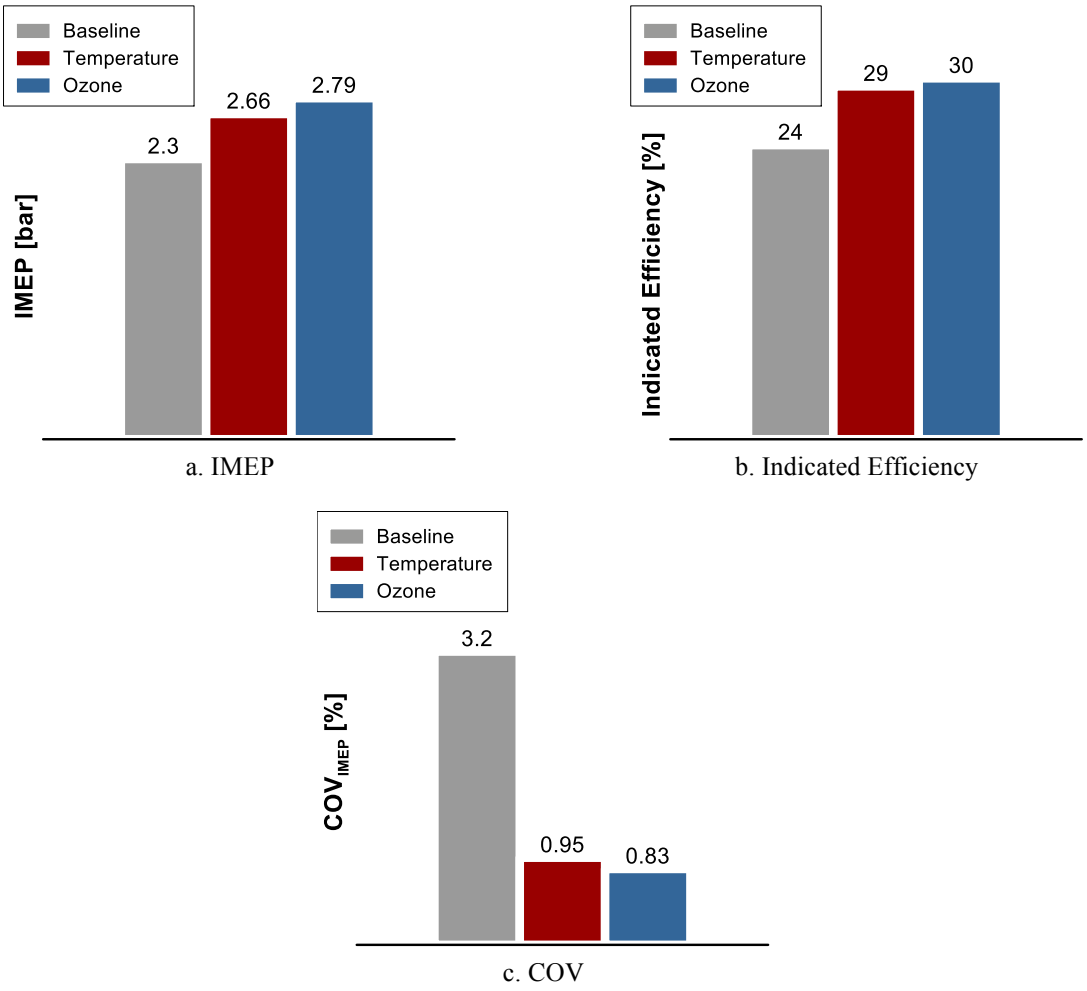

Figure 81. IMEP (a), Indicated Efficiency (b) and IMEP COV (c) for the experimental conditions listed in Table 10.

The results from experiments are collected in Figure 81 in which the main combustion characteristics are compared for the three previously described cases. As can be seen in Figure 81 (a), for a given combustion phasing, using ozone instead of the temperature to set a certain CA50 yields a higher IMEP, higher indicated efficiency and lower COV of IMEP. The values of IMEP and indicated efficiency reported in Figure 81 (a) and Figure 81 (b) demonstrated that more energy and more work are extracted for a given mass of fuel when

ozone seeded the engine intake. The COV values reported in Figure 81 (c) indicate that ozone can reduce the cycle-to-cycle variations. This means that, regardless of the combustion phasing, an improvement in the combustion process took place when ozone seeded the fresh intake charge. It can be deduced that the alteration of the oxidation reaction path occurring when ozone is present in the intake charge can chemically enhance the combustion process. More energy can be extracted from a unitary mass of fuel, improving the combustion efficiency. Adding ozone strengthens the oxidation process, reducing cycle to cycle variation and improving combustion stability.

5.3.2. Extension of the autoignition region

In the previous sub-section, the HCCI autoignition region of gasoline was defined, and the impact of ozone was investigated when the fuel-air mixture had already autoignited due to the effect of the in-cylinder pressure and temperature evolution. Starting from the diagram shown in Figure 73, it is possible to reduce the intake temperature or the mixture strength, i.e. equivalence ratio, and progressively exceed the conditions that allow autoignition of the fuel. When the autoignition limits are exceeded, combustion can no longer occur because the thermodynamic conditions obtained during the compression stroke do not provide the energy necessary to start and complete the oxidation of the fuel-air blend process. This section investigates the ability of ozone to extend the autoignition limits of commercial gasoline under HCCI conditions. In particular, two cases will be studied. In the first case, the possibility of using ozone to reduce the minimum mixture strength necessary for autoignition will be investigated. The second situation considered will concern the use of ozone to reduce the minimum intake temperature necessary for autoignition of a fuel-air mixture for a given equivalence ratio. In both cases, the discussion will show the advantages and disadvantages in terms of engine performance and combustion characteristics associated with the respective techniques.

5.3.2.1. Reduction of the lean limit

The experiments described in this section were intended to determine whether the beneficial properties of ozone on gasoline combustion were able to reduce the minimum equivalent ratio required for autoignition. An experimental point defined by a combination of intake temperature, pressure and equivalence ratio leading to a stable autoignition was chosen as a reference point. An arbitrary threshold of COV of IMEP < 3.5% was established as the stability limit. Starting from the reference conditions, whose properties are listed in Table 11, the equivalence ratio was systematically reduced. It was observed that combustion was very sensitive to variations in the equivalence ratio and that even going from ϕ 0.3 to 0.29 led to a deterioration of combustion stability and hence to a misfire. It can be stated that by reducing the equivalence ratio, the strength of the mixture was no longer sufficient to ensure stable combustion and that the limit of autoignition was exceeded. Under these conditions, it was found that the addition of ozone re-established

combustion while maintaining stability within the arbitrary threshold of COV < 3.5%. Figure 82 shows the evolution of the COV of IMEP as a function of ozone concentration, for different values of equivalence ratio. It should be noted that only the experimental conditions yielding a COV < 3.5% are included in the graph. As can be seen from Figure 82, without ozone, the minimum equivalence ratio value which guaranteed a sufficient combustion stability was ϕ=0.3. For ϕ values lower than 0.3 and no ozone seeding the engine intake, it was not possible to achieve stable combustion with a COV of IMEP below 3.5%. However, Figure 82 shows that ozone could also be employed to improve combustion under unfavorable conditions and achieve stable combustion of a lean mixture with ϕ below 0.3, which otherwise would not have autoignited. Specifically, it was found that, for a given ϕ below 0.3, a minimum ozone concentration was necessary to activate stable autoignition. Then, by supplying extra ozone at the intake, the combustion stability may have been further improved by moving the CA50 closer to TDC, as can be seen by comparing Figure 82 and Figure 83. It is interesting to note that the minimum ozone concentration necessary for stable autoignition was found to be a function of the equivalence ratio of the mixture. In Figure 84, plotting the minimum ozone required for stable autoignition as a function of the equivalence ratio of the mixture made it possible to identify an ozone-equivalence ratio curve which traces the boundary between stable and unstable combustion regions. For the given set of intake thermodynamic conditions indicated on the graph, no stable operation was possible for ozone concentrations lower than the one corresponding to the stability limit drawn in Figure 84. Starting from any of the ϕ- O_3 combinations lying on the stability boundary, adding ozone at the intake strengthened the combustion process by reducing the COV of IMEP and consequently improving the combustion stability by advancing the combustion phasing. As represented in Figure 84, the minimum amount of ozone required for stable combustion dramatically increased as the mixture got leaner.

Experimental Conditions								
	Engine Speed *[rpm]*	E.R *[-]*	Fuel Mass *[mg/cycle]*	Intake Pressure *[Bar]*	Intake Temperature *[°C]*	Ozone *[ppm]*	CA50 *[CAD]*	COV *[%]*
Reference Case	1500	0.3	10.68	1.3	134	0	9.5	3.5

Table 11. Values of the main engine parameters for the reference case considered for the lean limit extension by using ozone

To better understand these results, it is useful to observe Figure 85, in which the stability limit is represented by the value of the combustion phasing registered at the points shown in Figure 84. It is interesting to note what the link between stability and combustion phasing is. Figure 85 shows that as the mixture becomes leaner, the stability requirement means that more ozone has to be used to move the CA50 closer to the TDC. This is due to the lower energy density of mixtures with a lower equivalence ratio. In fact, the increasingly

smaller amount of energy provided by leaner intake charges must be released in smaller volumes. Only in this way is it possible to sufficiently concentrate the released energy and provide the optimum conditions to ensure the sustainability of the reactions that contribute to combustion oxidation. In other words, as the intake charge becomes leaner, avoiding the dispersion of the energy in excessively larger volumes becomes an increasingly binding factor to avoid quenching of the combustion and consequently to maintain the desired stability.

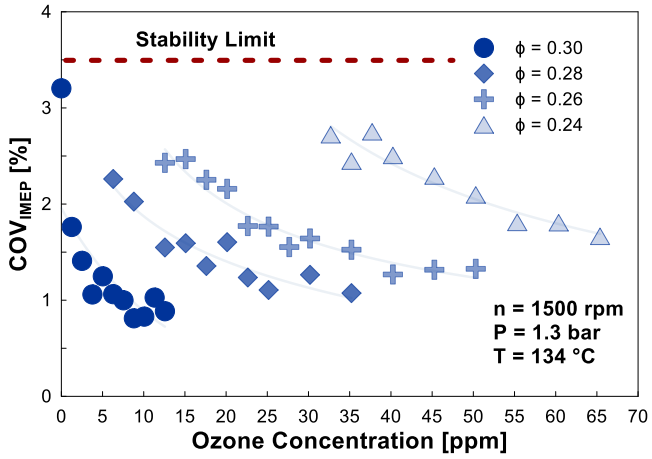

Figure 82. COV of IMEP as a function of ozone concentration, and for different values of fuel-air equivalence ratio.

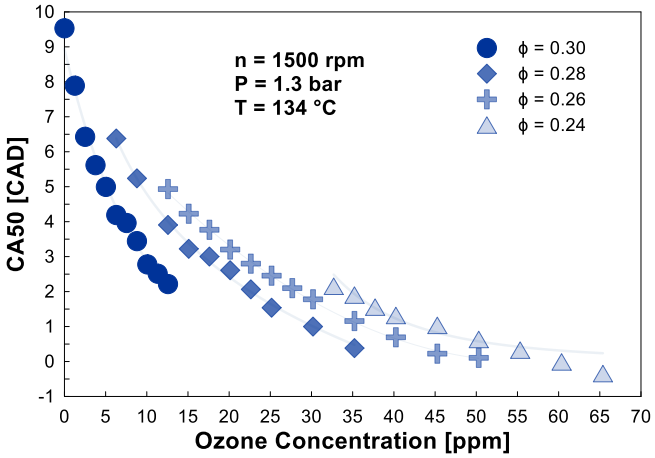

Figure 83. CA50 as a function of intake ozone concentration for different values of the equivalence ratio of the fuel-air mixture.

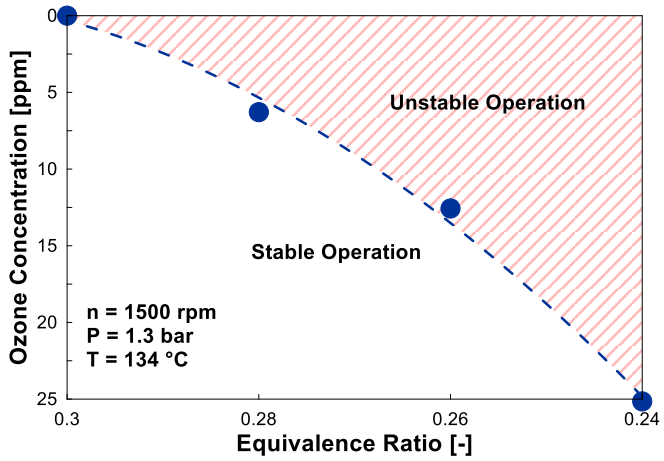

Figure 84. Ozone necessary to achieve stable operation as a function of the equivalence ratio of the mixture.

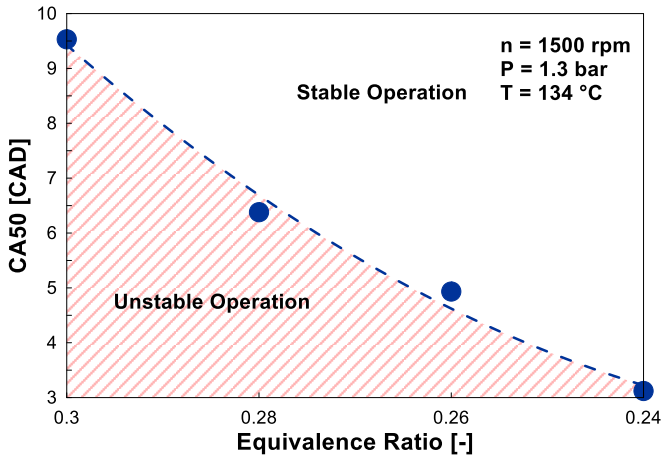

Figure 85. CA50 corresponding to the stability boundary as a function of the equivalence ratio of the mixture.

In the first part of this section, the mechanisms behind the ability of ozone to enable the autoignition of mixtures with a low equivalent ratio were analyzed. This section investigates what the effects on engine performance are when ozone is used to go beyond the stability limit.

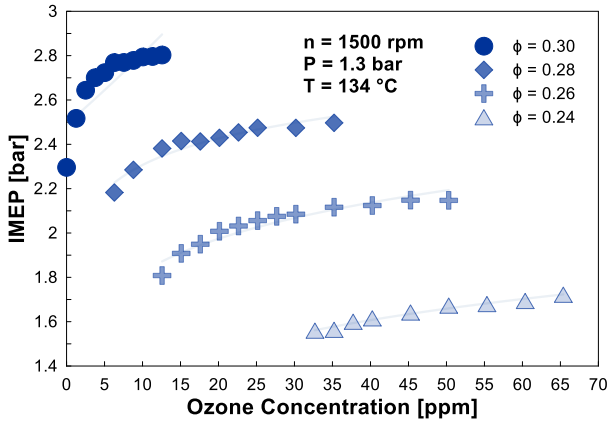

Figure 86.IMEP as a function of intake ozone concentration and for different fuel-air equivalence ratios

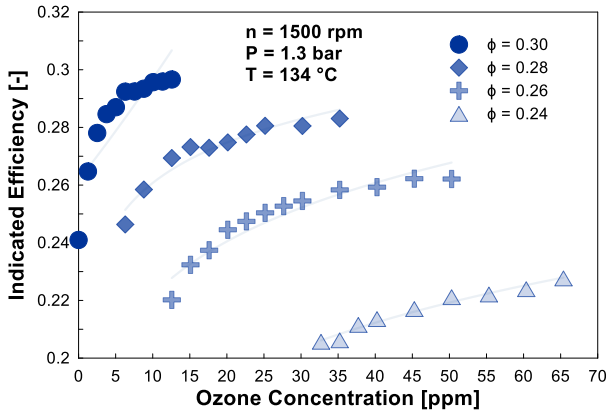

Figure 87. Indicated efficiency as a function of intake ozone concentration and for different fuel-air equivalence ratios.

In Figure 86 the values of IMEP are reported as a function of the concentration of ozone at the intake, for the different equivalence ratios tested. For the same experimental conditions, Figure 87 shows the values of the indicated efficiency. It should be recalled that for all the conditions, the COV was higher than 3.5%. What is worth noting here is that, for each equivalence ratio tested, any amount of ozone greater than the minimum required to guarantee the stability limit can be used to maximize the extractable IMEP from a given mass of fuel. This can consequently maximize the indicated efficiency. Another important factor to consider is the shape of the function that describes the performance of these two factors as a function of ozone. In fact, the increase in IMEP and efficiency, although it showed a progressive trend, exhibited a sort of saturation effect. This is due to the fact that there is a limit to the work that can be extracted from a given amount of fuel. This limit is reached when the amount of ozone is sufficient to maximize the combustion

efficiency and to initiate the combustion event so as to match the optimal combustion phasing. It follows that, depending on the equivalence ratio of the mixture, it is possible to define a maximum IMEP achievable through the promoting effect of ozone. Advantages in terms of engine performances are obtained if ozone enables the same mechanical work, i.e. IMEP, to be extracted from a mass below that required under non seeded operations.

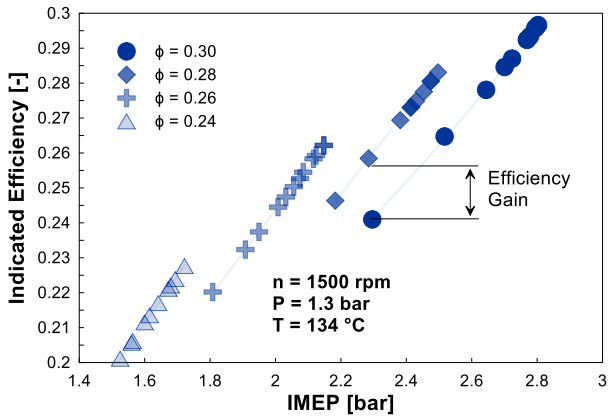

Figure 88. Indicated efficiency as a function of IMEP for different values of the fuel-air equivalence ratio.

To determine if these advantages could be obtained, the different combinations of IMEP and indicated efficiency obtainable from mixtures characterized by even lower equivalence ratios are represented in Figure 88. As can be seen from the curves shown in Figure 88, there are intervals in which the same IMEP can be generated by smaller fuel masses by exploiting the oxidizing power of ozone. For example, for IMEP higher than 2.2 bar, enhancing the combustion of mixtures with $\phi = 0.29$ provided the same IMEP as that generated by mixtures with $\phi = 0.3$. This led to a corresponding indicated efficiency gain of ~1.5%. Generalizing, it can be said that an advantage in terms of efficiency can be achieved by systematically reducing the fuel content of the mixture and employing ozone to extract the maximum possible IMEP. If this maximum IMEP has a greater value when compared to the minimum obtainable from a mixture with a slightly higher equivalent ratio, an efficiency gain will be obtained. From Figure 88, it can be seen that for the experimental case presented here, no more overlap was observed between IMEP–efficiency traces when the equivalence ratio decreased from 0.28 to 0.26. This condition marked the applicability limit of the technique described above.

5.3.2.2. Reduction of the autoignition temperature

The mechanism by which temperature has a promotional effect on combustion is well-known. Increasing the intake air temperature increases the rate at which chemical reactions take place, favoring the autoignition process of homogeneous mixtures. Conversely, a reduction in temperature leads to a reduction in charge

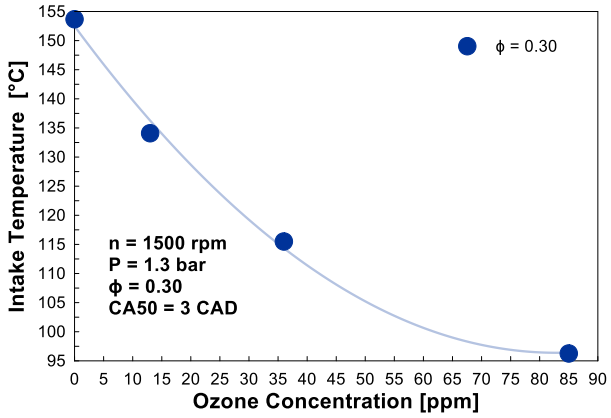

Figure 89. Intake temperature required to achieve combustion by placing the CA50 3 DA after TDC, as a function of the intake ozone concentration.

reactivity and moves the combustion phasing farther from TDC. As has been shown in this chapter, ozone has the same catalytic effect on the reactivity of the mixture, which increases or decreases according to the ozone concentration. The idea here is to allow the autoignition of the fuel at lower temperatures by seeding the engine intake with ozone. Starting from a reference condition, reducing the temperature causes a delay in the combustion phasing. The more the temperature is reduced, the more CA50 increases until misfire occurs. Under these conditions, enriching the air with ozone increases the reactivity of the charge, and leads combustion to occur again, but at a lower intake temperature. Experiments were conducted in which this procedure was repeated by systematically replacing the temperature with increasing concentrations of ozone. Figure 89 reports the results of the experiments.

Figure 89 shows the intake temperature required to achieve autoignition as a function of the intake concentration of ozone, while the CA50 was maintained constant at 3 CAD after TDC. As can be clearly seen, increasing the intake concentration of ozone made it possible to systematically reduce the intake temperature necessary for gasoline autoignition. With less than a hundred ppm of ozone, the intake temperature was reduced by 60°C, i.e. the temperature dropped from 155°C in the non-seeded case to 95°C with 85 ppm of ozone.

For the same experiments as those shown in Figure 89, Figure 90 gives the estimated in-cylinder gas temperature evaluated at a moment just following autoignition, i.e. at CA10, or CAD of 10 % of the heat release. With the correct approximations, the observed trend of this parameter is indicative of the

temperature at which combustion begins. Figure 90 clearly shows how the addition of ozone enables a systematic reduction in the temperature required for the autoignition of a mixture.

When combustion was achieved by means of pure air, autoignition took place when the in-cylinder charge temperature reached a temperature close to 1010 K. Seeding the engine intake with ozone increased the reactivity of the intake air flow and progressively reduced the minimum temperature required for autoignition. With 85 ppm of ozone injected in the intake plenum, combustion initiated at 920 K, i.e. a reduction of 90K in the temperature required for autoignition. It is interesting to note the improvement that such small concentrations of O_3 made to the reactivity of the intake flow. It can be deduced that the flammability limit of gasoline could be extended towards lower temperatures by enriching the intake air with a small concentration of ozone. Once again, the promoting effect of ozone was shown to allow for the extension of the autoignition region under compression ignition conditions. A possible interpretation of this result is that because of the introduction of O atoms in the intake air, ozone alters the reaction path, reducing the enthalpy of activation required to initiate oxidation of the fuel. The same procedure to reduce the intake

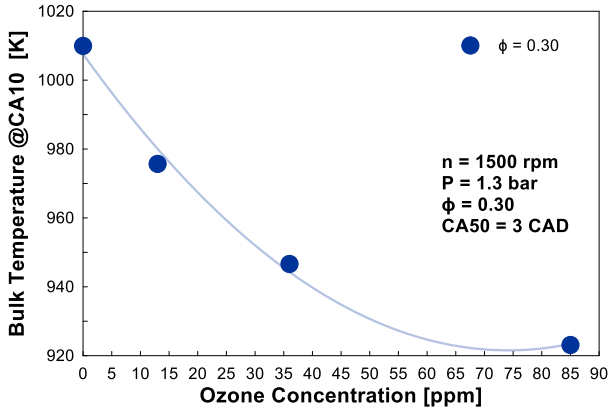

Figure 90. Intake temperature required to achieve combustion by placing the CA50 3 DA after TDC, as a function of the intake ozone concentration.

and autoignition temperature using the property of ozone was repeated by additionally varying the fuel concentration in the mixture. In particular, it was interesting to determine whether ozone could reduce the admission temperature of increasingly leaner fuel-air mixtures. Figure 91 shows the results of this experiment. In the graph, the ozone concentration required for combustion with CA50=3 CAD is plotted versus the equivalence ratio of the mixture and for different targeted intake temperatures. The results of the experiments revealed that, for a given target intake temperature, the leaner the mixture, the higher the ozone concentration necessary to obtain combustion. Likewise, for a fixed fuel-air equivalence ratio, a higher ozone concentration was required to enable the mixture to burn at a lower temperature. What is interesting

to note here is how the different ozone properties investigated separately, i.e. the ability to independently reduce the temperature

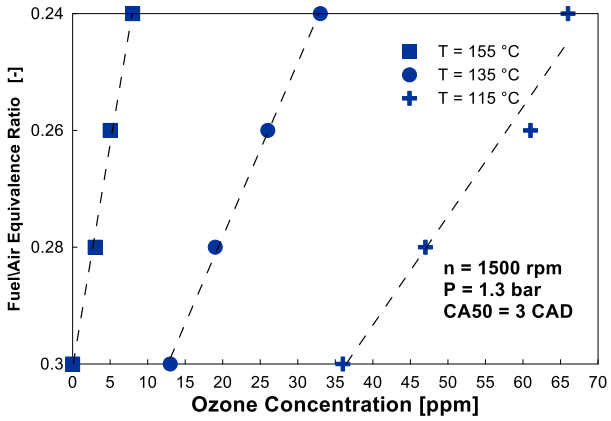

Figure 91. Equivalence ratio versus ozone concentration required the fuel-air mixture autoignition for different intake temperatures and for a fixed CA50 =3 CAD.

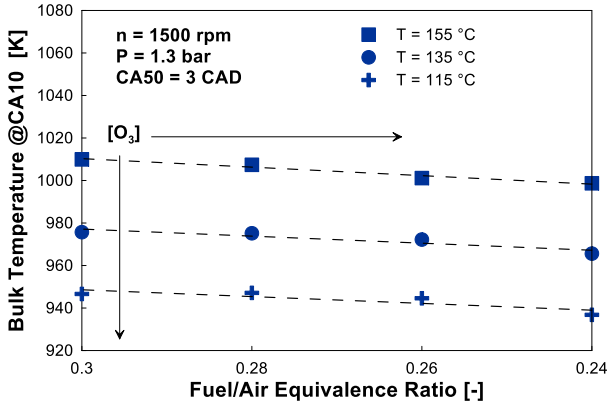

Figure 92. In-cylinder bulk temperature at CA10 as a function of the fuel-air mixture equivalence ratio and for different intake temperatures. Arrows are drawn to indicate the direction of the need for higher ozone concentrations.

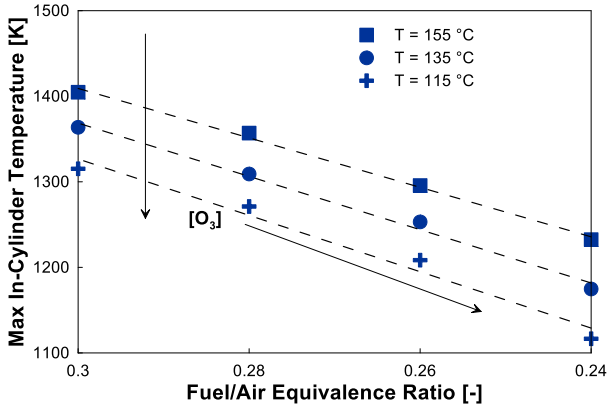

Figure 93. Maximum in-cylinder bulk temperature as a function of the fuel-air equivalence ratio and for different targeted intake temperatures. Arrows are drawn to indicate the direction of the need for higher ozone concentrations.

or the equivalence ratio required for autoignition, could be combined according to what appears to be a sort of superimposition effect principle.

Figure 92 shows the temperature at CA10 for several equivalence ratios and intake temperatures. The data suggest that the ignition temperature of the fuel is predominantly dependent on the initial intake temperature, and consequently on the ozone concentration permitting this temperature, whereas the fuel concentration does not appear to be very influential. For each intake temperature tested, the temperature at CA10 decreased by approximately ten degrees when the equivalence ratio was varied from 0.3 to 0.24. However, this small increase in the temperature observed in the case of the richer mixture may be due to the greater energy contained and released by such mixtures and not to a real increase in the temperature necessary for autoignition.

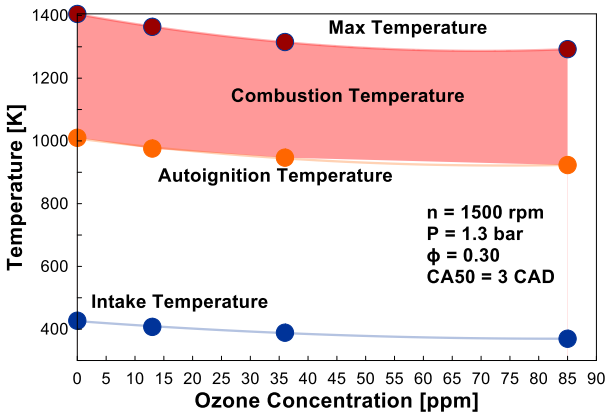

Figure 94. Intake, autoignition and maximum estimated in-cylinder temperature as a function of ozone concentration.

Figure 93 shows the maximum in-cylinder estimated gas temperature as a function of the intake temperature and of the equivalence ratio of the mixture. It can be seen that for a given equivalence ratio, the maximum gas temperature was considerably lower if the intake temperature was reduced by means of an increasingly higher ozone concentration seeding the intake manifold of the engine. For the case of ϕ=0.3, adding 35 ppm of ozone induced a reduction of approximately 100 K in the maximum combustion temperature, in spite of an intake temperature reduction of ~40 K, as can be seen by comparing Figure 93 with Figure 91. Observing the data related to leaner mixtures in Figure 93, it can be seen that the fuel-air equivalence ratio of the mixture does not alter the effect that ozone, and the reduction in intake temperatures, had on the maximum temperature reached in the cycle. The maximum estimated temperature always decreased when lower intake temperatures were achieved by using ozone to improve the reactivity of the intake charge. To summarize, Figure 94 shows on the same graph the intake temperature, the temperature at autoignition and the maximum gas temperature reached during the cycle, as a function of ozone, for a given ϕ=0.3. It can be concluded that

one consequence of achieving autoignition at a lower intake temperature is that the whole combustion process begins, develops and ends at lower temperatures.

5.4. CONCLUSIONS

The aim of the experiments described in this chapter was to study the impact of ozone on the homogeneous charge compression ignition combustion of commercial gasoline fuel.

The first part of the chapter described the effect of seeding the intake of the engine with ozone after combustion had already been established by means of intake thermodynamic conditions favorable to autoignition.

Gasoline HCCI combustion proved to be highly sensitive to ozone addition. The addition of a small concentration of ozone in the intake air flow induced an advance and an acceleration of the oxidation process. Results showed an increase and an advance of the heat released during combustion following ozone addition. Consequently, the in-cylinder pressure and temperature characterizing the combustion process increased consistently with the increase in ozone concentrations. Combustion related parameters were highly sensitive to ozone addition. The combustion phasing was strongly advanced when ozone was used to seed the intake of the engine. Moreover, the entire combustion process was shortened when an increased amount of ozone seeded the intake of the engine. The reduction in combustion duration was associated to the increased chemical activity and to the more favorable conditions in which oxidation reactions took place when ozone seeded the engine intake. Seeding the intake with ozone molecules induced an improvement in the IMEP and in the indicated efficiency. Results from experiments demonstrated that increasing the work extracted from a given mass of fuel was possible due to a combination of a better combustion phasing and of an improvement in the combustion efficiency induced by ozone addition. Moreover, results from the experiments indicated that adding ozone also strengthened the oxidation process, reducing the cycle to cycle variation and improving the combustion stability.

Ozone was also shown to be able to extend the autoignition limits of commercial gasoline under HCCI conditions. In a first section, ozone was shown to allow for the autoignition of increasingly leaner mixtures. Starting from a given set of intake thermodynamic conditions, reducing the mixture equivalence ratio led to misfire. Results showed that seeding the engine intake with ozone made it possible to restore the autoignition of leaner mixtures. The equivalence ratio reduction was proportional to the intake ozone concentration. Moreover, results showed that increasing the intake ozone concentration made it possible not only to obtain the combustion of poor mixtures, but also to control the combustion phasing. As a result, the same IMEP

could be achieved by simultaneously reducing the fueling rate and increasing the ozone concentration, yielding an effective improvement of the indicated efficiency.

In a second section, ozone was employed to reduce the intake temperature required for autoignition. Results showed that starting from a given set of intake thermodynamic conditions, reducing the intake temperature led to misfire. Enriching the intake air flow with ozone extended the flammability limit of gasoline towards lower temperatures. A possible explanation for this result is that because of the introduction of O atoms in the intake air, ozone alters the reaction path, reducing the enthalpy of activation required to initiate oxidation of the fuel. Results also showed that as a consequence of the lower intake temperature necessary for autoignition, the whole combustion process begins, develops and ends at lower temperatures. In the last part of the chapter, results indicated that by increasing the intake ozone concentration it was possible to simultaneously reduce the intake temperature and the equivalence ratio.

6. Optical investigation of the impact of ozone on HCCI combustion

6.1. INTRODUCTION

To provide a better understanding of the impact of ozone on gasoline combustion, the experiments reported in the previous chapter were repeated in an optically accessible engine.

The main purpose of these experiments was to understand the mechanisms underlying the impact of ozone on combustion by observing the evolution of the radicals which are significant in determining the evolution of the combustion process, i.e. CH2O, CH* and OH*. Different techniques were employed to detect these radicals.

To investigate the influence of ozone on the early stages of combustion, CH2O and CH radicals were tracked. CH2O was detected by means of CH2O PLIF, to study the low temperature heat release and to detect the possible occurrence of a cool flame. Then, CH* chemiluminescence was detected because it is generally present in the first stage of the oxidation process. OH* chemiluminescence was collected to identify the occurrence of the main high-temperature phase of the heat release rate.

As optical laser diagnostics were used, gasoline fuel could not be employed since light is emitted from the fluorescent compounds present in commercial fuel. Non-fluorescent iso-octane was therefore used as a gasoline surrogate. An important feature of iso-octane is that it is characterized by a single stage combustion behavior, as is also the case of the commercial gasoline previously tested. Because ozone showed a strong impact on the first stage of the oxidation process, it was deemed preferable not to introduce fuels with cool flame behavior, i.e. n-heptane, in order to simplify the detection of reactions in the early stage of ignition.

This chapter comprises two main sections. In the first section the impact of ozone addition on thermodynamically established combustion was investigated. In the second section, the impact on combustion was investigated when ozone was used to extend the autoignition limit of iso-octane fuel.

6.2. IMPACT OF OZONE ON THERMODYNAMICALLY ESTABLISHED COMBUSTION

This section summarizes the results of the experiments performed to investigate the impact of adding ozone after combustion had been already established by means of the intake thermodynamic conditions. Table 12 reports the experimental conditions used during the experiments. Because iso-octane has a higher ON than gasoline and because the optical engine is characterized by higher thermal losses, the intake thermodynamic conditions differed slightly from those used in the metallic engine experiments previously presented, with a higher intake temperature and pressure needed to achieve iso-octane autoignition.

Fuel	Engine Speed	Intake Temperature	Intake Pressure	Equivalence ratio	O_3	CA50
PRF100	1500 rpm	195 °C	1.39 bar	0.3	0 ppm	7 CAD
PRF100	1500 rpm	195 °C	1.39 bar	0.3	6 ppm	-2 CAD

Table 12. Experimental conditions for thermodynamically established combustion in the optically accessible engine.

As reported in Table 12, if no ozone was employed, the intake temperature had to be increased up to 195°C and pressure to 1.38 bar in order to achieve the autoignition of an iso-octane/air mixture with ϕ=0.3. Combustion was characterized by a CA50 = 7 CAD. Starting from the latter, the intake charge was then seeded by 6 ppm of O_3 molecules and the combustion phasing advanced due to the increased reactivity induced by the effect of O_3 molecules, as indicated by the CA50 = -2 CAD. The impact of ozone was firstly investigated by PLIF visualization of CH_2O and visualization of OH* chemiluminescence.

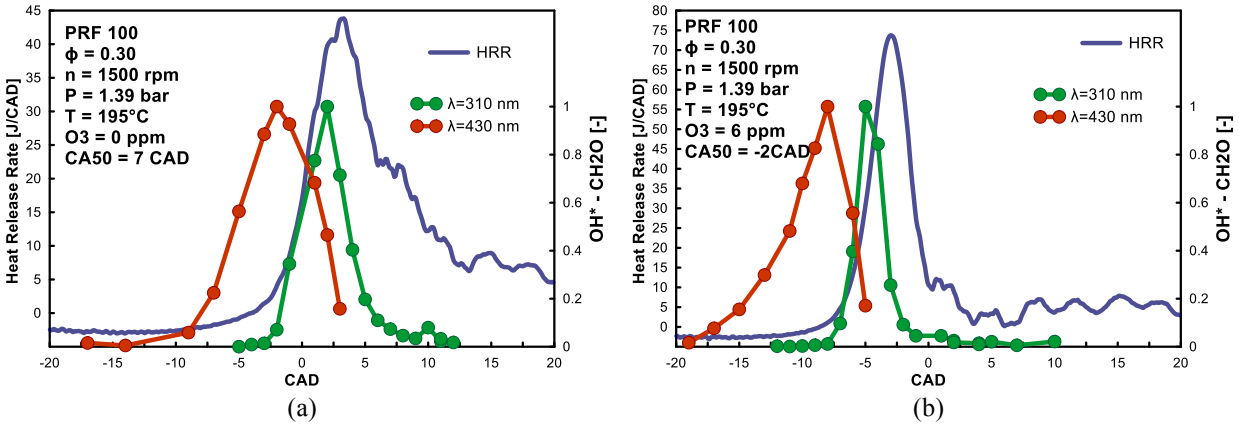

Figure 95. Impact of ozone addition on the heat release rate, CH2O and OH* integrated signal for thermodynamically induced combustion. Heat release, OH* and CH_2O are reported for the non-seeded case (a) and for the seeded case with the ozonizer capacity set to 4%,corresponding to 6 ppm of O_3. (b). Experimental conditions are reported in Table 12.

Figure 95 shows the CH_2O PLIF and the OH* chemiluminescence signals as a function of the CAD along with the heat release rate traces corresponding to the two experimental conditions reported in Table 12. Figure 95 (a) reports the results for the non-seeded case, while Figure 95 (b) shows the results when 6 ppm of ozone were employed to enhance combustion and advance the combustion phasing. In the non-seeded case, Figure 95 (a) shows how the heat from combustion began to be released close to TDC. The signal from CH_2O-PLIF started to be visible from -10 CAD aTDC, reached its maximum at -2 CAD aTDC and then started to decrease, until no CH_2O signal was recorded later than 5 CAD aTDC. Corresponding to the CH_2O signal drop near TDC, the first non-zero level of OH* chemiluminescence luminosity indicated the occurrence of the high-temperature phase of combustion. Figure 95 (b) reports that adding 6 ppm of ozone dramatically advanced the combustion event. The first appearance of heat release took place at -7 CAD aTDC and CA50= -2 CAD aTDC. In accordance with the advance in combustion phasing, the CH_2O signal was also advanced: it started to grow at -17 CAD aTDC, and reached its maximum at -8 CAD aTDC. Then, the CH_2O signal dropped and OH* chemiluminescence started to rise, indicating the onset of the high temperature heat release, which occurred between -7 CAD and -1 CAD aTDC. Results from Figure 95(a) and Figure 95 (b) indicate that the whole oxidation process was advanced when ozone was added to the engine intake. Under ozone seeded conditions, the heat release rate was advanced and both CH_2O and OH were both produced earlier but their relative phasing was not altered, with the conventional CH_2O-OH* transition taking place at the occurrence of the high temperature heat release. No CH_2O from cool flame of low temperature heat release was observed when ozone was used to advance the combustion phasing. For the same experimental conditions, simultaneous detection of the chemiluminescence signal of OH*(λ=310nm) and CH*(λ=430nm) radicals was performed by positioning two photomultipliers in front of the optical access of the engine. It should be noted that in this case, ozone concentrations were varied from 0 ppm to 6 ppm with additional intermediate steps of 2 ppm, 3 ppm and 4 ppm. Figure 96 shows the heat release traces and the corresponding chemiluminescence signals emitted by OH* and CH* in the non-seeded case and for the case in which combustion phasing was advanced by means of different ozone concentrations. During these experiments, the power supply voltage of the two photomultipliers was set to an intermediate level of 50% in order to avoid saturation of the acquisition card which is limited at 10V, and to capture the entire signal profile. In this way, it was possible to capture the impact of ozone on both the phasing and on the intensity of the CH* and OH* chemiluminescence signals. Figure 96 shows that the heat release enhancement induced by ozone was accompanied by a corresponding advance of the chemiluminescence signal emitted by OH* and CH* radicals. This trend confirms that the impact of ozone on the combustion phasing of premixed compression ignition combustion is due to the fact that the development of the chemical reactions governing fuel oxidation is advanced. All the combustion process advanced and became faster when ozone seeded the engine intake. The production of radicals was also

faster, as indicated by the advance in the emission of chemiluminescence from CH* and OH*. From Figure 96, it can be seen

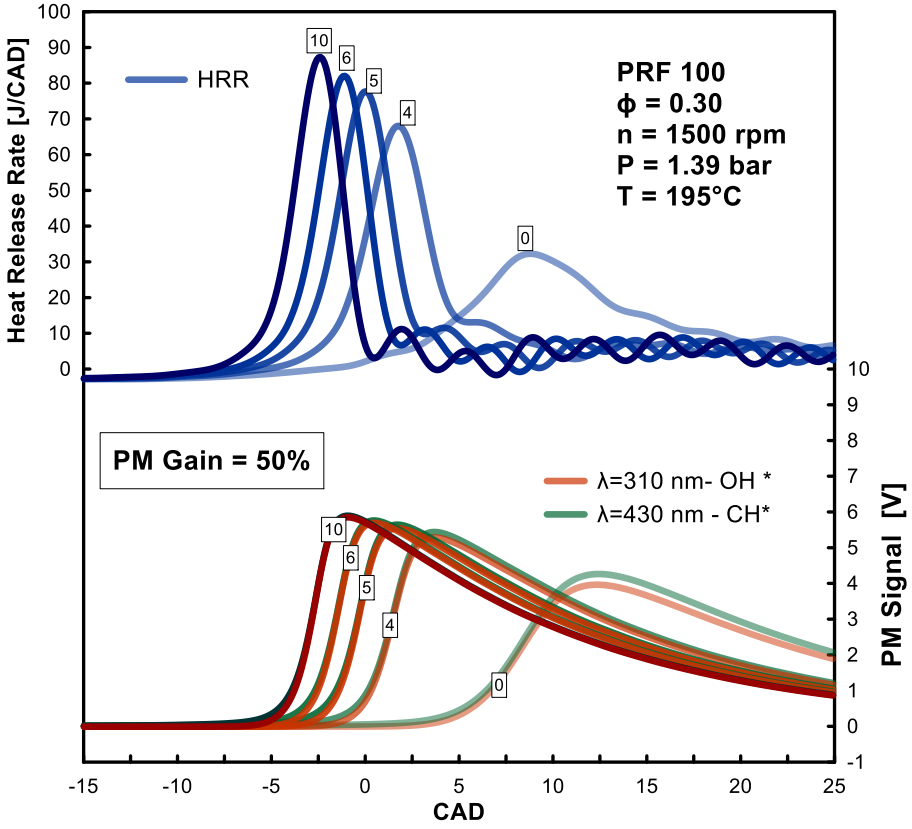

Figure 96. Heat Release rate traces, OH* and CH* signal from photomultipliers as a function of different ozone concentrations. Numbers in the boxes indicate the ozone concentration in ppm. Photomultiplier gain was set at 50% of the maximum capacity. Intake conditions are reported in Table 12.

that when ozone seeded the intake of the engine, the amplitude of the chemiluminescence signal from both radicals increased. This result is most likely related to the fact that ozone can improve the proliferation of radicals, leading to an increase in the concentration of CH* and OH* not only at the beginning but also during the entire development of the combustion process. However, chemiluminescence emission can also

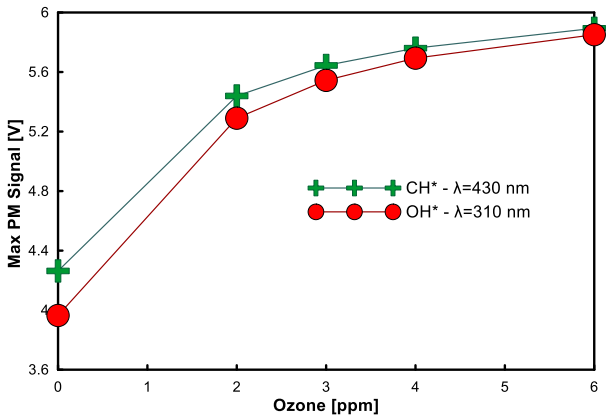

Figure 97. Impact of ozone concentration in ppm on the maximum intensity of the signal of CH* and OH* measured by photomultipliers. Experimental conditions are reported in Table 12.

be due to an increase in the combustion temperature. Further investigations should be performed to elucidate this point.

Figure 97 reports the maxima of CH* and OH* chemiluminescence signals as a function of the intake ozone concentration. It can be observed that the OH* / CH* peak signal increased so long as the combustion was enhanced by ozone. In [121], increasing trends of the OH* / CH* chemiluminescence signal were shown to be correlated with the fuel/air mixture equivalence ratio characterizing n-heptane/air premixed flames igniting in a spherical bomb. The authors found that the OH*/CH* ratio increased for combustion of a premixed flame characterized by a higher equivalence ratio. In the present work, the iso-octane/air equivalence ratio was maintained constant during the experiments, therefore a possible interpretation of the trends reported in Figure 97 is that more fuel was burned as increased concentrations of ozone were added at the intake. Such a hypothesis would entail that the addition of ozone induced an improvement in combustion efficiency. A third experiment consisted in repeating the same test, but by increasing as much as possible the input voltage supplied to the photomultipliers with the aim of increasing the sensitivity of the detection system. Results are reported in Figure 98. In the non-seeded case, the first signal detected was CH* emission, visible well before the occurrence of the heat release. The CH* signal was flat until -20 CAD aTDC, then abruptly increased, indicating the occurrence of early oxidation reactions promoting the proliferation of CH* radicals. The OH* chemiluminescence signal started to rise later, close to TDC, along with the HRR trace, indicating the occurrence of the main high temperature combustion phase. As expected, adding increased ozone concentrations at the intake led to a proportional acceleration and an advance of the main heat release. Moreover, results indicated that ozone impacted the initiation of combustion. Figure 98

shows that adding ozone modified the shape of the CH* signal early in the cycle. In the non-seeded case, the CH*

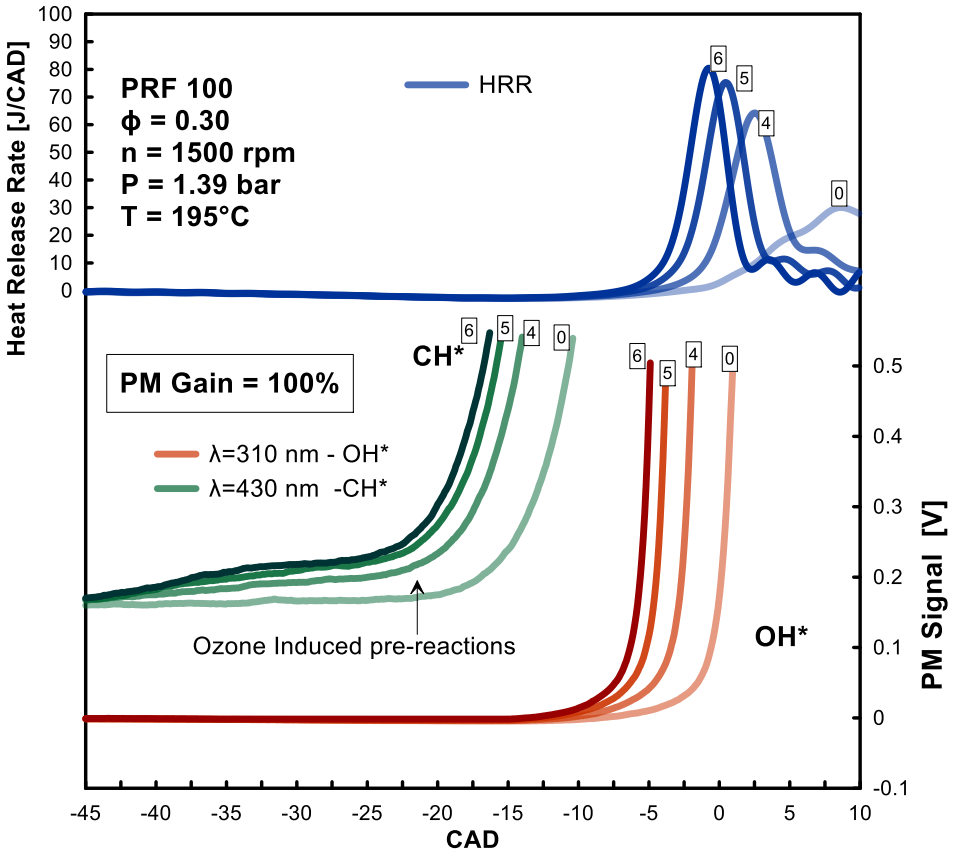

Figure 98. Heat Release Rate (HRR) traces, OH* and CH* signals from photomultipliers as a function of different ozone concentrations. Numbers in the boxes indicate the ozone concentration in ppm. Photomultiplier gain was set at full capacity. Experimental conditions are reported in Table 12.

signal was flat until -15 CAD aTDC and then abruptly increased. In the ozone seeded case, a weaker early CH* emission, with an intensity proportional to the intake ozone concentration, was observed between – 45 CAD and -20 CAD aTDC preceding the definitive rise in the CH* signal. The early presence of CH* is most likely the manifestation of the impact that ozone has on the early oxidation reactions. Indeed, this early O_3-induced CH* emission took place at the same CAD interval regardless of the fact that heat release was shifted by several CAD when different O_3 concentrations were added. This may be evidence that this early radical emission is related to the alteration of the fuel oxidation process typical of ozone seeding. Because of the introduction of O atoms, ozone induced chemical pre-reactions which are associated to new chemical pathways. Although these ozone-induced pre-reactions are not accompanied by a significant heat release, they have an important effect on the early chain branching and lead to the proliferation of reactive radicals. The macroscopic effect of this increase in the concentration of reactive radicals is an overall improvement in the fuel/air mixture reactivity and hence a faster heat release. This effect on the early stage of oxidation

can be identified as the main mechanism which causes the advance in the combustion phasing observed when ozone seeds the engine intake.

6.3. EXTENSION OF THE AUTOIGNITION REGION: OZONE INDUCED COMBUSTION

In this section, optical diagnostics were performed when high ozone concentrations were used to extend the autoignition range of iso-octane, allowing the fuel to autoignite in thermodynamic conditions in which combustion cannot generally occur.

6.3.1. OH* and CH_2O PLIF

Two experimental conditions were analyzed to understand the mechanism governing the ability of ozone to extend the ignition range of gasoline-like fuels. The details are reported in Table 13.

Tag	Engine Speed	Intake Temperature	Intake Pressure	Equivalence ratio	Ozone
TI	1500 rpm	195 °C	1.39 bar	0.3	0 ppm
OI	1500 rpm	110 °C	1.39 bar	0.3	100 ppm

Table 13. Experimental conditions for thermodynamically established combustion in the optically accessible engine.

A thermodynamically induced (TI) combustion case was compared to ozone-induced (OI) low temperature combustion. TI autoignition needed an intake temperature of 195°C to occur. To achieve OI relevant conditions, the intake temperature was lowered to 110°C, well below the minimum temperature required to achieve iso-octane TI autoignition, and then the ozonizer was activated by setting it to the maximum generation capacity: ~100 ppm of O_3 seeded the intake flow, and OI combustion was achieved. Figure 99 compares the heat release rate of the CH_2O-PLIF and OH* chemiluminescence signals for the TI and OI case.

It should be noted that the two cases showed a different CA50, which was 7 CAD in TI combustion and 2 CAD for OI combustion. Accordingly, the HRR associated to the OI trace was shifted by some CAD toward TDC and had a higher maximum value compared to the TI case. In the TI case, the heat release started to increase close to TDC, reached a maximum 5 CAD aTDC, and then decreased, indicating the end of the combustion process. Accordingly, the corresponding OH* signal was recorded in the same CAD range. As

expected for conventional HCCI combustion, the CH_2O-PLIF emission preceded the OH* signal by a few CAD. Setting the ozone generator at its maximum capacity made it possible to reduce the intake temperature required for iso-octane autoignition by ~80°C. In these conditions iso-octane experienced ozone-induced (OI) combustion. The OI case showed interesting phenomena occurring earlier during the first stage of combustion.

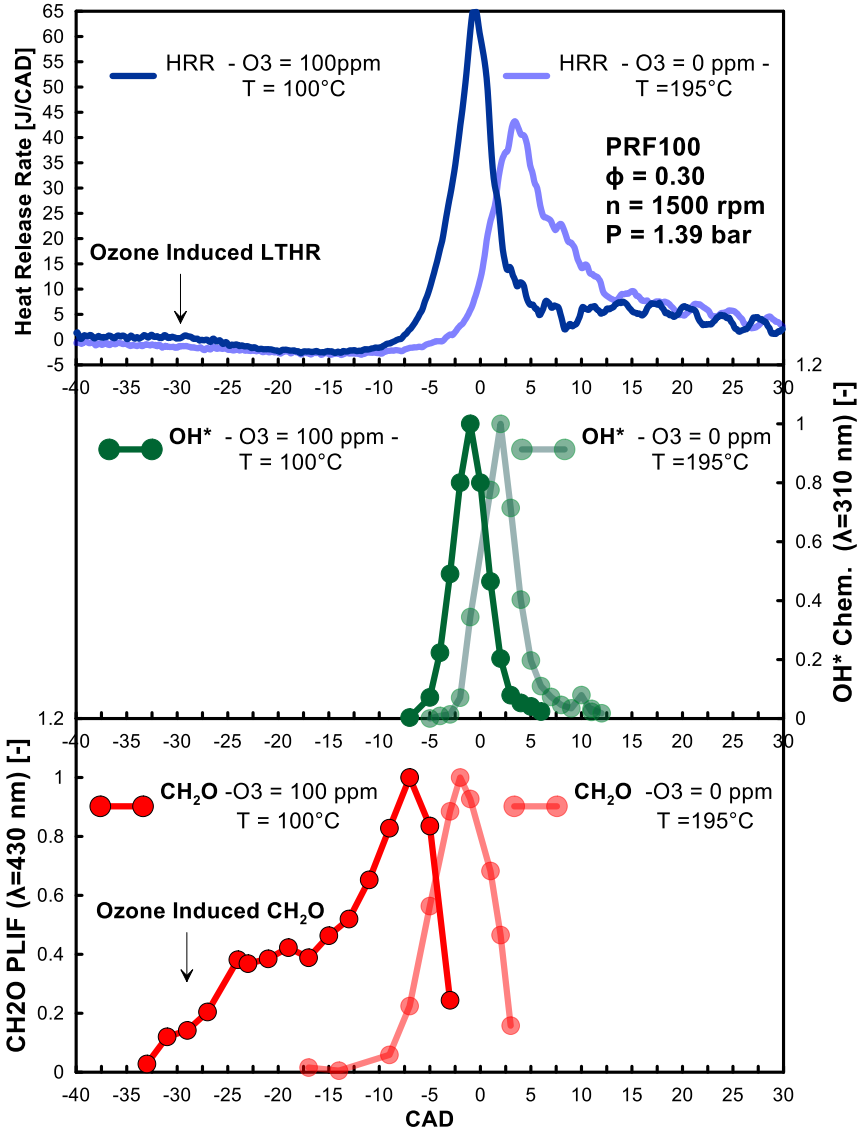

Figure 99. Heat release rate trace, OH* and CH_2O PLIF emission under TI and OI conditions. Experimental conditions are reported in Table 13.

The first phenomenon which differentiated OI from TI combustion was the appearance of an early low temperature heat release (LTHR) with an intensity of ~2J/CAD between -35 CAD and -25 CAD aTDC. An additional phenomenon which differentiated OI from TI combustion is the shape of the CH_2O-PLIF. The presence of formaldehyde was detected starting from -35 CAD aTDC. After its appearance, the CH_2O signal showed a first increase and reached 40% of its maximum at -25 CAD aTDC. Then, CH_2O remained constant

until -25 CAD aTDC, when it started to rise again, reaching its maximum some CAD before TDC. Then, the CH_2O signal started to fall at -7 CAD aTDC and OH* emission, which was not observable before, started to rise. The early heat release and the CH_2O emission observed for the OI case in Figure 99 are similar to those characterizing the LTHR in HCCI combustion of fuel exhibiting a double-stage heat release [110,122–124]. This demonstrated that ozone, by carrying highly reactive O atoms in the fuel/air mixture, has the ability to alter the oxidation process and promote new reaction pathways responsible for a LTHR and early CH_2O formation. The induction of a LTHR is most likely the mechanism through which ozone addition stimulates the reactivity of the system, allowing for the compression ignition of the lean iso-octane/air mixture which otherwise would not have ignited at such a low intake temperature.

6.3.2. Analysis of Ozone Induced (OI) combustion by means of CH* and OH* detection by photomultipliers

In the previous section the simultaneous analysis of the CH_2O-PLIF and OH* signals demonstrated that the improved reactivity caused by ozone, which enabled the ignitability range of iso-octane to be extended, is strictly related to the ability of this chemical agent to induce a LTHR similar to that which characterizes low octane fuels such as naphtha or n-heptane. In this way, ozone was shown to be capable of activating the combustion process even at temperatures well below the minimum values required for autoignition in the non-seeded case. To acquire more details about the mechanism governing the ability of ozone to extend the ignitability range of gasoline, further investigations into OI combustion were performed by means of the simultaneous measurements of the in-cylinder pressure and the CH* and OH* chemiluminescence signals.

In the experiments, the engine was initially run by setting the intake temperature and pressure which define the OI intake conditions (P_{intake} = 1.39 bar and T_{intake} = 110°C), but with the ozonizer turned off. Accordingly, combustion did not occur at such a low temperature.

Tag	Engine Speed	Intake Temperature	Intake Pressure	Equivalence ratio	Ozone
OI	1500 rpm	110 °C	1.39 bar	0.3	0-50-75-100 ppm

Table 14. Experimental conditions used to investigate the OI combustion process in the optically accessible engine.

Then, as indicated in Table 14, the ozonizer was turned on and its capacity progressively increased in order to observe the in-cylinder process transition from misfire to the establishment of ozone-induced combustion. Figure 100 shows the in-cylinder pressure, temperature and the mean heat release rate in OI experimental

conditions and for different ozone concentrations. For the same experiments, the chemiluminescence emissions of OH* and CH* recorded by two photomultipliers are reported in Figure 101.

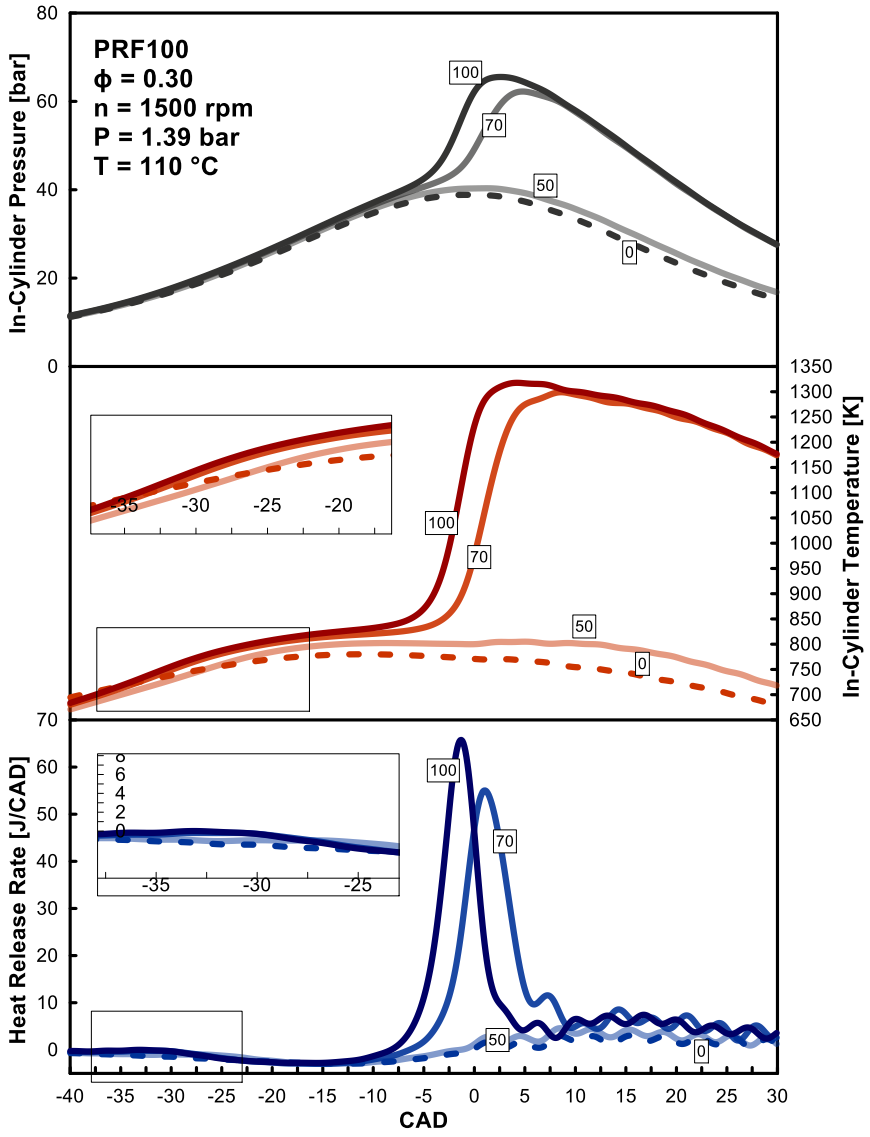

Figure 100. In-cylinder pressure, temperature and heat release rate as a function of the ozone concentration in ppm under OI intake conditions. Numbers in the boxes indicate the ozone concentration in ppm. Experimental conditions are reported in Table 14 .

The in-cylinder data reported in Figure 100 clearly show that no combustion occurred when the ozonizer was turned off. Accordingly, the OH* chemiluminescence signal was flat, indicating the absence of any high-temperature combustion process leading to the formation of this radical. An extremely weak signal coming from CH* chemiluminescence is observable in Figure 101, indicating the presence of a weak chemical activity even if combustion did not occur. By adding 50 ppm of ozone, it was possible to observe the first macroscopic effects of ozone addition. Following the presence of a certain ozone concentration in the cylinder, an overall increase in reactivity was registered, as demonstrated by the weak but observable

LTHR between -35 CAD and -25 CAD aTDC reported in both Figure 100 and Figure 101. Figure 101 also shows that this LTHR was immediately followed by CH* chemiluminescence emission starting at -25 CAD aTDC. The presence of such early CH* emission demonstrates that ozone alters

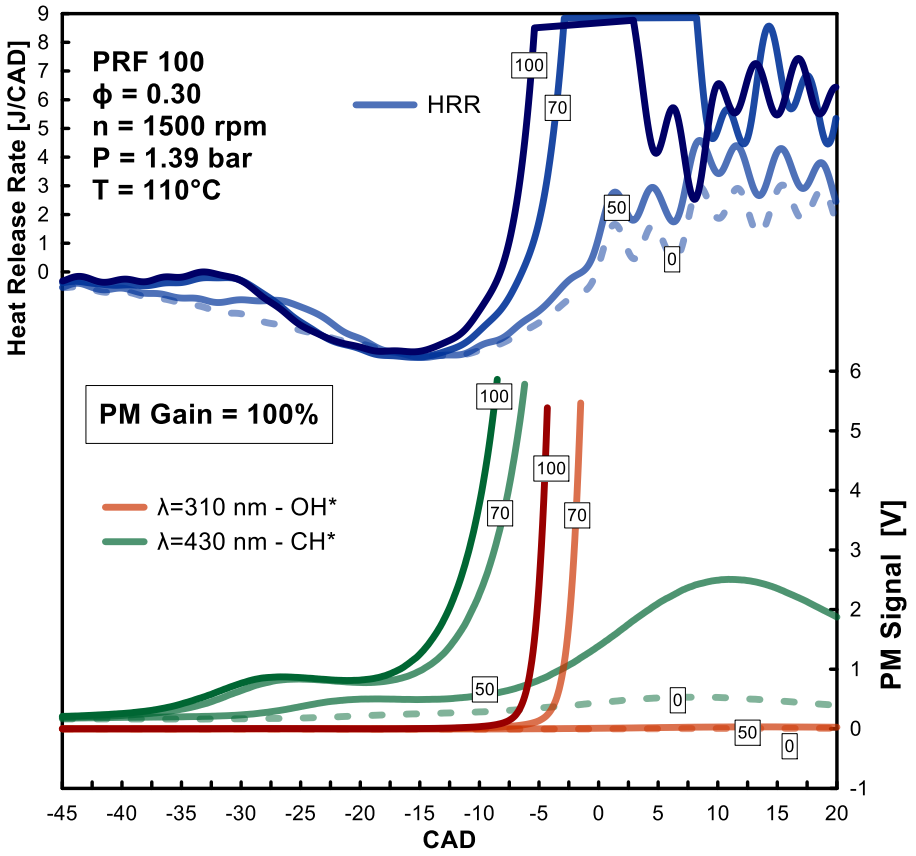

Figure 101. Impact of ozone addition on the heat release rate, OH* and CH* signals from photomultipliers. Numbers in the boxes indicate the ozone concentration in ppm. Photomultiplier gain at 100%. Experimental conditions are reported in Table 12.

the reaction path, stimulating earlier chain branching reactions and thus yielding the production of radicals which were not produced in the absence of ozone nor in the conventional oxidation process (cf. Figure 98). It can also be seen that the CH* signal increased later in the cycle, in the region just after TDC. However, as reported in Figure 100, although some substantial fluctuations of the in-cylinder pressure and temperature were recorded some CAD after TDC, the enhancement of the reactivity induced by this level of ozone was not significant enough to enable the full development of the reactions leading to autoignition of the fuel. Therefore misfire occurred, as can also be deduced by the lack of any appreciable OH* chemiluminescence signal or high-temperature heat release visible in Figure 101 when the 50 ppm of ozone seeded the intake of the engine. Increasing the ozone concentration up to 70 ppm, led to an overall improvement in reactivity which was accompanied by the occurrence of fuel autoignition, as indicated by the well-developed HRR, pressure and temperature traces observable in Figure 100 when O_3=70 ppm. The higher O_3 concentration

allowed the establishment and the complete development of the oxidation process which was instead only partially initiated when the ozone concentration was O_3=50 ppm. It can therefore be said that ozone-induced OI autoignition was achieved with the 70 ppm of ozone, even though the in-cylinder pressure and temperature were well below the minimum values required for the ignition of such a lean iso-octane/air mixture under conventional, non-seeded operations.

It can be noticed from the heat release rate (HRR) traces reported in Figure 100 and Figure 101, that in this case of a well-established and developed OI combustion process, a clear LTHR preceding the main heat release was observable 35 CAD before TDC. Figure 101 shows that the LTHR was immediately followed by CH* chemiluminescence emission that is visible starting from -35 CAD aTDC. However, unlike the case of O_3 =5 0 ppm the early CH* signal was more intense and occurred earlier in the cycle, indicating a strengthening of the LTHR reactions. Moreover, after remaining at a constant level, the CH* emission abruptly increased starting from -15 CAD aTDC, leading to the saturation of the photomultiplier signal. Figure 101 shows that the dramatic increase in the CH* signal took place close to the main heat release, and that it was followed by a strong OH* chemiluminescence emission indicating the occurrence of the main heat release phase of the ozone-induced OI combustion. The previously shown increase in the CH* emission indicated that thanks to the higher ozone concentration, the alternative ozone-induced oxidation pathway was strengthened, promoting the chain branching reactions that led to the proliferation of highly reactive radicals and the production of the excited state of CH. It can also be noticed that the early LTHR observable in both Figure 100 and Figure 101 was accompanied by a small but clear increase of the in-cylinder temperature in the same CAD interval. The resulting in-cylinder temperature however was low if compared to the in-cylinder temperature required to achieve iso-octane autoignition in the non-seeded case, which was 100 K higher. This result, along with the CH* trends discussed above, suggests that the increased ozone-induced reactivity is merely associated with a chemical effect related to the proliferation of radicals, rather than to a thermal effect. Setting the intake ozone concentration at 100 ppm led to a further increase in the intake ozone concentration, enhancing the autoignition process leading to the well-known advance of the heat release, followed by the corresponding simultaneous advance and increase of the in-cylinder pressure and temperature. Observing Figure 101, it can be seen that the advance in the heat release rate is associated to a slight advance and increase in the heat generated during the LTHR. Accordingly, an advance and an increase in early CH* emission was observed, indicating that the promoting effect of ozone on combustion was related to the strengthening of the alternative ozone-induced chemical mechanism which governs the occurrence of an iso-octane cool flame and its associated LTHR.

6.4. CONCLUSIONS

In this chapter, HCCI combustion of iso-octane, a gasoline surrogate fuel, was investigated by means of an optically accessible engine. The aim was to identify the mechanism underlying the promoting effect of ozone. In the first part of this chapter, the impact of ozone on thermodynamically induced combustion was investigated. Results indicated that when ozone seeded the engine intake, CH_2O-OH* production advanced in accordance with the advance experienced by the heat release. The relative phasing of the CH_2O and OH* signals was not altered, with the conventional CH_2O-OH* transition occurring at the main heat release phase. No CH_2O from cool flame of low temperature heat release was observed when low amounts of ozone were used to advance the combustion phasing. Despite no low temperature heat release, photomultiplier measurements showed that ozone induced an increased chemical activity characterized by the early emission of CH* chemiluminescence, indicating the stimulating impact of ozone on the chain branching reactions promoting the autoignition event. In the second part of the chapter, ozone was employed to extend the autoignition range of iso-octane. Specifically, using an ozone concentration of ~112 ppm made it possible to reduce the intake temperature required for autoignition by about 90°C. The appearance of an early low temperature heat release and a CH_2O-PLIF emission taking place -35 CAD aTDC characterized the ozone-induced OI combustion. Moreover, the presence of early CH* emission was also observed at this LTHR. This demonstrates that under ozone-induced combustion, the highly reactive O atoms carried by the O_3 molecules alter the fuel's oxidation reaction path, introducing alternative chemical pathways and stimulating the earlier chain branching reactions that lead to an increased production of radicals which are not produced in the absence of ozone during the conventional oxidation process. The modified fuel oxidation chemistry, characterized by the increased radical production and followed by a LTHR in the case of high intake ozone concentrations was identified as the mechanism through which ozone addition stimulates the reactivity of the system, allowing for the autoignition of a lean iso-octane/air mixture which otherwise would not have ignited at such a low intake temperature.

7. Ozone-assisted GCI low load operation

7.1. INTRODUCTION

In a GCI engine, the in-cylinder process is characterized by a certain degree of PFS to achieve Gasoline PPC. To achieve such a GPPC mode, GCI engines rely on a complex injection strategy. Using the promoting effect of ozone to improve gasoline combustion and overcome GCI limitations at low load brings with it the need to understand how the beneficial properties of ozone are impacted by the injection strategy employed to supply the fuel.

7.2. OZONE IMPACT UNDER DIRECT-INJECTION GCI OPERATION

7.2.1. Ozone decomposition in a D-I CI engine

Previous studies [85] demonstrated that the effect of ozone on hydrocarbon oxidation is mainly related to its ability to decompose and yield highly-reactive O atoms, as reported in Figure 102. The highly reactive O atoms then improve fuel combustion by introducing new pathways in the fuel oxidation process. Assessing the way in which ozone behaves and decomposes once introduced into the combustion chamber is therefore of primary importance, even more so when the fuel direct injection strategy can be employed to vary the timing of the fuel supply. The decomposition of ozone can be studied through kinetic modelling using the Senkin [125] code. A model simulating the in-cylinder volume variation as a function of time was employed. In input, the model was fed by the engine geometry, the intake thermodynamic conditions and gas composition. To assess ozone decomposition during the compression stroke of the engine, a chemical mechanism including the ozone sub-mechanism provided by [72] was used. Initial conditions for Senkin calculations simulate the engine setup used for the experiments, and are reported in Table 15. After being introduced inside the cylinder, ozone is subject to the effect of the in-cylinder pressure and temperature evolution. Under such in-cylinder thermodynamic conditions, ozone molecules are not stable and decompose according to a chemical mechanism which can be described by the following reactions:

$$O_3 + N_2 \leftrightarrow O_2 + O + N_2 \quad (27)$$

$$O_3 + O_2 \leftrightarrow 2O_2 + O \quad (28)$$

$$O_3 + M \leftrightarrow M + \mathrm{O} + O_2 \quad (29)$$

As indicated in Figure 102, under engine relevant conditions, ozone decomposition leads to the presence of molecular O2 oxygen and the highly reactive O atoms responsible for the ozone-induced combustion

enhancement. Results from simulation indicated that highly-reactive O atoms are generated during the last part of the compression stroke.

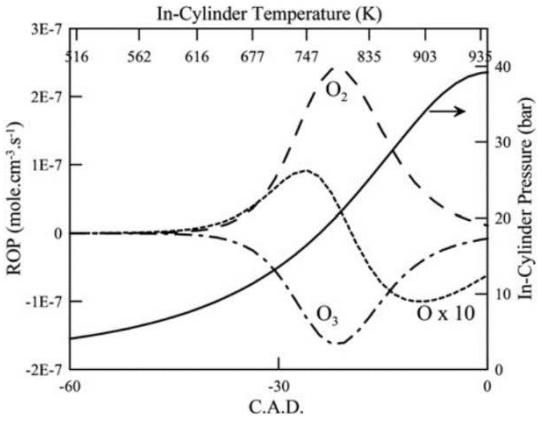

Figure 102. O atoms mole fraction and in-cylinder pressure as a function of CAD for different ozone concentrations at the intake, from [85].

O2/N2 ratio	Engine Speed	Intake Temperature	Intake Pressure	Ozone
21% / 79%	1500 rpm	187 °C	1 bar	Variable

Table 15. Initial conditions employed for Senkin calculations.

Figure 103 shows the in-cylinder concentration of free radicals of oxygen coming from the decomposition of different intake ozone concentrations. Whatever the initial O_3 concentration at the intake, results of calculations showed that the concentration of O atoms presented a maximum some crank angle degrees before top dead center (TDC), then decreased because highly reactive O atoms recombined, yielding O_2 molecules. Both the value and the phasing of the maximum availability of O atoms depended on the initial ozone concentration. The concentration of the highly reactive O atoms increased in the case of higher intake ozone concentrations. This explains why higher ozone concentrations have a higher promoting impact on combustion. Moreover, higher ozone concentrations resulted in a faster decomposition of ozone, followed by an advance of the maximum O availability in the cycle. The calculated O evolutions suggest that the injection timing could play an important role in determining the ability of ozone seeding to enhance the combustion process. Looking at the O recombination occurring in the final part of the compression stroke shown in Figure 102, it is questionable whether late fuel injections may still be subject to the influence of

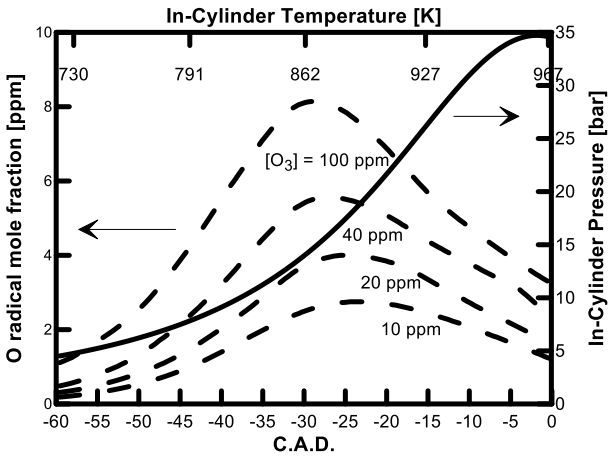

Figure 103. O atoms mole fraction and in-cylinder pressure as a function of CAD for different ozone concentrations at the intake.

ozone despite the recombination of O atoms into O_2 molecules. The final purpose of the use of ozone is to systematically reduce the intake air temperature required for low load gasoline autoignition.

Therefore, the impact of the intake temperature on the ozone behavior was investigated. Figure 104 shows the in-cylinder concentration of O free radicals coming from the decomposition of 100 ppm of O_3 as a function of the crank angle degree and for different intake temperatures. It can be seen that the ozone behaves similarly whatever the intake temperature, with O_3 decomposition leading to a release of O atoms that recombine in O_2 molecules close to TDC. However, the maximum value and its relative position are strongly temperature dependent.

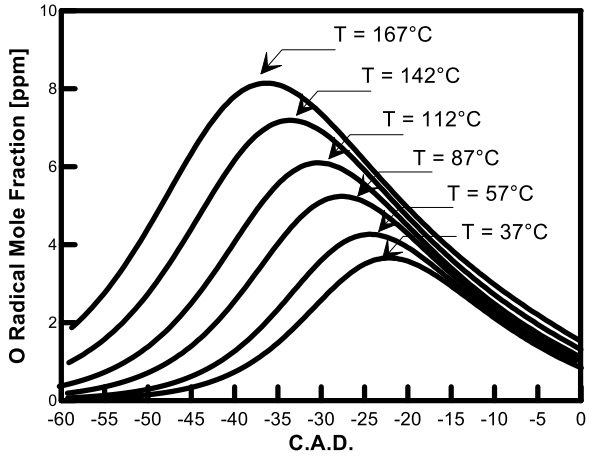

Figure 104. In-cylinder O atoms mole fraction as a function of the CAD for different intake temperatures for an intake Ozone concentration of 100ppm.

To clarify the impact of temperature, Figure 105 reports on the same graph the maxima in O concentration and the corresponding position in the cycle as a function of the intake temperature. In addition, in the upper y axis, the maximum in-cylinder temperatures reached during each cycle are reported. Results show that

both the O maxima and their relative phasing are linearly correlated with the in-cylinder temperature evolution during the compression stroke. These results indicate that the chemical kinetics of ozone decomposition is strongly temperature dependent. If the entire decomposition of ozone takes place at a lower temperature, the production rates of the chemical reactions leading to O atoms are slowed down, with a consequent delay and reduction of the maximum O availability. According to these results, the increased reduction in the intake temperature can be a significant parameter affecting the capacity of ozone to release the O atoms necessary for enhancing autoignition.

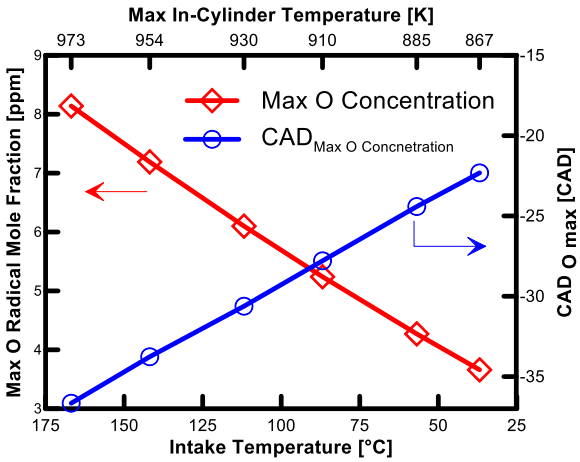

Figure 105. Maximum in-cylinder O atoms concentration, crank angle positions of the maximum O concentration and maximum in-cylinder temperature as a function of the intake temperature for a constant intake ozone concentration of 100 ppm. Results from Senkin simulations.

7.2.2. Impact of the fuel injection timing on the promoting effect of ozone

In the premixed combustion reported in the previous chapter, ozone and fuel molecules were introduced together in the engine. Accordingly, under all the conditions investigated, fuel and ozone coexisted in the cylinder throughout the engine cycle. Moreover, the local conditions of temperature and equivalence ratio can be considered homogeneous. Inhomogeneities induced by spray fuel injection were excluded, reducing the number of parameters affecting the impact of ozone on combustion. In GCI Direct-Injection operation, the fuel is injected with a variable timing. Ozone and the O atoms coming from its decomposition come into contact with fuel molecules only after the start of injection (SOI) has occurred. Hence, the time available for the fuel molecules and the O atoms to mix and react together changes depending on the fuel injection strategy. Moreover, fuel injection timing also determines the characteristics of the spray-induced inhomogeneities, which strongly impact the local chemical and thermodynamic conditions in which the

chemical reactions induced by ozone have to occur. It is clear that a small variation in injection timing can considerably complexity the phenomena determining the ozone impact on gasoline combustion.

For these reasons, the first step necessary for understanding the impact of ozone on PPC combustion of gasoline consisted in the assessment of the impact that the fuel injection timing may have on the ability of ozone to alter the fuel oxidation reactions.

Experiments were performed to analyze the impact of ozone as a function of the fuel injection timing. Experimental conditions are reported in Table 16.

Engine operating conditions			
Fuel	SPB95 Gasoline	**Injector**	UA90/UA156
Engine Speed	1500 rpm	**Rail Pressure**	400 bar
Intake Pressure	1 bar	**Injected Mass**	7.8 mg/cycle
Intake Temperature	187° C	**Equivalence ratio**	0.3
Ozone concentration	Variable	**SOI**	Variable

Table 16. Engine baseline operating conditions used to study the effect of ozone under different fuel injection timings.

To investigate low load GCI operation, a fixed mass of 7.8 mg/cycle commercial RON95 gasoline was directly injected in a single injection event. This fueling rate corresponded to an equivalence ratio of ϕ=0.3. For all the tests, an injection pressure of 400 bar was employed. The intake pressure was kept constant at 1 bar in order to simulate the low load operation of a GCI engine, in which the exhaust enthalpy is too low to provide the energy necessary to activate intake boosting by a turbocharger. Gasoline combustion was first thermodynamically established by heating the intake air flow up to 187°C, well above the intake air temperature available in commercial CI engines at low load. For a given start of injection SOI, the thermodynamically established combustion was characterized by a certain CA50. The engine intake was then seeded with different ozone concentrations and the shift in the CA50 induced by a certain amount of

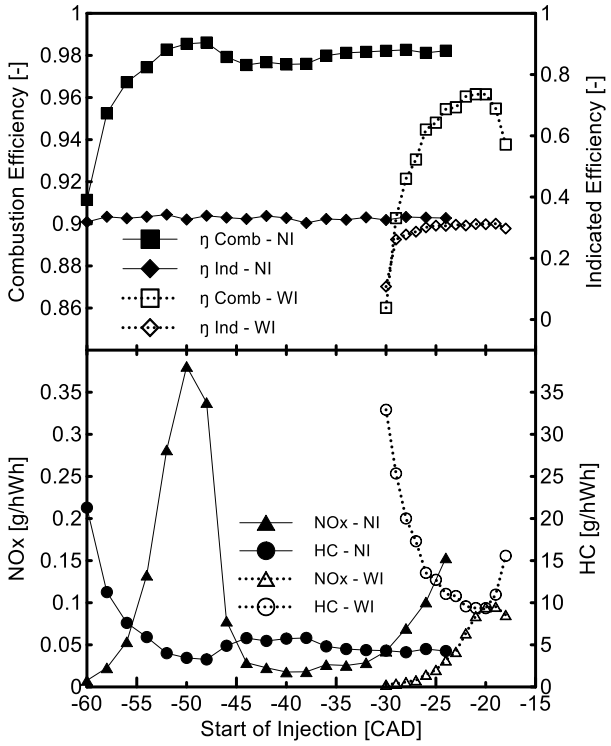

Figure 106. Combustion efficiency, Indicated efficiency, NOx and HC emissions as a function of SOI and injector type: WI=156° and NI=90° umbrella angle.

O_3 molecules was used to quantify the impact of ozone at a given SOI. The effect of ozone was then evaluated at different SOI and for different intake ozone concentrations.

A first attempt to investigate ozone-SOI interaction was conducted employing the baseline 156° Diesel injector (WI). In the experimental conditions described above, thermodynamically established combustion was achieved. Starting from TDC, the gasoline injection timing was advanced up to SOI = -24 CAD, but more advanced injection timings were not possible since the gasoline did not autoignite because of the excessive overleaning, as indicated by the results reported in Figure 106. Moreover, in this SOI range, no effect of ozone on combustion was observed. No variation in the combustion phasing was observed even though the ozone generator was set at the maximum capacity. This was most likely due to the fact that for such late SOI, fuel is injected when the O atoms coming from O_3 decomposition have already started to recombine, forming molecular oxygen. No O atoms are then available to improve the fuel oxidation. Moreover, as indicated by the experiments reported in the previous chapter, optical diagnostics revealed that the ozone-induced pre-reactions in the premixed case occurred approximately 40 CAD before TDC, as shown in Figure 98. Later injection timings are therefore not impacted by ozone because of the limited time available for the low temperature reactions to occur. In order to extend the SOI range, the experiments were repeated by mounting an injector with a narrower umbrella angle, the UA90. Figure 106 reports the results

of the swipe in injection timing in the case of thermodynamically induced combustion, when no ozone seeded the intake of the engine, for both the UA90 and UA156 injectors. Experimental conditions are reported in Table 16. It should be noted that although the intake temperature was different from the one employed for the GPPC characterization discussed in Chapter 4, results from the experiments evidence the same trends and phenomena. In detail, Figure 106 shows that using a 90° umbrella angle extended the injection range up to 58° CAD before TDC, while maintaining combustion efficiency around 98%. A bump in NO_X emission from the UA90 injector can be observed between SOI =-55 CAD and SOI = -45CAD. This was a further manifestation of the NOx excitation mechanism explained in Chapter 4. NOx production abruptly increased due to geometric interference between spray and bowl conformation. Because of the particular injection timing, spray orientation and bowl geometry caused the fuel to remain accumulated and constrained at the bottom of the bowl. In the latter condition, the local equivalence ratio value in the range of ϕ 0.9-1.1 can increase, incentivizing the formation of NO according to the Zeldovich thermal mechanism.

Using the UA90 injector, the impact of ozone on the combustion of gasoline was evaluated for different injection timings and for different intake ozone concentrations, while all the other parameters were kept constant. Experimental conditions are summarized in Table 16. Results are reported in Figure 107 (a). Figure 107 (a) clearly shows that over the SOI range investigated, the effect of ozone did not follow a monotonic trend. Thus, ozone decomposition and the O trends reported in Figure 102 and Figure 103 are not sufficient to explain the ozone behavior. At SOI = -60 CAD, adding 15 ppm of O_3 advanced CA50 by 6 CAD, and increasing O_3 concentration up to 124 ppm corresponded to a further shift of 11.5 CAD. In these conditions, the CA50 shift induced by ozone increased with the increase in ozone intake concentration. At this early injection timing, the improved fuel-air mixing enabled the premixed combustion of gasoline, ozone fuel residence times are longer if compared to later SOI, and the effect of ozone was comparable to that obtained under HCCI conditions for gasoline and iso-octane combustion in similar conditions.

Moving SOI closer to TDC caused a substantial reduction in the ozone effect, as indicated by the lower sensitivity of the CA50 to increase ozone concentration. This can be attributed to a lower residence time between the fuel and the O atoms induced by later SOI. However, a reduction in the residence time of fuel

and ozone cannot explain the phenomena observed between SOI=-52 and -48 CAD. In this SOI range, indeed, adding ozone actually caused a delay in CA50.

This behavior is due to the chemical interaction between ozone and the Nitrogen Oxide (NO) contained in the Residual Burnt Gases [94,126].

Figure 107 (b) reports the exhaust NO emissions in the non-seeded case and the fraction of the NO produced that was trapped in the residual burnt gases, experimentally measured with the method developed and described in Chapter 4. Indeed, due to the reaction

$$O_3 + NO \quad \leftrightarrow O_2 + NO_2 \qquad (30)$$

of which the effects were discussed in [17], the NO trapped in the residual gases consumes a portion of O_3 molecules, with a one by one ratio, before O_3 can decompose and interact with the fuel. If the initial concentration of NO is lower than that of ozone, a fraction of O_3 molecules reacts, leading to NO_2, while the remainder initiates fuel oxidation. The impact of ozone in this case is only reduced proportionally to the initial NO concentration. If the initial concentration of NO is higher than that of ozone, all the O_3 molecules are consumed by the $NO+O_3 \rightarrow NO_2+O_2$ reaction. No residual O_3 is available to initiate fuel oxidation, and also the initial concentration of NO, which was responsible for accelerating combustion phasing in the non-seeded case, is reduced, leading to a global delay in combustion phasing. To support this interpretation, Figure 108 shows, as a function of the concentration of ozone at the intake, the evolution of CA50, the exhaust NO concentration, and the estimated residual NO in two representative cases. At SOI = -48 CAD, ozone delays combustion because of interaction with NO. Without O_3 molecules, CA50=2.6 CAD, and combustion generated 680 ppm of NO, of which 25 ppm were estimated to be trapped in the cylinder. According to previous considerations, an ozone concentration below 25 ppm should delay combustion. Experiments confirmed this hypothesis. Ozone delayed CA50 for concentrations below 30ppm, the point at which CA50 reached the maximum 3.2 CAD. Then, increasing the O_3 concentration monotonically reduced CA50. It is also shown that for $[O_3]< 30$ ppm, as ozone increased, the NO concentration decreased, indicating that part of the NO reacted with O_3 yielding NO_2 and O_2. Figure 108(b) shows the results for SOI=-44CAD. The initial trapped NO concentration was 2 ppm, and because a minimum $[O_3]$ = 12 ppm was added, an advancing effect was directly observed.

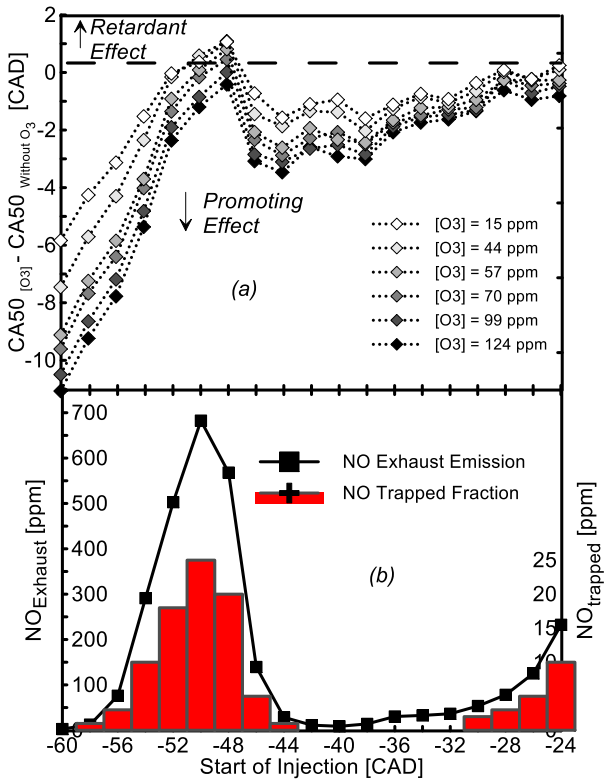

Figure 107. Shift in CA50 induced by different intake ozone concentrations as a function of the injection timing (a). Exhaust NO concentration and estimated NO trapped concentration as a function of the injection timing. Experimental conditions are reported in Table 16. The UA90 injector was employed during the experiments (b).

The considerations reported above clearly describe the trends in CA50 observed between SOI=-60 and -48 CAD, when combustion is mainly driven by residual NOx. However, over the SOI range between -44 CAD and -24 CAD, the trapped NO fraction is negligible, so that an ozone impact similar to the one observed at SOI = -60 or 58 CAD should have been expected according to previous considerations. The results in Figure 107 show a shift in CA50 that is halved if compared to that at early injection. This is related to the shorter time in which fuel and ozone coexist inside the cylinder. In Figure 98, under similar conditions, ozone-induced precreation occurred approximately 40 CAD before TDC. This suggests that retarding the injection event may lead to a shorter time in which ozone and fuel coexist, thus reducing the promoting effect that ozone has on hydrocarbon oxidation. This can explain the results reported in Figure 107, which shows a

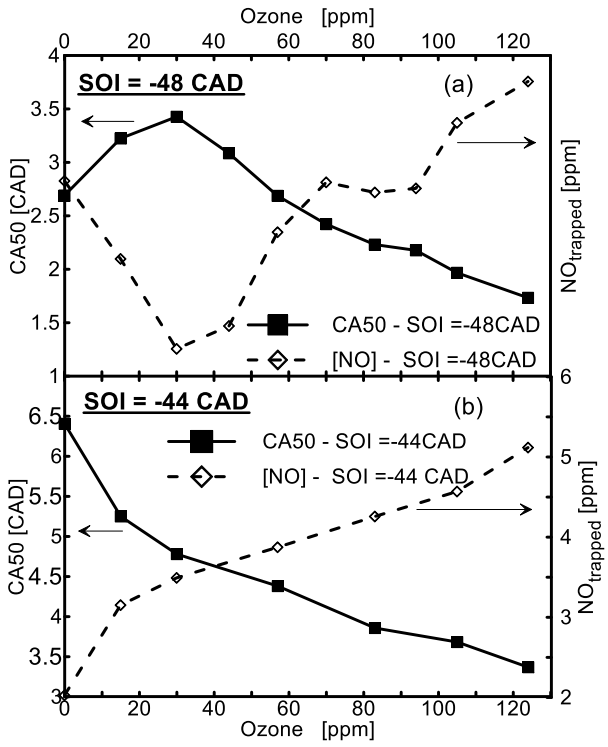

Figure 108. Combustion efficiency, Indicated efficiency, NOx and HC emissions as a function of SOI and injector type: WI=156° and NI=90° umbrella angle.

reduced sensitivity of the combustion phasing to ozone addition for SOI occurring later than -45 CAD compared to earlier injection timing.

7.3. EXTENDING THE LOW LOAD LIMIT OF A GCI ENGINE BY MEANS OF OZONE SEEDING

Extending the low load limit of a GCI means achieving autoignition of a reduced mass of fuel without the need to increase the intake temperature. Therefore, in this section the use of ozone to achieve gasoline autoignition at ambient intake temperature is investigated under direct injection operation.

7.3.1. Maximization of the ozone effect through adaptation of the fuel injection strategy

In the previous section ozone showed a potential for improving the autoignition propensity of gasoline under direct injection operation. Results showed that ozone can enhance gasoline combustion as much as the injection event is advanced. Experiments were then performed in order to reduce the intake temperature required for the gasoline autoignition and to investigate whether ozone could be used to overcome the limitations of GCI at low load, by reducing the intake temperature necessary for autoignition without any

boosting or VVT system to enhance fuel autoignition. In the experiments illustrated in the previous section, the maximum effect of ozone was observed for SOI = -60 CAD after TDC. However, even if the ozone generator capacity was set to the maximum power, the intake temperature was reduced by only a few degrees Celsius if gasoline was injected during the last part of the compression stroke.

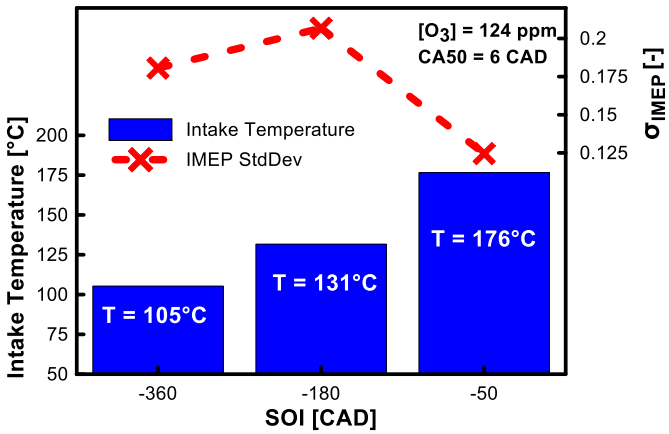

Figure 109. In blue: Minimum intake temperature required for autoignition of gasoline at a constant CA50 = 6 CAD, for three different Start of Injection: SOI = -50 CAD, SOI = -180 CAD and SOI = -360 CAD. In red dotted line and cross symbol: standard deviation of IMEP as a function of SOI. Fuel mass = 7.8 mg/cycle, P intake = 1 bar, n = 1500 rpm, the injection timing. Constant Ozone concentration of 124 ppm. Injector UA90°.

As in the previous experiment the residence time between the injected fuel and the ozone molecules proved to be of primary importance, additional tests were performed to investigate the influence of this parameter. Experiments were performed with a constant concentration of 124 ppm ozone seeding the engine intake. The intake temperature was varied in order to obtain the autoignition of a constant amount of fuel of 7.8 mg/cycle for three different injection timings. Figure 109 shows that if the injection was fixed at 50 CAD before TDC, gasoline did not autoignite at intake temperatures below 176°C. If the injection was advanced up to 180 CAD before TDC, the intake temperature necessary for gasoline autoignition was 131°C. The lowest intake temperature required for gasoline autoignition was observed when fuel was injected 360 CAD before TDC, at the beginning of the intake stroke. The results in Figure 109 suggest that for temperature reduction applications, injection timing close to TDC during the compression stroke is not suitable to capitalize on the effect of ozone, mainly because of the shortened residence time. Instead, early injections during the compression stroke or even injecting the fuel during the intake stroke, represent a better solution to enable the low temperature autoignition of gasoline. In order to assess the combustion stability,Figure 109 shows the standard deviation of IMEP for the three cases investigated. Results showed that besides offering the most reactive conditions, injecting the fuel at SOI=-360 CAD before TDC was also favorable to achieve stable operation if compared to the SOI = -180 CAD case. According to previous experiments the most reactive condition which also offers stable combustion is injection at SOI=-360 CAD. However, even for low load operations in which a reduced amount of fuel is injected, a strategy consisting of a single

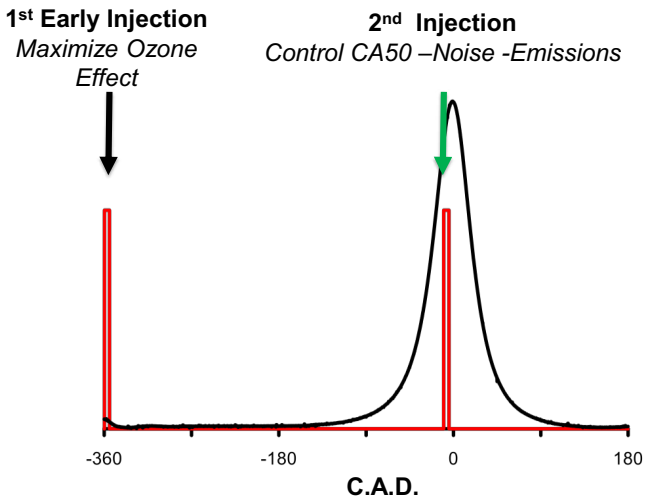

Figure 110.Schematic of the Injection Strategy employed to maximize the effect of Ozone.

injection during the intake stroke is not suitable for real engine applications because of the excessive noise and because of the impossibility of controlling the combustion phasing. Therefore, as shown in Figure 110, a double injection strategy was employed for ozone-assisted GCI at low load operations. The first injection event is located at the beginning of the intake stroke, and has the task of maximizing the residence time and improving the mixing between ozone and fuel, capitalizing on the promoting effect of the O atoms coming from O_3 decomposition. The second injection event takes place in the late compression stroke, close to TDC and is necessary to control the combustion phasing, noise and pollutant emissions, as will be shown later.

7.3.2. Using Ozone to reduce the Intake temperature required for gasoline autoignition

The goal of the experiments presented in this section was to demonstrate that with ozone, the GCI low load limitations could be overcome. Seeding the intake of the engine with ozone in order to extend the low load limitation of a GCI engine means achieving stable autoignition at room temperature and pressure. However, stable operations at low load were not possible when only one ozone generator was employed. In the following experiments, four ozone generators were connected in parallel to provide the necessary ozone concentration to enable the gasoline autoignition at 40°C. For all the tests in this section, the engine speed and the intake pressure were respectively 1500 rpm and 1 bar. As already discussed, because of the high octane number of gasoline, low load operations require the intake air to be heated up in order to allow the fuel to autoignite. However, as reported in Chapter 5, ozone can be used to reduce the intake temperature required for autoignition. In fact, while the intake temperature is maintained constant, adding ozone

advances the combustion phasing. Therefore, the intake temperature can be reduced in order to restore the original CA50. If this process is systematically repeated, ozone can systematically substitute the intake temperature required for autoignition, until gasoline combustion takes place at ambient temperature.

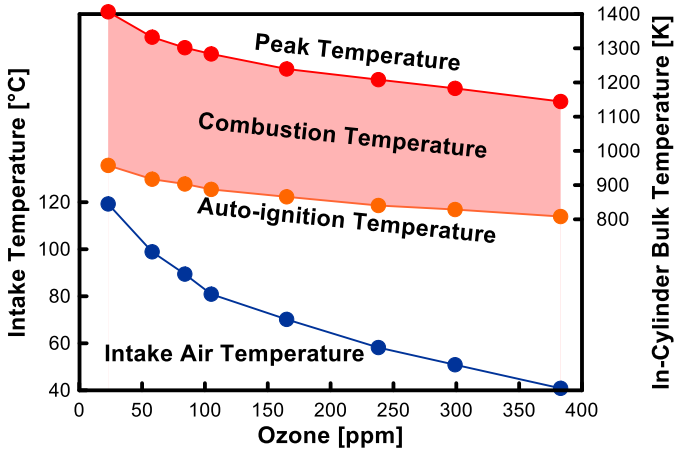

Figure 111. Blue line: intake temperature as a function of the intake concentration of ozone. Orange line: bulk temperature as a function of the ozone concentration at the intake. Red line: the maximum bulk temperature as a function of the ozone concentration at the intake. All the data were taken at fixed CA50 = 6 CAD and for a double injection strategy with SOI1=-360 CAD and SOI2 =-5CAD after TDC. Fuel distribution: 50/50 between the 2 events. IMEP = 3 bar.

Figure 111 shows the results of the experiment described above. The ozone-assisted GCI injection strategy was employed, with the fuel equally divided into two injection events, the first at SOI = -360 CAD and the second at SOI = -6 CAD. A fuel mass corresponding to 3 bar IMEP was maintained constant for all the experiments. Combustion phasing was maintained constant at 6 CAD after TDC, while by systematically increasing the ozone concentration seeding the intake of the engine up to 380 ppm the intake temperature required for autoignition was reduced to 40°C, which was considered the target temperature. Figure 111 also reports for the same experimental conditions the trends for the autoignition temperature, here estimated as the gas bulk temperature at CA10, and the maximum gas bulk temperature estimated from the in-cylinder pressure measurements. As highlighted in Figure 111, when the intake temperature was set at 120°C, autoignition of gasoline occurred at 980 K and combustion generated a maximum flame temperature of 1400K.

7.3.3. Characteristics of low intake temperature combustion induced by ozone

As a higher concentration of ozone was employed to substitute for the intake temperature required for autoignition, gasoline combustion initiated at systematically lower temperatures, thanks to the ability of O atoms coming from O_3 decomposition to alter the oxidation reaction and to directly generate OH radicals. In order to reach the target temperature of 40°C, 380 ppm of ozone were necessary. In these conditions, gasoline combustion began and developed at a lower temperature. The autoignition temperature was

lowered to 800 K and the maximum bulk temperature was drastically reduced to 1150 K. Results clearly show that ozone enabled the low temperature combustion of gasoline, and Figure 112 reports the consequences of the temperature reduction over the pollutant emissions generated by gasoline combustion. In Figure 112 NOx, HC and CO emissions are reported as a function of the ozone concentration at the intake (corresponding to increasingly reduced temperature). The lowering of the temperature at which the entire combustion process took place had a directly beneficial effect on NOx emissions, that were reduced from 680 ppm to 480 when the ozone concentration went from 25 to 380 ppm and the intake temperature from 120 to 40°C. The increased ozone concentration and the intake temperature reduction were also beneficial for unburned hydrocarbon (HC) emissions, which decreased from 4900 ppm to 4680 ppm. However, the conversion of CO into CO_2 dramatically suffered from the reduction of the overall combustion temperature, as indicated by the increase in CO exhaust emissions from 0.32% to 0.42% when the intake temperature was reduced to 40°C. Figure 113 shows the change in the maximum in-cylinder pressure gradient and in the combustion duration with the ozone concentration at the intake. Results show that while the intake temperature was reduced to ambient temperature, the in-cylinder pressure rose at a reduced rate when the intake temperature went from 120°C to 40°C.

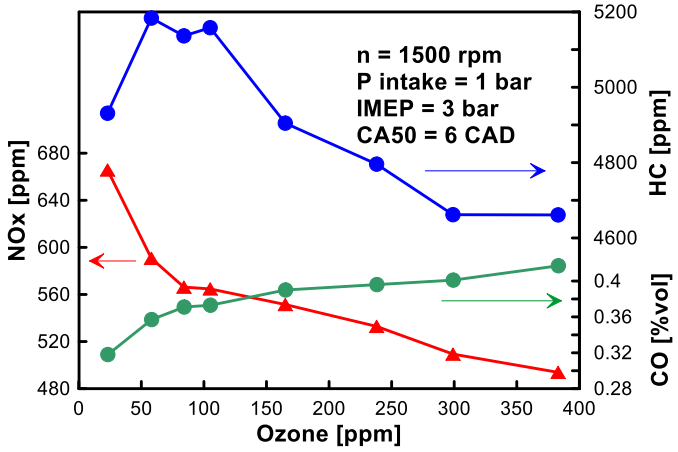

Figure 112. Pollutant emissions of NOx, CO and HC as a function of the ozone concentration employed to reduce the intake temperature.

The heat release traces as a function of the crank angle degree are reported in Figure 114. A cool flame occurring between -30 CAD and -20 CAD before TDC is a further manifestation of the alteration of the reaction path previously described. Figure 114 shows that the intensity of the cool flame heat release increased as the ozone concentration was increased from 23 to 383 ppm, mainly because an increasingly larger fraction of the fuel was affected by the modification in the oxidization reactions caused by the O atoms generated during ozone breakdown.

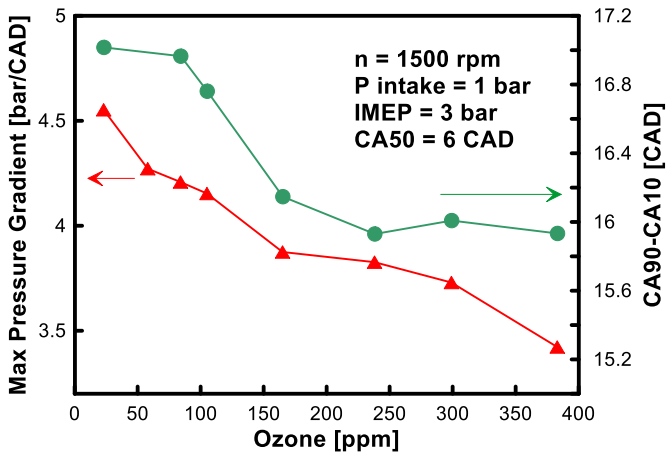

Figure 113. Maximum in-cylinder pressure gradient and combustion duration as a function of the ozone concentration used to reduce the intake temperature.

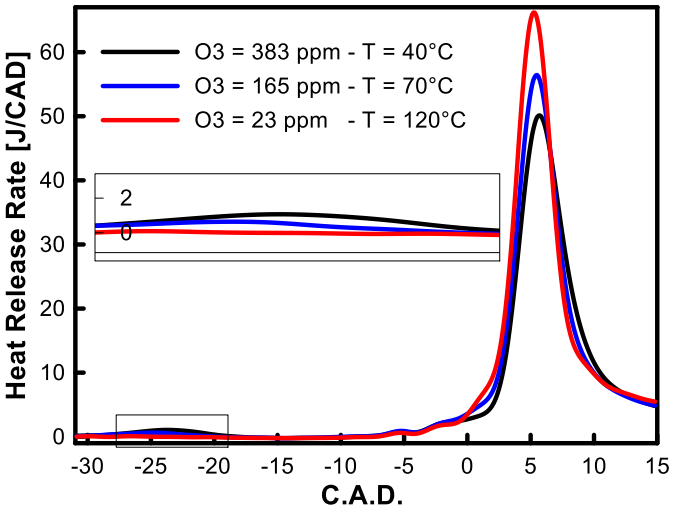

Figure 114. Heat Release Rate traces for three different ozone concentrations and intake temperatures. CA50 = 6 CAD. IMEP = 3 bar. Engine speed 1500 rpm. Injection Pressure 400 bar. Intake pressure 1 bar.

7.3.4. Control of GCI combustion via the timing of the second injection.

As mentioned in the previous section, for ozone-assisted GCI operation a second injection during the compression stroke is necessary to enable partial fuel stratification and hence control gasoline combustion via the injection event. Figure 115, Figure 116, Figure 117 and Figure 118 show the results of a sweep of the timing of the second injection (SOI2) when a constant O_3 concentration of 383 ppm was used to enable stable combustion of gasoline at 40°C. For all the tests, the fuel mass, equally split between the two injections, was adjusted in order to maintain a constant IMEP of 3 bar IMEP. For all the tests, COV of IMEP

was lower than 3%. As can be seen in Figure 115, by adjusting the timing of the second injection from SOI2 = 0 CAD to SOI2 = -10 CAD after TDC the combustion phasing could be set between 9.5 CAD and 2.7 CAD after TDC. While on the one hand, injection timings after TDC were not considered because of a significant decrease in combustion stability due to the long injection dwell time, on the other, earlier injection timings were limited at 10 CAD to meet the target of 5 bar/CAD as a maximum pressure gradient to avoid excessive noise and mechanical stresses. The increase in the pressure rise rate with the advance in injection timing is due to the more advanced combustion phasing and to the combustion being generated after both the first and the second injected charges had mixed and autoignited together under premixed conditions. This can be observed in Figure 117 in which the heat release rate and the in-cylinder pressure traces are reported as a function of the injection timings. According to Figure 115 for SOI2 earlier than -6 CAD after TDC, both injections are completed before the onset of combustion and both the heat release rate and the in-cylinder pressure traces present a single intense peak, indicating a premixed behavior, and accordingly, higher pressure gradient if compared to the one observed for more delayed injection timing. For injection timings corresponding to SOI2=-4 CAD and SOI2 = 0 CAD after TDC, the second injection took place after the combustion of the first premixed fuel portion had already started. Accordingly, the heat release and pressure traces showed two peaks where one can discern the mark of the cooling effect that the second injection has on the first premixed burning charge. However, because the last injection is not completed before the onset of combustion, the double peak shape cannot be referred to as bi-modal combustion generating from lean and reaching the phi-region induced by particular fuel stratification as discussed in [37]. In fact, for the SOI2 range from -4 to 0 CAD after TDC, the second injection interrupted the combustion of the first injected mass, and after a period in which oxidation is slowed down because of the heat necessary for the evaporation of the second charge, a more intense combustion event results from the rich and reactive mixture generated by the second injection.

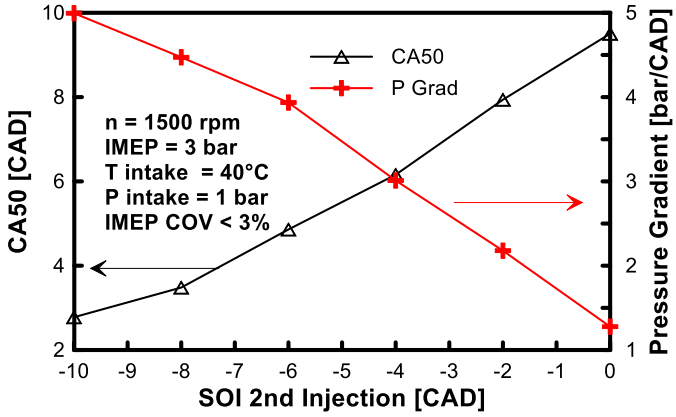

Figure 115.CA50 and Maximum Pressure Gradient as a function of the start of the second Injection SOI2

Moreover, the longer the second injection is delayed, the more time is available for the development of the oxidation of the premixed charge, as shown by the increased ratio between the intensity of the first and the second peak in the heat release rate. Because of the split and the lengthening of the heat release rate for injections taking place after SOI = -4 CAD, the slope of the pressure gradient as a function of SOI2 in Figure 115 is less steep if compared to injections taking place earlier than SOI = -4 CAD after TDC. Figure 118 reports the data from the exhaust gas analysis for the same experimental conditions. Results show a reduction in NOx emissions in accordance with the delay of the CA50 as the second injection moved toward TDC. NOx concentration at the exhaust decreased from 550 ppm to 110 ppm when SOI2 was moved toward TDC. However, delaying the second injection toward TDC and consequently the combustion phasing far from it had a detrimental effect on the exhaust emissions of Soot, HC and CO. Figure 118 shows that even though always under the limit of 1 FSN, soot emission abruptly increased for SOI2 later than -4 CAD after TDC. In fact, in accordance with the above observations on the heat release, the lack of separation between the injection event and the combustion process led the oxidation process to initiate from rich fuel pockets, incentivizing the production of soot. Figure 118

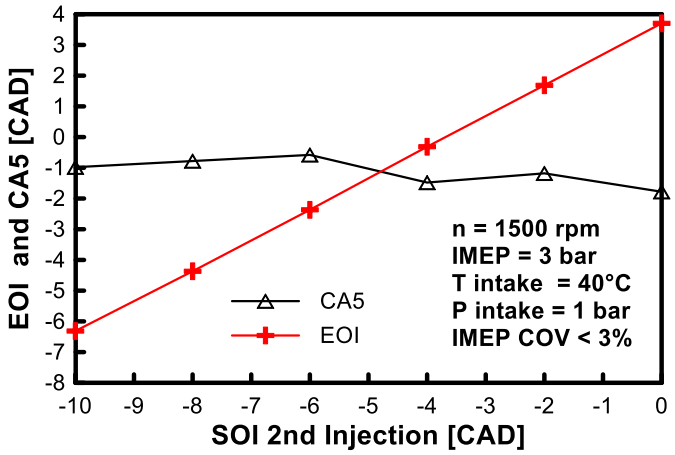

Figure 116. End of Injection and CA10 as a function of the SOI2

shows the influence of SOI2 on CO and HC exhaust concentrations. Both pollutants followed the same trend, showing lower sensitivity to the injection timing when SOI2 varied from -10 to -4 CAD after TDC, and a higher responsiveness for injection between SOI2 -4 and 0 after TDC, with a peak in SOI2 = -2 CAD after TDC. The latter is due to the interaction between the premixed combustion of the first injected mass and the spray coming from the second injection event, which arrested the rise of the in-cylinder temperature as shown in Figure 117(b), hindering the completion of CO to CO_2 conversion. However, even the minimum

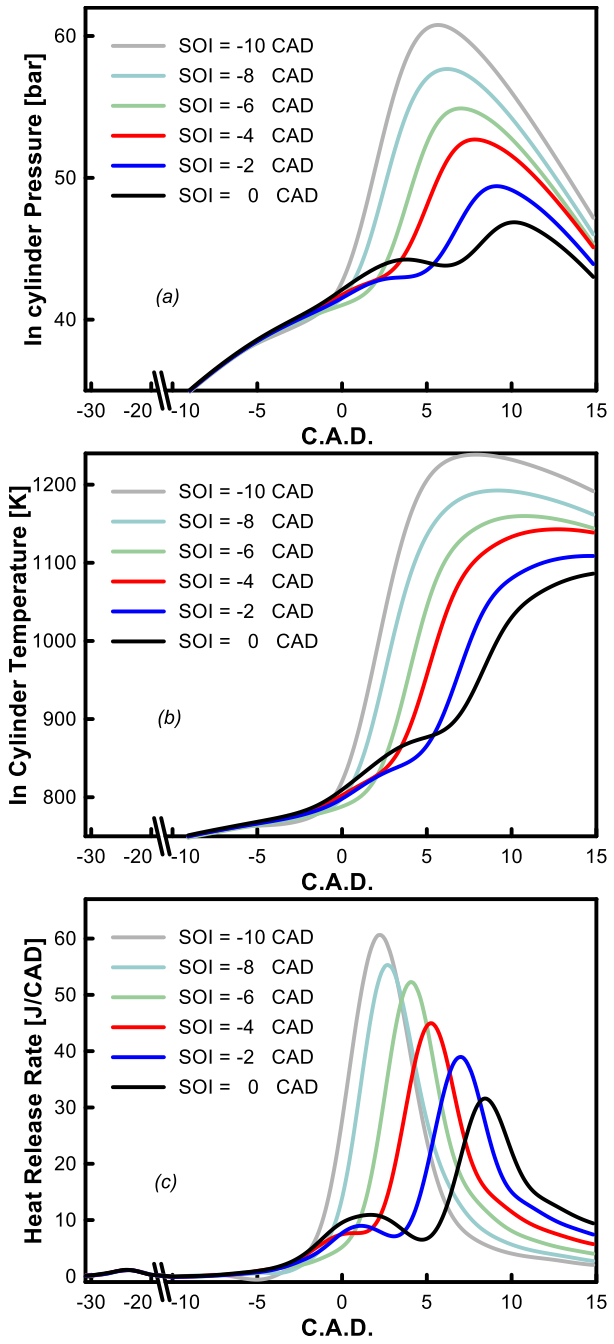

Figure 117.In-Cylinder Pressure (a), In-Cylinder Temperature (b) and Heat Release Rate (c) as a function of CAD for different SOI2.

concentrations of HC and CO measured at the exhaust, respectively 2900 ppm and 0.24 %, were extremely high. The main reason is the injection strategy employed. Because under ozone-

assisted GCI operation at low load the first injection takes place at TDC of the intake stroke, due to the proximity with the piston at the moment of injection spray fuel impingement can occur, leading to unburned hydrocarbon emission from the liquid pool. Moreover, because of the long ignition delay and the long

injection dwell time, overleaning occurred and the local values of equivalence ratio were too low to ensure complete and efficient fuel oxidation. All these phenomena have a detrimental impact on combustion efficiency, the values of which are shown in Figure 119. As can be observed, the highest combustion efficiency achieved was 87%, which also limited the gross indicated efficiency to a maximum value of approximately 35%. These values are low if compared to the values of efficiency presented in other studies [63,127,128]. However, it should be borne in mind that in the experiments presented in this work, no modifications were made to the original engine, which is optimized for conventional Diesel operations. Therefore, the optimization of the combustion chamber and of the injection system for better HC emission and combustion efficiency will be a further development necessary for the improvement of the overall engine performance under ozone-assisted GCI operation.

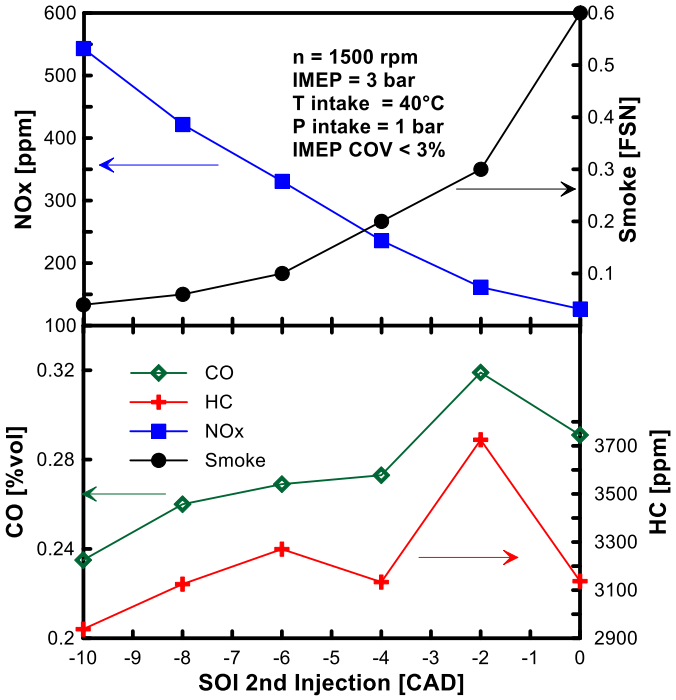

Figure 118.Exhaust emissions of NOx, HC, CO and Soot as a function of SOI2.

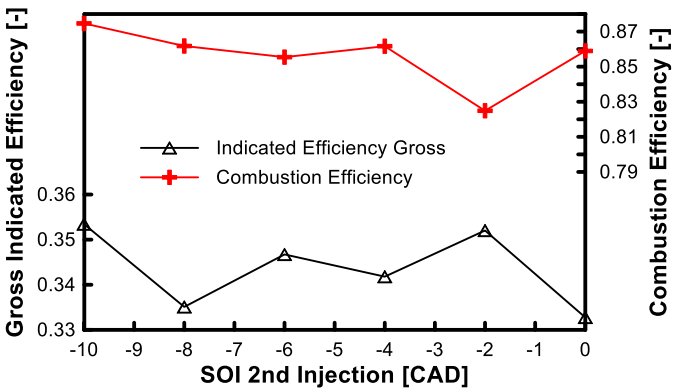

Figure 119. Combustion Efficiency and Gross Indicated Efficiency as a function of the SOI2.

7.3.5. Conclusions

In this chapter, the impact of ozone was investigated when fuel was directly injected into the cylinder inducing a certain fuel stratification. In the first part of the work, the ozone effect was investigated over a wide range of injection timing. The shift in the CA50 induced by ozone seeding was employed as a parameter to quantify the impact of ozone. The results from experiments highlighted the need to advance the fuel supply to obtain the effect of ozone. Injections close to TDC were not impacted by the ozone effect even when the ozonizer was set at its maximum capacity. This was most likely due to the fact that the O atoms coming from O_3 decomposition had already recombined, yielding molecular oxygen instead of reacting with fuel. Advancing the injection timing improved the impact of ozone. A stronger impact of ozone, comparable to that observed in HCCI conditions, was observed at early injection timing, i.e. SOI = -60 CAD. Experimental results also showed that if the operating range is characterized by higher NOx emission, the residual NO trapped in the residual gases can strongly limit the effect of ozone. In these conditions, O_3 reacts with NO, leading to NO_2 and O_2 before ozone breakdown can occur. O atoms are not produced and fuel oxidation is not improved. The residence time between ozone and fuel was also identified as an important parameter affecting the effect of ozone on GCI operations. It was therefore concluded that the fuel injection timing plays a fundamental role in determining the effectiveness of ozone to improve gasoline combustion under direct injection operation. In the second part of the chapter, a strategy based on ozone seeding to achieve stable GCI low load operations was developed. The fuel injection strategy was identified as a tool which can be employed to indirectly promote the impact of ozone on combustion. A double injection strategy was employed to maximize the effect of ozone on combustion. A first injection during the intake stroke was necessary to maximize the impact of ozone while a second injection during the compression stroke was necessary for the control of combustion phasing, noise, and pollutant emissions. Under these conditions, systematically increasing the ozone concentration at the intake enabled stable GCI low load operation at room temperature and pressure, with reduced amounts of soot and NOx. However, the

high emission of CO and HC due to the large separation between the two injection events may limit the combustion efficiency and the indicated efficiency. The potential of using ozone to achieve stable low load and idle GCI operations was demonstrated, but an optimization of the combustion chamber will be necessary to avoid excessive HC and CO. The injection system and the development of an ozone generator to be installed on light duty vehicles are necessary steps to be undertaken before making ozone-assisted GCI engines suitable for real car applications.

8. Conclusions and Perspectives

In this work, a comprehensive study on the potential of ozone to enable low load gasoline compression ignition operation was conducted.

Low load GCI operation requires burning a lean ($\phi = 0.3$) gasoline/air mixture. In conventional CI engines, the intake thermodynamic conditions at low load are not suitable to attain autoignition of high ON commercial gasoline. Increasing the temperature at the intake is a possible way to meet the autoignition chemistry requirements of gasoline. Under these conditions, the first part of the study focused on understanding the autoignition process and combustion in a GCI engine. It was found that in the conditions investigated and according to the chemical scheme employed for simulations, autoignition occurred in fuel lean regions which are characterized by a high local temperature. Therefore, a sequential ignition of increasingly richer fuel pockets occurs. The presence of rich fuel pockets in the moments prior to combustion is therefore associated to high combustion temperatures which can promote NOx production. Depending on the fuel injection strategy, the in-cylinder temperature equivalence ratio distribution can be strongly altered. Under certain operating conditions, an abnormal NOx emission occurred at early injection timing. Experiments and simulations demonstrated that the NO contained in the residual gases chemically promoted fuel oxidation, leading to a strong advance in combustion phasing. The impact of the injector umbrella angle on combustion was investigated: results showed that under single injection operation, different combinations of injection timing and umbrella angle corresponded to the spray targeting the same position of the piston head bowl. Although different injectors gave slightly different performances, a similar combustion behavior was observed for similar spray target positions. The impact of the injector umbrella angle was also investigated under double injection low load operation. The injector umbrella angle had a relatively small impact on low load combustion. The results suggested that the choice of the injection system has therefore to be made by considering the whole operating map of the engine and the combustion strategy to be adopted.

Ozone, a strong oxidizing agent, can be produced from natural air by means of an ozone generator. Its promoting effect on hydrocarbon oxidation was identified as a possible solution to extend the ignition range of lean gasoline/air mixture and achieve GCI low load operation without using VVT or changing the fuel properties.

The impact of ozone was investigated on the compression ignition combustion of commercial gasoline fuel. HCCI engine operation was chosen as an experimental environment in which the effect of ozone on combustion could be investigated by limiting the number of parameters affecting the fuel-ozone interaction. Results from experiments demonstrated that gasoline fuel is highly sensitive to the chemical impact of ozone, which was shown to improve the combustion process. The effects of seeding the engine intake with ozone on gasoline combustion were shown to be an advance and an increase in the heat released induced by

an overall improvement in combustion efficiency. Ozone was shown to be able to extend the range of conditions in which gasoline can autoignite, since adding zone allowed the compression ignition of lean mixtures which otherwise would not have burnt. In this way, the same amount of work was extracted by burning a reduced fuel mass, leading to a gain in indicated efficiency. Seeding the intake of the engine with ozone was also shown to be an effective way to reduce the intake temperature required for autoignition. Moreover, by increasing the intake ozone concentration, a simultaneous reduction of the equivalence ratio and of the intake temperature can be achieved, indicating that HCCI gasoline combustion can be substantially improved if the intake availability of ozone is high enough.

The impact of ozone on gasoline HCCI combustion was investigated in an optically accessible engine with iso-octane as a surrogate fuel. Results from experiments demonstrated that ozone alters the reaction path, stimulating the earlier chain branching reactions yielding a production of radicals which were not produced in absence of ozone and in the conventional oxidation process. The induction of a LTHR was identified as the mechanism through which ozone addition stimulates the reactivity of the system, allowing for the combustion of lean iso-octane/air mixtures which otherwise would not have ignited at very low intake temperatures.

In the last part of the work, the promoting effect of ozone on gasoline combustion was used to reduce the minimum load attainable in a GCI engine. To do that, the impact of ozone on combustion had to be investigated under fuel direct injection operation. Its impact on combustion turned out to be indirectly sensitive to the method employed to supply the fuel. Fuel had to be injected before the O atoms responsible for the combustion improvement had recombined to form molecular oxygen. Moreover, earlier injection timing promoted the impact of ozone because of the longer time available to ozone O atoms to interact with fuel. The presence in the combustion chamber of NO was demonstrated to negatively affect the impact of ozone on combustion because the strong chemical affinity between O_3 and NO prevented the release of the highly reactive O atoms.

An injection strategy for ozone-assisted GCI low load operation was designed based on the results obtained in the previous study to maximize the ozone effect on combustion and minimize the size and energy requirement for the ozone generator. A double injection strategy was shown to be effective to simultaneously maximize the promoting effect of ozone by means of an early injection during the intake stroke, and to enable control of the combustion process with a second injection in the final part of the compression stroke.

The results from the investigation reported in this work have demonstrated the potential of ozone to improve the reactivity of gasoline under low load GCI relevant conditions.

Other studies focused on extending low load GCI operation. Two main ways were considered. First, a short term solution to reduce CO_2 emissions from ICE consists in adapting the intake thermodynamic conditions to meet the autoignition requirements of the high ON gasoline currently available on the market. The second effective method, which also aims to be a long term solution closer to the demands of engine producers, fuel producers and final customers, is to use more reactive gasoline-like fuels in the naphtha range.

The use of ozone can be seen as a mix of these two strategies. On the one hand, an ozone generator is an actuator which could be employed to introduce a further degree of freedom in determining the intake air reactivity. By means of an ozone generator positioned in the intake manifold of a CI engine, not only temperature and pressure, but also the ozone concentration could be tuned to attain the intake air reactivity which best matches the load-speed conditions in which the engine would operate. Moreover, results from this work showed that when ozone made it possible to burn high ON fuel in thermodynamic conditions generally not suitable for autoignition, gasoline actually behaved like a more reactive double stage heat release fuel. The use of an ozone generator could also be seen as a method to attain an on-demand adaptation of the fuel properties according to the requirements of the engine operating conditions. Irrespective of the fuel used to run a CI engine, ozone has shown its potential to help engineers overcome some of the challenges related to the practical application of advanced compression ignition engines. Ozone can be employed to overcome several issues related to the use of high ON or low Cetane number fuels in CI engines: cold start and idle, stability at low load, emissions of CO and HC. In this work, a single operating condition was used to show the potential of ozone to enable low load GCI operation. GCI low load issues however involve a large set of combinations of load and speed in which fuel reactivity impedes autoignition. The ozone output concentration supplied by the ozone generator could be defined according to the engine operating conditions. In this context, the last part of the present research can be considered as the first step toward the development of a practical procedure to define the ozone concentration necessary to attain a targeted IMEP below the ignitability limit of the fuel used to run the engine. This procedure can be included in the design of an ozone generator for real passenger car applications.

In order to enable the use of ozone to be extended over a wide range of operating conditions, more research has to be done. The use of chemical simulation and 3D-CFD simulations would be an additional tool in increasing the understanding of the impact of ozone on combustion in ICE. Further investigations are therefore necessary to include ozone-related reactions in the chemical mechanisms for gasoline surrogate fuel. The application of optical diagnostic techniques is therefore of primary importance in acquiring additional knowledge of the chemistry of ozone decomposition and of the impact of the in-cylinder

distribution of temperature and equivalence ratio which can alter the effect of ozone on hydrocarbon oxidation. The impact on fuel oxidation of other chemical species such as nitric compounds should also be included in the reduced chemical mechanism suitable for 3D CFD simulations, due to the ever wider application of IGR, EGR and the relevance that these species may have in knock-related phenomena in SI engines.

Commercial ozone generators designed for purposes far from automotive applications were used in this study. The development of compact ozone generators to be installed in the intake system of a light-duty engine is therefore the next task to be performed before considering ozone for real automotive applications. It should be mentioned that engine prototypes [97] equipped with an ozone generator were released while this research was being carried out. This is a further demonstration of the potential of ozone to reduce the CO_2 emissions of the future light-duty internal combustion engine.

9. References

[1] Nederhoff E. Transport energy co2 - Moving Toward Sustainability. 2009. doi:10.1787/9789264073173-en.

[2] Sieminski A. International Energy Outlook 2016. US Energy Inf Adm 2016. doi:DOE/EIA-0484(2014).

[3] International Energy Agency n.d. https://www.iea.org/statistics/.

[4] United Nations. World Population Prospects: The 2017 Revision, Key Findings and Advance Tables 2017:46.

[5] U.S. Energy Information Administration. Transportation Sector Energy Consumption 2016;2016:127–37.

[6] https://www.eia.gov/opendata/ n.d. https://www.eia.gov/opendata/ (accessed January 1, 2017).

[7] International Energy Agencey (IEA). CO2 Emissions From Fuel Combustion. 2016.

[8] Miller JD, Façanha C. The state of clean transport policy - A 2014 synthesis of vehicle and fuel policy developments. ICCT Rep 2014:73.

[9] Stocker TF, Qin D, Plattner G-K, Tignor MMB, Allen SK. Climate Change 2013: The Physical Science Basis. Contribution of Working Group I to the Fifth Assessment Report of the Intergovernmental Panel on Climate Change. Intergov Panel Clim Chang Work Gr I Contrib to IPCC Fifth Assess Rep (AR5)(Cambridge Univ Press New York) 2013:1535.

[10] Berni F, Breda S, D'Adamo A, Fontanesi S, Cantore G. Numerical Investigation on the Effects of Water/Methanol Injection as Knock Suppressor to Increase the Fuel Efficiency of a Highly Downsized GDI Engine, 2015. doi:10.4271/2015-24-2499.

[11] Kim J, Park H, Bae C, Choi M, Kwak Y. Effects of water direct injection on the torque enhancement and fuel consumption reduction of a gasoline engine under high-load conditions. Int J Engine Res 2016;17:795–808. doi:10.1177/1468087415613221.

[12] Hwang J, Bae C, Park J, Choe W, Cha J, Woo S. Microwave-assisted plasma ignition in a constant volume combustion chamber. Combust Flame 2016;167:86–96. doi:10.1016/j.combustflame.2016.02.023.

[13] Dec JE. Advanced compression-ignition engines - Understanding the in-cylinder processes. Proc Combust Inst 2009;32 II:2727–42. doi:10.1016/j.proci.2008.08.008.

[14] Saxena S, Bedoya ID. Fundamental phenomena affecting low temperature combustion and HCCI engines, high load limits and strategies for extending these limits. Prog Energy Combust Sci 2013;39:457–88. doi:10.1016/j.pecs.2013.05.002 Review.

[15] Xie H, Li L, Chen T, Zhao H. Investigation on gasoline homogeneous charge compression ignition (HCCI) combustion implemented by residual gas trapping combined with intake preheating through waste heat recovery. Energy Convers Manag 2014;86:8–19.

doi:10.1016/j.enconman.2014.05.022.

[16] Lü X-C, Chen W, Huang Z. A fundamental study on the control of the HCCI combustion and emissions by fuel design concept combined with controllable EGR. Part 1. The basic characteristics of HCCI combustion. Fuel 2005;84:1074–83. doi:10.1016/j.fuel.2004.12.014.

[17] Albayrak Çeper B, Yildiz M, Akansu SO, Kahraman N. Performance and emission characteristics of an IC engine under SI, SI-CAI and CAI combustion modes. Energy 2015;136:72–9. doi:10.1016/j.energy.2016.08.038.

[18] Wang X, Xie H, Li L, Xie L, Chen T, Zhao H. Effect of the thermal stratification on SI-CAI hybrid combustion in a gasoline engine. Appl Therm Eng 2013;61:451–60. doi:10.1016/j.applthermaleng.2013.07.049.

[19] Gray AW, Ryan TW. Homogeneous Charge Compression Ignition (HCCI) of Diesel Fuel, 1997. doi:10.4271/971676.

[20] Christensen M, Hultqvist A, Johansson B. Demonstrating the multi-fuel capability of a homogeneous charge compression ignition engine with variable compression ratio. SAE Trans 1999;108:2099–113.

[21] Ryan TW, Callahan TJ. Homogeneous Charge Compression Ignition of Diesel Fuel. SAE Tech Pap 1996;961160. doi:10.4271/961160.

[22] Peng Z, Zhao H, Ladommatos N. Effects of Air / Fuel Ratios and EGR Rates on HCCI Combustion of n-heptane , a Diesel Type Fuel Reprinted From : Homogeneous Charge Compression Ignition 2003;2003. doi:10.4271/2003-01-0747.

[23] Takeda Y, Keiichi N. Emission Characteristics of Premixed Lean Diesel Combustion with Extre?me Early Staged Fuel Injection. Soc Automot Eng 1996:938–47. doi:10.4271/961163.

[24] Harada A, Shimazaki N, Sasaki S, Miyamoto T, Akagawa H, Tsujimura K. The Effects of Mixture Formation on Premixed Lean Diesel Combustion Engine. SAE Tech Pap 980533 1998:DOI: 10.4271/980533. doi:10.4271/980533.

[25] Kim MY, Kim JW, Lee CS, Lee JH. Effect of compression ratio and spray injection angle on HCCI combustion in a small DI diesel engine. Energy and Fuels 2006;20:69–76. doi:10.1021/ef0501694.

[26] Akagawa H, Miyamoto T, Harada A, Sasaki S, Shimazaki N, Hashizume T, et al. Approaches to Solve Problems of the Premixed Lean Diesel Combustion. Soc Automot Eng 1999;1:120–32. doi:10.4271/1999-01-0183.

[27] Iwabuchi Y, Kawai K, Shoji T, Takeda Y. Trial of New Concept Diesel Combustion System - Premixed Compression-Ignited Combustion -. SAE Pap 1999-01-0185 1999. doi:10.4271/1999-01-0185.

[28] Walter B, Gatellier B. Development of the High Power NADITM Concept Using Dual Mode Diesel Combustion to Achieve Zero NOx and Particulate Emissions. SAE Tech Pap 2002-01-1744 2002. doi:10.4271/2002-01-1744.

[29] Sjöberg M, Dec JE, Hwang W. Thermodynamic and Chemical Effects of EGR and Its Constituents

on HCCI Autoignition.pdf 2007.

[30] Ojeda W, Ojeda W, Kumar R, Kumar R, Zoldak P, Zoldak P, et al. Development of a Fuel Injection Strategy for Diesel LTC - 2008-01-0057. Sae 2008;2008. doi:10.4271/2008-01-0057.

[31] Murata Y, Kusaka J, Daisho Y, Kawano D, Suzuki H, Ishii H, et al. Miller-PCCI Combustion in an HSDI Diesel Engine with VVT. SAE Int J Engines 2008;1:444–56. doi:10.4271/2008-01-0644.

[32] He X, Durrett RP, Sun Z. Late intake valve closing as an emissions control strategy at Tier 2 Bin 5 engine-out NOx level. SAE Tech Pap 2008;1:2008-01–0637. doi:10.4271/2008-01-0637.

[33] Dec JE, Sjöbera M. Isolating the effects of fuel chemistry on combustion phasing in an HCCI engine and the potential of fuel stratification for ignition control. SAE Trans 2004;113:239–57. doi:10.4271/2004-01-0557.

[34] Sjöberg M, Dec JE. Smoothing HCCI Heat-Release Rates Using Partial Fuel Stratification with Two-Stage Ignition Fuels. SAE Tech Pap 2006;2006. doi:10.4271/2006-01-0629.

[35] Hwang W, Dec JE, Sjöberg M. Fuel Stratification for Low-Load HCCI Combustion: Performance & amp; Fuel-PLIF Measurements. Library (Lond)., 2007, p. 776–0790. doi:10.4271/2007-01-4130.

[36] Yang Y, Dec JE, Dronniou N, Sjöberg M, Cannella W. Partial Fuel Stratification to Control HCCI Heat Release Rates: Fuel Composition and Other Factors Affecting Pre-Ignition Reactions of Two-Stage Ignition Fuels. SAE Int J Engines 2011;4:2011-01–1359. doi:10.4271/2011-01-1359.

[37] Yang Y, Dec JE, Dronniou N, Sjöberg M. Tailoring HCCI heat-release rates with partial fuel stratification: Comparison of two-stage and single-stage-ignition fuels. Proc Combust Inst 2011;33:3047–55. doi:10.1016/j.proci.2010.06.114.

[38] Dempsey AB, Curran SJ, Wagner RM. A perspective on the range of gasoline compression ignition combustion strategies for high engine efficiency and low NOx and soot emissions: Effects of in-cylinder fuel stratification. Int J Engine Res 2016;1. doi:10.1177/1468087415621805.

[39] Dec JE, Yang Y, Dernotte J, Ji C. Effects of Gasoline Reactivity and Ethanol Content on Boosted, Premixed and Partially Stratified Low-Temperature Gasoline Combustion (LTGC). SAE Int J Engines 2015;8:935–55. doi:10.4271/2015-01-0813.

[40] Ji C, Dec J, Dernotte J, Cannella W. Boosted Premixed-LTGC / HCCI Combustion of EHN-doped Gasoline for Engine Speeds Up to 2400 rpm. SAE Int J Engines 2016;9:2016-01–2295. doi:10.4271/2016-01-2295.

[41] Kalghatgi GT, Risberg P, Angstrom H-E. Partially Pre-Mixed Auto-Ignition of Gasoline to Attain Low Smoke and Low NOx at High Load in a Compression Ignition Engine and Comparison with a Diesel Fuel. SAE Tech Pap 2007:SAE 2007-01-0006. doi:10.4271/2007-01-0006.

[42] Kalghatgi G, Johansson B. Gasoline compression ignition approach to efficient, clean and affordable future engines. Proc Inst Mech Eng Part D J Automob Eng 2017:95440701769427. doi:10.1177/0954407017694275.

[43] Kalghatgi GT, Gosling C, Jo M. The outlook for transport fuels : Part 2. Pet Technol Q 2016.

[44] Kalghatgi GT, Gosling C, Jo M. The outlook for transport fuels : Part 1. Pet Technol Q 2016.

[45] Kalghatgi GT. Developments in internal combustion engines and implications for combustion science and future transport fuels. Proc Combust Inst 2015;35:101–15. doi:10.1016/j.proci.2014.10.002.

[46] Viollet Y, Chang J, Kalghatgi G. Compression Ratio and Derived Cetane Number Effects on Gasoline Compression Ignition Engine Running with Naphtha Fuels. SAE Int J Fuels Lubr 2014;7:412–26. doi:10.4271/2014-01-1301.

[47] Kalghatgi GT, Kumara Gurubaran R, Davenport a., Harrison a. J, Hardalupas Y, Taylor a. MKP. Some advantages and challenges of running a Euro IV, V6 diesel engine on a gasoline fuel. Fuel 2013;108:197–207. doi:10.1016/j.fuel.2012.10.059.

[48] Al-Abdullah MH, Kalghatgi GT, Babiker H. Flash points and volatility characteristics of gasoline/diesel blends. Fuel 2015;153:67–9. doi:10.1016/j.fuel.2015.02.070.

[49] Kalghatgi GT, Risberg P, Ångström H-E. Advantages of Fuels with High Resistance to Auto-ignition in Late-injection, Low-temperature, Compression Ignition Combustion. SAE Tech Pap 2006. doi:10.4271/2006-01-3385.

[50] Manente V, Zander C, Johansson B, Tunestal P, Cannella W. An Advanced Internal Combustion Engine Concept for Low Emissions and High Efficiency from Idle to Max Load Using Gasoline Partially Premixed Combustion. SAE Tech Pap 2010;1. doi:10.4271/2010-01-2198.

[51] Vittorio Manente. Gasoline Partially Premixed Combustion An Advanced Internal Combustion Engine Concept Aimed to High Efficiency, Low Emissions and Low Acoustic Noise in the Whole Load Range. 2010.

[52] Manente V, Johansson B, Tunestal P, Sonder M, Serra S. Gasoline partially premixed combustion: high efficiency, low NOx and low soot by using an advanced combustion strategy and a compression ignition engine. Int J Veh Des 2012;59:108–28. doi:10.1504/IJVD.2012.048689.

[53] Dec JE, Yang Y, Dronniou N. Boosted HCCI - Controlling Pressure-Rise Rates for Performance Improvements using Partial Fuel Stratification with Conventional Gasoline. SAE Int J Engines 2011;4:2011-01–0897. doi:10.4271/2011-01-0897.

[54] Sellnau M, Sinnamon J, Hoyer K, Husted H. Gasoline Direct Injection Compression Ignition (GDCI) - Diesel-like Efficiency with Low CO2 Emissions. SAE 2011-01-1386 2011. doi:10.4271/2011-01-1386.

[55] Sellnau MC, Sinnamon J, Hoyer K, Husted H. Full-Time Gasoline Direct-Injection Compression Ignition (GDCI) for High Efficiency and Low NOx and PM. SAE Int J Engines 2012;5:2012-01–0384. doi:10.4271/2012-01-0384.

[56] Sellnau MC, Sinnamon J, Hoyer K, Kim J, Cavotta M, Husted H. Part-Load Operation of Gasoline Direct-Injection Compression Ignition (GDCI) Engine. SAE Int J Engines 2013:1–24. doi:10.4271/2013-01-0272.

[57] Hoyer KS, Sellnau M, Sinnamon J, Husted H. Boost System Development for Gasoline Direct-Injection Compression-Ignition (GDCI). SAE Int J Engines 2013;6:815–26. doi:10.4271/2013-01-0928.

[58] Sellnau MC, Sinnamon J, Hoyer K, Kim J, Cavotta M, Husted H. Part-Load Operation of Gasoline Direct-Injection Compression Ignition (GDCI) Engine. SAE 2013-01-0272 2013. doi:10.4271/2013-01-0272.

[59] Sellnau M, Foster M, Hoyer K, Moore W, Sinnamon J, Husted H. Development of a Gasoline Direct Injection Compression Ignition (GDCI) Engine. SAE 2014-01-1300 2014. doi:10.4271/2014-01-1300.

[60] Sellnau M, Foster M, Moore W, Sinnamon J, Hoyer K, Klemm W. Second Generation GDCI Multi-Cylinder Engine for High Fuel Efficiency and US Tier 3 Emissions. SAE Int J Engines 2016;9:2016-01–0760. doi:10.4271/2016-01-0760.

[61] Kodavasal J, Kolodziej CP, Ciatti SA, Som S. Computational Fluid Dynamics Simulation of Gasoline Compression Ignition. J Energy Resour Technol 2015;137:32212. doi:10.1115/1.4029963.

[62] Sellnau M, Moore W, Sinnamon J, Hoyer K, Foster M, Husted H. GDCI Multi-Cylinder Engine for High Fuel Efficiency and Low Emissions. SAE Int J Engines 2015;8:775–90. doi:10.4271/2015-01-0834.

[63] Kolodziej C, Kodavasal J, Ciatti S, Som S, Shidore N, Delhom J. Achieving Stable Engine Operation of Gasoline Compression Ignition Using 87 AKI Gasoline Down to Idle. SAE Tech Pap 2015-01-0832 2015. doi:10.4271/2015-01-0832.

[64] Borgqvist P, Tunestal P, Johansson B. Gasoline Partially Premixed Combustion in a Light Duty Engine at Low Load and Idle Operating Conditions, 2012. doi:10.4271/2012-01-0687.

[65] Borgqvist P, Tuner M, Mello A, Tunestal P, Johansson B. The Usefulness of Negative Valve Overlap for Gasoline Partially Premixed Combustion, PPC, 2012. doi:10.4271/2012-01-1578.

[66] Borgqvist P, Tunestal P, Johansson B. Comparison of Negative Valve Overlap (NVO) and Rebreathing Valve Strategies on a Gasoline PPC Engine at Low Load and Idle Operating Conditions. SAE Int J Engines 2013;6:2013-01–0902. doi:10.4271/2013-01-0902.

[67] Chang J, Viollet Y, Amer A, Kalghatgi G. Fuel Economy Potential of Partially Premixed Compression Ignition (PPCI) Combustion with Naphtha Fuel. SAE Tech Pap 2013. doi:10.4271/2013-01-2701.

[68] Chang J, Kalghatgi G, Amer A, Adomeit P, Rohs H, Heuser B. Vehicle Demonstration of Naphtha Fuel Achieving Both High Efficiency and Drivability with EURO6 Engine-Out NOx Emission. SAE Int J Engines 2013;6:101–19. doi:10.4271/2013-01-0267.

[69] Caprio V, Insola a., Lignola PG. Ozone Activated Low Temperature Combustion of Propane in a C.S.T.R. Combust Sci Technol 1983;35:215–24. doi:10.1080/00102208308923713.

[70] Ombrello T, Won SH, Ju Y, Williams S. Flame propagation enhancement by plasma excitation of oxygen. Part I: Effects of O3. Combust Flame 2010;157:1906–15. doi:10.1016/j.combustflame.2010.02.005.

[71] Starik AM, Kozlov VE, Titova NS. On the influence of singlet oxygen molecules on the speed of flame propagation in methane-air mixture. Combust Flame 2010;157:313–27. doi:10.1016/j.combustflame.2009.11.008.

[72] Halter F, Higelin P, Dagaut P. Experimental and Detailed Kinetic Modeling Study of the Effect of Ozone on the Combustion of Methane. Energy & Fuels 2011;25:2909–16. doi:10.1021/ef200550m.

[73] Wang ZH, Yang L, Li B, Li ZS, Sun ZW, Aldén M, et al. Investigation of combustion enhancement by ozone additive in CH4/air flames using direct laminar burning velocity measurements and kinetic simulations. Combust Flame 2012;159:120–9. doi:10.1016/j.combustflame.2011.06.017.

[74] Liang X, Wang Z, Weng W, Zhou Z, Huang Z, Zhou J, et al. Study of ozone-enhanced combustion in H2/CO/N2/air premixed flames by laminar burning velocity measurements and kinetic modeling. Int J Hydrogen Energy 2013;38:1177–88. doi:10.1016/j.ijhydene.2012.10.075.

[75] Won SH, Jiang B, Diévart P, Sohn CH, Ju Y. Self-sustaining n-heptane cool diffusion flames activated by ozone. Proc Combust Inst 2015;35:881–8. doi:10.1016/j.proci.2014.05.021.

[76] Weng W, Nilsson E, Ehn A, Zhu J, Zhou Y, Wang Z, et al. Investigation of formaldehyde enhancement by ozone addition in CH4/air premixed flames. Combust Flame 2015;162:1284–93. doi:10.1016/j.combustflame.2014.10.021.

[77] Pinchak M, Ombrello T, Carter C, Gutmark E, Katta V. The effects of hydrodynamic stretch on the flame propagation enhancement of ethylene by addition of ozone. Phil Trans R Soc A 2015;373:20140339. doi:10.1098/rsta.2014.0339.

[78] Gao X, Zhang Y, Adusumilli S, Seitzman J, Sun W. The Effect of Ozone Addition on Flame Propagation 2015:1–27. doi:10.2514/6.2016-0960.

[79] Gao X, Zhang Y, Adusumilli S, Seitzman J, Sun W, Ombrello T, et al. The effect of ozone addition on laminar flame speed. Combust Flame 2015;162:3914–24. doi:10.1016/j.combustflame.2015.07.028.

[80] Ehn A, Zhu JJ, Petersson P, Li ZS, Aldén M, Fureby C, et al. Plasma assisted combustion: Effects of O3 on large scale turbulent combustion studied with laser diagnostics and Large Eddy Simulations. Proc Combust Inst 2015;35:3487–95. doi:10.1016/j.proci.2014.05.092.

[81] Gao X, Zhang Y, Adusumilli S, Seitzman J, Sun W, Ombrello T, et al. The effect of ozone addition on laminar flame speed. Combust Flame 2015;162:3914–24. doi:10.1016/j.combustflame.2015.07.028.

[82] Kribs JD, Shah P V., Hutchins AR, Reach WA, Muncey RD, June MS, et al. The stabilization of partially-premixed jet flames in the presence of high potential electric fields. J Electrostat 2016;84:1–9. doi:10.1016/j.elstat.2016.08.002.

[83] Reuter CB, Won SH, Ju Y. Flame structure and ignition limit of partially premixed cool flames in a counterflow burner. Proc Combust Inst 2017;36:1513–22. doi:10.1016/j.proci.2016.06.067.

[84] Hajilou M, Ombrello T, Won SH, Belmont E. Experimental and numerical characterization of freely propagating ozone-activated dimethyl ether cool flames. Combust Flame 2017;176:326–33. doi:10.1016/j.combustflame.2016.11.005.

[85] Foucher F, Higelin P, Mounaïm-Rousselle C, Dagaut P. Influence of ozone on the combustion of n-heptane in a HCCI engine. Proc Combust Inst 2013;34:3005–12. doi:10.1016/j.proci.2012.05.042.

[86] Tachibana T, Hirata K, Nishida H, Osada H. Effect of ozone on combustion of compression ignition engines. Combust Flame 1991;85:515–9. doi:10.1016/0010-2180(91)90154-4.

[87] Aceves SM, Flowers D, Martinez-Frias J, Espinosa-Loza F, Pitz WJ, Dibble R. Fuel and Additive Characterization for HCCI Combustion. SAE Tech Pap 2003:2003-01–1814. doi:10.4271/2003-01-1814.

[88] Mohammadi A., Kawanabe H., Ishiyama T., Shioji M., Komada A. Study on combustion control in natural-gas PCCI engines with ozone addition into intake gas. SAE Tech Pap 2006;2006. doi:10.4271/2006-01-0419.

[89] Nishida H, Tachibana T. Homogeneous Charge Compression Ignition of Natural Gas/Air Mixture with Ozone Addition. J Propuls Power 2006;22:151–7. doi:10.2514/1.14991.

[90] Masurier J-B, Foucher F, Dayma G, Mounaïm-Rousselle C, Dagaut P. Towards HCCI Control by Ozone Seeding, 2013. doi:10.4271/2013-24-0049.

[91] Masurier JB, Foucher F, Dayma G, Dagaut P. Homogeneous charge compression ignition combustion of primary reference fuels influenced by ozone addition. Energy and Fuels 2013;27:5495–505. doi:10.1021/ef401009x.

[92] Masurier J, Foucher F, Dayma G, Dagaut P. Effect of Additives on Combustion Characteristics of a Natural Gas Fueled HCCI Engine. SAE Tech Pap 2014. doi:10.4271/2014-01-2662.

[93] Masurier J-B, Foucher F, Dayma G, Dagaut P. Ozone applied to the homogeneous charge compression ignition engine to control alcohol fuels combustion. Appl Energy 2015;160:566–80. doi:10.1016/j.apenergy.2015.08.004.

[94] Masurier J-B, Foucher F, Dayma G, Dagaut P. Investigation of iso-octane combustion in a homogeneous charge compression ignition engine seeded by ozone, nitric oxide and nitrogen dioxide. Proc Combust Inst 2015;35:3125–32. doi:10.1016/j.proci.2014.05.060.

[95] Masurier J, Foucher F, Dayma G, Rousselle C, Dagaut P. Application of an Ozone Generator to Control the Homogeneous Charge Compression Ignition Combustion Process. SAE Pap 2015-24-2456 2015. doi:10.4271/2015-24-2456.Copyright.

[96] Pinazzi PM, Masurier J-B, Dayma G, Dagaut P, Foucher F. Towards Stoichiometric Combustion in HCCI Engines: Effect of Ozone Seeding and Dilution. SAE Tech. Pap., 2015. doi:10.4271/2015-24-2450.

[97] Nagatsu K, Inoue A, Matsumoto K, Kaminaga T, Miyamoto T, Youso T. Control Device for Compression Ignition-Type Engine. US 9,719,441 B2, 2017.

[98] Fenimore CP. Formation of nitric oxide in premixed hydrocarbon flames. Symp Combust 1971;13:373–80. doi:10.1016/S0082-0784(71)80040-1.

[99] Lavoie GA, Heywood JB, Keck JC. Experimental and Theoretical Study of Nitric Oxide Formation in Internal Combustion Engines. Combust Sci Technol 1970;1:313–26. doi:10.1080/00102206908952211.

[100] Merryman EL, Levy A. Nitrogen oxide formation in flames: The roles of NO2 and fuel nitrogen. Symp Combust 1975;15:1073–83. doi:10.1016/S0082-0784(75)80372-9.

[101] C.T. Bowman, R.K. Hanson, D.F. Davidson, W.C. Gardiner, Jr., V. Lissianski, G.P. Smith, D.M. Golden MF and MG. http://www.me.berkeley.edu/gri_mech/ n.d.

[102] Dagaut P, Dayma G. The high-pressure reduction of nitric oxide by a natural gas blend. Combust Flame 2005;143:135–7. doi:10.1016/j.combustflame.2005.06.006.

[103] Lenner M. Nitrogen dioxide in exhaust emissions from motor vehicles. Atmos Environ 1987;21:37–43. doi:10.1016/0004-6981(87)90268-X.

[104] Dubreuil A, Foucher F, Mounaïm-Rousselle C, Dayma G, Dagaut P. HCCI combustion: Effect of NO in EGR. Proc Combust Inst 2007;31 II:2879–86. doi:10.1016/j.proci.2006.07.168.

[105] Moréac G, Dagaut P, Roesler JF, Cathonnet M. Nitric oxide interactions with hydrocarbon oxidation in a jet-stirred reactor at 10 atm. Combust Flame 2006;145:512–20. doi:10.1016/j.combustflame.2006.01.002.

[106] Anderlohr JM, Bounaceur R, Pires Da Cruz A, Battin-Leclerc F. Modeling of autoignition and NO sensitization for the oxidation of IC engine surrogate fuels. Combust Flame 2009;156:505–21. doi:10.1016/j.combustflame.2008.09.009.

[107] Benajes J, López JJ, Molina S, Redón P. New 0-D methodology for predicting NO formation under continuously varying temperature and mixture composition conditions. Energy Convers Manag 2015;91:367–76. doi:10.1016/j.enconman.2014.12.010.

[108] Contino F, Foucher F, Dagaut P, Lucchini T, D'Errico G, Mounaïm-Rousselle C. Experimental and numerical analysis of nitric oxide effect on the ignition of iso-octane in a single cylinder HCCI engine. Combust Flame 2013;160:1476–83. doi:10.1016/j.combustflame.2013.02.028.

[109] Kopp M, Brower M, Mathieu O, Petersen E, Güthe F. CO2* chemiluminescence study at low and elevated pressures. Appl Phys B Lasers Opt 2012;107:529–38. doi:10.1007/s00340-012-5051-4.

[110] Collin R, Nygren J, Richter M, Aldén M, Hildingsson L, Johansson B. Simultaneous OH- and Formaldehyde-LIF Measurements in an HCCI Engine. SAE 2003 Trans J Fuels Lubr 2003;112–4:1–8. doi:10.4271/2003-01-3218.

[111] Reitz RD, Diwakar R. Structure of High-Pressure Fuel Sprays, 1987. doi:10.4271/870598.

[112] Senecal PK, Richards KJ, Pomraning E, Yang T, Dai MZ, McDavid RM, et al. A New Parallel Cut-Cell Cartesian CFD Code for Rapid Grid Generation Applied to In-Cylinder Diesel Engine Simulations 2007;2007:776–90. doi:10.4271/2007-01-0159.

[113] Schmidt DP, Rutland CJ. A New Droplet Collision Algorithm. J Comput Phys 2000;164:62–80. doi:10.1006/jcph.2000.6568.

[114] Liu AB, Mather D, Reitz RD. Modeling the Effects of Drop Drag and Breakup on Fuel Sprays, 1993. doi:10.4271/930072.

[115] Mehl M, Chen JY, Pitz WJ, Sarathy SM, Westbrook CK. An Approach for Formulating Surrogates for Gasoline with Application toward a Reduced Surrogate Mechanism for CFD Engine Modeling. Energy & Fuels 2011;25:5215–23. doi:10.1021/ef201099y.

[116] Mehl M, Pitz WJ, Westbrook CK, Curran HJ. Kinetic modeling of gasoline surrogate components

and mixtures under engine conditions. Proc Combust Inst 2011;33:193–200. doi:10.1016/j.proci.2010.05.027.

[117] Chen Y, Wolk B, Mehl M, Cheng WK, Chen J-Y, Dibble RW. Development of a re duce d chemical mechanism targeted for a 5-component gasoline surrogate: A case study on the heat release nature in a GCI engine. Combust Flame 2016;178:268–76. doi:10.1016/j.combustflame.2016.12.018.

[118] Chen J-Y. A General Procedure for Constructing Reduced Reaction Mechanisms with Given Independent Relations. Combust Sci Technol 1988;57:89–94. doi:10.1080/00102208808923945.

[119] Som S, Longman D, Aithal S, Bair R, García M, Quan S, et al. A Numerical Investigation on Scalability and Grid Convergence of Internal Combustion Engine Simulations, 2013. doi:10.4271/2013-01-1095.

[120] Kim HJ, Park SH, Lee KS, Lee CS. A study of spray strategies on improvement of engine performance and emissions reduction characteristics in a DME fueled diesel engine. Energy 2011;36:1802–13. doi:10.1016/j.energy.2010.12.026.

[121] Tinaut F V., Reyes M, Giménez B, Pastor J V. Measurements of OH* and CH* chemiluminescence in premixed flames in a constant volume combustion bomb under autoignition conditions. Energy and Fuels 2011;25:119–29. doi:10.1021/ef1013456.

[122] Skeen SA, Manin J, Pickett LM. Simultaneous formaldehyde PLIF and high-speed schlieren imaging for ignition visualization in high-pressure spray flames. Proc Combust Inst 2015;35:3167–74. doi:10.1016/j.proci.2014.06.040.

[123] Brackmann C, Nygren J, Bai X, Li Z, Bladh H, Axelsson B, et al. Laser-induced fluorescence of formaldehyde in combustion using third harmonic Nd:YAG laser excitation. Spectrochim Acta - Part A Mol Biomol Spectrosc 2003;59:3347–56. doi:10.1016/S1386-1425(03)00163-X.

[124] Tang Q, Liu H, Li M, Yao M, Li Z. Study on ignition and flame development in gasoline partially premixed combustion using multiple optical diagnostics. Combust Flame 2017;177:98–108. doi:10.1016/j.combustflame.2016.12.013.

[125] Chemkin. Senkin: a fortran program for predicting homogeneous gas phase chemical kinetics with sensitivity analysis. 1997.

[126] Pinazzi PM, Foucher F. Influence of injection parameters, ozone seeding and residual NO on a Gasoline Compression Ignition (GCI) engine at low load. Proc Combust Inst 2017;36:3659–68. doi:10.1016/j.proci.2016.06.075.

[127] Borgqvist P, Tunestal P, Johansson B. Comparison of Negative Valve Overlap (NVO) and Rebreathing Valve Strategies on a Gasoline PPC Engine at Low Load and Idle Operating Conditions. SAE Int J Engines 2013;6:366–78. doi:10.4271/2013-01-0902.

[128] Sellnau M, Moore W, Sinnamon J, Hoyer K, Foster M, Husted H. GDCI Multi-Cylinder Engine for High Fuel Efficiency and Low Emissions. SAE Int J Engines 2015;8:775–90. doi:10.4271/2015-01-0834.

Pietro Matteo PINAZZI

POTENTIEL DE L'OZONE POUR ATTEINDRE LE FONCTIONNEMENT EN FAIBLE CHARGE D'UN MOTEUR ESSENCE A ALLUMAGE PAR COMPRESSION.

Le moteur essence à allumage par compression (GCI), reposant sur la combustion partiellement prémélangée de l'essence (GPPC), peut potentiellement assurer des opérations efficaces et propres. Le moteur GCI s'est avéré efficace à forte charge, mais l'indice d'octane élevé de l'essence limite considérablement les opérations à faible charge. Le présent travail étudie le potentiel de l'utilisation de l'ozone, fort agent oxydant, pour améliorer la réactivité de l'essence et permettre le fonctionnement à faible charge de GCI. L'ozone peut être produit *on board* en équipant le moteur d'un générateur d'ozone, sans impact dramatique sur le coût du moteur et sur la complexité du contrôle du moteur. Les essais effectués avec un moteur monocylindre ont montré que l'ozone favorise la combustion HCCI de l'essence, permettant d'étendre la limite d'auto-inflammation et de réduire la température minimale nécessaire de celle-ci. Les diagnostics optiques ont montré que ces propriétés sont liées à une prolifération radicale accrue, amenées par des réactions à basse température induites par l'ozone. En parallèle, le processus de combustion GCI a été étudié dans des conditions de faible charge. Sans ozone, la température d'admission doit être considérablement augmentée pour permettre l'auto-inflammation des mélanges essence-air pauvres. De plus, les résultats indiquent que le monoxyde d'azote (NO) contenu dans les gaz brûlés résiduels peut, dans certaines conditions, favoriser fortement la combustion GCI. Ensuite, l'effet de l'ozone a été étudié dans des conditions d'injection directe GCI. Les résultats démontrent qu'une stratégie avec double injection est nécessaire pour maximiser l'effet promoteur de l'ozone et pour contrôler le processus de combustion GCI. Enfin, l'utilisation d'une forte concentration d'ozone a permis d'atteindre des opérations à faible charge en mode GCI, avec des faibles émissions de NOx et de suie, et cela, sans avoir besoin d'augmenter la température ou la pression d'admission.

Mots clés : *Moteur essence allumage par compression (GCI), Combustion essence partiellement prémélangée (GPPC), Combustion à basse température (LTC), Ozone.*

POTENTIAL OF OZONE TO ENABLE THE LOW LOAD OPERATION OF A GASOLINE COMPRESSION IGNITION ENGINE.

Gasoline Compression Ignition (GCI) engine, relying on Gasoline Partially Premixed Combustion (GPPC) has potential for efficient and clean operations. GCI engine showed to be effective at high load, however, the high octane number of gasoline dramatically limits low load operations. The present work investigates the potential of using ozone, a strong oxidizing agent, to improve gasoline reactivity and enabling low load GCI operation. Ozone can be produced in-situ and on-demand by equipping the engine with an ozone generator, without a dramatic impact on the engine cost and the engine control complexity. Experiments in a single cylinder engine showed that ozone promotes gasoline HCCI combustion, making possible to extend the lean limit and reducing the minimum temperature needed for autoignition. Optical diagnostics showed that these properties are related to an increased radical proliferation related to ozone-induced low temperature reactions. In parallel, GCI combustion process was investigated under low load conditions. Without ozone, the intake temperature should be considerable increased to enable autoignition of lean gasoline-air mixtures. Moreover, results indicated that the NO contained into residual burnt gases can strongly promote GCI low load combustion. Finally, the effect of ozone was investigated under GCI direct-injection conditions, demonstrating that low load GCI operation with low NOx and Soot emission can be achieved by seeding the intake of the engine with ozone without needing of increasing the intake charge temperature or boosting the intake pressure.

Keywords : Gasoline Compression Ignition (GCI), Gasoline Partially Premixed Combustion (GPPC), Low Temperature Combustion (LTC), Ozone

Laboratoire PRISME
Université d'Orléans